

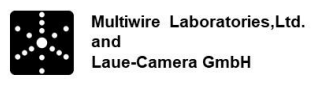
DKT 2020

**Deutsche
Kristallzüchtungstagung
11.-13. März 2020 in
München/Garching**

**50 Jahre Deutsche
Gesellschaft für
Kristallwachstum und
Kristallzüchtung e. V.**



ISBN 978-3-00-064845-8



Editorial

A warm welcome to everybody to the Annual German Crystal Growth Conference ("Deutsche Kristallzüchtungstagung, DKT 2020") of the German Association of Crystal Growth DGKK (Deutsche Gesellschaft für Kristallwachstum und Kristallzüchtung e. V.) !

This year we are happy and proud to celebrate the 50th anniversary of DGKK. It was founded in April 1970 and later in October the first general assembly took place in Munich together with the colloquium "Kristallzüchtung" of the German Research Foundation (DFG). With actually just nearly 400 individual and institutional members, the DGKK is an important part of the crystal growth community in Europe and well connected worldwide. From the very beginning until today the success of the association is based on the interdisciplinarity of the members coming from all fields of natural sciences and engineering and united in the complexity of the single crystal growth and the cutting edge technology needed. Such a widespread collection of interests and topics, all focusing on structural perfection, optimum performance for technical applications, unique physical properties and last not least in the aesthetic and beauty of crystals may be unique. The DGKK combines and promotes all of the fundamental and applied knowledge in crystal growth science and technology, which is documented in the special issue of the Journal Crystal Research & Technology Vol 55(2) 2020, dedicated to the 50th Anniversary of the German Association for Crystal Growth and this book of extended abstracts. It mirrors our very active crystal growth community and our vital working groups in all its facets. Certainly the retrospection on occasion of our commemorative session on Thursday afternoon followed by the gala dinner is the central event and we wish at this place to express our thanks to all our members for their unwearied efforts to boost our community all the years. We are pleased to welcome some of the merited "veterans" of the very first years and we would like to express our thanks and very best wishes to all of our fellows, who cannot join our celebration because of health reasons.

Beside the look back, the future perspectives are our central concern for the DKT 2020. The talks given by former and actual laureates of the DGKK prize as well by the invited speakers are supposed to inspire our discussion about our future challenges ranging from basic research, new materials and complex engineering technology to new computing methods and artificial intelligence.

Finally we would like to express our gratitude to all the institutions and companies named on the front cover for generous financial support. We wish you all a fruitful and unforgettable conference and look ahead a successful future of our DGKK,

Andreas Erb, Wolfram Miller, Andreas Danilewsky

Grußworte der Vorsitzenden des Exzellenzclusters ORIGINS

Liebe Mitglieder der DGKK,

im Namen der Mitglieder des Münchner ORIGINS Clusters gratulieren wir ganz herzlich der DGKK zum 50-jährigen Jubiläum.

Der Exzellenzcluster ORIGINS untersucht die Entstehung des Weltalls und den Ursprung des Lebens. Er geht aus der sehr fruchtbaren Zusammenarbeit zwischen Astro-, Teilchen- und Kernphysikern innerhalb des vorherigen Exzellenzclusters Universe hervor, der die grundlegenden Eigenschaften des Universums erforschte. Hochreine Kristalle spielen hierbei eine ganz wichtige Rolle: sie werden zur Suche nach der dunklen Materie verwendet, zum Nachweis von Neutrinos bei niedrigsten Energien, zur Spurensuche was mit der anfänglichen Anti-Materie im Universum geschehen ist, oder um die Kopplung von hypothetische Teilchen an Photonen zu vervielfachen. Grundlagenforschung in der Kern-, Astro- und Teilchenphysik und Kristallwachstum sind eng mit einander verbunden und die aktuelle Forschung in einem der Forschungsfelder beflügelt oft das andere.

Wir wünschen Ihnen eine erfolgreiche Jahrestagung 2020!

Herzliche Grüße
Ihr

Prof. Stephan Paul

Prof. Andreas Burkhart

Co-Sprecher des Exzellenzcluster ORIGINS, München



Deutsche Gesellschaft für Kristallographie

Grußwort vom Vorsitzenden der DGK

Liebe Mitglieder der DGKK,

im Namen der Deutschen Gesellschaft für Kristallographie gratulierte ich der DGKK ganz herzlich zu ihrem 50-jährigen Bestehen. Kristallzüchtung und Kristallwachstum haben in den 50 Jahren nicht an Bedeutung verloren, im Gegenteil, manche Fragen sind heute aktueller sind denn je.

Die DGKK und die DGK sind nicht nur durch ihre ähnlichen Namen verbunden, sondern auch durch gemeinsame wissenschaftliche Interessen, wie z.B. in den Materialwissenschaften. Dies spiegelt sich auch in gemeinsamen Aktivitäten wieder, wie ein gemeinsam organisiertes Mikrosymposium im Rahmen der DGK Jahrestagung 2018 sowie in 2019 beim GPPCG-3 in Poznań und einer DGK Summer School in Mühlheim, denen in Zukunft hoffentlich weitere gemeinsame Veranstaltungen folgen werden.

Ich wünsche Ihnen eine erfolgreiche Jahrestagung 2020!

Herzliche Grüße

Ihr

Ralf Ficner
Georg-August-Universität Göttingen
Vorsitzender der DGK

DGM - Deutsche Gesellschaft für Materialkunde e.V.
Postanschrift: DGM c/o DGM-Inventum GmbH
Marie-Curie-Straße 11 – 17, D-53757 Sankt Augustin

An die

Deutsche Gesellschaft für
Kristallwachstum und Kristallzüchtung e.V.

12. Januar 2020

Grußwort zu 50 Jahre DGKK

Manche Erfindungen verdanken sich dem glücklichen Zufall. Als Jan Czochralski 1913 beim Verfassen seines Tagesberichts im Metall-Forschungslabor der AEG seine Feder statt in die Tinte in die heiße Zinnlösung für seine Experimente tauchte, entdeckte er, wie man einen Einkristall aus einer Zinnschmelze zieht: eine neue Methode zur Herstellung von einkristallinen Werkstoffen. Das Czochralski-Verfahren ist heute eines der wichtigsten Züchtungsverfahren – und damit von großer Bedeutung nicht nur für die Metallurgie, sondern in besonderem Maße auch für die Deutsche Gesellschaft für Kristallwachstum und Kristallzüchtung e.V. (DGKK), deren 50. Geburtstag wir 2020 feiern können.

Im vergangenen Jahr wurde die Deutsche Gesellschaft für Materialkunde e.V. (DGM) 100 Jahre alt – und Jan Czochralski war eines ihrer Gründungsmitglieder! Über seinen Namen und sein Wirken sind die beiden Gesellschaften also seit rund einem halben Jahrhundert miteinander verbunden – eine Verbindung, die durch die Zusammenarbeit in der Bundesvereinigung MatWerk längst auch praktischen Nutzen für DGKK und DGM nach sich gezogen hat.

In diesem Sinne ist es uns eine große Freude, der DGKK hiermit herzlich zu ihrem runden Jubiläum zu gratulieren. Die von ihr geförderte Forschung, Lehre und Technologie auf den Gebieten Kristallwachstum, Kristallzüchtung und Epitaxie etwa durch Ausbildungs- und Fortbildungsveranstaltungen hat auch auf die von der DGM vertretenen Bereiche der Materialwissenschaft und Werkstofftechnik zurückgewirkt. Auch ihre erfolgreiche Nachwuchsförderung hat uns immer wieder sehr beeindruckt.

Wir freuen uns im Namen unserer Mitglieder auf die weitere gemeinsame Zukunft.

Mit freundlichen Grüßen



Prof. Dr.-Ing. Frank Mücklich
Präsident der Deutschen Gesellschaft für Materialkunde e.V.



Dr. Oliver Schauerte
Präsident der Deutschen Gesellschaft für Materialkunde e.V.

Grußwort zum 50-jährigen Bestehen der Deutschen Gesellschaft für Kristallwachstum und Kristallzüchtung e.V. (DGKK)

Dr. phil. nat. Ursula Eul

*Bundesvereinigung Materialwissenschaft und Werkstofftechnik e.V. (BV MatWerk)
E-mail: vorstand-bv@matwerk.de*

Zu ihrem 50-jährigen Bestehen gratuliert die Bundesvereinigung Materialwissenschaft und Werkstofftechnik e.V. (BV MatWerk) der Deutschen Gesellschaft für Kristallwachstum und Kristallzüchtung e.V. (DGKK) sehr herzlich.

Hochwertige Kristalle halfen in der präparativen Chemie der 1950er Jahre, das Rätsel unserer Erbsubstanz zu lösen. Ohne technische Kristalle gäbe es heute weder WLAN noch Laser Pointer, weder Ultraschall-Gerät noch Körperscanner. Siliziumkristalle bilden die unverzichtbare Materialbasis für die Halbleiterindustrie und für die Solarindustrie. Ohne die wissenschaftlichen und technischen Erfolge in der Kristallographie wäre unsere Welt heute nicht so, wie sie ist.

In den 50 Jahren ihres Bestehens hat die DGKK mit ihrem Einsatz für Forschung, Lehre und Technologie von Kristallwachstum, Kristallzüchtung und Epitaxie maßgeblich zum hohen Entwicklungsstand dieser Disziplinen in Deutschland und damit zu zahlreichen technischen und wirtschaftlichen Erfolgen beigetragen. Durch die kontinuierliche Optimierung der Kristallstrukturanalyse konnten immer wieder neue Einsatzgebiete erschlossen werden, z.B. in der Landwirtschaft, in der pharmazeutischen Industrie, im Bauwesen oder in der Textilindustrie.

Für die Entwicklung neuer Materialien spielt die Analyse komplexer Kristallstrukturen eine wichtige Rolle: Erst wenn bekannt ist, welche Struktur zugrunde liegt, können zusätzliche Eigenschaften integriert werden. Bei smarterer Kleidung werden z.B. verschiedene physiologische Parameter, wie Körpertemperatur oder Herzfrequenz, über Sensoren erfasst. Je nachdem, wie das Messergebnis ausfällt, können die verarbeiteten Stoffe einen kühlenden oder wärmenden Effekt erzeugen.

Als Gründungsmitglied von BV MatWerk verbindet DGKK und BV MatWerk eine langjährige vertrauensvolle Zusammenarbeit. Beide Institutionen eint das Anliegen, die kontinuierliche interdisziplinäre Zusammenarbeit unter ihren Mitgliedern ebenso wie den wissenschaftlichen Nachwuchs zu fördern, den Austausch mit Politik, Wirtschaft und Gesellschaft zu intensivieren und die Wahrnehmung von Materialwissenschaft und Werkstofftechnik in Politik und Öffentlichkeit positiv zu beeinflussen.

Die BV MatWerk bedankt sich ausdrücklich für das große Engagement der DGKK für Materialwissenschaft und Werkstofftechnik und wünscht ihr im Namen aller Mitglieder eine weiterhin erfolgreiche Zukunft.

Dr. phil. nat. Ursula Eul

Vorstandsvorsitzende der BV MatWerk e. V.

PROGRAMME

WEDNESDAY, 11.03.2020

10:00 – 10:10 OPENING ANDREAS DANILEWSKY, ANDREAS ERB

SESSION 1

CHAIR PROF. DR. ANDREAS DANILEWSKY

10:10 – 10:50 **PROF. OLIVIER GUILLON**, FORSCHUNGSZENTRUM JÜLICH GMBH
(INVITED) *Crystalline materials for electrochemical energy storage*

10:50 – 11:10 **DR. DIRK KOK**, RADBOUD UNIVERSITEIT NIJMEGEN, NL
Thermochemical heat storage using alcohol solvates

11:10 – 11:30 **DR-ING. MATTHIAS GERMANN**, ISABELLENHÜTTE, DILLENBURG
VGF-Growth of Half-Heusler-material for industrial production of thermoelectric-material

11:30 – 11:50 **TOM SCHNEIDER**, TU BERGAKADEMIE FREIBERG
3D interlayer growth in the high temperature vapor phase epitaxy of GaN

11:50 – 12:10 **DR. NIKOLAY ABROSIMOV**, LEIBNIZ-INSTITUT FÜR KRISTALLZÜCHTUNG, BERLIN
Growth of ²⁸Si crystals for the preparation of Si spheres

12:10 – 13:20 LUNCHBREAK

SESSION 2

CHAIR PROF. DR. PETER WELLMANN

13:20 – 14:00 **DR. MATTHIAS SCHRECK**, UNIVERSITÄT AUGSBURG
(INVITED) *Single crystal diamond wafers by heteroepitaxy: Synthesis and potential applications*

14:00 – 14:20 **DR. LUTZ KIRSTE**, FRAUNHOFER IAF, FREIBURG
X-Ray Diffraction analysis of the defect structure of diamond substrates and Thick Diamond Films

14:20 – 14:40 **DR. STEPHAN MÜLLER**, FRAUNHOFER IISB, ERLANGEN
PVT growth of large freestanding C-doped AlN crystals

14:40 – 15:00 **DR. THOMAS STRAUBINGER**, LEIBNIZ-INSTITUT FÜR KRISTALLZÜCHTUNG, BERLIN
Growth of bulk AlN crystals: Influence of the temperature field on growth rate, optical absorption and dislocation density

15:00 – 16:30 POSTERSESSION WITH DRINKS AND SNACK

SESSION 3

CHAIR PROF. DR. ANDREAS ERB

- 16:30 – 17:10 **PROF. DR. GÜNTHER EGGELER**, RUHR-UNIVERSITÄT BOCHUM
(INVITED) *On mosaicity and the formation of defects during Bridgman processing of Ni-base single crystal superalloys*
- 17:10 – 17:30 **TIMMY REIMANN**, INNOVENT E.V, JENA
Magneto-optical Bismuth substituted rare-earth iron garnet sensor films for characterization of electrical steel sheets
- 17:30 – 17:50 **DARREN PEETS PhD**, TECHNISCHE UNIVERSITÄT DRESDEN
Self-flux growth of single crystals of BaCoSO
- 17:50 – 18:10 **MARIUS PETERS**, GOETHE UNIVERSITÄT FRANKFURT AM MAIN
Crystal growth of the valence fluctuating system EuPd_2Si_2
- 18:30 – 20:30 MITGLIEDERVERSAMMLUNG (GENERAL ASSEMBLY)
WITH DRINKS AND SNACK
-

THURSDAY, 12.03.2020

SESSION 4

CHAIR DR. WOLFRAM MILLER

-
- 08:30 – 09:10 **PROF. DR. JÖRG NEUGEBAUER**, MAX-PLANCK-INSTITUT FÜR EISENFORSCHUNG,
(INVITED) DÜSSELDORF
Modeling crystal growth and materials design in high dimensional chemical and structural configuration spaces
- 09:10 – 09:30 **DR. NORA WOLFF**, HELMHOLTZ-ZENTRUM BERLIN FÜR MATERIALIEN UND ENERGIE
Growth of CuFeO₂ single crystals by the optical floating-zone technique
- 09:30 – 09:50 **DR. NATALIJA VAN WELL**, LUDWIG-MAXIMILIANS-UNIVERSITÄT MÜNCHEN
Investigation of orthorhombic and tetragonal phases of Cs₂CuCl_{4-x}Br_x mixed system
- 09:50 – 10:10 **SEBASTIAN GRUNER**, FRAUNHOFER THM FREIBERG
Investigation of facet growth in heavily doped silicon single crystals grown in the mirror furnace
- 10:10 – 10:40 COFFEEBREAK

SESSION 5

CHAIR PROF. DR. MATTHIAS BICKERMANN

-
- 10:40 – 11:00 **PROF. DR. MICHAEL HEUKEN**, AIXTRON, SE HERZOGENRATH
Control of AlInN composition in closed coupled showerhead MOCVD reactors
- 11:00 – 11:20 **DR. ANDREAS POPP**, LEIBNIZ-INSTITUT FÜR KRISTALLZÜCHTUNG IKZ, BERLIN
Growth of modulation-doped β-Ga₂O₃ multilayers by MOVPE
- 11:20 – 11:40 **DR. CARSTEN DUBS**, INNOVENT E.V, JENA
Nanometer-thin iron garnet films grown by liquid phase epitaxy
- 11:40 – 12:00 **MANUEL KOLLMUß**, FRIEDRICH-ALEXANDER-UNIVERSITÄT ERLANGEN-NÜRNBERG
Status of 3C-SiC bulk growth using sublimation epitaxy
- 12:00 – 13:00 LUNCHBREAK

SESSION 6

CHAIR PROF. DR. MICHAEL HEUKEN

-
- 13:00 – 13:40 **DR. ALEXANDER KILLI**, TRUMPF LASER GMBH, SCHRAMBERG
(INVITED) *Significance of Optical Crystals for the laser industry*
- 13:40 – 14:00 **PROF. DR. MATTHIAS BICKERMANN**, LEIBNIZ-INSTITUT FÜR KRISTALLZÜCHTUNG,
BERLIN
Crystal growth of oxides and fluorides at the IKZ
- 14:00 – 14:20 **ANASTASIA UVAROVA**, LEIBNIZ-INSTITUT FÜR KRISTALLZÜCHTUNG IKZ, BERLIN
Growth of high-melting sesquioxides for laser applications
- 14:20 – 14:50 COFFEEBREAK

COMMEMORATIVE EVENT 50 YEARS DGKK A. ERB, W. MILLER, A. DANILEWSKY

14:50 – 15:00 **OPENING**

15:00 – 15:15 GRUßWORTE - WELCOMING SPEECHES

15:15 – 16:00 GESCHICHTE DER DGKK UND DER ARBEITSGRUPPE "KRISTALLISATION" IN DER VFK
PROF. DR. HELMUT KLAPPER, AACHEN
PROF. DR. PETER RUDOLPH, SCHÖNEFELD

16:00 – 16:20 PRIZES FOR SCHOLAR'S COMPETITION "WER ZÜCHTET DEN SCHÖNSTEN KRISTALL?"
16:20 – 16:25 POSTER PRIZE

16:25 - 16:50 **DR. ANTON JESCHE**, UNIVERITÄT AUGSBURG
Solution Growth as a powerful tool for the solid-state physicist

16:50 – 17:20 DGKK NACHWUCHSPREIS: **ROBIN LANG**, FRAUNHOFER ISE FREIBURG
MOVPE Growth of GaAs with Growth Rates up to 280 $\mu\text{m}/\text{h}$

17:20 – 17:50 DGKK PREIS: **DR. STACIA KELLER**, UNIVERSITY OF CALIFORNIA ST. BARBARA (USA)
The "amazing" group-III nitrides - epitaxy for optical and electronic applications

19:00 – 22:00 GALA DINNER AT THE MUNICH TOWNHALL (RATSKELLER, ALTE KÜFEREI)

FRIDAY, 13.03.2020

SESSION 7

CHAIR LEV KADINSKI

-
- 08:30 – 09:00 **PROF DR. KOICHI KAKIMOTO**, KYUSHU UNIVERSITY, JAPAN
(INVITED) *Collaboration of experiment and numerical analysis of crystal growth of semiconductors*
- 09:00 – 09:20 **DR. KASPARS DADZIS**, LEIBNIZ-INSTITUT FÜR KRISTALLZÜCHTUNG, BERLIN
Model experiments for crystal growth technique
- 09:20 – 09:40 **STANISLAUS SCHWANKE**, FRAUNHOFER IISB, ERLANGEN
Numerical modeling of metallic impurity incorporation during directional solidification of multi-crystalline silicon assisted by experimental proof
- 09:40 – 10:00 **OLIVER HARDER**, LUDWIG-MAXIMILIANS-UNIVERSITÄT MÜNCHEN
Forced convection by high-speed rotation in Czochralski growth from high temperature solutions
- 10:00 – 10:20 **DR. D.V. BERKOV**, GENERAL NUMERICS RESEARCH LAB. , JENA
Theoretical analysis, critique and validity limits of Haasen-Alexander-Model for predicting the dislocation density
- 10:20 – 11:00 COFFEEBREAK

SESSION 8

CHAIR DR. JOCHEN FRIEDRICH

-
- 11:00 – 11:30 **PROF. DR. STEFAN SCHÖNERT**, TU MÜNCHEN
(INVITED) *High-purity single crystals for experiments in astroparticle physics research*
- 11:30 – 11:50 **DR. RADHAKRISHNAN SUMATHI** LEIBNIZ-INSTITUT FÜR KRISTALLZÜCHTUNG, BERLIN
Towards 80 mm diameter ultra-high purity germanium single crystals by Czochralski growth
- 11:50 – 12:10 **KEVIN-PETER GRADWOHL**, LEIBNIZ-INSTITUT FÜR KRISTALLZÜCHTUNG, BERLIN
Formation of vacancy related defects in high-purity germanium
- 12:10 – 12:30 **ANGELINA KINAST**, TU MÜNCHEN
CaWO₄ crystal growth for the CRESST dark matter search
- 12:30 – 12:50 **DR. THOMAS JAUß**, ALBERT-LUDWIGS UNIVERSITÄT, FREIBURG
Investigation of particle incorporation in a transparent melt system under μg conditions
- 12:50 – 13:00 CLOSING REMARKS

POSTERS

- 1 MATTHIAS ARZIG**, FRIEDRICH-ALEXANDER-UNIVERSITÄT ERLANGEN-NÜRNBERG
Influence of the surface morphology on the defect distribution in the faceted region of 4H-SiC single crystals
- 2 MICHAEL SCHÖLER**, FRIEDRICH-ALEXANDER-UNIVERSITÄT ERLANGEN-NÜRNBERG
Limitations during Vapor Phase Growth of Bulk (100) 3C-SiC Using 3C-SiC-on-SiC Seeding Stacks
- 3 MELISSA RÖDER**, ALBERT LUDWIGS UNIVERSITY FREIBURG
X-Ray Analysis of Defects in 4H-SiC
- 4 JOHANNES STEINER**, FRIEDRICH-ALEXANDER-UNIVERSITÄT ERLANGEN-NÜRNBERG
Impact of Varying Parameters on the Temperature Gradients in 100 mm Silicon Carbide Bulk Growth in a Computer Simulation Validated by Experimental Results
- 5 DR. KLAUS BÖTTCHER**, LEIBNIZ-INSTITUT FÜR KRISTALLZÜCHTUNG, BERLIN
Numerical Modelling of the Czochralski Growth of Neodymium-scandate single crystals
- 6 FRANZISKA GRUßLER**, UNIVERSITY OF AUGSBURG
Synthesis and characterization of the triangular antiferromagnets NaYbO₂, KYbO₂ and NaYbS₂
- 7 ELLA SUPIK** ALBERT LUDWIGS UNIVERSITY FREIBURG
The Influence of Sodium Dodecyl Sulfate on the Growth and Properties of Triglycine Sulfate Crystals
- 8 ALEXANDER ENGELHARDT**, TECHNISCHE UNIVERSITÄT MÜNCHEN
Single-crystal growth and magnetic phase diagram of TbFeO₃
- 9 FRANZISKA BREITNER**, UNIVERSITY OF AUGSBURG
Crystal Growth of Fe-doped Li₃N
- 10 GLORIA KIRSTE**, LEIBNIZ-INSTITUT FÜR FESTKÖRPER- UND WERKSTOFFFORSCHUNG, DRESDEN
Microstructural evolution of intermetallics under the influence of magnetic field annealing – exemplified by Mn₃Ga

- 11 PATRIZIA FRITSCH**, LEIBNIZ-INSTITUT FÜR FESTKÖRPER- UND WERKSTOFFFORSCHUNG, DRESDEN
ZF NMR as a tool to clarify crystallographic, magnetic, and electronic structure of magnetically ordered materials
- 12 DR. KRISTIN KLIEMT**, GOETHE-UNIVERSITÄT FRANKFURT
 LnMn_2Ge_2 ($\text{Ln} = \text{Nd}, \text{Sm}, \text{Dy}$): Single crystal growth and characterization
- 13 DR. MATTHIAS SCHUSTER**, FRIEDRICH-ALEXANDER-UNIVERSITÄT ERLANGEN-NÜRNBERG
Directly analyzing the depth dependent properties of $\text{Cu}(\text{In}, \text{Ga})(\text{S}, \text{Se})_2$ wedges manufactured by exfoliation and a nontoxic, adjustable etching process
- 14 JIAONA ZOU**, MATERIALS RESEARCH CENTER FMF, FREIBURG
Crystal growth of $(\text{Cd}, \text{Zn})\text{Te}$ under microgravity Vampir-F: Characterization of ground experiments
- 15 ANDREAS-GABRIEL SCHNEIDER**, UNIVERSITY OF AUGSBURG
In-situ detection of crystallization processes and seed selection in high temperature solutions
- 16 DR. WOLFRAM MILLER**, LEIBNIZ-INSTITUT FÜR KRISTALLZÜCHTUNG, BERLIN
A KMC model for homoepitaxial growth of Ga_2O_3
- 17 JAN PHILLIP WÖHRLE**, ALBERT-LUDWIGS-UNIVERSITY FREIBURG
Investigation of soluto-capillary convection in $\text{Ge}_x\text{Si}_{1-x}$ melts
- 18 IRYNA BUCHOVSKA**, LEIBNIZ-INSTITUT FÜR KRISTALLZÜCHTUNG, BERLIN
Parameter study on n-type multicrystalline ingots with tailored resistivity profiles
- 19 DR. FRANK M. KIESSLING**, LEIBNIZ-INSTITUT FÜR KRISTALLZÜCHTUNG, BERLIN
Investigation of directionally solidified quasi-mono silicon for future gravitational- wave detector test-mass mirrors
- 20 STEFAN PÜSCHEL**, LUDWIG-MAXIMILIANS-UNIVERSITÄT MÜNCHEN
Single crystal growth of Sn- and Ge-substituted GaPd_2 for basic research in catalysis
- 21 DR. HANS-JOACHIM ROST**, LEIBNIZ-INSTITUT FÜR KRISTALLZÜCHTUNG, BERLIN
Thermally stimulated dislocation generation in silicon crystals grown by the Floating Zone method

Invited Talks

CRYSTALLINE MATERIALS FOR ELECTROCHEMICAL ENERGY STORAGE

O. Guillon^{abc}

^a Forschungszentrum Jülich GmbH, Institute of Energy and Climate Research (IEK-1: Materials Synthesis and Processing), D-52425 Jülich, Germany

^b Jülich-Aachen Research Alliance, JARA-Energy

^c Helmholtz-Institute Münster, c/o Forschungszentrum Jülich GmbH, D-52425 Jülich, Germany

E-mail: o.guillon@fz-juelich.de

Summary

Electrochemical battery cells can be operated reversibly (in charging/discharging modes) in order to temporarily store electrical energy. Among the already commercially available battery systems, the Li-ion technology has been continuously further developed since its discovery acknowledged in 2019 by the Nobel Prize in Chemistry. Reaching high energy densities, Li-ion batteries have enabled new applications in consumable electronics, power tools, battery electric vehicles or even electric flight. Current and future developments focus on the use of new electrode materials, solid-state electrolytes for higher safety and capacity, as well as alternative chemistries such as Na-ion.

Inorganic crystals and polycrystals play a key role in all these type of cells [1]. On the one hand, compounds which can reversibly accommodate mobile Li- or Na-ions in their lattice are used as electrode materials. Today commercial cathode materials for Li-ion batteries are all oxide particles with well-defined stoichiometry and structure. On the other hand, crystalline ionic conductors with negligible electronic conductivity are potentially candidates for solid-state batteries. Their larger electrochemical stability may enable to combine a high-capacity metallic anode with high-voltage cathode materials.

The presentation will give an overview of recent developments in the field and highlight the importance of controlling composition, crystalline phase, morphology and microstructure of crystalline materials by advanced synthesis and processing as well as characterization methods.

[1] Y. Arinicheva, M. Wolff, S. Lobe, C. Dellen, D. Fattakhova-Rohlfing, O. Guillon, D. Böhm, F. Zoller, R. Schmuch, J. Li, Martin Winter, E. Adamczyk, V. Pralong, *Ceramics for electrochemical storage*, in “Advanced Ceramics for Energy Conversion and Storage”, Ed. O. Guillon, Elsevier, 2020.

Single crystal diamond wafers by heteroepitaxy: Synthesis and potential applications

M. Schreck,^a S. Gsell,^b M. Fischer^b

^aInstitut für Physik, Universität Augsburg, Universitätsstraße 1, 86135 Augsburg, Germany

^bAugsburg Diamond Technology GmbH, Am Technologiezentrum 5, 86159 Augsburg, Germany

E-mail: matthias.schreck@physik.uni-augsburg.de

Summary

Diamond is a crystalline material with a unique combination of extreme material parameters that form the base for various potential applications in mechanics, optics and electronics. Since the 1950s two alternative routes for the synthesis have been explored: The first one is the high pressure high temperature (HPHT) method which copies the natural formation process using typical pressures of 5 - 6 GPa and temperatures of 1300 - 1600 °C. The second one is chemical vapor deposition (CVD) that works at conditions below ambient pressure (10 - 300 mbar) and at more moderate temperatures (500 – 1200°C). While the HPHT technique can deliver crystals of high structural quality, it suffers from severe limitations in size (< 1 inch). In contrast, CVD methods can readily be scaled to large lateral dimensions. However, CVD grown films are typically polycrystalline which hinders their use for high end applications like electronic devices. To tackle this dilemma, heteroepitaxy of diamond on foreign single crystals has been explored. The success of this approach was recently documented by the first report of a 3.5 inch size single crystal diamond wafer (s. Fig. 1).

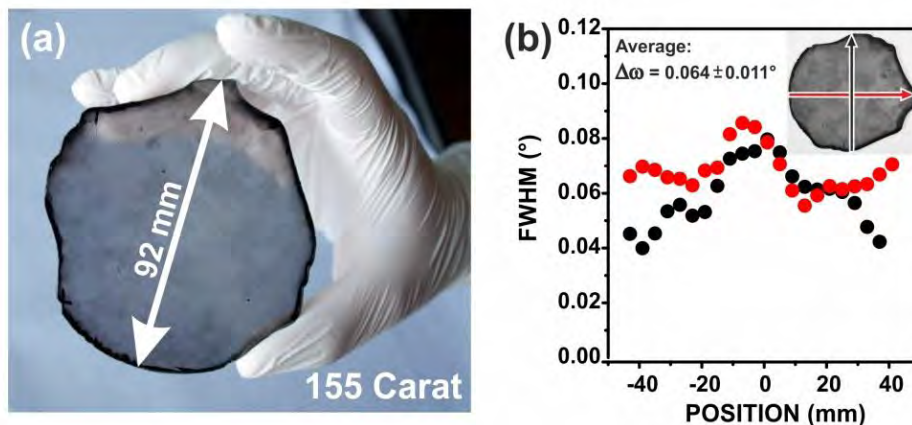


Fig. 1: (a) Free-standing single crystal diamond wafer grown heteroepitaxially on Ir/YSZ/Si(001). (b) Width of rocking curve measured along two perpendicular lines across the wafer. The corresponding average azimuthal width (dia(311) reflection) was $0.12 \pm 0.04^\circ$ and the Raman line width $1.75 \pm 0.07 \text{ cm}^{-1}$ [1].

In this presentation the efforts towards the realization of single crystal diamond in wafer-size will be reviewed. Important milestones, like the selection of iridium as growth surface, the use of the bias enhanced nucleation (BEN) procedure to generate oriented nuclei, the transformation of highly oriented diamond layers into real single crystals, the development of the multilayer substrate Ir/YSZ/Si and its scaling to wafer-size are described. Special attention is paid to threading dislocations, their role in stress formation and strategies to reduce their density. The state of the art in terms of structural quality for (001)- and (111)-oriented layers is presented and the potential for

further improvement is critically discussed. In addition, the model explaining the non-classical diamond nucleation on Ir by the BEN procedure will be briefly outlined [1].

The second part is focused on the material properties relevant for different applications. These comprise

- 1) detectors for high energy particles at accelerator facilities [2]
- 2) Schottky barrier diodes [3]
- 3) monochromators for neutrons [3]
- 4) host material for color centers as single photon emitters and quantum sensors [4]
- 5) UV-VIS and IR optical components
- 6) cutting tools for high precision machining of optical quality surfaces
- 7) scalpels for eye surgery

While some applications are already in a mature stage with first products being available on the market (<http://www.audiatec.de>), for others strong further efforts will be required, e.g. to develop high power electronic devices that can compete with alternative wide bandgap semiconductor materials.

- [1] M. Schreck, S. Gsell, R. Brescia, M. Fischer, "Ion bombardment induced buried lateral growth: the key mechanism for the synthesis of single crystal diamond wafers," *Sci. Rep.* **7**, 44462 (2017).
- [2] C. Stehl, M. Fischer, S. Gsell, E. Berdermann, M.S. Rahman, M. Traeger, O. Klein, M. Schreck, "Efficiency of dislocation density reduction during heteroepitaxial growth of diamond for detector applications," *Appl. Phys. Lett.* **103**, 151905 (2013).
- [3] M. Schreck and J.-C. Arnault "Heteroepitaxy of diamond on Ir/metal-oxide/Si substrates" in S. Koizumi, H. Umezawa, J. Pernot, M. Suzuki (Eds), *Power Electronics Device Applications of Diamond Semiconductors*, A volume in Woodhead Publishing Series in Electronic and Optical Materials, 58 - 80 (Elsevier 2018).
- [4] R. Nelz, J. Görlitz, D. Herrmann, A. Slablab, M. Challier, M. Radtke, M. Fischer, S. Gsell, M. Schreck, S. Becher, E. Neu, "Toward wafer-scale diamond nano and quantum technologies," *APL Mater.* **7**, 011108 (2019).

On mosaicity and the formation of defects during Bridgman processing of Ni-base single crystal superalloys

F. Scholz, P. Hallensleben, J. Frenzel, G. Eggeler

Lehrstuhl Werkstoffwissenschaft, Ruhr-Universität Bochum, Universitätsstr. 150,
44801 Bochum, Germany
E-mail: gunther.eggeler@rub.de

Summary

Ni-base single crystal superalloys (SX) are used to make blades for turbines which operate in aero engines and power plants and have to withstand mechanical loads at temperatures close to the melting point of the complex alloys. The materials are produced following an ingot metallurgy processing route, where melts are directionally solidified using a Bridgman process. Directional solidification is the first step in a processing chain, where specific heat treatments follow to establish the final microstructure. However, the dendritic solidification of the metallic melt is the first process which coins the SX microstructure, Figure 1 [1].

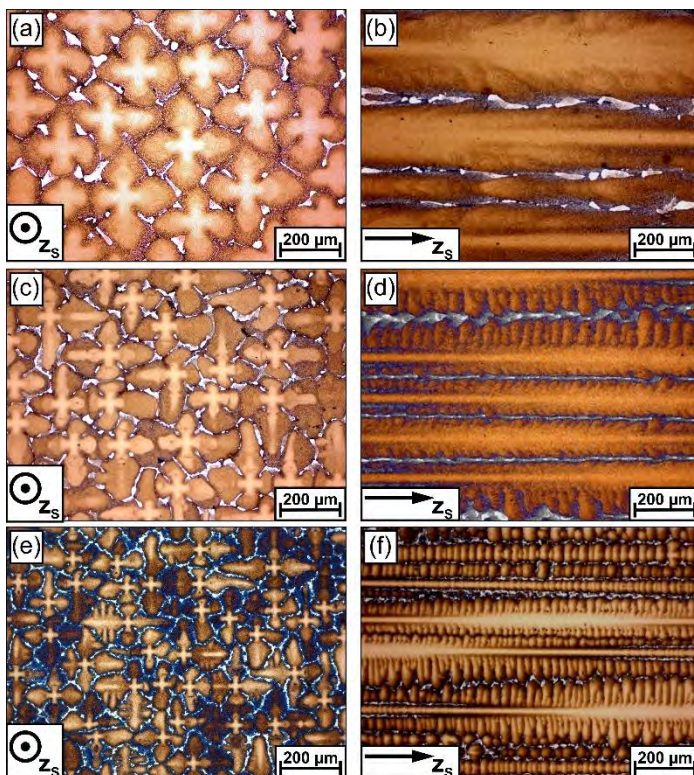


Fig. 1: Dendritic microstructures after Bridgman processing of SX. (a), (c) and (e): Metallographic cross sections perpendicular to the solidification direction. (b), (d) and (f): Longitudinal cross sections. Solidification rates: Top - 45 mm/h; Middle - 180 mm/h; Bottom 720 mm/h.

The Ruhr-University Bochum and the Friedrich-Alexander University Erlangen Nürnberg have joined forces in the collaborative research center SFB/TR 103, which focusses on basic aspects which help to design a new generation of SX. In this context, elementary processes which occur during single crystalline solidification and which lead to the formation of crystal defects require careful attention. With this in mind, a seeded Bridgman process was developed which allows to produce cylindrical crystals of 12 mm diameter and 120 mm. Nucleation and competitive growth of dendrites is

investigated using optical scanning electron microscopy.

In order to characterize misorientations between dendrites, a new orientation imaging SEM technique was developed, which allows to document and quantify crystal mosaicity at a high angular resolution [2]. In the present work we describe our seeded Bridgman procedure. We describe the elementary microstructural processes which we have identified. Finally, we present our new orientation imaging SEM method, which has an angular resolution $< 0.03^\circ$.

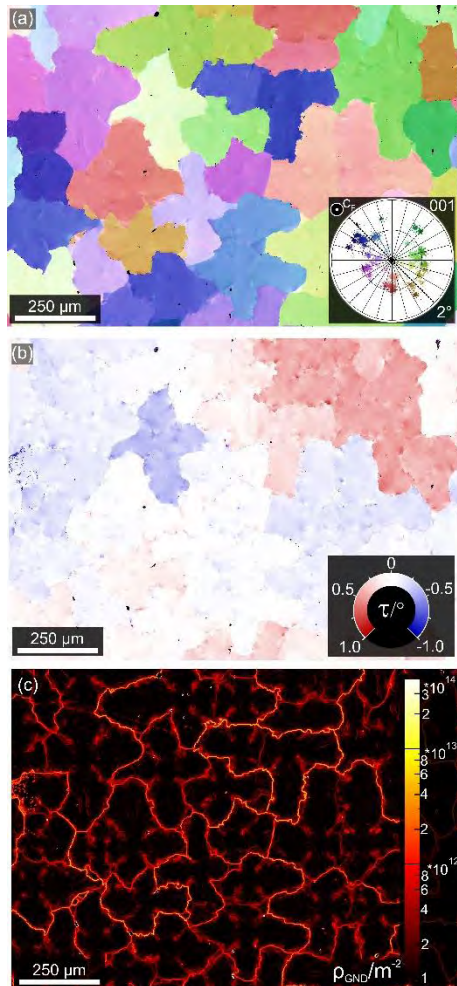


Fig. 2: Results obtained with the new orientation imaging scanning electron microscopy method (the rotation vector base line method, RV-EBSD method) [2]. (a) Out of plane misorientations due to bending processes. (b) Torsional misorientations. (c) Interpretation of misorientations in terms of geometrically necessary dislocations.

The results of the present work are discussed in the light of results which were previously published in the literature. Areas in need of further work are outlined.

Acknowledgement

The authors acknowledge funding through projects A2 and B7 of the collaborative research center SFB/Tr 103 funded by the German research association DFG

[1] P. Hallensleben, H. Schaar, P. Thome, N. Jons, A. Jafarizadeh, I. Steinbach, G. Eggeler, J. Frenzel, On the evolution of cast microstructure during processing of single crystal Ni-base superalloys using a Bridgman seed technique, *Materials & Design*, 128 (2017) pp. 98-111

[2] P. Hallensleben, F. Scholz, P. Thome, H. Schaar, I. Steinbach, G. Eggeler, J. Frenzel, On crystal mosaicity in single crystal Ni-base superalloys, 2019, *Crystals*, 9 (2019), article number: 149

Modeling crystal growth and materials design in high dimensional chemical and structural configuration spaces

Liverios Lymperakis^a, Jan Janssen^a, Liam Huber^a, Tilmann Hickel^a, and Jörg Neugebauer^a

^a *Max-Planck-Institut für Eisenforschung, Max-Planck-Str. 1, 40237 Düsseldorf, Germany*

E-mail: neugebauer@mpie.de

Modern engineering materials have evolved from chemically and structurally simple alloys with well-established design rules to chemically, thermodynamically and structurally highly complex materials. This complexity presents a severe challenge to designing this new generation of materials, since experimental trial-and-error approaches, as successfully used in the past, are often no longer feasible. Ab initio approaches with their inherent predictive accuracy provide perfect tools to explore and identify design strategies, but face serious challenges to efficiently handle the vast high-dimensional configuration spaces resulting from this complexity. To address this challenge, we have developed a python based framework called pyiron that combines (i) rapid prototyping of the complex simulation protocols as needed to achieve computational efficiency and accuracy, (ii) a seamless integration to big data analytics and machine learning tools, as well as (iii) a simple upscaling from interactive prototyping to high-throughput calculations on supercomputer frameworks. The flexibility and the predictive power of this approach will be discussed for examples covering various aspects of crystal growth and materials design.

SIGNIFICANCE OF OPTICAL CRYSTALS FOR THE LASER INDUSTRY

A. Killi^a

^a *TRUMPF Laser GmbH, Aichhalder Straße 39,
78713 Schramberg, Germany
E-mail: alexander.killi@trumpf.com*

Summary

TRUMPF Laser is a leading manufacturer of high-power laser systems for industrial applications. The product portfolio of solid-state lasers ranges from high power CW lasers used for welding and cutting applications, to pulsed lasers used in micro machining applications [1].

In this presentation the significance of high-quality optical crystals is shown for a variety of use cases in industrial high-power laser systems.

The first presented use-case is the optical isolator, which is a system critical component for high power pulsed laser systems such as short pulsed and ultrafast lasers [2].

The second use-case is the electro-optical modulator that can be deployed in cavity dumped resonators and regenerative amplifiers. TRUMPF offers a range of kW-class ns lasers based on the principle of cavity dumping [3]. On the other hand, the well-established product line TruMicro 5000 uses regenerative amplification and in our case an electrooptical modulator [4]. On the very high-performance range of regenerative amplifiers TRUMPF offers the “Dira”, a high energy (100s of mJ) high power (up to kW range) ultrafast laser that can be used for various scientific applications such as a drive laser for OPCPA [5, 6].

The third use-case is the conversion of infrared laser radiation into the visible spectral range and ultraviolet regime using nonlinear optical crystals. Many industrial micromachining processes are unthinkable without frequency conversion of CW, short pulse and ultrafast lasers. A prominent example is the lift-off of flexible displays from their mother glass [7], another one the welding of copper using a green CW laser [8].

Acknowledgment

The author thanks the EU and the BMBF for various grants that enabled research projects in the forefront of product development.

- [1]https://www.trumpf.com/en_INT/products/lasers/
- [2]https://www.trumpf.com/en_INT/products/lasers/short-and-ultrashort-pulse-laser/
- [3]https://www.trumpf.com/en_INT/products/lasers/short-and-ultrashort-pulse-laser/trumicro-series-7000/
- [4]https://www.trumpf.com/en_INT/products/lasers/short-and-ultrashort-pulse-laser/trumicro-series-5000/
- [5]<https://www.trumpf-scientific-lasers.com/products/dira-series/>
- [6]Proceedings Volume 11034, Short-pulse High-energy Lasers and Ultrafast Optical Technologies; 110340N (2019) <https://doi.org/10.1117/12.2525028>
- [7]https://www.trumpf.com/en_INT/products/lasers/short-and-ultrashort-pulse-laser/trumicro-series-8000/
- [8]https://www.trumpf.com/en_INT/products/lasers/disk-lasers/trudisk-with-green-wavelength/

Collaboration of experiment and numerical analysis of crystal growth of semiconductors

K. kakimoto

*Research Institute for Applied Mechanics, Kyushu University, 6-1, Kasuga-koen, Kasuga,
816-8580 Fukuoka, JAPAN
kakimoto@riam.kyushu-u.ac.jp*

Summary

Silicon (Si) and wide bandgap crystals are one of the main materials for solar cells, power devices and/or large scale integrated circuits. For the present power devices, Si crystals grown by the floating zone method are used so far [1]. To satisfy the demand for solar cells and electric vehicles in society, a huge amount of cells and electric power equipment is required; thus, driving demand for Si crystals used in power devices. To satisfy the large demand, it is necessary to grow Si crystals by the Czochralski (CZ) method, and it is particularly essential to concentrate on the carrier's long lifetime in the crystal. Several papers have reported the increased lifetime, and it has been reported that the lifetime of the Si crystals grown by the CZ process is affected by oxygen and/or carbon-related defects [2, 3].

Many papers have reported the carbon impurity in crystals and the formation of oxygen-related defects, such as oxygen precipitates, thermal donors, and new thermal donors [4, 5]. Several papers have also reported that the concentration of carbon in the crystals depends on the process parameters, such as total pressure and flow rate of argon (Ar) gas in a furnace [3, 6]. However, no research has been conducted to measure the level of carbon monoxide (CO) during the Si crystal growth.

We focused on in-situ measurement of CO gas concentration after the melting process of raw materials in the CZ growth method to qualitatively understand the CO contamination mechanism into the Si melt in this paper. We succeeded in to measure the CO concentration in the furnace after the melting process, which is the most crucial process in which CO gas could contaminate the Si melt [6, 7]. The contamination process was then observed and discussed using a simple mass transfer model. Although the results obtained by numerical simulation were reported [8-10] the experimental results have not been reported quantitatively.

We carried out in-situ measurements of CO concentration in a CZ furnace using a gas chromatographic method. Two sampling monitors were set up above the Si melt and the Ar gas exhaust, respectively. The gas samples were collected into the tubes at the two sampling monitors, then introduced to an analyzer made by GL Science. The sampling interval was set at 660 seconds. The melt was made with 25 kg of commercially available polycrystalline silicon in a quartz crucible 45.7 cm in diameter. CO was mainly generated by a heater which caused a chemical reaction at high temperature. In this case, we measured the concentration after melting process without growing crystal.

Figure 1 shows the total pressure dependence of CO concentrations in the furnace measured. The cross indicates the values obtained from the experiment without the Si melt and the quartz crucible. The CO concentration linearly increased as the total pressure in the furnace increased. The value was well above one order of magnitude smaller than that with the Si melt and the crucible. The two measurements linearly increased with one order of magnitude difference. Both values of measured CO concentration proportionally increased with the total pressure in the furnace.

The average velocity of Ar gas decreased as a function of the total pressure based on the ideal gas law. Therefore, as the gas velocity in the furnace declined, back diffusion of CO was enhanced. Consequently, the CO concentration increased as a function of the total pressure in the furnace. As

CO flowed from the heater to the exhaust, the CO concentration at position A near the exhaust increased.

Figure 2 shows the measured CO concentrations as a function of the total flow rate of Ar gas in the furnace. As the total flow rate of Ar gas increased, the CO concentration decreased. The significant decrease in CO concentration as a function of gas flow rate was due to the higher Péclet number (the ratio between the convective and the diffusive mass transfer of Ar gas flow).

The increase in gas flow could also remove more SiO from the system, which was the reactant of the CO generation. Such decrease in CO contamination was attributed to the increase of flow velocity as well as the effective removal of SiO from the chemically reactive area in the furnace.

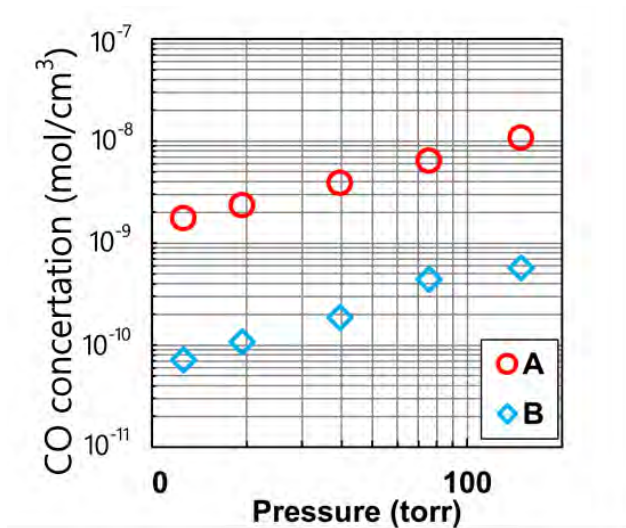


Fig. 1: Measured CO concentration as a function of Ar gas pressure in the furnace.

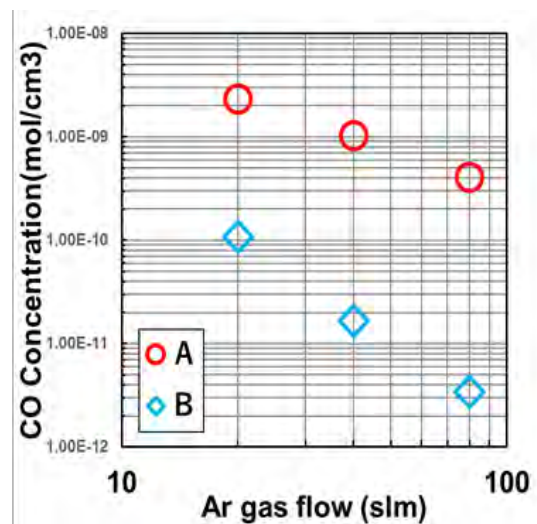


Fig. 2 Measured CO concentration as a function of Ar gas flow rate.

Acknowledgment

This work was partly supported by the New Energy and Industrial Technology Development Organization under the Ministry of Economy, Trade and Industry (METI).

- [1] G. Eranna, Crystal Growth and Evaluation of Silicon for VLSI and ULSI, CRC Press, New York, 2014.
- [2] B.O. Kolbesen, A. Mühlbauer, Carbon in silicon: Properties and impact on devices, Solid-State Electronics, 25 (1982), 759.
- [3] Y. Nagai, S. Nakagawa, K. Kashima, Crystal growth of MCZ silicon with ultralow carbon concentration, Journal of Crystal Growth, **401** (2014), 737.
- [4] S. Kishino, M. Kanamori, N. Yoshida, M. Tajima, I. Iizuka, J. Appl. Phys., **50** (1979) 8240.
- [5] T. Nozaki, Y. Yatsurugi, N. Akiyama, J. Electrochem. Soc. **117** (1970) 1566.
- [6] L. Raabe, O. Paetzold, I. Kupka, J. Ehrig, S. Wurzer, M. Stelter, J. Crystal Growth, **318** (2011) 234.
- [7] R. Series and K. G. Barraclough, J. Crystal Growth, **63** (1983) 219.
- [8] L. Xin, Hirofumi Harada, Yoshiji Miyamura, Xue-feng Han, Satoshi Nakano, Shin-ichi Nishizawa, Koichi Kakimoto, J. Crystal Growth, **499** (2018) 8.
- [9] Xin Liu, Bing Gao, Koichi Kakimoto, J. Crystal Growth, **417** (2015) 58.
- [10] G. Müller, A. Mühe, R. Backofen, E. Tomzig, W. v. Ammon, J. Crystal Growth, **45** (1999) 135.

High-purity single-crystals for astroparticle physics research

S. Schönert^a

^a (Ex) Physik-Department E15, Technische Universität München, James-Frank-Str. 1, 85748 Garching
85748 Garching, Germany
E-mail: schoenert@ph.tum.de

Summary

The dynamics of galaxies, larger structures, and the overall expansion and structure formation in the universe require about six times more gravitating mass than can be ascribed to ordinary matter. As this type of matter is invisible, it is called dark matter (DM). It probably consists of a hitherto undetected type of weakly interacting elementary particle and is searched for in many experiments around the globe. DM particles with masses from sub-GeV to the TeV would occasionally hit nuclei in the laboratory and the small recoil energies in the tens-of-keV range can be identified in direct detection experiments using high-purity single crystals. High-purity CaWO₄ crystals are operated in the CRESST dark matter experiment [1] at a few tens of mK temperature, where it serves as target material for the interaction with dark matter particles. Energy thresholds below 100 eV for nuclear recoils have been achieved and the average background rate measured with CaWO₄ crystals grown at TUM [2] corresponds to about 3.51 kg⁻¹ keV⁻¹ d⁻¹ in the energy region between 1-40 keV [3], which is significantly lower compared to crystals of the same material with different origin.

High-purity crystals are also employed to address another fundamental question in particle physics, astrophysics and cosmology, namely why matter is so much more abundant than anti-matter in today's Universe. The question might be closely related to the observation that neutrino masses are more than five orders of magnitude smaller than that of the electron. This raises the question whether the origin of neutrino masses differs from that of the other elementary fermions. The leading models on neutrino masses, rooted in unified field theories, predict that neutrinos are their own antiparticles, usually referred to as Majorana neutrinos. Given that they do not carry electrical charge, neutrinos are the only known elementary fermions where the strict distinction between particle and antiparticle could be void. Majorana neutrinos would not only explain naturally the lightness of neutrinos, but would also shed light on the mechanism why matter is so much more abundant than anti-matter in today's Universe. Majorana neutrinos lead to a nuclear decay which violates lepton number conservation and is therefore forbidden in the standard model of particle physics. The so called neutrinoless double beta decay transforms in a nucleus with mass number A and atomic number Z, two neutrons simultaneously into two protons, under the emission of two electrons, 2e⁻, but without the emission of two electron anti-neutrinos. The two electrons carry the available decay energy and the resulting mono-energetic signal is the prime experimental signature. A positive detection would manifest the first observation of a matter-creating process, without the balancing emission of antimatter. The GERDA experiment at the Gran Sasso underground laboratory is operating background-free [4] high-purity germanium single crystals, enriched in the isotope ⁷⁶Ge. A world leading median sensitivity of the half-life of $T_{1/2} > 1.1 \cdot 10^{26}$ yr (90% C.L.) has been reached recently [5].

This presentation will discuss the science motivations, the state-of-the-art and the future the needs for high-purity crystals in astroparticle physics experiments of the current and next generation.

Acknowledgment

This work is supported in part by the SFB1258, by the Cluster of Excellence “Origins” and the BMBF Verbundforschung Astroteilchenphysik.

Acknowledgment

- [1] CRESST Collaboration, Phys.Rev.D 100 (2019) 10, 102002
- [2] A. Erb and J.-C. Lanfranchi, CrystEngComm, 2013, 15, 2301
- [3] CRESST Collaboration, Eur. Phys. J. C (2014) 74
- [4] GERDA collaboration Nature 544 (2017) 47
- [5] GERDA collaboration, Science 365, 1445 (2019);

Contributed Talks

Session 1
Wednesday 11.03.2020
10:10 - 12:10

Thermochemical heat storage using alcohol solvates

D.J. Kok, H. Meekes & E. Vlieg

Solid State Chemistry, Radboud University, Heyendaalseweg 135, 6525 AJ Nijmegen,
The Netherlands

E-mail: dirkkok@science.ru.nl

Summary

Renewable energy sources tend to be inflexible: energy is either currently available or not. With the continuing drive towards a larger fraction of renewables in our power mix, the need for energy storage capacity is rising. Since an average household in Europe consumes about 70% of its energy in the form of heat for hot water and space heating [1], storing heat is an attractive option.

Currently, there are three ways of storing heat:

- Sensible heat storage: storing a warm substance
- Latent heat storage: storing heat in a phase transition
- Thermochemical heat storage: storing heat in a reversible chemical reaction, often hydrate or solvate formation

Thermochemical heat storage has several advantages: it has a very high energy density, and the dehydrated compound can be stored indefinitely, whereas sensible heat will always leak away. In addition, latent heat is difficult to partially release while a rehydration reaction stops when the solvent vapor flow ceases.

The general principle of seasonal thermochemical heat storage is shown in fig. 1. The discharged reactor, containing the host-solvent complex, is heated using a solar thermal collector. The solvent is stored, and in winter, the solvent vapor is allowed to flow back to the dry host, exothermically forming the complex again.

Good candidate materials need to have a high energy density ($\approx 1 \text{ GJ/m}^3$ or more), release the solvent at a useful temperature (roughly between 70 and 130 °C for domestic applications) and not have any side reactions with the solvent or the reactor. Also, the material should not be highly toxic or too expensive.

Most research into these systems has focused on hydrates (see for example [2]), but the vapor pressure of water is inconveniently low. At 10°C, it is 12 mBar while ethanol has a vapor pressure of 29 mBar and methanol has a vapor pressure of 68 mBar. This makes alcoholate complexes interesting candidates for heat storage systems.

Since alcoholate complexes are not nearly as well studied as hydrates, current work is focusing on determining the energy density and cycle stability of different materials. First, it must be determined whether there is an exothermic solvate formation or not and whether the complex also forms from gaseous solvent or only in solution. The latter is done in a thermogravimetric analysis (TGA) setup with an alcohol bubbler attached. This setup is also used to test how many cycles the compound will last. Alcoholate crystals are grown from solution to determine or confirm their structures. These crystals are then also investigated with differential scanning calorimetry (DSC) and TGA to determine their energy density. Some example curves for $\text{CaBr}_2 \cdot 6\text{MeOH}$ are shown in fig. 2. It took between 463 and 544 J/g to remove the methanol from the crystals, which gives an energy density of 0.72-0.85 GJ/m^3 .

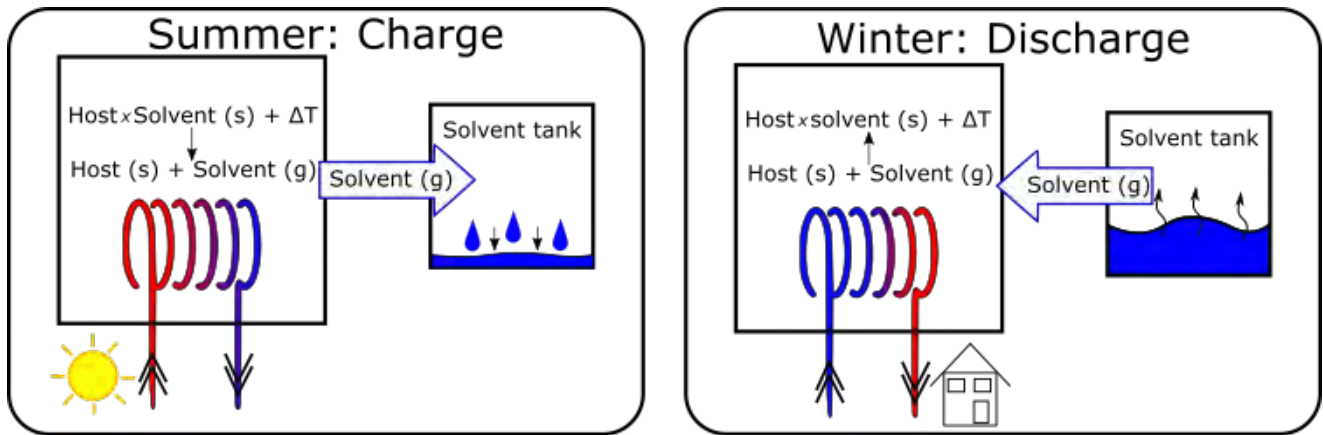


Fig. 1: General principle of seasonal heat storage based on a thermochemical system.

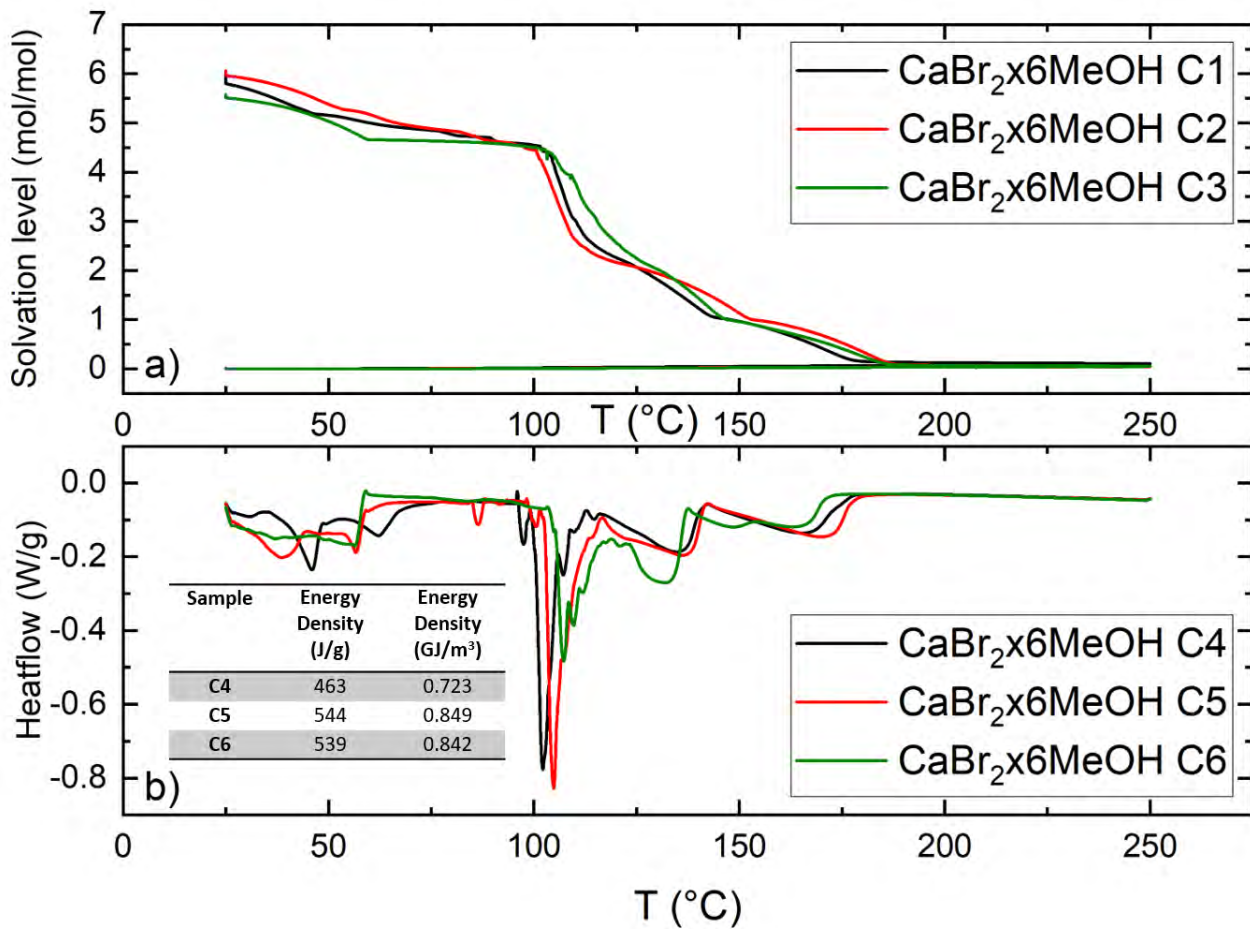


Fig. 2: Thermal analysis results for $\text{CaBr}_2 \times 6\text{MeOH}$. a) Solvation level calculated from TGA measurements b) DSC heating curves.

Acknowledgment

We kindly acknowledge funding by Topsector Energie under project number TEUE117062 (SWeKOS).

[1] F. Belaïd, Energy Policy, **92**, 220-233 (2016)

[2] P.A.J. Donkers, L.C. Sögütögl, H.P. Huinink, H.R. Fischer, O.C.G. Adan, Applied Energy, **199**, 45-68 (2017)

VGF-Growth of Half-Heusler-material for industrial production of Thermoelectric-material

M. Germann^{a*}, D. Zuckermann^a, A. Fey^a, S. Herbert^a, C. Klingelhöfer^a, V. Macin^a, D. Eirich^a

^a Isabellenhütte Heusler GmbH & Co KG, Eibacher Weg 3-5, 35683 Dillenburg, Germany

* Corresponding Author: mathias.germann@isabellenhuetten.de

The industrialization and automation of material and module manufacturing technologies is one of the important topics to reduce the costs of thermoelectric technology. The company Isabellenhütte Heusler GmbH & Co. KG (ISA) is engaged in the industrialization of the thermoelectric (TE) technology based on Half-Heusler-materials (HH).

The ISA has a long tradition in Heusler-compound research. The great grandfather of the actual CEO Dr. Felix Heusler was Dr. Fritz Heusler. Dr. Fritz Heusler developed the first Heusler alloy in 1901 at the Isabellenhütte. Unfortunately there was no economic use for this kind of compounds for the company until today.

Since 2009 the Isabellenhütte is actively involved in Heusler alloy research again. The purpose of the project activities is the development of a melt metallurgical manufacturing process for an appropriate HH-material, which can be industrialized. A second objective in this context is the development of thermoelectric modules using the developed Half-Heusler-material.

In 2017 the Isabellenhütte built up an industrial pilot line production, which starts with the raw material and ends up with thermoelectric modules. The ambition is to demonstrate an industrial scale material manufacturing and an automated assembling process of HH-TE-modules in a constant high quality.



Figure 1 – L: VGF-furnace with a 10kg and the 25kg ingot. R: Pilot line process.

A key feature for the industrial scale material manufacturing is the mass production of the raw material. Following the silicon mass production, for solar cells, etc., the VGF-method got judged as a promising process for the preparation of the HH-materials in an industrial scale. We succeeded to grow 10kg ingots of HH-material with the VGF-method. Both classes of HH-materials, p- and n-type, were grown with a reproducible quality. Additionally the process was used to grow ingots up to 25kg (see Fig. 1).

Due to the industrialization of the thermoelectric module manufacturing, Isabellenhütte developed a two-step module design concept (see Fig. 2). The first step is the production of an unicouple. The second step is the mounting of many unicouples on the surface of a special cold side substrate without the classical massive ceramic sheet. In this way it is possible to produce different module geometries with one type of unicouple. Additionally it's possible to process different materials.

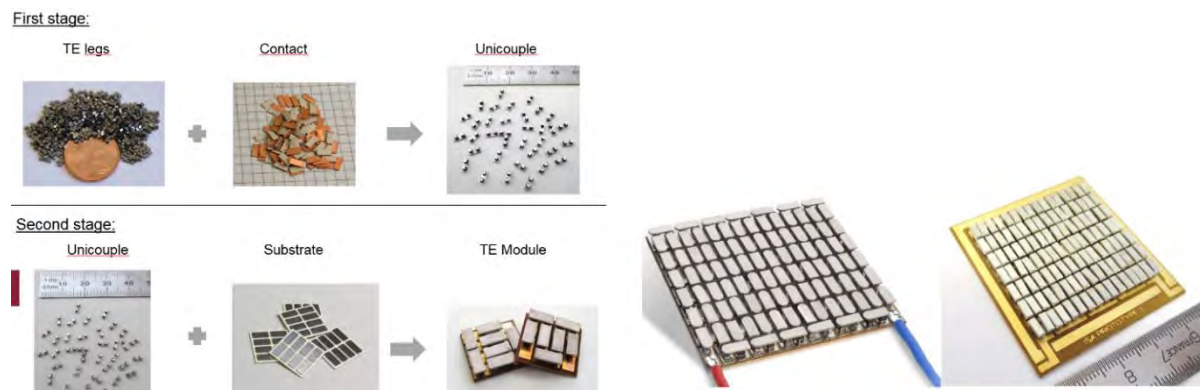


Figure 2 – 2 step manufacturing and prototype modules from an industrial like production.

The raw material for the unicouples are legs cut from the VGF-grown ingots. The VGF-ingot is getting cut with a band saw into a cuboid. Then wafers are cut from the cuboid with an inner diameter saw. The legs for the unicouple are fabricated with a blade saw. Finally one p-type and one n-type leg are getting assembled on top of a hot side contact to a unicouple.

For the second step IH built up an automated production line for a standard type of thermoelectric modules to investigate an industrial manufacturing. The line has a theoretical production capacity of 5.8 million unicouples p.a.. This amount of unicouples is enough to equip 50.000 modules with a size of 40mm by 40mm. Isabellenhütte developed a first standard module with 40 x 40 mm² for qualification testing and customer sampling (figure 3.).

3D interlayer growth in the high temperature vapor phase epitaxy of GaN

T. Schneider^a, M. Förste^a, P. Fischer^b, C. Röder^c, E. Niederschlag^a, O. Pätzold^a, D. Rafaja^b, M. Stelter^a

^a Institute of Nonferrous Metallurgy and Purest Materials, TU Bergakademie Freiberg, Leipziger Straße 34, 09599 Freiberg, Germany

^b Institute of Materials Science, TU Bergakademie Freiberg, Gustav-Zeuner-Straße 5, 09599 Freiberg, Germany

^c Institute of Applied Physics, TU Bergakademie Freiberg, Leipziger Straße 23, 09599 Freiberg, Germany

E-mail: Tom.Schneider@inemet.tu-freiberg.de

Summary

The growth of GaN by high temperature vapor phase epitaxy (HTVPE) is based on the physical vapor transport of gallium. Thermally evaporated gallium is transported to a substrate, where it reacts with ammonia to form a GaN layer according to $2\text{Ga} + 2\text{NH}_3 \rightarrow 2\text{GaN} + 3\text{H}_2$. This method has attracted interest, because aggressive or toxic substances are widely avoided and high growth rates can be reached. In the last years, advanced HTVPE techniques with improved process control and stability were developed [1–6]. The potential of the method for the deposition of GaN seed layers on sapphire substrates [1-4] and for the deposition of GaN bulk layers with a growth rate of up to 200 $\mu\text{m}/\text{h}$ [5,6] was demonstrated.

This contribution addresses recent progress in the growth of GaN layers by HTVPE. A novel multi-step process aimed at the in-situ deposition of 3D interlayers to control the dislocation density and the stress level is described. A series of GaN samples deposited on 15 x 15mm² sapphire substrates under different growth conditions is presented. The results of SEM, XRD and Raman measurements are shown and the influence of a 3D interlayer on the dislocation density and the residual stress is discussed.

Fig. 1a shows the HTVPE reactor used for the experiments. The main components are made of refractory metals, glassy carbon, pyrolytical boron nitride and fused silica. The reactor provides a flexible setting of the process parameters in wide ranges [3,4]:

- Separate control of the substrate temperature T_S and the temperature of the Ga melt T_{Ga} in the ranges of 500 – 1350°C and 1100 – 1350°C, respectively.
- Variation of the reactor pressure from 20 to 1000 mbar.
- Control of the growth rate between 0.1 – 160 $\mu\text{m}/\text{h}$.

A scheme of the presented GaN samples is shown in Fig. 1b. Starting from a sapphire substrate, the samples are formed by a seed layer – 3D interlayer – top layer sequence. The process steps used for the deposition of the seed layers can be summarized as follows [3,4]:

- Deposition of a nucleation layer with a thickness of about 20 nm at a reactor pressure of 985 mbar, a substrate temperature of 500°C and with a typical growth rate of 240 nm/h.
- Recrystallization of the nucleation layer at the substrate temperature of 1080°C under an ammonia and hydrogen containing atmosphere.
- High-temperature (HT) growth to form a coalesced GaN seed layer with a thickness of about 2 – 5 μm at a reactor pressure of 985 mbar and a substrate temperature of 1100°C with a growth rate of about 2.5 $\mu\text{m}/\text{h}$.

The interlayers were deposited at a reactor pressure of 55 mbar under different substrate temperatures (900°C, 950°C, 1000°C) and Ga melt temperatures (1300°C, 1320°C, 1340°C) with growth rates in the range of 27 – 57 $\mu\text{m}/\text{h}$. Under these conditions, 3D growth dominates leading to a

preferred formation of voids and pyramidal facets (see Fig. 1c). In the final process step, the interlayers were coalesced within 90 min at a reactor pressure of 985 mbar, a substrate temperature of 1100°C and a Ga melt temperature of 1300°C to form a 2D top layer (see Fig. 1d). First XRD and Raman investigations of the samples indicate that a 3D interlayer mainly influences the residual compressive stress, whereas the dislocation density remains essentially unchanged in comparison with a reference sample without interlayer.

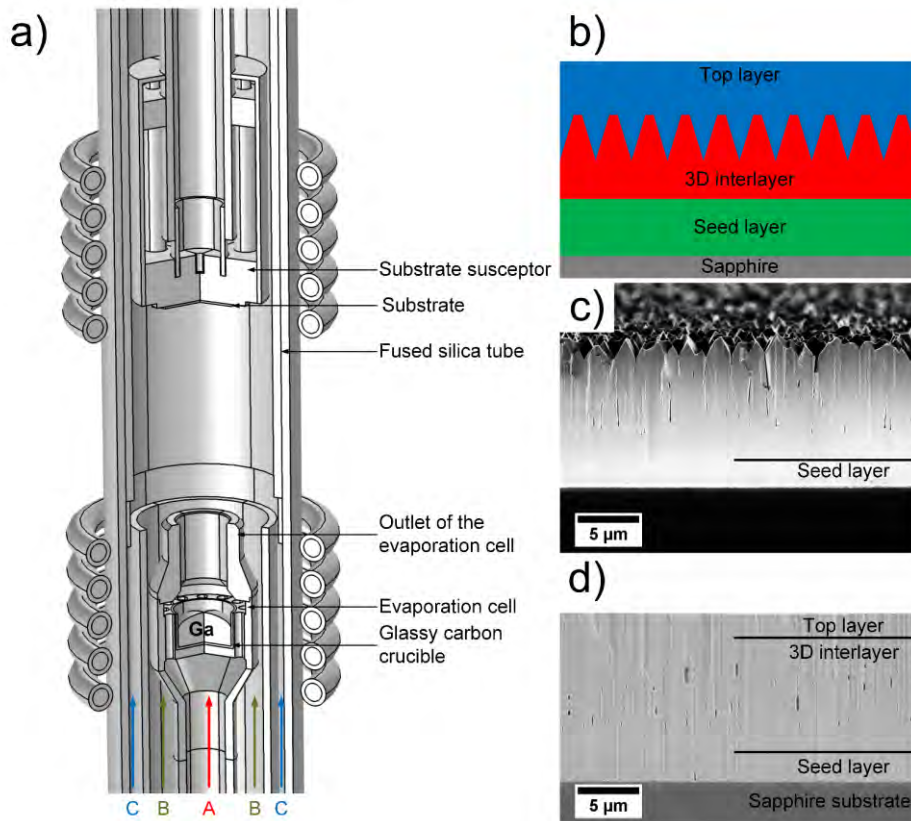


Fig. 1: a) Scheme of the HTVPE reactor. A, B, and C indicate different gas flows: A – Ga transport flow (Ar, H₂), B – separation flow (N₂), C – NH₃ transport flow (H₂, N₂). b) Cross-section scheme of the layer sequence of the presented GaN samples. c)/d) Cross-section SEM images of an interlayer-terminated/a complete GaN sample with a coalesced top layer.

Acknowledgment

The financial support by the German Research Foundation (projects PA 1236/3 and RA 1050/28) is gratefully acknowledged.

- [1] G. Lukin, C. Röder, M. Barchuk, G. Schreiber, O. Pätzold, J. Kortus, D. Rafaja, M. Stelter, *Physica Status Solidi C*, **11**, 491-494 (2014)
- [2] G. Lukin, T. Schneider, M. Barchuk, F. Zimmermann, E. Niederschlag, O. Pätzold, M. Stelter, *Physica Status Solidi A*, **214**, 1600753 (2017)
- [3] G. Lukin, T. Schneider, M. Förste, M. Barchuk, C. Schimpf, C. Röder, F. Zimmermann, E. Niederschlag, O. Pätzold, F. C. Beyer, D. Rafaja, M. Stelter, *Journal of Crystal Growth*, **524**, 125185 (2019)
- [4] T. Schneider, M. Förste, G. Lukin, P. Fischer, M. Barchuk, C. Schimpf, E. Niederschlag, O. Pätzold, D. Rafaja, M. Stelter, *Journal of Crystal Growth*, **533**, 125465 (2020)
- [5] D. Nakamura, T. Kimura, *Applied Physics Express*, **10**, 95503 (2017)
- [6] D. Nakamura, T. Kimura, K. Horibuchi, *Applied Physics Express*, **10**, 45504 (2017)

Growth of ^{28}Si crystals for preparation of Si spheres

N.V. Abrosimov, H. Riemann, H.-J. Rost, L. Lehmann, M. Renner, S. Weiß, R. Menzel

Leibniz-Institut für Kristallzüchtung (IKZ), Max-Born-Straße 2, 12489 Berlin, Germany
nikolay.abrosimov@ikz-berlin.de

Summary The manufacturing chain of ^{28}Si crystals from the enrichment procedure up to the growth of the final 4 inch crystals by the Floating Zone (FZ) technique is described systematically. As a result, six ^{28}Si dislocation free single crystals of 100 mm in diameter were grown in the frame of “Avogadro”, “Kg-2” and “Kg-3” projects for preparation of Si spheres used for a more precise determination of the Avogadro constant, which has been crucial for the new definition of the mass unit - kilogram.

On the 16th of November 2018, the General Conference on Weights and Measures in Paris passed a new definition of the kilogram, which has been successfully entered into force on the 20th of May 2019. There are seven fundamental units: meter, second, kilogram, ampere, candela, kelvin, and mole which are organized in the International System of Units (SI). The main idea of metrology in the last decade was to define these units in terms of fundamental natural constants and one of them is the Avogadro constant N_A - the number of atoms contained in a certain quantity of a substance, i.e. in one mole. N_A is used then for determining of the Planck constant as the basis for the new definition of the kilogram standard that was the last unit based on an artefact - the so-called prototype kilogram (Urkilogramm) in Sevre near Paris.

The IKZ was involved in several projects, such as “Avogadro”, “Kg-2” and “Kg-3” under the initiative and management of the Physikalisch Technische Bundesanstalt (PTB; the German National Metrology Institute) aiming at a more precise determination of the Avogadro constant. It was done by counting the atoms in ^{28}Si silicon spheres prepared by PTB with less than 20 nm shape deviation at a diameter of approximately 93.6 mm and with a surface polished free of defects. These spheres were used for measurements to establish a connection between the volume and the number of atoms in the highly ordered crystalline structure. To make Si spheres one needs to grow perfect Si crystals of about 100 mm in diameter. Six ^{28}Si dislocation free single crystals of 100 mm in diameter were grown by FZ technique over the last 12 years (Fig.1).

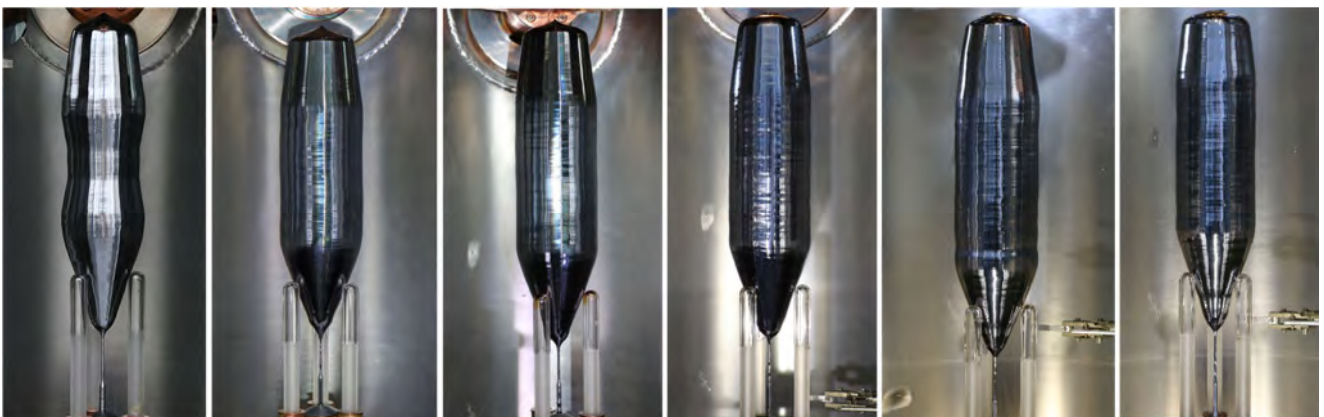


Fig. 1: ^{28}Si dislocation free single crystals of 100 mm in diameter grown by FZ technique in the frame of “Avogadro”, “Kg-2” and “Kg-3” projects

Manufacturing chain of the ^{28}Si highly enriched crystals includes five main steps (Fig. 2). A big challenge relating to the production of highly enriched ^{28}Si is saving the isotopic enrichment of the starting material during all technological steps and improving the high chemical purity at the same time.

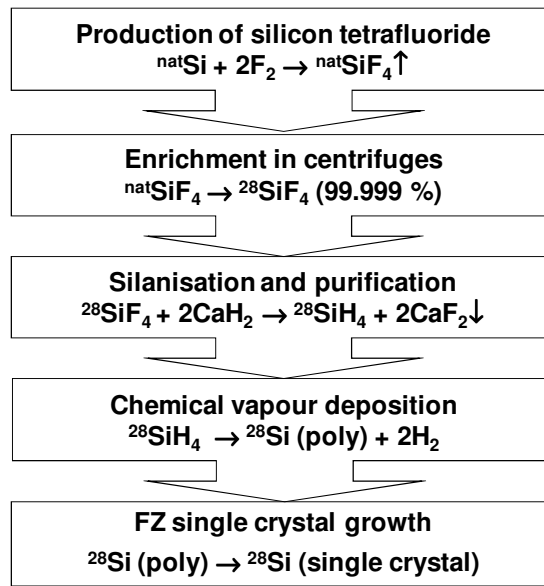


Fig. 2. Main technological steps of the ^{28}Si crystal production [1].

Crystal growth techniques such as FZ, pedestal and Czochralski (CZ) are used for the single crystal growth and recycling of ^{28}Si residues after different steps of the manufacturing chain (Fig. 2) and material characterization. To improve the chemical purity of the starting polycrystalline material several FZ runs, partly in vacuum in order to remove oxygen, were carried out. For the CZ growth, the quartz crucible was coated with ${}^{28}\text{SiO}_2$ to avoid the introduction of other Si isotopes by erosion of the inner crucible surface in contact with molten ^{28}Si . As a result, dislocation free ^{28}Si single crystals of about 4" diameter with an enrichment of up to 99.9995 at% and weights of about 5.5 kg could be grown using the FZ technique.

FZ grown ^{28}Si crystals were also used for the investigation of the basic properties of the novel material. In natural Si the stable isotopes ^{28}Si , ^{29}Si , ^{30}Si , mixed in the crystal lattice, influencing the average molar mass, changing the whole phonon spectrum and causing inhomogeneous line broadening. For instance, the thermal conductivity of a ^{28}Si crystal enhances according to the enrichment level from $45.5 \text{ Wcm}^{-1}\text{K}^{-1}$ to ca. $450 \text{ Wcm}^{-1}\text{K}^{-1}$ at 24K in a crystal of ^{28}Si (99.995 %) being the highest ever measured value for thermal conductivity of dielectrics at any temperature [2]. The absence of the ^{29}Si nuclear magnetic dipoles enables a spin-free "semiconductor vacuum" making them very promising for quantum information technologies and for the development of Si-based quantum computer [3].

- [1] N.V. Abrosimov, D.G. Aref'ev, P. Becker, H. Bettin, A.D. Bulanov, M.F. Churbanov, S.V. Filimonov, V.A. Gavva, O.N. Godisov, A.V. Gusev, T.V. Kotereva, D. Nietzold, M. Peters, A.M. Potapov, H.-J. Pohl, A. Pramann, H. Riemann, P.-T. Scheel, R. Stosch, S. Wundrack, S. Zakel, *Metrologia* **54**, 599 (2017).
- [2] A.V. Inyushkin, A.N. Taldenkov, J.W. Ager III, E.E. Haller, H. Riemann, N.V. Abrosimov, H.-J. Pohl, P. Becker, *JApplPhys* **123**, 095112 (2018).
- [3] M. Steger, K. Saeedi, M.L.W. Thewalt, J.J.L. Morton, H. Riemann, N.V. Abrosimov, P. Becker, H.-J. Pohl, *Science* **336**, 1280 (2012).

Session 2
Wednesday 11.03.2020
13:20 – 15:00

X-Ray Diffraction Analysis of the Defect Structure of Diamond Substrates and Thick Diamond Films

L. Kirste, J. Engels, T. Fuchs, P. Knittel, J. Langer, M. Prescher, P. Reinke, J. Weippert,
V. Cimalla, & V. Lebedev

*Fraunhofer Institut für Angewandte Festkörperphysik (IAF),
Tullastraße 72, 79108 Freiburg, Germany
E-mail: lutz.kirste@iaf.fraunhofer.de*

Diamond is a wide band-gap semiconductor with a number of extraordinary physical properties promising for emerging devices such as power transistors, high frequency electro-acoustic filters, integrated photonic circuits and quantum-effect sensors.

Defect density and substrate size are still bottlenecks for the development of reliable and cost-effective diamond based devices. In the past years, a number of approaches have been developed to produce larger substrates, as well as substrates with relatively low defect density. Using a bulk crystal growth technique like the high-pressure high-temperature method (HPHT) for diamond, dislocation densities below $5 \times 10^3 \text{ cm}^{-2}$ were demonstrated. However, for the diamond HPHT crystal growth process, the resulting levels of impurities are typically high and additional wafer diameters are still small and the yield of devices is therefore low. On the other side, for larger substrates and low impurity levels, concepts based on heteroepitaxy are used, e.g. chemical vapor deposition (CVD) of diamond on Ir/YSZ/Si (001) template. The drawback of these heteroepitaxial method is that the density of dislocation is typically high (e.g. $\approx 10^8 - 10^{10} \text{ cm}^{-2}$). Since a low content of crystal defects is a critical requirement for the realization of demanding diamond-based devices with high efficiency, performance and lifetime, it is necessary to determine the types of defects and their density in the substrate crystals.

In this work we will present a detailed analysis of the defect structure of freestanding diamond substrates grown by HPHT and CVD and thick ($> 10 \mu\text{m}$) diamond layers grown by CVD. Aspects such as defect types and defect densities depending on crystal growth method, seed material and doping (e.g. boron doping for power transistors or nitrogen doping for quantum sensing devices based on spin properties of the nitrogen vacancy (NV) center in diamond) will be discussed. X-ray topography (XRT) and high resolution X-ray diffraction (HRXRD) are used for this combined study. XRT in two principal ways is used in the course of this analysis, namely the projection transmission mode and the section transmission mode. HRXRD (reciprocal space mapping, $\omega/2\theta$ -scans and ω -scans) is used for the analysis of subsurface damage, strain and mosaicity of the diamonds. The combination of these analytical methods allows a detailed statement of the nature, density and distribution of typical defects in diamond bulk substrates and epitaxial CVD grown diamond layers.

Fig.1 and Fig.2 show as examples type 220 reflection X-ray topographies (projection mode and section mode, Mo-radiation) of large CVD-grown (001) diamond substrates from two different vendors. The diamond crystal of Fig.1 was grown heteroepitaxially on an Ir/YSZ/Si (001) seed (Vendor: Audiatec). The projection topography (Fig. 1a) of this diamond shows a mosaic-like blurred contrast (orientation contrast) of a mosaic crystal with tilted and twisted grains. No sharp contrast of individual dislocations is observable. However, the projection topography shows some kind of texture (Fig.1b). Important information can be extracted from the section topographies (Fig.1c and 1d). While the image of the $\bar{2}\bar{2}0$ reflex is very diffuse, the topography of the $\bar{2}\bar{2}0$ reflex shows a lateral domain structure, which suggests an epitaxial lateral overgrowth (ELOG) technique. Fig. 2a shows the projection topography of

a diamond grown by CVD on a high quality HPHT diamond seed (Vendor: ElementSix). In the center of the crystal the defect density is low and only single threading dislocations are visible. In contrast, dislocation bundles with a high density appear at the $\{100\}$ growth sector boundaries. The high material quality in the center of the crystal is confirmed by the visibility of Kato-fringes in the section topographies of Fig.2b.

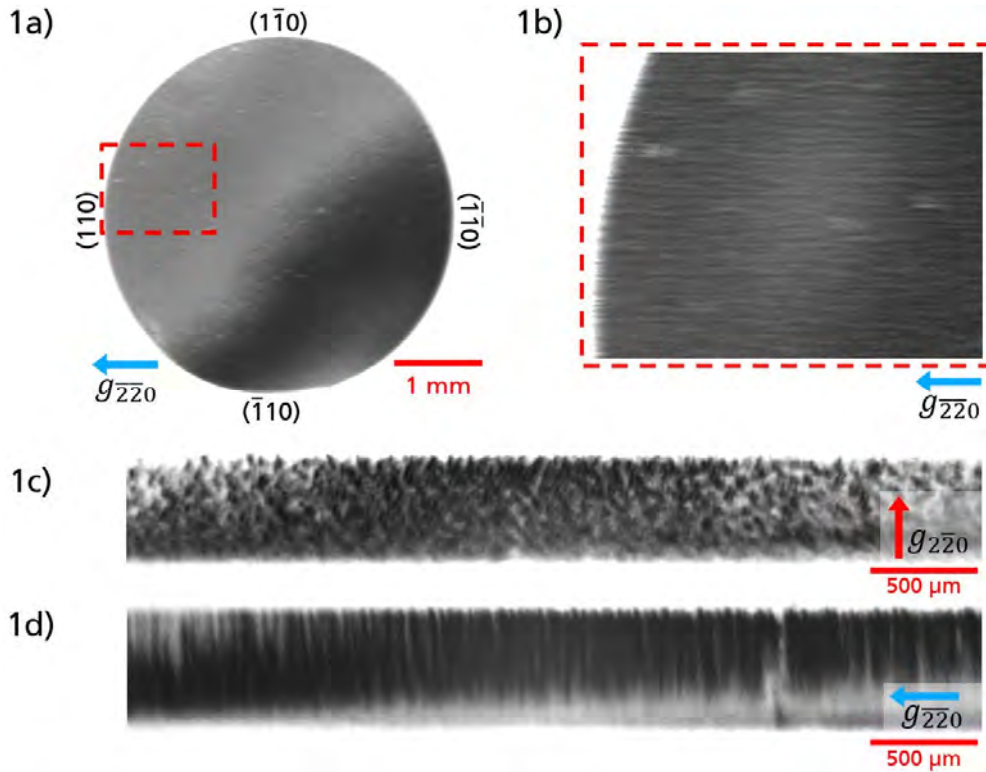


Fig. 1: XRT of a diamond crystal (diameter: 9 mm) grown heteroepitaxially by CVD on an Ir/YSZ/Si (001) seed. The seed was removed after growth. (Fig. 1a and 1b: projection topographies, Fig. 1c and 1d: section topographies)

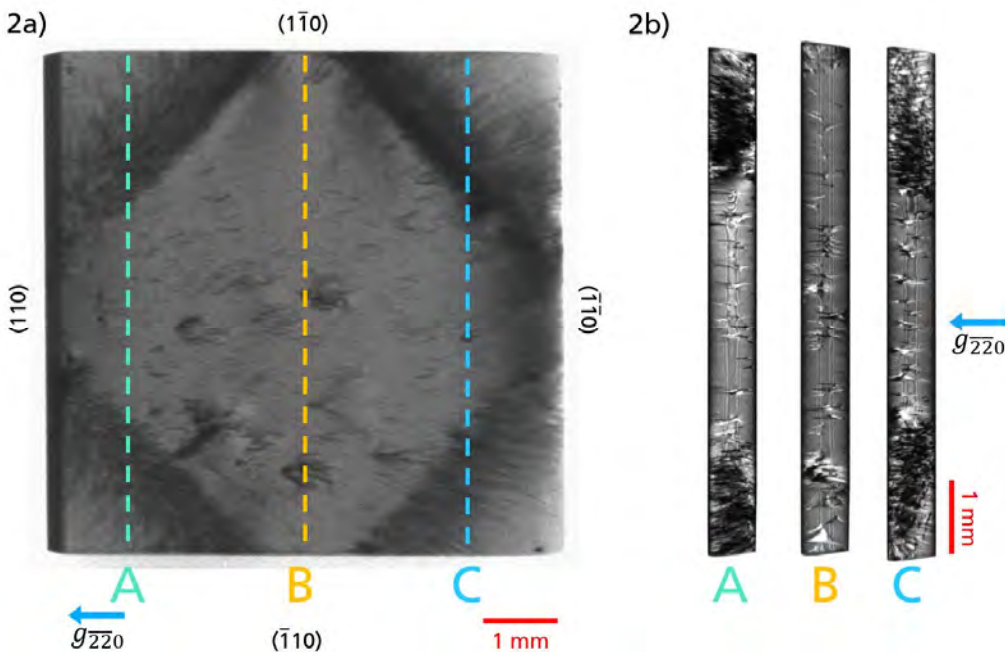


Fig. 2: XRT of a diamond crystal (size: 7 mm × 7 mm) grown homoepitaxially by CVD on a HPHT diamond (001) seed. The seed was removed after growth. (Fig. 2a: projection topography, Fig. 2b: section topographies)

PVT GROWTH OF LARGE FREESTANDING C-DOPED ALN CRYSTALS

S. Müller, B. Epelbaum, T. Wicht, S. Besendörfer, R. Weingärtner, D. Jockel
E. Meissner and J. Friedrich

Fraunhofer IISB, Schottkystr. 10, 91058, Germany
E-mail: stephan.mueller@iisb.fraunhofer.de

Summary

The availability of large size, high quality AlN substrates is critical for a high yielding, cost-effective production process of the next generation of AlGaN devices via homoepitaxy for UV-optoelectronics and power electronics. Despite considerable efforts and recent progress [1], high quality 2" AlN substrates are still far from being widespread commercially available. Moreover, for applications in power electronics, an even larger substrate sizes will be necessary to take advantage of the economy of scale and advanced equipment of existing fab lines. While a slow but steady increase of crystal size by repeated PVT bulk growth has been demonstrated, only very limited data is available on changes of the AlN crystals defect microstructure during growth both within the regular growth direction ($[0001]$ or $[000\bar{1}]$) or within any lateral expansion areas. It is of particular interest, if the new crystal material added by lateral expansion differs in structural quality from the original material in the center area. Possible reasons for such difference include: (i) thermomechanical stress build up in the growing crystal, and (ii) differences in the growth modes for various crystallographic directions. It is well known from other PVT grown semiconductors like SiC, that the diameter expansion geometry needs to be chosen very carefully to avoid stress and any related deterioration of the crystal quality [2].

In order to minimize thermomechanical stress and specifically investigate this aspect (ii) for the AlN material system, we employed a dedicated PVT growth geometry based on the concept of Lely growth [3]. By establishing conditions with low thermal gradients, we were able to investigate the *fundamental* possibility to maintain both, the crystal quality in axial and lateral portions of material grown in quite different growth modes. The seed wafers used for this study were cut from previous bulk AlN crystals grown in our laboratory with approximately one inch diameter and mainly wafer halves. The seed thickness was about 600 μm , with both surfaces polished mechanically with 1 μm diamond slurry. On some of seed wafers we added differently oriented edge flats in order to facilitate the formation of side facets and to investigate lateral growth (Fig. 1). All seed wafers were annealed at temperature of 2250-2300°C in isothermal conditions in slightly undersaturated AlN vapor during 2-5 hours prior to setting them into the growth cell. Thermal anneal was essential for the removal of residual surface damage, in particular on seed edges and added flats. These seeds were mounted in a Lely-type growth assembly shown schematically in Fig. 1A. Hereby the main structure used for growth was a central cavity build by sintered blocks of coarse grained (1 to 3 mm) AlN of high purity inside of a loosely-closed TaC crucible, also acting as background C-source for doping. All charge material was carefully purified by repeated re-sublimation in W-crucibles in a carbon-free reactor, resulting in slightly Al-rich material. The seeds were clamped at a targeted position with tungsten or tantalum stripes. Growth experiments were performed during 24-48 hours runs at $T > 2300^\circ\text{C}$ and 700-900 mbar of nitrogen pressure in a growth reactor with indirect heating of a dense graphite susceptor via an induction coil. Due to the very low T-gradients in our system, the habitus of grown crystals clearly reflects differences in the growth rates in various crystallographic directions (Wulff shape), with the biggest portion of new material always grown in $[000\bar{1}]$ -direction on the N-polar face (normally facing towards the hotter crucible bottom), and only 200-400 μm grown on Al-polar face. As-grown crystals (Fig. 1 B, C) were first evaluated using optical microscopy, while the crystal surfaces morphology, formed in the course of the growth process, have been investigated in more details by AFM and SEM. The dislocation structures in the grown crystals were analyzed by X-ray diffraction (XRD), X-ray

topography (XRT)) and defect selective KOH/NaOH etching. The diffraction vectors chosen for XRT were $\vec{g} = [0004]$ (reflection geometry.), $\vec{g} = \langle 1\bar{1}00 \rangle$ (transmission geometry) and $\vec{g} = \langle \bar{2}021 \rangle$ (transmission).

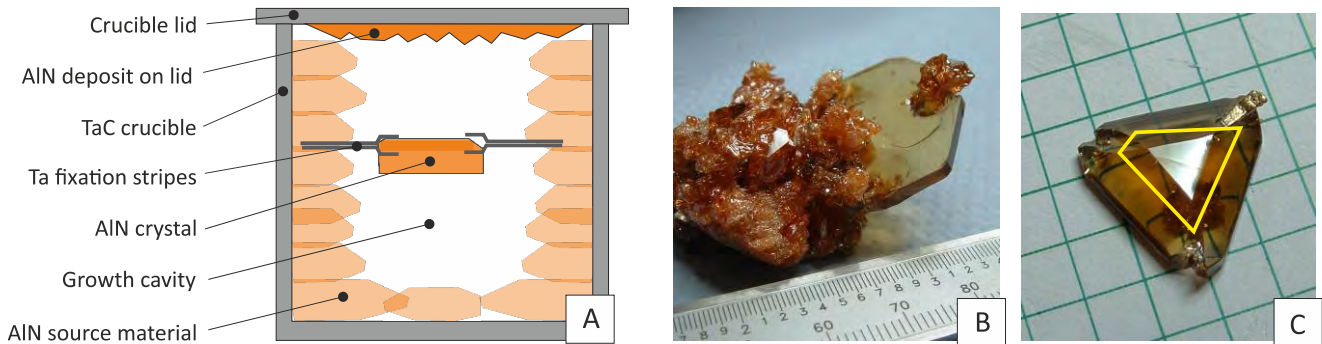


Fig. 1: Growth assembly for growth of unstrained AlN crystals (A) and some characteristic examples: crystal seeded on round wafer grows into hexagonal prism (B); triangle-shaped seed (marked yellow) produces large amount of lateral growth (C), grid scale in C is 5 mm.

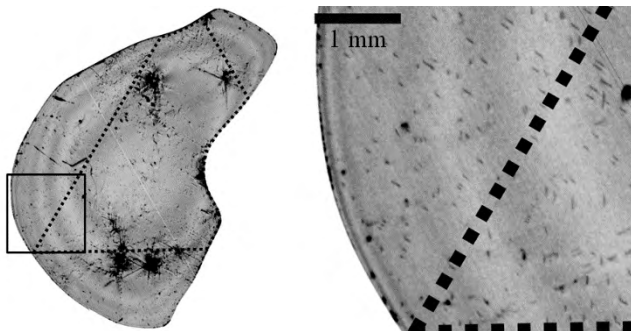


Fig. 2: XRT $\vec{g} = [\bar{2}021]$ measurements of an AlN wafer in transmission. The dotted triangle illustrates the border between material grown axially on top of the seed, and the lateral expansion area

XRD $(0\bar{1}10)$ -rocking-curve mappings result in a mean FWHM of 13-17 arcsec which is in line with a low density of Basal Plane Dislocations (BPDs) as well as 2θ -shift values in between ± 15 arcsec, again in line with a low density of Threading Edge Dislocations (TEDs) in the range of $2\text{-}4 \cdot 10^3 \text{ cm}^{-2}$ for the great majority of the crystal volume i.e. for both regions the axially and the laterally grown crystal portions (excluding the areas of parasitic nucleation). These results are within the expectation for the low thermal gradient conditions employed for the growth. The comparison of XRT images of subsequent wafers sliced from the same crystal resulted in an identical Total Dislocation Density (TDD), demonstrating no deterioration of the high crystal quality during axial growth on N-polar $(000\text{-}1)$ -face. On the other hand, locally increased FWHM and 2θ -shift are found for parasitic grains and defect clusters. It is shown, that the latter were accommodated by both grain boundaries and by the formation of Basal Plane Screw Dislocations (BPSs) in adjacent areas during growth, identified as such for the first time in AlN bulk material. Most significantly, the crystal quality was typically the same in expansion areas compared to the center of the crystal (Fig. 2), despite the rather large laterally added area within a single growth run. In summary, it was shown, that fundamentally the high structural quality of bulk AlN material could be preserved within both, axial and lateral growth, independent on very strong differences in growth morphologies characteristic for differently oriented facets of carbon-doped AlN. Important differences in surface morphologies and their influence on growth rate, resulting crystal habit and defect formation will be presented as well.

- [1] Dalmau, R., Craft, H. S., Britt et al. *Materials Science Forum*, **924**, 923–926 (2018)
- [2] Drachev, R. V.; Hansen, D.; Loboda, M. J. *MRS Proc.* **1246** (2010) K2.18.1.
- [3] Lely, J. A., US Patent US2854364A, March 7, (1955)

Growth of bulk AlN crystals: Influence of the temperature field on growth rate, optical absorption and dislocation density

T. Straubinger, C. Hartmann, L. Matiwe, J. Wollweber, I. Gamov, K. Irmischer, M. Bickermann

Leibniz-Institut für Kristallzüchtung (IKZ), Max-Born-Str. 2, 12489 Berlin, Germany
E-mail: thomas.straubinger@ikz-berlin.de

Summary

Light emitting diodes (LEDs) for ultra-violet (UV) applications are typically processed on sapphire substrates and typically show threading dislocation densities (TDD) in the range of 10^9 cm^{-2} in the light emitting AlxGa1-xN multi-quantum well layers strongly reducing the radiative recombination efficiency [1]. One solution to overcome this issue is to use native aluminum nitride (AlN) substrates to grow device layers with TDD multiple orders lower compared to AlN on sapphire, typically $< 10^5 \text{ cm}^{-2}$ [2, 3].

AlN bulk crystals (Fig. 1, left) are grown with the physical vapor transport (PVT) method [3, 4] by evaporation of an AlN-powder source with low impurity level at temperatures of approx. 2250 °C and recrystallization at a colder AlN-seed at temperatures of approx. 2200 °C.

One key for successful AlN bulk growth is a fundamental understanding of the correlation of temperature field and growth rate which was investigated by growing crystals at five different growth conditions (T_{seed} , ΔT) and comparing the results to a simple model based on diffusion and step-flow-growth [5]. The growth rate R is directly proportional to the absolute supersaturation S_{Al} (excess partial pressure of gaseous Al at the seed) and increases with both the temperature T_{seed} and the temperature difference ΔT between source and seed.

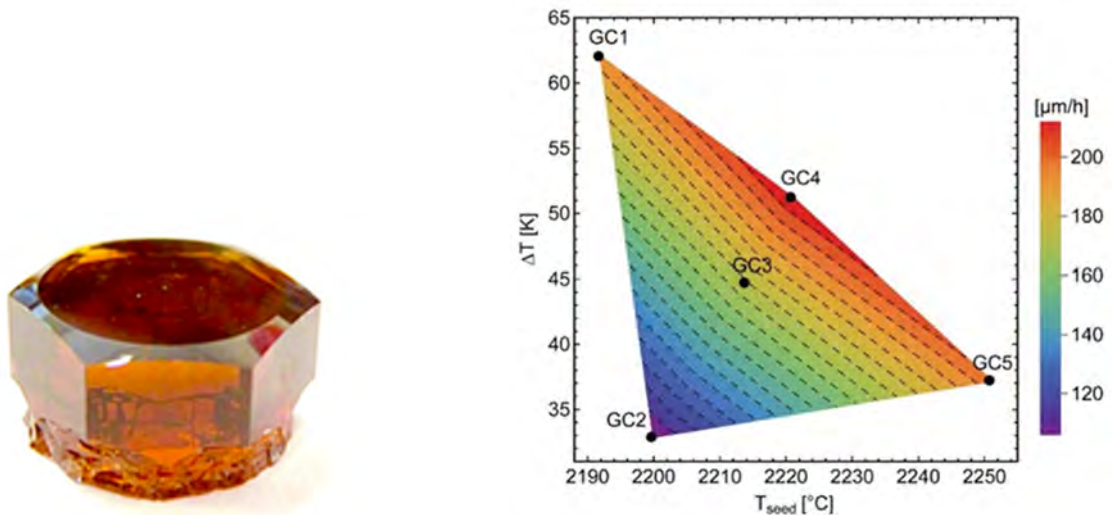


Fig. 1: Left - typical AlN crystal grown in c-direction with m-facets on side walls and 8 mm diameter. Right - contour plot of experimentally observed growth rates R (T_{seed} , ΔT). The five growth conditions (GC-x) used in the investigation are marked with black data points.

Prior to the analysis of structural and optical properties the AlN-crystals were sliced with an inner diameter saw and both side polished using diamond and SiO_2 (chemo mechanical polishing) abrasives. The absorption in AlN is mainly determined by the concentrations of the elements O, C and Si and their ratios. In all samples [Fig. 2] the carbon related absorption at 4.7 eV [6] is completely quenched

due to the shift in the Fermi level because $[O] + [Si] > 3 [C]$ [7]. The lowest absorption in the crucial wavelength range for, e.g., water disinfection (265 nm) is achieved for the crystal grown at the highest T_{seed} .

For the determination of the dislocation densities defect selective etching was performed using molten KOH. The dislocation density was then exclusively counted in the central area as the crystal rims showed defect clusters caused by contact to polycrystalline AlN which was nucleated next to the seed rim. The dislocation density significantly decreases with increasing T_{seed} while it seems not to be influenced by the growth rate and the temperature difference between source and seed.

In conclusion growth of AlN-crystals at high temperatures and low axial temperature gradients is favorable to gain AlN-substrates with low dislocation density ($< 10^4 \text{ cm}^{-2}$) and high UV-transparency for AlGaN-based deep-UV emitters.

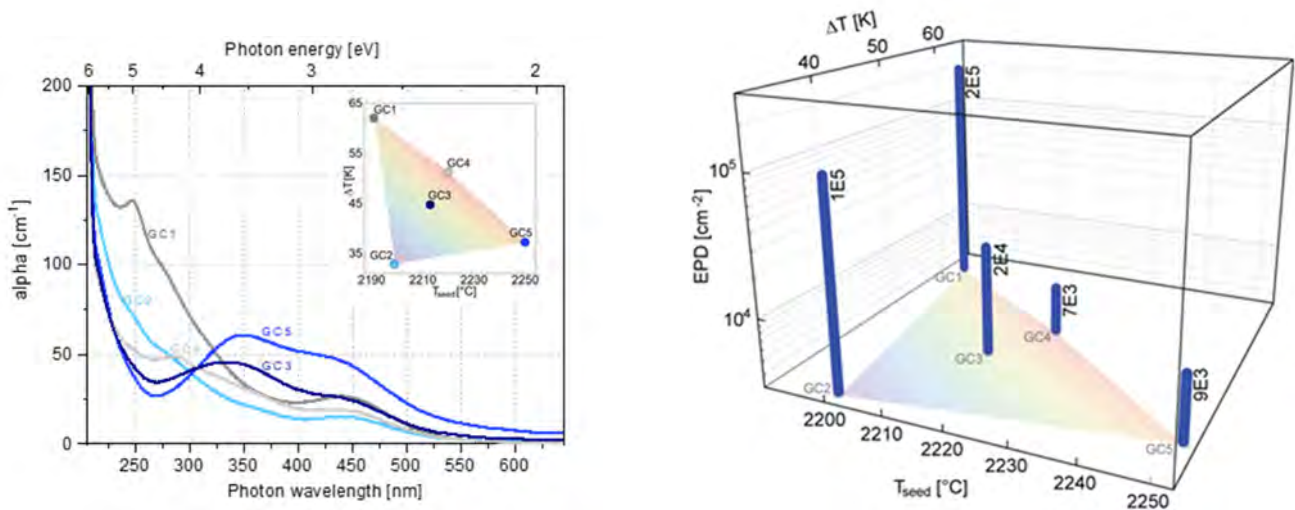


Fig. 2: Left - UV/VIS absorption spectra for the five crystals grown with different T -field and subsequent growth rates. Right - etch pit density (EPD) (z -axis) and subsequent growth rates (xy -plane) for the same crystals.

Acknowledgment

This work is financially supported by the Bundesministerium für Bildung und Forschung (Zwanzig20 Advanced UV for Live, 03ZZ0112A and 03ZZ0138A). This work is financially supported by the Bundesministerium für Bildung und Forschung (Zwanzig20 Advanced UV for Live, 03ZZ0112A and 03ZZ0138A). Parts of the work were also performed using funding from the German Research Foundation under grant no. BI781/11-1.

- [1] M. Kneissl et al., Nature Photonics, **13**, pp. 233-244 (2019)
- [2] R. Dalmau et al., Journal of the Electrochemical Society, **158** (5), pp. 530-535 (2011)
- [3] R. Dalmau et al., Materials Science Forum, **924**, pp. 923-926 (2018)
- [4] C. Hartmann et al., CrystEngComm, **18**, pp. 3488-3497 (2016)
- [5] B. Epelbaum et al., Materials Science Forum, **457-460**, pp. 1537-1540 (2004)
- [6] R. Collazo et al., Applied Physics Letters, **100**, p. 191914 (2012)
- [7] K. Irmscher et al., Journal of Applied Physics, **114**, p. 123505 (2013)

Session 3
Wednesday 11.03.2020
16:30 – 18:10

MAGNETO-OPTICAL BISMUTH SUBSTITUTED RARE-EARTH IRON GARNET SENSOR FILMS FOR CHARACTERIZATION OF ELECTRICAL STEEL SHEETS

T. Reimann^a, M. Lindner^a, B. Wenzel^a, R. Holzhey^a

^a INNOVENT e.V. Technologieentwicklung, Dept. Magnetic and Optical Systems, Prüssingstr. 27B,
07745 Jena, Germany

E-mail: tr@innovent-jena.de

Summary

Bismuth-substituted rare-earth iron garnets (Bi-REIG) are well known for their high specific Faraday rotation of few degrees per micrometer film thickness. The principle of magneto-optical (MO) imaging using Faraday rotation (MOIF) is shown in Fig. 1. The local magnetic north and south pole of the magnetic sample results in an antipodal direction of the magnetic polarization of the Bi-REIG sensor film. The resulting opposing rotation of the polarized light leads to an optically visible black-white contrast. Therefore, the magnetic domain structure can be observed using a standard camera. The low optical absorption, high sensitivity for weak magnetic stray field strengths and high lateral resolution of Bi-REIG materials enables MOIF of magnetic domains in grain oriented electrical steel sheets (GOES). These are widely used as core material for inductive power transformers [1]. The investigation of the correlation between the magnetic properties and the crystallographic orientation of the GOES grains, was subject to research activities within the last years [2] [3]. In this work, the magnetic domain structure of a GOES (thyssenkrupp AG) was characterized by MOIF technique and the results were compared with texture measurements from XRD.

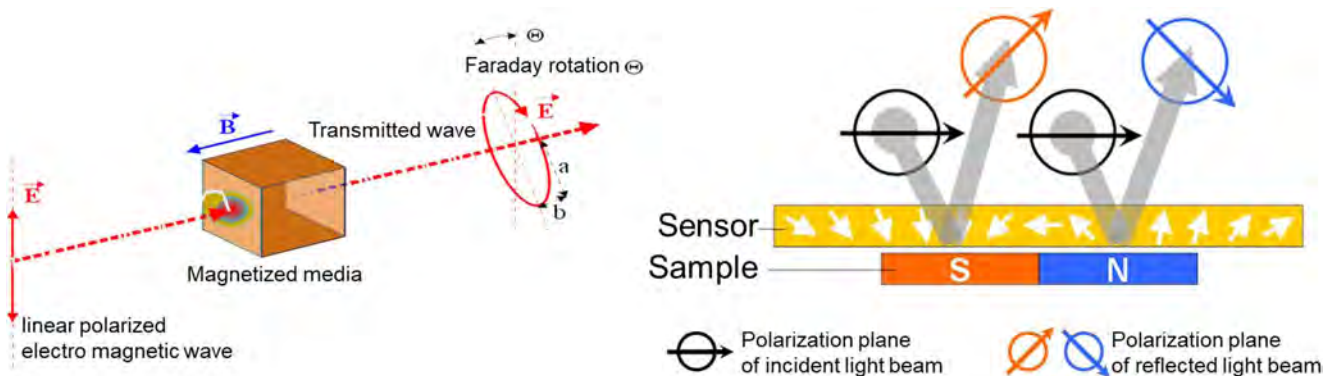


Fig. 1: Faraday effect of magnetized material (left) and illustration of the MO imaging principle (right).

Bi-REIG films were made by liquid phase epitaxy (LPE), with dipping technique in $\text{PbO-Bi}_2\text{O}_3\text{-B}_2\text{O}_3$ based flux. Single crystalline $\text{Gd}_3\text{Ga}_5\text{O}_{12}$ garnet disks ([111] oriented) with very low surface roughness and a diameter up to three inches were used as substrates. The deposition process was done under air atmosphere in a 3 zone furnace using platinum crucibles. After the LPE process, the coated substrates were cleaned and the Bi-REIG layer was removed from one side by polishing. For use as MO sensor, the residual Bi-REIG film was coated with an additional mirror layer and a hard coating layer, in order to increase the scratch resistance. The MO sensor was cut into chips of size 20 mm x 15 mm. This sensor chips are used in a camera based measuring system for MOIF (CMOS Magview S, Matesy GmbH).

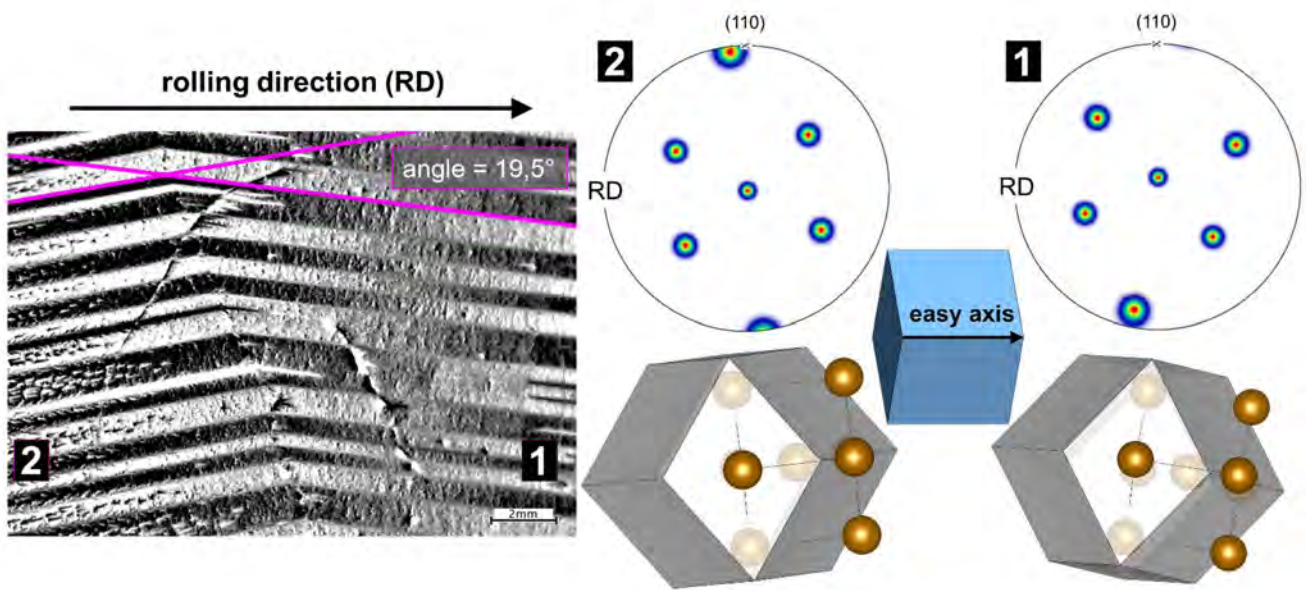


Fig. 2: MO image of grain oriented electrical steel (left), via CMOS-MagView technique and pole figures with illustrated crystal orientation of the two grains, measured by XRD texture analysis (right).

The measured magnetic domain structure of two grains of the GOES sample, is shown in Fig. 2. The XRD texture analysis (Bruker Discover, Co-K-alpha radiation) of these grains shows a typical rolling texture of the GOES. This is called Goss texture, where the (110) plane is ideally parallel to the surface and the magnetic easy axis [001] is oriented in the rolling direction (RD) (Fig. 2.). The XRD data was evaluated by MTEX toolbox for Matlab [2]. However, a misorientation of the easy axis according to the rolling direction in the x-y-plane can be detected by the XRD and MOIF analysis. As a result, the angle between the two domain directions in die MO image was 19.5°. Evaluation of the XRD data revealed the same angle between the intersection lines of the (110) planes of the two grain orientations with the x-y-plane. Because the magnetic domain structure is determined by the direction of the [001] axis, the MO image also gives a information on the actual crystallographic orientation of the GOES grains. This could be very suitable for the quality management of GOES production process. The MOIF techniques enables a very fast and sample preparation free measurement of the domain structure, compared to structure analysis techniques like XRD or EBSD.

Acknowledgment

We would like to thank Mr. Arne Bochmann from the Ernst-Abbe-University of applied Science Jena for providing support at the XRD texture measurements and evaluation.

- [1] Hendryk Richert, Heidemarie Schmidt, Sandra Lindner, Morris Lindner, Benjamin Wenzel, Rocco Holzhey, and Rudolf Schäfer, steel research int., **No. 2**, 232-240 (2016)
- [2] I. Gutierrez-Urrutia, A. Bottcher, L. Lahn, D. Raabe, J Mater Sci, **49**, 269-276 (2014)
- [3] A. Nadouma, F. Robinsonb, S. Biroasca, Journal of Magnetism and Magnetic Materials **Volume 494**, 165772 (2020)
- [4] F. Bachmann, R. Hielscher, H. Schaeben, Solid State Phenomena, **Vol. 160**, 63-68 (2010)

Self-flux Growth of Single Crystals of BaCoSO

Y.H. Song ^a, D.C. Peets ^{a,b}, X.S. Liu ^a, Maxim Avdeev ^c, and D.L. Feng ^{a,d}

^a Department of Physics and Advanced Materials Laboratory, Fudan University, 2005 SongHu Road, Yangpu District, Shanghai 200438, China

^b Institut für Festkörper- und Materialphysik, Technische Universität Dresden, Häcklstr. 3, 01169 Dresden, Germany

^c Australian Nuclear Science and Technology Organisation, Lucas Heights, NSW 2234, Australia

^d Hefei National Laboratory for Physical Science at Microscale and Department of Physics, University of Science and Technology of China, Hefei, Anhui 230026, China

^e Collaborative Innovation Center of Advanced Microstructures, Nanjing 210093, China
E-mail: darren.peets@tu-dresden.de

Summary

Doped BaCoSO was recently predicted to be a high-temperature superconductor in an entirely new class based on Co and Ni. BaCoSO has been recently prepared as a powder [1,2], but crystals have not been available. Based on its layered crystal structure, significant anisotropy would be expected in its electronic and magnetic response, which will require single-crystalline samples to elucidate. Single crystals will also be a prerequisite for several doping and measurement schemes in the quest to verify the prediction of superconductivity. We were unable to inject carriers or induce superconductivity in this study.

Using a Co-S self-flux method with a 5:1 flux ratio, we synthesized the first single crystals of the antiferromagnetic insulator BaCoSO from BaO, Co, and S. The growth was performed in a sealed quartz tube between 1000 and 880°C using an alumina crucible. Excess flux was removed at the conclusion of growth using a centrifuge. The resulting single crystals were up to 2×2×0.2 mm³ in size, black, with mirror surfaces largely free of flux [see Fig. 1(b) for an example].

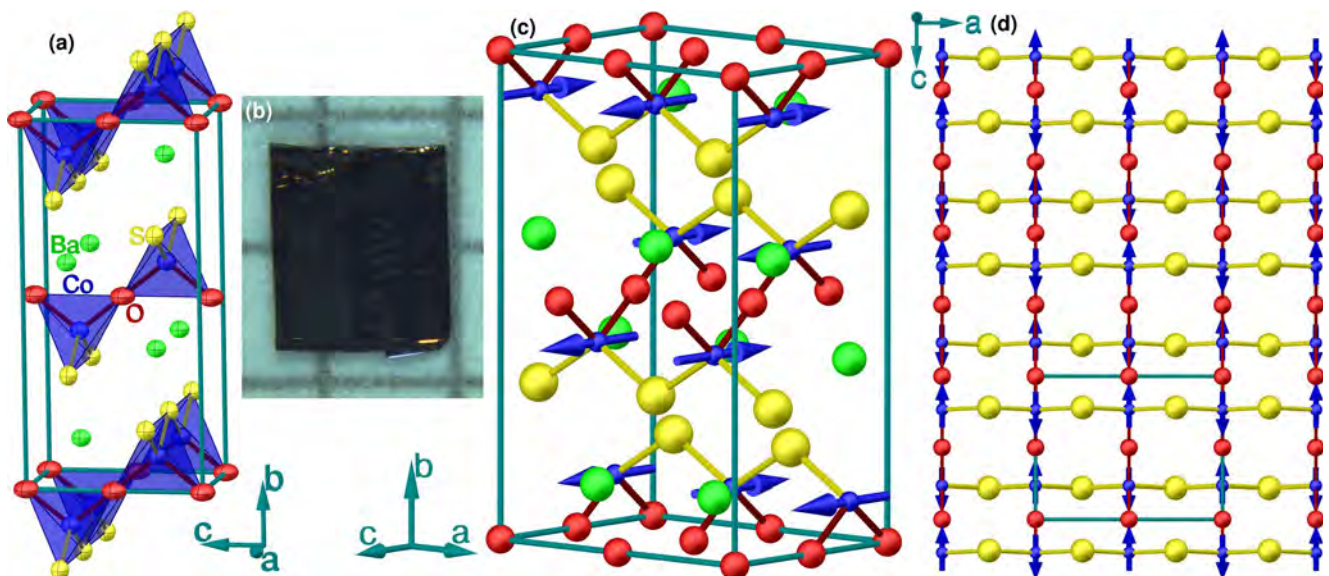


Fig. 1: Crystal and magnetic structure of BaCoSO, also now reported in our Ref. [3]. (a) Crystal structure of BaCoSO. (b) An example of one of the single crystals grown in this study, on millimetre-ruled graph paper. (c,d) Magnetic structure of BaCoSO.

Our magnetic and specific heat measurements and neutron single-crystal diffraction results provide previously-unavailable details of its magnetic anisotropy and order. The refined crystal and magnetic structure are shown in Fig. 1. We find a different magnetic space group from that reported previously, and a rather different magnetic response for fields along c than a or b . The vast majority of magnetic entropy is not released near the transition, suggesting the survival of significant short-range order to far higher temperatures. Our white-beam neutron Laue diffraction experiment was not sensitive to diffuse scattering, and was unable to confirm this.

Acknowledgment

This work is supported by the Science Challenge Project (grant No. TZ2016004), the National Key R&D Program of the MOST of China (grant No. 2016YFA0300203), the German Science Foundation from the project C03 of the Collaborative Research Center SFB 1143 at the TU Dresden (project-ID 247310070), and the National Natural Science Foundation of China (projects No. 11650110428, 11421404, U1532266, 11790312, and 11674367). D.C.P. is supported by the Chinese Academy of Sciences through 2018PM0036.

- [1] M. Valldor, U.K. Rößler, Y. Prots, C.-Y. Kuo, J.-C. Chiang, Z.W. Hu, T.-W. Pi, Rüdiger Kniep, and L.H. Tjeng, *Chem. Eur. J.*, **21**, 10821–10828 (2015)
- [2] E.J.T. Salter, J.N. Blandy, and S.J. Clarke, *Inorg. Chem.*, **55**, 1697–1701 (2016)
- [3] Y.H. Song, X.S. Liu, D. Wu, Q. Yao, C.H.P. Wen, M. Avdeev, R. Peng, H.C. Xu, J. Miao, X. Lou, Y.F. Fang, B.L. Pan, N.L. Wang, D.C. Peets, and D.L. Feng, *Phys. Rev. B*, **100**, 205130 (2019), also available as arXiv:1911.03076

Crystal growth of the valence fluctuating system EuPd_2Si_2

Marius Peters, Doan-My Tran, Eunhyung Cho, Franz Ritter, Kristin Kliemt, and Cornelius Krellner

Kristall- und Materiallabor, Physikalisches Institut, Goethe-Universität Frankfurt, Max-von-Laue-Str. 1,
60438 Frankfurt am Main

E-mail: marius.peters@stud.uni-frankfurt.de

The study of collective phenomena arising from enhanced coupling between electrons and phonons is focussed on materials exhibiting phase transitions involving both electronic and lattice-degrees of freedom. One system providing such a strongly coupled phase transition is EuPd_2Si_2 of the ThCr_2Si_2 structural type, showing a temperature induced valence transition of europium between the energetically vicinal valence states Eu^{2+} and Eu^{3+} at about 160 K [1]. First reports on the synthesis of single crystals came up only recently [2], but a deep investigation of the valence transition in this compound is still missing.

We approached the ternary Eu-Pd-Si system using differential thermal analysis to map the local composition phase diagram. The target compound, its melting temperature and the remainders for certain starting stoichiometries could be identified and utilised to conduct larger scaled growth experiments.

We used the Bridgman method to gain a seed of EuPd_2Si_2 for an iterative Czochralski method for the successful growth of mm-sized single crystals of EuPd_2Si_2 (see Fig. 1). These experiments were performed testing various levels of Europium excess in the starting composition.

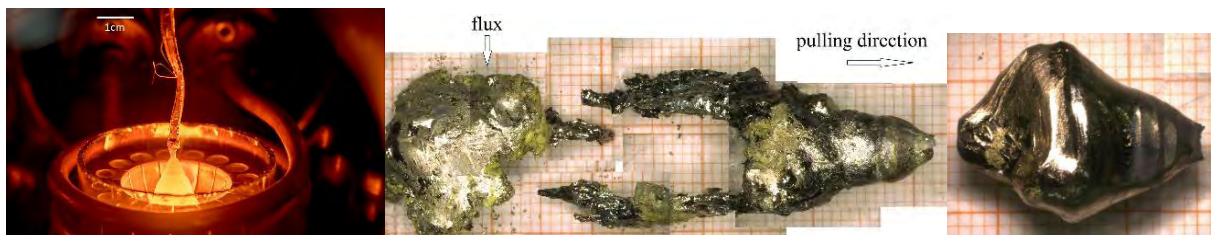


Fig. 1, left to right: Czochralski growth, sample MP401 (generation 1), sample MP411 (generation 3).

The characterisation of this system is highly interdependent between the three pillars of stoichiometrical, structural and physical characterisation. Structural characterization was done by powder X-ray diffraction (XRD). With this technique, we determined the temperature dependence of the lattice parameters by measuring XRD down to 50 K. The respective curves are depicted in Fig. 2a. We first focus on the (004) reflection at $2\Theta = 36.3^\circ$. It is apparent that this peak is nearly temperature independent with a tendency of a shift to smaller angles at low temperatures, which corresponds to a constant c parameter through the valence transition with only a slight increase at low temperature (see Fig. 2c). In contrast, the a parameter decreases strongly (around 2%) when cooling through the valence transition, visible in the raw data as a significant shift of the (200) reflection and in the refined lattice parameter in Fig. 2b.

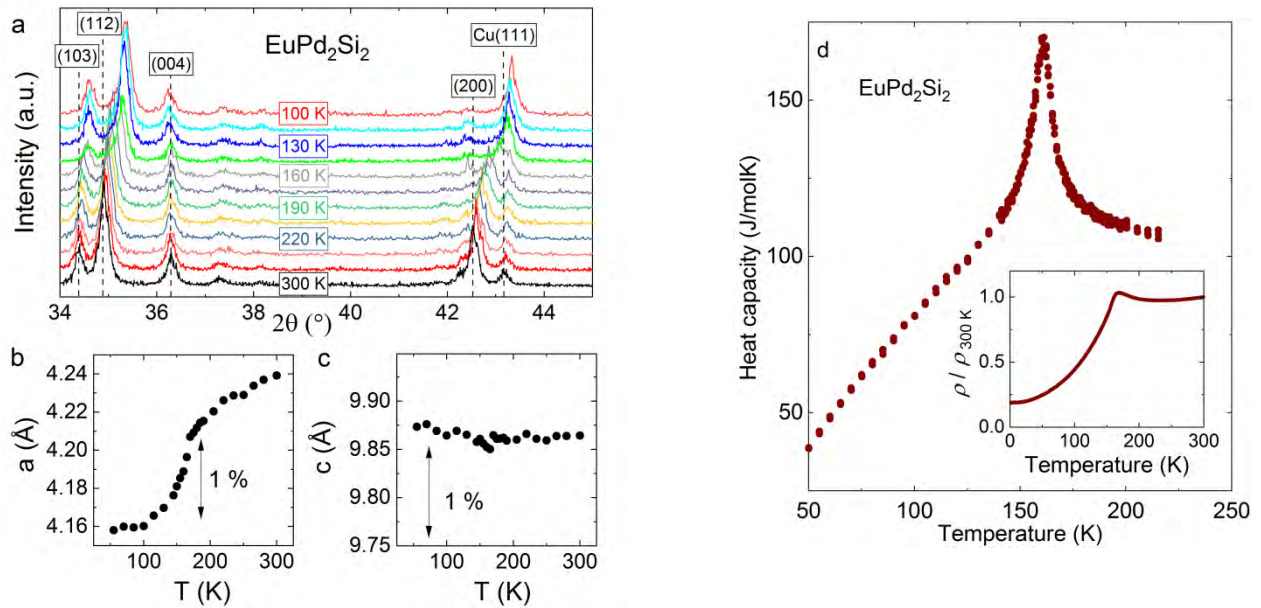


Fig. 2: a) Temperature-dependent powder XRD data of EuPd_2Si_2 . The refined lattice parameters as function of temperature are shown in b) and c). The change of the a parameter is very large with relative changes of about 1%, whereas the c parameter is nearly temperature independent. d) Heat capacity of an EuPd_2Si_2 single crystal. A sharp anomaly is visible at the valence transition, $T_V = 160$ K. The inset presents the resistivity for current along the crystallographic c direction. Also there a pronounced anomaly is apparent at T_V .

The valence transition was further investigated by temperature-dependent measurements of the heat capacity and the resistivity using the standard options of a Physical Property Measurement System (PPMS). In Fig. 2d we present the heat capacity of a single crystal, grown using the Czochralski technique described above. A pronounced anomaly is visible around $T_V = 160$ K. As the standard option of the PPMS determines the heat capacity with a relaxation method, where one easily can miss first-order transitions, we carefully checked the temperature-time curves but did not find any evidence of latent heat. Therefore, we can exclude a first-order phase transition for this particular crystal.

The resistivity of that sample is shown in the inset of Fig. 2d and also there a pronounced anomaly is visible at T_V . The residual resistivity ratio (RRR = 5) of that sample is comparable to what was reported by Onuki *et al.* [2].

Acknowledgment

We acknowledge funding through the Deutsche Forschungsgemeinschaft (DFG), grant No. KR3831/5-1 and Fermi-NESt.

[1] E. V. Sampathkumaran *et al.*, Journal of Physics **C14**, L237 (1981).

[2] Y. Onuki *et al.*, Philosophical Magazine **97**, 3399 (2017).

Session 4
Thursday 12.03.2020
8:30 – 10:10

Growth of CuFeO_2 single crystals by the optical floating-zone technique

N. Wolff^{a,b}, T. Schwaigert^a, D. Siche^a, D. G. Schlom^{c,d}, D. Klimm^a

^a Leibniz-Institut für Kristallzüchtung, Max-Born-Str. 2, 12489 Berlin

^b Helmholtz-Zentrum Berlin für Materialien und Energie, Hahn-Meitner-Platz 1, 14109 Berlin

^c Department of Materials Science and Engineering, Cornell University, Ithaca, NY 14853-1501, USA

^d Kavli Institute at Cornell for Nanoscale Science, Ithaca, NY 14863-1501, USA

E-mail: nora.wolff@helmholtz-berlin.de

Oxide materials based on the ABO_2 delafossite structure are of particular interest due to the novel properties that accompany their cation variation at A and B sites. Usually the semiconductor delafossites consists of Ag or Cu at A-site and several trivalent cations as Al, Fe or Ga at B-site. Pd and Pt-based compositions are the metallic delafossite oxides where B-site cations are transition metals like Co, Cr or Rh [1-3]. Among these, the growth of single crystalline PdCoO_2 came in our focus due to its ultra-high conductivity at room temperature. An in-plane resistivity of $\rho_{ab} = 2.6 \mu\Omega\text{-cm}$ at 295 K makes this material the most conductive oxide known, comparable to the best metallic conductors Ag, Cu, Au and Al [4]. [5]

So far, epitaxial layers of PdCoO_2 have mainly been grown on sapphire substrates with degraded quality resulting from the not well matched crystallographic lattice [6-8]. For the growth of high quality epitaxial layers, isostructural single crystalline substrates with similar lattice constants are required. CuFeO_2 is the only delafossite compound, which can be grown on a larger scale and has suitable lattice parameters (PdCoO_2 : $a = 2.830 \text{ \AA}$, $c = 17.743 \text{ \AA}$ [9] and CuFeO_2 : $a = 3.0351 \text{ \AA}$, $c = 17.166 \text{ \AA}$). [5]

The aim of this work was to grow CuFeO_2 single crystals, which can be used as substrates for the growth of high quality PdCoO_2 films. Crystals with diameters up to 10 mm were grown from stoichiometric sintered rods by the optical floating-zone technique (Fig. 1). Due to the incongruent melting behavior of CuFeO_2 and redoxprocesses of iron- and copperoxide during growth (Fig. 2), low growth rates of 0.4 mm/h are necessary. [5]

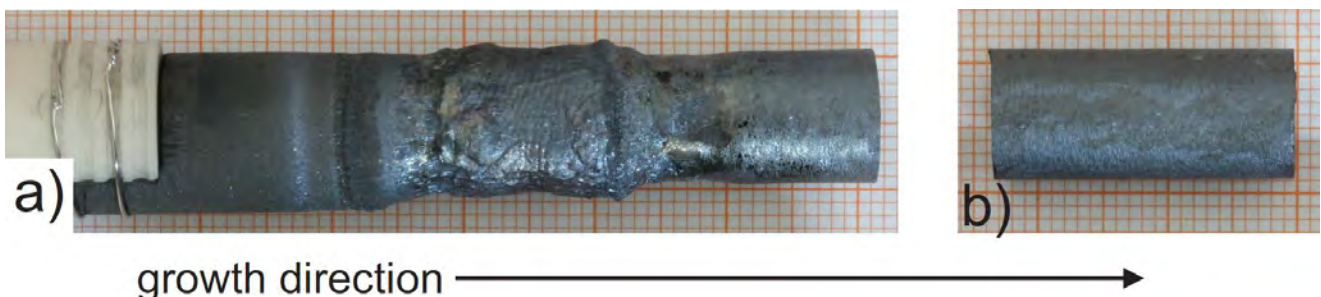


Fig. 1: (a) Unstable growth of CuFeO_2 in the initial growth state. (b) Single crystal part of the same rod. [5]

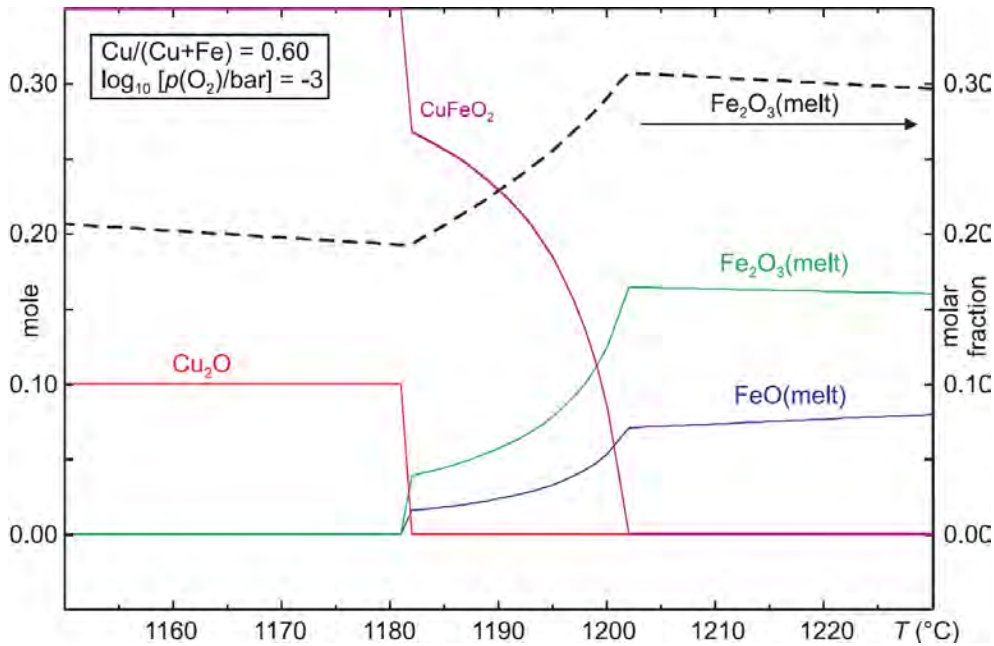


Fig. 2: Crystallization of the Cu-Fe-oxide melt under a constant oxygen fugacity of 1bar. Even if only $\text{CuFe}^{3+}\text{O}_2$ starts to crystallize around 1200 °C, the amount of Fe^{2+}O in the melt drops. [5]

Acknowledgment

A. Kwasniewski is acknowledged for performing X-ray powder analysis and Laue measurements. We are indebted to C. Gugushev who performed energy-dispersive Laue mappings and X-ray fluorescence spectroscopy and to S. Ganschow for continuous support of this work. The authors acknowledge funding by the German Research Foundation (DFG) under project SI 463/9-1. D.G.S. acknowledges funding provided by the Alexander von Humboldt Foundation for his sabbatical stay at the Leibniz-Institut für Kristallzüchtung and support from the U.S. Department of Energy, Office of Basic Sciences, Division of Material Sciences and Engineering, under Award No. DE-SC0002334

- [1] R.D. Shannon, D.B. Rogers, C.T. Prewitt, Chemistry of noble metal oxides. I. Syntheses and properties of ABO_2 delafossite compounds, *Inorg. Chem.* 10 (1971) 713–718.
- [2] C.T. Prewitt, R.D. Shannon, D.B. Rogers, Chemistry of noble metal oxides. II. crystal structures of PtCoO_2 , PdCoO_2 , CuFeO_2 , and AgFeO_2 , *Inorg. Chem.* 10 (1971) 719–723.
- [3] D.B. Rogers, R.D. Shannon, C.T. Prewitt, J.L. Gillson, Chemistry of noble metal oxides. III. electrical transport properties and crystal chemistry of ABO_2 compounds with the delafossite structure, *Inorg. Chem.* 10 (1971) 723–727.
- [4] C.W. Hicks, A.S. Gibbs, A.P. Mackenzie, H. Takatsu, Y. Maeno, E.A. Yelland, Quantum oscillations and high carrier mobility in the delafossite PdCoO_2 , *Phys.Rev. Lett.* 109 (2012) 116401.
- [5] N. Wolff, T. Schwaigert, D. Siche, D.G. Schlom, D. Klimm, Growth of CuFeO_2 single crystals by the optical floating-zone technique, *J. Cryst. Growth.* 532 (2020) 125426.
- [6] M. Brahlek, G. Rimal, J.M. Ok, D. Mukherjee, A.R. Mazza, Q. Lu, H.N. Lee, T.Z. Ward, R.R. Unocic, G. Eres, S. Oh, Growth of metallic delafossite PdCoO_2 by molecular beam epitaxy, *Phys. Rev. Mater.* 3 (2019) 093401.
- [7] T. Harada, K. Fujiwara, A. Tsukazaki, Highly conductive PdCoO_2 ultrathin films for transparent electrodes, *APL Mater.* 6 (2018) 046107.
- [8] P. Yordanov, W. Sigle, P. Kaya, M.E. Grunder, R. Pentcheva, B. Keimer, H.U. Habermeier, Large thermopower anisotropy in PdCoO_2 thin films, *Phys. Rev. Mater.* 3 (2019) 085403.
- [9] H.Takatsu, S.Yonezawa, S.Mouri, S.Nakatsuji, K.Tanaka, Y.Maeno, Roles of high frequency optical phonons in the physical properties of the conductive delafossite PdCoO_2 , *J. Phys. Soc. Japan* 76 (2007) 104701.

Investigation of orthorhombic and tetragonal phases of $\text{Cs}_2\text{CuCl}_{4-x}\text{Br}_x$ mixed system

Natalija van Well^a

^a Department of Earth and Environmental Sciences, Crystallography Section, Ludwig-Maximilians-University Munich, D-80333 Munich, Germany
E-mail: Natalija.vanwell@lrz.uni-muenchen.de

Low-dimensional quantum spin systems are a large class of materials, which have been studied intensively in condensed matter physics for the last decades [1]. These systems also include the $\text{Cs}_2\text{CuCl}_{4-x}\text{Br}_x$ mixed system, which exists in orthorhombic and tetragonal polymorphs [2,3]. For this mixed system, the centre of interest are the different Cu^{2+} environments and their influence on the magnetic properties of the orthorhombic and tetragonal compositions. Additionally, the understanding of such influence is important to understand the change of magnetic behaviour by applying magnetic field.

The crystals are grown from aqueous solution using the evaporation method and different temperatures for growing orthorhombic and tetragonal phases. The compounds of the orthorhombic phase of this mixed system can be grown in the full Br concentration range for $0 \leq x \leq 4$ from aqueous solution at a temperature of 50°C [4]. The structure was analysed by x-ray powder diffraction and showed the orthorhombic symmetry $Pnma$ in the full Br concentration range [4]. The compositions of the tetragonal phase are grown for a Br concentration range between $1 \leq x \leq 2$ at a temperature of 24°C . At 8°C , the mixed system can be supplemented with the tetragonal realization of Cs_2CuCl_4 [2]. The compositions of the tetragonal phase show the tetragonal symmetry $I4/mmm$ in x-ray powder diffraction analysis. Fig. 1 presents a schematic phase diagram of this mixed system.

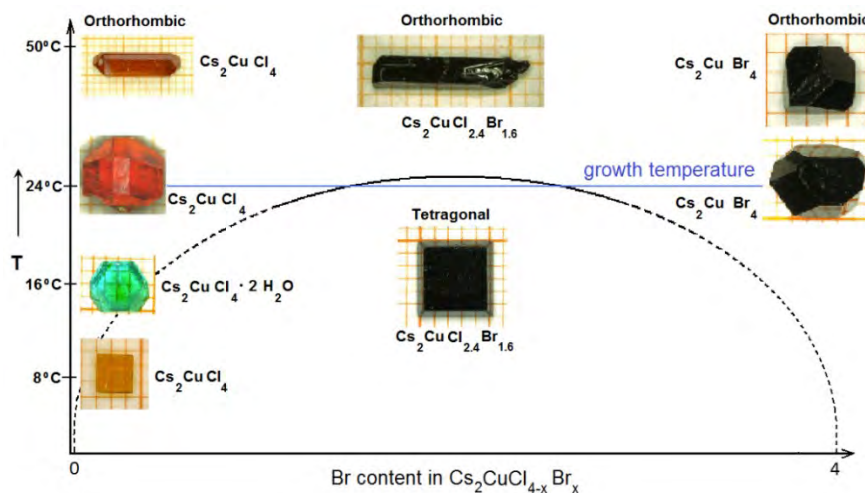


Fig. 1: Schematic phase diagram of the $\text{Cs}_2\text{CuCl}_{4-x}\text{Br}_x$ mixed system grown from aqueous solution.

The physical properties demonstrate differences for the orthorhombic and the tetragonal phases. The investigation of the orthorhombic compounds with neutron diffraction results in a rich magnetic phase diagram, based on four regimes, which is shown in Fig. 2. The regimes are characterized by different exchange coupling mechanisms [3]. In Fig. 2, a long-range antiferromagnetic order at lower temperatures is observed for some compositions (red circles) in regimes I and IV. The black circles show the data from literature for Cs_2CuCl_4 and Cs_2CuBr_4 [5,6]. The horizontal arrow bars ± 0.1 represent the uncertainties of the EDX results of the chemical composition. In the magnetic phase diagram, the two ordered magnetic phases in regimes I and IV seem to be separated by quantum critical

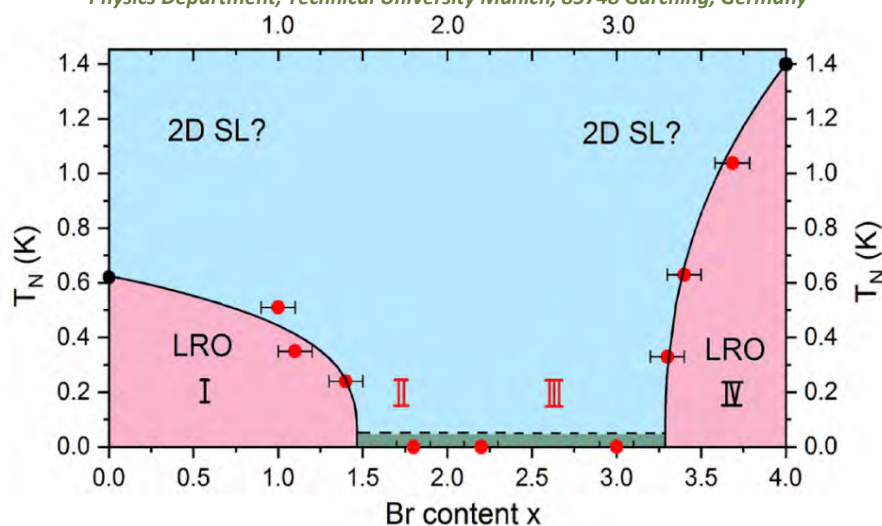


Fig. 2: Magnetic phase diagram of orthorhombic compounds of $\text{Cs}_2\text{CuCl}_{4-x}\text{Br}_x$.

points (QCP), QCP1 near $x = 1.5$ and QCP2 near $x = 3.2$, respectively. Whereas in regimes I and IV (with a long-range antiferromagnetic order) investigations in a magnetic field show new results, in regimes II and III no magnetic order was observed. 2D spin liquid (2D SL) might exist for a still to be defined Br concentration range of this mixed system. As this still has to be confirmed with inelastic neutron scattering, 2D SL are marked in Fig. 2 with “?”.

For the compounds of the tetragonal phase, the magnetic behaviour remains antiferromagnetic down to 1.5 K, evidenced by neutron diffraction experiments [2]. One of the key points for understanding the magnetic structure of the investigated tetragonal compounds is, to clarify, whether there is a relationship between the spin ordering and the crystallographic ordering of the $[\text{CuX}_6]$ octahedra. To answer this question, single crystal neutron diffraction measurements are envisaged.

Subject: Abstract Oral

Acknowledgment

The author thanks W. Aßmus from Goethe-University, Frankfurt am Main. The neutron diffraction experiments were performed on ZEBRA with crystals orientated on ORION at PSI, Villigen, Switzerland and on D23 with crystals orientated on OrientExpress at ILL, Grenoble, France, and on MIRA with crystals orientated on the neutron-laue diffractometer RESI at FRM II of MLZ, Garching. This work was supported by Paul Scherrer Institute, Institut Laue-Langevin, University of Bayreuth, Heinz Maier-Leibnitz Zentrum and Physik Department E21, Technische Universität München, and the Deutsche Forschungsgemeinschaft through the research fellowship for the project WE-5803/1-1 and WE-5803/2-1, and through the fellowship A 4576 – 1/3 of the University of Bayreuth. This work was additionally supported by the Swiss State Secretariat for Education, Research and Innovation (SERI) through a CRG-grant.

[1] M. Vojta, *Rep. Prog. Phys.*, 81, 064501 (2018); [2] N. van Well, C. Eisele, S. Ramakrishnan, T. Shang, M. Medarde, A. Cervellino, M. Skoulatos, R. Georgii, S. van Smaalen, *Cryst. Growth Des.*, 19, 11, 6627-6635 (2019); [3] van Well, N.; Zaharko, O.; Delley, B.; Skoulatos, M.; Georgii, R.; van Smaalen, S.; Rüegg, Ch., *Ann. Phys. (Berlin, Ger.)*, 530, 201800270 (2018); [4] N. Kruger, S. Belz, F. Schossau, A. A. Haghghirad, P. T. Cong, B. Wolf, S. Gottlieb-Schoenmeyer, F. Ritter, W. Assmus, *Cryst. Growth Des.*, 10, 4456 (2010); [5] Ono, H. Tanaka, T. Nakagomi, O. Kolomiyets, H. Mitamura, F. Ishikawa, T. Goto, K. Nakajima, A. Oosawa, Y. Koike, K. Kakurai, J. Klenke, P. Smeibidle, M. Meißner, H. A. Katori, *J. Phys. Soc. Jpn.*, 74, 135 (2005); [6] R. Coldea, D. A. Tennant, R. A. Cowley, D. F. McMorrow, B. Dorner, Z. Tylczynski, *J. Phys., Condens. Matter*, 8, 7473 (1996)

Investigation of facet growth in heavily doped silicon single crystals grown in the mirror furnace

S. Gruner^{a,b}, S. Hürner^b, C. Kranert^{a,b}, T. Jauß^c, T. Sorgenfrei^c, C. Reimann^b, J. Friedrich^b

^a Fraunhofer THM, Am St. Niclas Schacht 13, 09599 Freiberg, Germany

^b Fraunhofer IISB, Schottkystraße 10, 91058 Erlangen, Germany

^c University of Freiburg, Crystallography, Hermann-Herder-Str. 5, 79104 Freiburg, Germany

E-mail: Sebastian.Gruner@iisb.fraunhofer.de

Summary

When an atomically rough and atomically smooth interface coexist simultaneously during growth of a crystal, their growth kinetics differ, which will affect the properties of the grown crystal like dopant homogeneity or content of extended crystal defects e.g. in form of dislocations or twins. The atomically smooth interface regions form typically along the (111) facets at a certain supercooling during growth of silicon or germanium crystals either at the crystal periphery known as edge facet or growth ridge or as central facet in the bulk for <111> crystal orientation.

In order to obtain a deeper understanding of the relationship between facet growth, growth conditions and the resulting crystal properties, systematic investigations have been carried out in the present work. For that purpose, heavily As-doped, <100>- and <111>- oriented silicon crystals with 8 mm in diameter were grown by the floating zone technique in a mirror furnace at translation speeds of 1 mm/min up to 8 mm/min. Partially the crystals were grown with a free melt surface, partially the melt surface was covered by an oxide layer to prevent Marangoni convection. The grown crystals were characterized with regard to the length of the central facet, the width of the growth ridge, the shape of the phase boundary, the emergence of constitutional supercooling, and the presence of dislocations and twins.

It was found that the macroscopic deflection of the growth interface decreases with increasing growth velocity in the <100>-oriented crystals because the temperature gradient in the crystal becomes steeper. As a result the diameter of the central facet in the <111>-oriented crystals becomes smaller. The diameter of the central facet is also influenced by dislocations. In some experiments it was not possible to apply a dash necking procedure. Therefore, dislocations are present in the crystal already at the beginning of the growth process. As a result, the central facet is shorter compared to the dislocation free crystals because a smaller supercooling is sufficient for the facet to grow when dislocations and therefore growth steps at the facet are present. In some cases an irregular instability of the central facet diameter has been observed apart from periodically oscillations (Fig. 1).

Edge facets appear only when the crystal surface is not covered by an oxide layer. The width of the growth ridge is shorter for <111>-orientation than for <100>-orientation which can be explained simply by the geometrical relation of the (111) edge facet with respect to the growth orientation. However, no influence of the growth velocity and the axial temperature gradient on the width of the growth ridge was found. In addition, the edge facet grows deeply into the bulk of the small diameter crystal and is not limited to the growth ridge, as it is for large diameter crystals. Both findings cannot be explained by the existing theory of Voronkov.

In agreement to our theoretical considerations, interface instability due to constitutional supercooling was found only during final solidification in the atomically rough interface region at the crystal periphery, when the growth velocity exceeds 10 mm/min and the temperature gradient

becomes very small with reducing the heating power. The faceted region showed to be more stable and was not affected by the starting morphological instabilities.

In addition to the experimental investigations, a global numerical model with Ansys Fluent was developed to describe the temperature field in the mirror furnace (Fig. 2). For that purpose experimental data from facet length analysis, phase boundary deflection in etched cross-sections and temperature measurements were used for its validation. The model is applied to analyze the influence of buoyant convection e.g. on the interface shape and to predict a possible influence of microgravity conditions on the growth behavior.

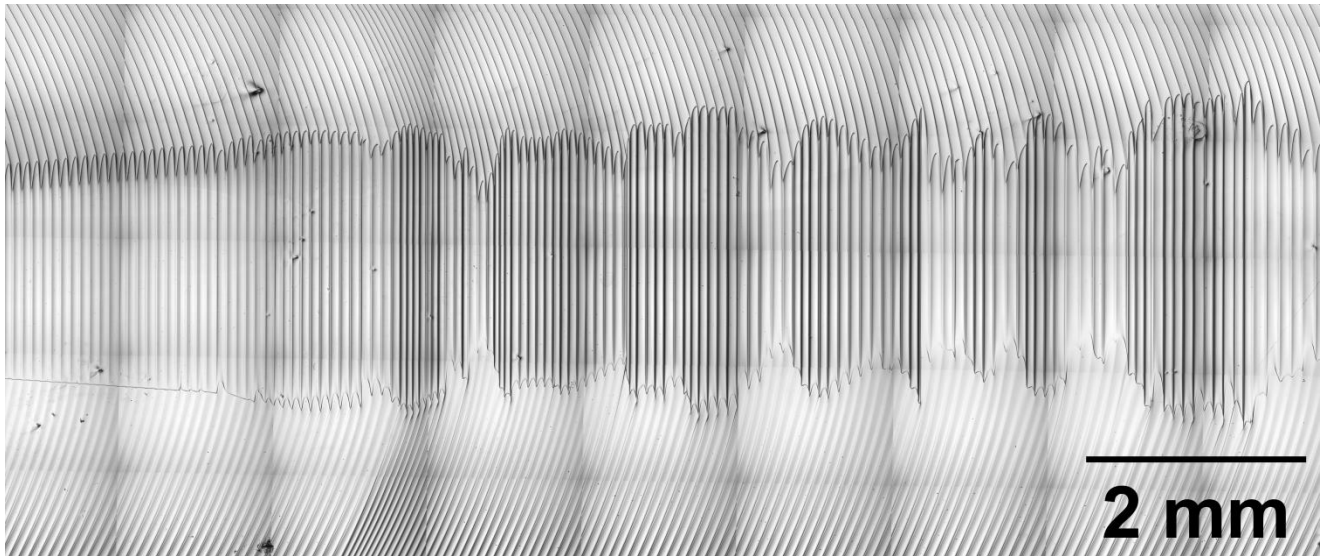


Fig. 1: Instability of the central facet diameter in heavily As-doped silicon

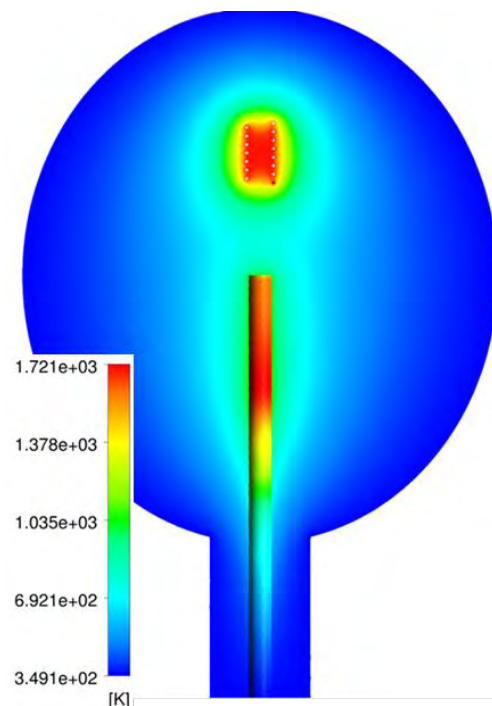


Fig. 2: Modelling of the temperature field for the mirror furnace with Ansys Fluent

Acknowledgment

This work is supported by the DLR within the project „Einfluss der Stabilität des Facettenwachstums auf die Entstehung von Kristalldefekten bei der Halbleiterkristallzuchtung“, FKZ50WM1844 and FKZ50WM1845.

Session 5
Thursday 12.03.2020
10:40 – 12:00

CONTROL OF AlInN COMPOSITION IN CLOSED COUPLED SHOWERHEAD MOCVD REACTORS

M. Heuken^{ab}, D. Meyer^b, F. Sandbaumhüter^{ab}, O. Rockenfeller^b, C. Mauder^b, and A. Boyd^b

^a RWTH Aachen University, Compound Semiconductor Technology, 52074 Aachen, Germany

^b AIXTRON SE, Dornkaulstraße 2, 52134 Herzogenrath, Germany

E-mail: m.heuken@aixtron.com

Nitride-based electronic devices continuously gain attention and are envisioned as driving force for next-generation of RF-HEMT for 5G applications. Therein, InAlN is most promising as barrier material. However, it has been reported that InAlN suffers from gallium contamination if grown in a reactor based on the Close Coupled Showerhead (CCS) architecture. Yet, a conclusive picture explaining the presence of Ga in the InAlN has not emerged. We have intensively studied the mechanism of the reported gallium incorporation as a function of precursor materials, process conditions and reactor hardware. In order to investigate the mechanism of the incorporation of gallium in InAlN, we studied the growth of InAlN on GaN templates, either with or without in-situ re-grown GaN, in a 3x2 CCS reactor in a 1x4 inch configuration. To grow InAlN and GaN layers, trimethylaluminum (TMAl), trimethylgallium (TMGa), trimethylindium (TMIn) and ammonia (NH₃) have been used to deposit Al, Ga, In, and N, respectively. The growth of the epitaxial layers have been in-situ monitored using LayTec EpiTT optical reflectance measurement. It is known, that opening and cleaning the reactor between the growth steps of GaN and InAlN results in Ga-free barrier layers. Growing InAlN directly on a GaN template or cleaning the reactor between these two steps are facile options to avoid Ga carry over in InAlN [1]. It also indicates that the origin of Ga cannot be explained by a diffusion of atoms from the GaN layer into InAlN. Moreover, opening the reactor without any additional cleaning of the reactor (for 20 minutes inside the Glovebox) has led to only 0.5% Ga in InAlN, indicating that a volatile and reactive process coating of the reactor affects the purity of InAlN. Residual amounts of oxygen in the glovebox seem to be sufficient to passivate this process coating. In addition, Mrad and co-workers could also show that the amount of Ga in InAlN scales with the thickness of the GaN layer [2].

To further shed light into the mechanism of the contamination, we have investigated the roles of the precursors for In and Ga. We can confirm the vital role of TMIn from an experiment, in which AlN is grown on GaN under conditions equal to those for InAlN, except no TMIn is introduced into the reactor. Growing AlN on in-situ re-grown GaN showed no difference to a sample grown on a GaN template. It is thus unlikely that condensed TMGa molecules slowly desorb during the process subsequent to GaN growth, as this should also affect AlN. We have furthermore investigated the Ga uptake in InAlN when using the precursors TEGa during GaN growth and TEIn during InAlN growth. Both experiments revealed no significant difference to the standard precursors with a Ga pollution in the range of 20-30%, so the fundamental mechanism of the contamination remained and its origin stems from reactants that are present for both trimethyl- and triethyl-based precursors.

We already concluded that desorption of condensed, unreacted TMGa molecules during InAlN growth unlikely cause the Ga uptake. It is also known that metallic Ga covers the Showerhead surface during GaN growth [3]. The effect of metallic gallium on the growth of InAlN has been

investigated by an etching experiment, in which the GaN layer has been etched in H₂. This generates free Ga atoms, which agglomerate on the Showerhead [4]. Starting with a cleaned reactor, we have applied this method to coat the initially clean Showerhead with metallic gallium without introducing any Ga precursor to the reactor. After etching approx. 2 μm of GaN from a template sample, we subsequently grew InAlN without opening the reactor using conventional process parameters. Growth rate and elemental analysis then revealed a high Ga contamination of more than 22%. Apparently, the combination of metallic gallium with the precursor for indium in the reactor plays a key role for the unintentional Ga incorporation. Metallic gallium is generated in both processes using TMGa and TEGa. Based on the low vapor pressure of metallic gallium, we can explain that gallium does not simply evaporate during subsequent processes, as evidenced by the missing Ga uptake in AlN grown on GaN. Instead, a chemical reaction takes place between gallium and the precursor for indium, upon which methyl units are exchanged. This reaction is energetically favorable based on the calculations published in ref. [5]. Molecules of TMIIn in the vicinity of metallic gallium in the reactor then lead to spontaneous formation of Ga precursor, which travel back into the gas phase and efficiently incorporate during the growth of InAlN.

Avoiding gallium to be incorporated into InAlN thus requires a method to inhibit the reaction between gallium and TMIIn. Changing the surface temperature of the Showerhead displays one route to transform the metallic gallium into a more stable coating. Due to its low thermal conductivity, a quartz-based deposition shield fixed to the Showerhead is a facile way to achieve a hot surface above the wafer. Not only reduces a hot surface the condensation rate of gallium, it also seems to enable the formation of a low-quality GaN composition on the deposition shield. As a result, a contamination of InAlN by Ga is almost entirely suppressed when using a quartz-based deposition shield with traces of gallium in the order of 0.1%.

With our current study, we discuss a contamination of InAlN by gallium if the barrier layer is grown subsequent to GaN. Here, we present a concise experimental study that reveals the Ga uptake in InAlN to originate from a metallic gallium coating, which diffuses back into the gas phase upon an alkyl exchange reaction with the precursor for In (e.g., TMIIn or TEIn). A quartz-based deposition shield fixed to the Showerhead leads to a high surface temperature, which enable the formation of a more stable coating during GaN growth, which is unaffected by the presence of TMIIn during InAlN growth. Thus we can provide Ga-free InAlN barrier layers, grown directly subsequent to GaN.

[1] Kim, et al. "Effect of Group-III precursors on unintentional gallium incorporation during epitaxial growth of InAlN layers by metalorganic vapor deposition," *Journal of Applied Physics*, **no. 118**, p. 125303 (2015)

[2] M. Mrad, et al. "Understanding and controlling Ga contamination in InAlN barrier layers," *Journal of Crystal Growth*, **no. 507**, pp. 139-142 (2019)

[3] J. Kim, et al. "Origins of unintentional incorporation of gallium in InAlN layers during epitaxial growth, part II: effects of underlying layers and growth chamber conditions," *Journal of Crystal Growth*, **no. 388**, pp. 143-149 (2014)

[4] E. E. Zavarin, et al. "In-situ investigations of GaN chemical instability during MOCVD," *Proceedings of the EUROCVI-15*, p. 299 (2005)

[5] B. H. Cardelino et al. "Dissociative Chemisorption of Trimethylgallium, Trimethylindium, and Ammonia on Gallium and Indium Nitride Substrates. A computational Study," *The Journal of Physical Chemistry C*, **no. 115**, pp. 9090-9104 (2011)

Growth of modulation-doped β -Ga₂O₃ multilayers by MOVPE

A. Popp^a, S. Bin Anooz^a, R. Grüneberg^a, A. Fiedler^a, Z. Galazka^a, R. Schewski^a,
M. Albrecht^a, K. Irmscher^a and G. Wagner^a.

^a Leibniz-Institut für Kristallzüchtung (IKZ), Member of the Forschungsverbund Berlin e.V.,
Max-Born-Str. 2, 12489 Berlin, Germany
E-Mail: andreas.popp@ikz-berlin.de

Summary

The wide bandgap (4.8 eV) oxide material β -Ga₂O₃ is characterized by a breakdown field strength of 8MV/cm [1]. Transistors based on β -Ga₂O₃ benefit from a low on-resistance at a given breakdown voltage, which leads to less power losses. Due to these properties β -Ga₂O₃ meets the requirements to become the next generation of high-performance material for power electronic applications.

In this contribution we report on the growth of homoepitaxial β -Ga₂O₃ layers by metal-organic vapor phase epitaxy (MOVPE) on (010) and (100) oriented substrates. To avoid the formation of twin lamellae for the (100) orientation substrates with a miscut of 6° towards the [00-1] direction were used [2, 3]. At IKZ two inch diameter bulk β -Ga₂O₃ single crystals were grown by the Czochralski method [4]. Out of these crystals the (100) oriented substrates were prepared. (010) oriented substrates were grown by the EFG method and supplied by Tamura Corp., Japan.

The focus of this work was the deposition of modulation Si-doped layer structures. To use the promising material properties of β -Ga₂O₃ the epi layers have to have a high structural perfection, a smooth surface morphology and a low defect density to achieve the best electrical properties. To meet the requirements for modern devices multilayer structures with different doping regimes are necessary. The interfaces between the substrate and layers, and especially between the single doped epi layers play an important role for the device performance. Figure 1 shows the comparison for a 200 nm layer grown on a (010) oriented substrate and a (100) 6° off oriented substrate.

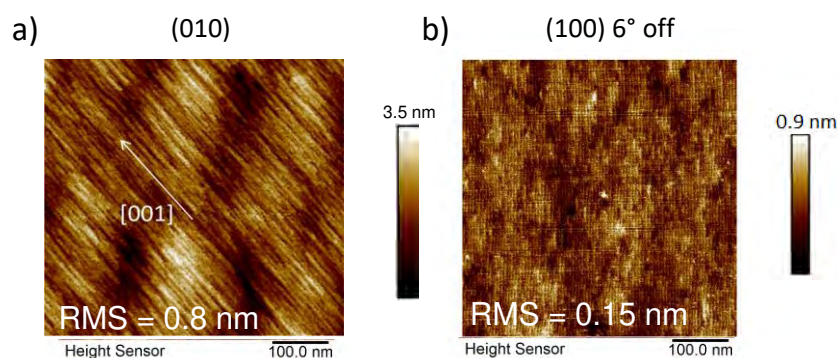


Figure1: AFM pictures of the layer morphology grown by MOVPE on a) a (010) oriented substrate and b) on a (100) 6° off oriented substrate.

The layer grown on the (010) oriented substrate shows elongated two dimensional islands, indicating a faceted surface morphology with a roughness of about 800 pm. In contrast to that, the layer grown on (100) 6° off oriented substrate is characterized by a smooth step flow growth with a surface roughness of < 200 pm, a quarter the value of the (010) layer. This is a good prerequisite to achieve very sharp interfaces for multilayer structures with different doping regimes. In contrast to that, gradual transition of doping regimes between layers will result in scattering of free charge carries that leads to a decrease of the carrier mobility and overall device performance. Therefore, it is crucial to

ensure that the interfaces are as sharp as possible. This depends strongly on the orientation of the β - Ga_2O_3 substrate.

We demonstrated in this work that β - Ga_2O_3 Si-doped multilayer structures homoepitaxially grown by MOVPE in the same run on (100)6° off oriented substrates and (010) substrates revealed sharper interfaces in the Si-depth profile for the (100) orientated substrates (see Fig. 2).

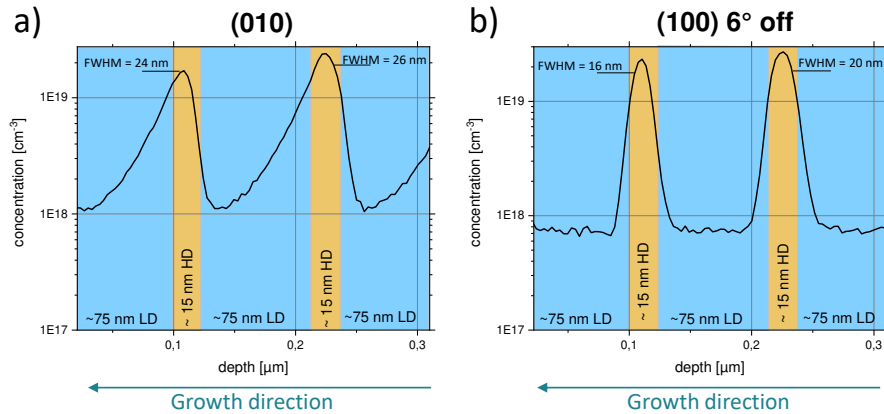


Figure 2: Si-depth profile measured by secondary ion mass spectroscopy (SIMS) of a multilayer structure grown by MOVPE on a) a (010) oriented substrate and b) on a (100) 6° off oriented substrate. The nomenclature LD and HD denotes “Low Si-Doping” and “High Si-Doping”, respectively.

The SIMS Si-depth profile for the multilayer grown on the (010) substrate shows a gradual transition from a high to the low Si doping regions. The reason seems to be the surface morphology. For the faceted (010) layer surface the incorporation of Si is inhomogeneous resulting in blurred interfaces. The Si depth profile of the multilayer grown on (100) 6° off substrate instead shows sharp interfaces between the high and low doping regions since the (100) orientation is a cleavage plane with the lowest surface energy [3]. The use of (100) oriented substrates may, therefore, reduce the leakage current and improve the device performance, pointing out at the same time a direction for the device development.

The surface morphology and electrical properties of the obtained layers were analyzed by AFM and Hall Effect measurements, respectively. Ellipsometry measurements of the layers were performed with the use of Al_2O_3 substrates in the same run to determine the layer thickness. The depth profile and the silicon concentration of the multilayer stack was measured by using secondary ion mass spectroscopy (SIMS). The shape of the interfaces between the layers and the structural perfection were analyzed by SIMS and high resolution transmission electron microscopy (HRTEM), respectively.

Acknowledgment

This work was performed in the framework of GraFOx, a Leibniz ScienceCampus. The work was partially funded by the BMBF under grant number 03VP03712, the European Community (Europäische Fonds für regionale Entwicklung- EFRE) under grant number 1.8/15 and by the Air Force Office of Scientific Research under award number FA9550-17-1-0279.

- [1] M. Higashiwaki et al., *Semicond. Sci. Technol.* **31**, 034001, (2016)
- [2] A. Fiedler et al., *J. Appl. Phys.*, **122**, no. 16, 165701, (2017)
- [3] R. Schewski et al., *APL Mater.* **7**, 022515 (2019)
- [4] Z. Galazka, *Semicond. Sci. Technol.*, **33**, no. 11, 113001, (2018)

NANOMETER-THIN IRON GARNET FILMS GROWN BY LIQUID PHASE EPITAXY

C. Dubs,^a O. Surzhenko,^a R. Thomas,^b J. Osten,^b T. Schneider,^b K. Lenz,^b J. Grenzer,^b R. Hübner,^b
E. Wendler^c

^a INNOVENT e.V. Technologieentwicklung, Prüssingstr. 27B, 07745 Jena, Germany

^b Institut für Ionenstrahlphysik und Materialforschung, Helmholtz-Zentrum Dresden-Rossendorf,
Bautzner Landstr. 400, 01328 Dresden, Germany

^c Institut für Festkörperphysik, Friedrich-Schiller-Universität Jena, Helmholtzweg 3, 07743 Jena,
Germany

E-mail: cd (ad) innovent-jena.de

Summary

Future magnonic components for data processing technology could be used as an integral part of magnon spintronics concepts. They are necessary for large-scale integrated circuit technology beyond standard CMOS applications, since the manipulation of spin waves rather than electron transport processes plays the key role here (see, e.g., [1]).

The ferrimagnetic insulator yttrium iron garnet (YIG) is a promising candidate. Its ultra-low ferromagnetic resonance losses allow long spin wave lifetimes in prospective nanoscopic magnonic waveguide structures in the GHz and THz frequency range. For magnonic applications, however, nanometer-thin epitaxial films, with perfect structural and magnetic properties and large diameters, are required to enable efficient wafer-scale circuit fabrication for a future YIG planar technology.

In our contribution we report on the structural and magnetic properties of 10 to 100-nm-thin YIG films grown by liquid phase epitaxy (LPE) on (111) gadolinium gallium garnet (GGG) substrates [2]. High-resolution X-ray diffraction analysis (HR-XRD), Rutherford backscattering spectrometry (RBS), high-resolution transmission electron microscopy (HR-TEM), and magneto-static and dynamic characterization techniques such as vibrating sample magnetometry (VSM) and ferromagnetic resonance spectrometry (FMR) were used to characterize the sample performance. The results show that both the expected high structural perfection of epitaxial YIG films, and the well-known low magnetic damping of YIG single crystals, are preserved for LPE films down to a film thickness of 20 nm.

Our sub-100-nm-thin LPE YIG films reveal RMS values ranging between 0.2 and 0.4 nm, independent of the film thickness. Sometimes, however, partial remnants of dendritic overgrowth increase the surface roughness to RMS values above 0.4 nm for inspection areas larger than 400 μm^2 .

HR-XRD measurements confirm a fully strained pseudomorphous film growth with perfect coherent in-plane lattice match to the GGG substrate. Besides the nearly symmetrical intensity distribution along the [111] out-of-plane direction, only a very weak diffuse scattering is visibly close to the Bragg peaks; pointing towards a nearly perfect crystal lattice without significant compositional strain or geometric mosaicity. Using the best fit of both, the (444) and (888) reflections, the out-of-plane lattice misfit values $\delta d_{\text{film}}^{\perp}$ were determined and a weak monotonous increase of $\delta d_{\text{film}}^{\perp}$ with decreasing film thickness was observed for films with thicknesses between 106 nm and 21 nm.

For all LPE films studied, the Fe to Y ratio determined by RBS measurements was $R = 1.67$. This corresponds to the ideal iron garnet stoichiometry of $\text{Y}_3\text{Fe}_5\text{O}_{12}$.

HR-TEM investigations show that the LPE technology is suitable for growing nm-thin YIG films without lattice defects and without significant interdiffusion at the film/substrate interface (Fig. 1).

FMR measurements, within a frequency range of 1 to 40 GHz, were carried out to investigate the magnetostatic and dynamic behavior of the nanometer-thin films. A key parameter is the so-called Gilbert damping parameter α , which can be interpreted as the viscous damping contribution of

the movement of the magnetization vector in an external magnetic field. The Gilbert damping coefficient, obtained for sub-100-nm films, is $\alpha \leq 1.3 \times 10^{-4}$ and corresponds to the best values previously reported for 100 nm LPE YIG films [3]. No significant increase in Gilbert damping at room temperature with decreasing film thickness down to 11 nm was observed for LPE films. This correlates with the high microstructural perfection and homogeneity of the volume and interfaces of LPE-grown films with film thicknesses larger than 11 nm.

The magnetic hysteresis loops obtained by VSM measurements show extremely small coercivity fields with H_c values of ~ 0.2 Oe. The determined saturation moments are independent of thickness except for the thinnest sample and are very close to the YIG volume values ($4M_s \sim 1800$ G). The most likely explanation for the observed reduction of the $4\pi M_s$ for the 11-nm-thin film is that the YIG layers at the substrate/film interface exhibit a reduced saturation magnetization due to a magnetically diluted iron sublattice. We assume that the reason for this could be a high-temperature diffusion of gallium ions from the GGG substrate into the YIG film. Curie temperature measurements and SIMS investigations confirm this assumption.

In summary, we are able to show that LPE technology can be used to fabricate sub-100-nm YIG films with high microstructural perfection, smooth surfaces and sharp interfaces, as well as excellent microwave properties down to a minimum film thickness of 21 nm. We expect, that these results will provide the basis for a possible application of nanometer-thin LPE films for the fabrication of nano- and microscaled circuits, such as nano-sized magnonic conduits [4], magnon transistors [5], directional couplers [6] etc. This deposition technique is easily scalable for future YIG sample diameters of several inches.

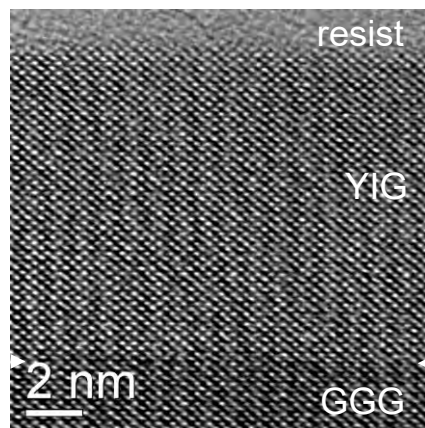


Fig. 1: Cross-sectional HR-TEM image of an 11-nm-thin YIG/GGG (111) LPE film (see also [3]).

Acknowledgment

C. D. and O. S. thank R. Köcher for AFM measurements, A. Hartmann for the DSC measurements and R. Meyer and B. Wenzel for technical support. This research was financially supported by the Deutsche Forschungsgemeinschaft (DFG), via Grant No. DU 1427/2-1.

- [1] A.V. Chumak, V.I. Vasyuchka, A.A. Serga, B. Hillebrands, *Nature Physics*, **11**, 453 (2015)
- [2] C. Dubs et al, *J. Phys. D : Appl. Phys.*, **50**, 204005 (2017)
- [3] C. Dubs et al.; arXiv: 1911.09400 (2019)
- [4] B. Heinz et al.; arXiv: 1910.08801 (2019)
- [5] A.V. Chumak, A.A. Serga, B. Hillebrands, *Nature Communications*, **5:4700** (2014)
- [6] Q. Wang et al.; arXiv 1905.12353 (2019)

Status of 3C-SiC bulk growth using sublimation epitaxy

M. Kollmuß^a, M. Schöler^a, P. Schuh^a, F. La Via^b, M. Mauceri^c, M. Zielinski^d, P. Wellmann^a

^a Crystal Growth Lab, Materials Science Department 6, Friedrich-Alexander-Universität Erlangen-Nürnberg, Martensstraße 7, 91058 Erlangen, GERMANY

^b CNR-IMM, sezione di Catania, Stradale Primosole 50, I-95121 Catania, Italy

^c LPE S.P.A., Sedicesima Strada, I-95121 Catania, Italy

^d NOVASiC, Savoie Technolac, BP267, F-73375 Le Bourget-du-Lac Cedex, France
E-mail: manuel.kollmuss@fau.de

Summary

The cubic polytype of silicon carbide (3C-SiC) has attracted particular interest for decades. 3C-SiC is a promising candidate for power electronic device applications, as well as applications in the field of energy saving, such as intermediate band solar cells (IBSC) [1] and photo-electrochemical water splitting [2]. Some point defects in 3C-SiC are even investigated for future quantum applications [3]. However, the lack of high-quality material with reasonable size and in relevant quantities hinders the breakthrough of this material. High numbers of defects and considerable amounts of stress are still an obstacle and subject of current research.

Since Nishino et al. [4] proposed the pioneering work about a multi-step chemical vapor deposition (CVD) process, significant progress has been made in the growth of high-quality 3C-SiC by CVD. Using such material as seed for a subsequent vapor growth process, thickness as well as quality of the 3C-SiC can be further improved [5-7]. In this work, the growth of high-quality 3C-SiC by sublimation epitaxy (SE) on CVD-grown 3C-SiC-on-Si seeding layers is presented.

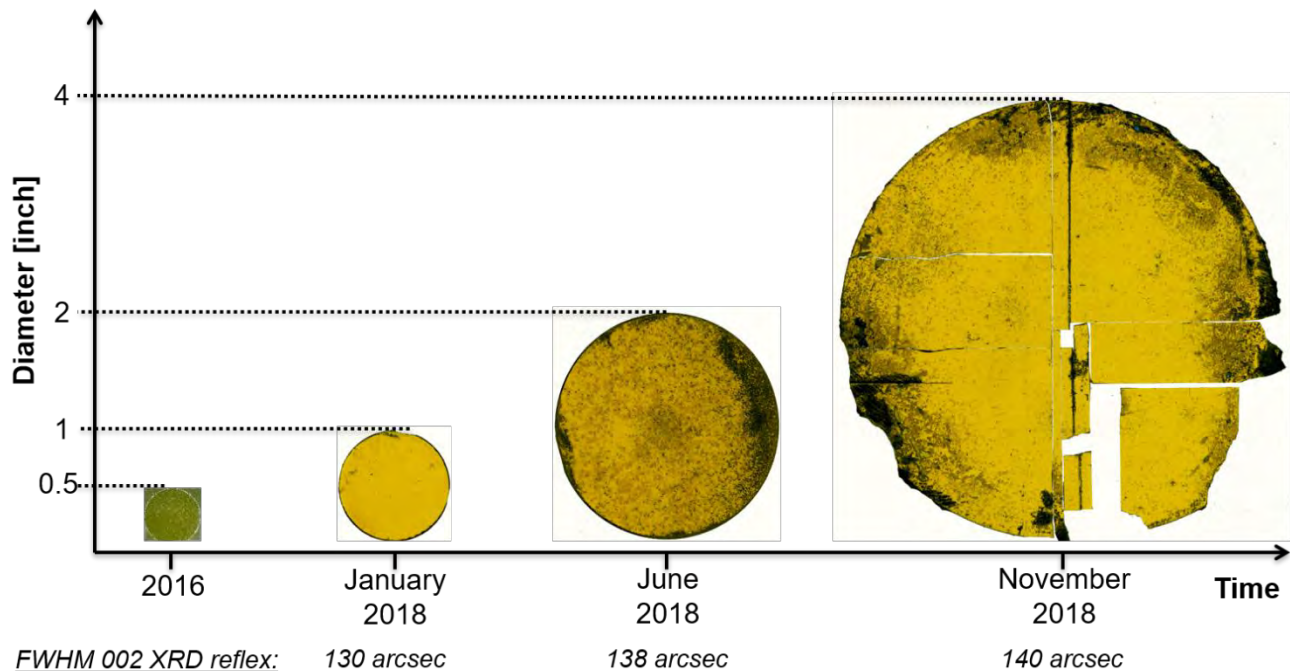


Fig. 1: Evolution of diameters for bulk 3C-SiC crystals grown by sublimation epitaxy. The timeline and the full-width-at-half-maximum (FWHM) values from XRD-rocking curve measurements are indicated.

A method for the reproducible growth of free-standing epitaxial layers up to 52 x 52 mm² using a laser ablation process is presented. The path towards growth of four inch material is presented, too. However, for increased dimensions, cracking of the seeds occurred during wet-chemical etching. The resulting vapor grown layers exhibit a thickness between 320 μm and 520 μm and were grown at growth rates between 190 μm/h and 320 μm/h. All crystals exhibit a bright yellow color which is typical for cubic silicon carbide. XRD analysis and Raman spectroscopy confirmed the growth of the 3C-SiC polytype. Moreover, the analysis of the bulk material proved the growth of stress-free-material. Typical defects in (100) oriented 3C-SiC are stacking faults and protrusions. While the number of stacking faults decreases with increasing thickness of the SE-layer, protrusions can be considered as one of the most critical defects when it comes to the growth of thick, “bulk-like” layers. Protrusions increase in size with increasing layer-thickness. This effect limits the achievable maximal thickness and leads to a surface roughening of the crystal.

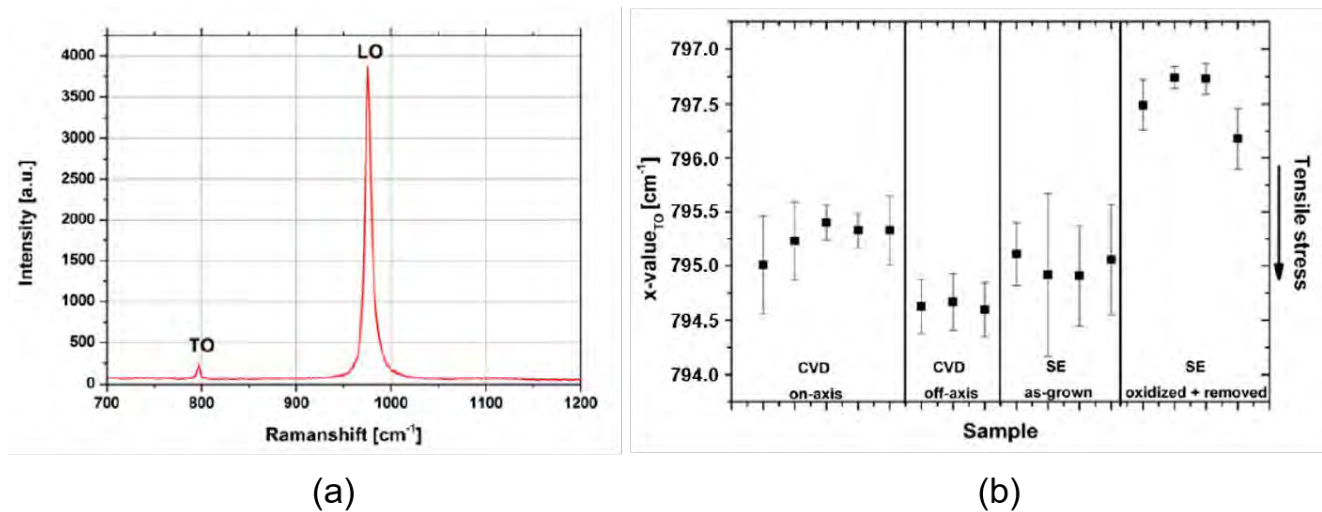


Fig. 2: (a) Raman spectrum of typical sublimation grown material acquired in a protrusion-free surface area. (b) Comparison of the x-value for the transverse optical (TO) Raman mode of 3C-SiC epitaxial layers grown by chemical vapor deposition (CVD) on on-axis and 4° off-axis substrates, homoepitaxial as-grown material produced by epitaxial sublimation growth (SE), and SE-material after temperature treatment.

Acknowledgment

Financial support by the European Union in the frame of the Horizon 2020 program (CHALLENGE project, grant number 720827) is greatly acknowledged.

- [1] M. Syvajarvi et al., *Solar Energy Materials and Solar Cells*, vol. 145, pp. 104-108, (2016).
- [2] N. Ichikawa, M. Kato, and M. Ichimura, *Applied Physics Express*, vol. 8, no. 9, (2015).
- [3] D. J. Christle et al., *Physical Review X*, vol. 7, no. 2, (2017).
- [4] S. Nishino, J. A. Powell, and H. A. Will, *Applied Physics Letters*, vol. 42, no. 5, pp. 460-462, (1983).
- [5] P. Schuh et al., *Journal of Crystal Growth*, vol. 478, pp. 159-162, (2017).
- [6] F. La Via et al., *Materials Science in Semiconductor Processing*, vol. 78, pp. 57-68, (2018).
- [7] M. Schöler, P. Schuh, J. Steiner, and P. J. Wellmann, *Materials Science Forum*, vol. 963, pp. 157-160, (2019).

Session 6
Thursday 12.03.2020
13:00 – 14:20

CRYSTAL GROWTH OF OXIDES AND FLUORIDES AT THE IKZ

Matthias Bickermann, Zbigniew Galazka, Christo Gugushev, Detlev Schulz, Hiroki Tanaka,
Detlef Klimm, Steffen Ganschow, Christian Kränkel, and Thomas Schröder

*Leibniz-Institut für Kristallzüchtung (IKZ), Max-Born-Str. 2, 12489 Berlin, Germany
E-mail: matthias.bickermann@ikz-berlin.de*

Summary

The growth of volume crystals of oxides and fluorides has a long tradition at the IKZ but is also characterized by modern topics with outstanding international visibility. Our publications on the Czochralski method to grow big gallium oxide (β -Ga₂O₃) bulk crystals from the melt are “highly cited” in the field of bulk crystal growth [1,2]. The former head of the IKZ team, Reinhard Uecker, was awarded the IOCG Frank Prize in 2019 (together with Darrell Schlom) for pioneering “strain engineering” by providing substrates for “lattice mis-matched” films [3,4]. Recently, we succeeded in the growth of the first KTb₃F₁₀ bulk crystals that can be used as optical isolators for high-power near infrared lasers.

In the presentation we will show how the preparation of β -Ga₂O₃ substrates of highest structural quality helped to provide a breakthrough in demonstration of novel power electronics devices [5]. Regarding crystal growth, the control of the local oxygen partial pressure is crucial to minimize the formation of suboxides and metallic gallium in the melt that would attack the crucible [2]. The growth of highly n-conductive β -Ga₂O₃ with large diameter remains a challenge, not only due to the self-absorption of heat radiation [1]. Current research is focused on the investigation of the segregation and doping of various elements during growth [6,7]. Also, the preparation and potential applications of gallates with spinel structure such as ZnGa₂O₄ [8] are discussed.

Perovskite-type substrates, originally used to prepare superconducting thin films, have been employed to push the limits of novel ferroelectric, superconducting, ferromagnetic, piezoelectric, multiferroic or high-mobility oxide electronic materials [9]. The rare earth scandates REScO₃ (RE = Dy...Pr) grown at IKZ are in worldwide use to cover any desired pseudo-cubic lattice parameter in the range from about 3.95 to 4.02 Å [3,4]. Recently, novel promising materials with lattice constants in the range of 4.08–4.15 Å have been developed at IKZ jointly with Cornell University [10,11] to accommodate promising thin film materials such as La:BaSnO₃, BiScO₃, BiFeO₃ or PbZrO₃ with high structural quality. This success was strongly based on thermochemical assessments of stability of compounds such as Ba₂ScNbO₆ and BaSnO₃ under melt growth conditions and phase diagram calculations in the La₂O₃–Lu₂O₃–Sc₂O₃–Nd₂O₃ system. We will present these results and also highlight perovskite-type crystals SrHfO₃ and SrZrO₃ grown by the IKZ in collaboration with the Institute of Physics CAS in Prague [12].

Regarding fluorides, we will briefly introduce our activities and demonstrate first crystals of KTb₃F₁₀ that can be used to prepare superior optical isolators. The crystal growth is impeded by a peritectic phase transition slightly below the melting point, while accurate thermodynamic data is not available [13]. Formation of scattering centers as well as oxygen contamination must be mitigated by employing the right off-stoichiometry and purified starting materials.

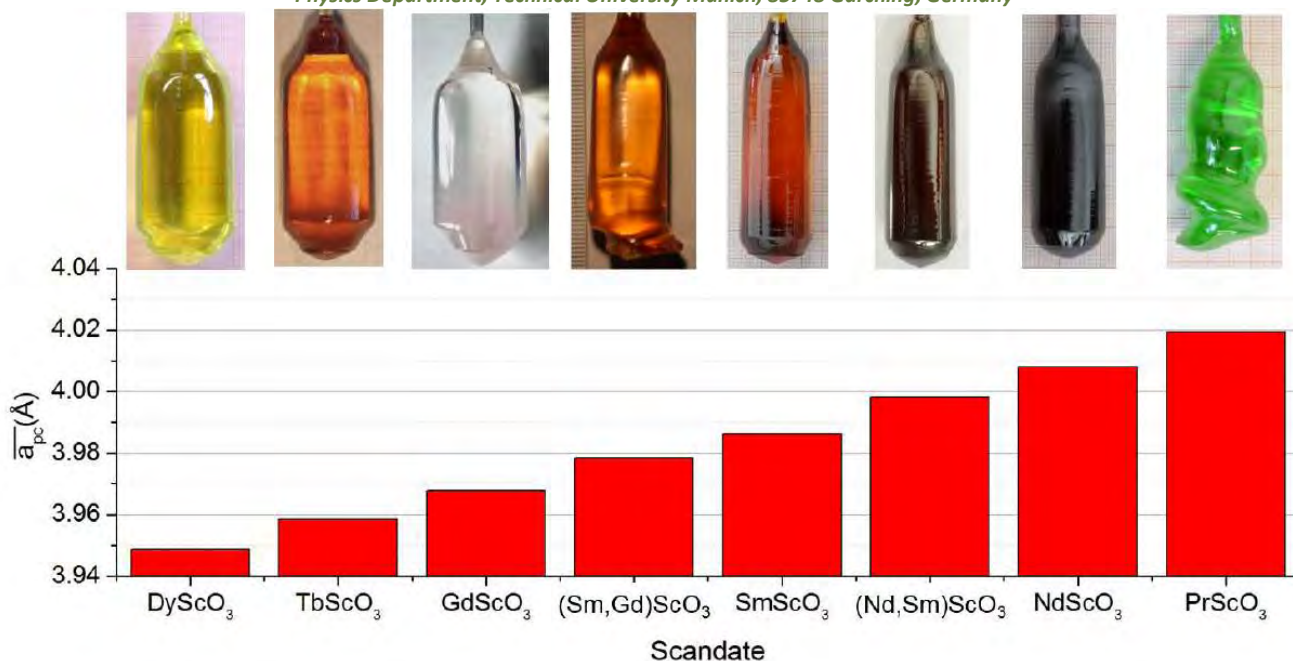


Fig. 1: Pseudo-cubic lattice parameters of different rare earth scandate single crystals (from [4])

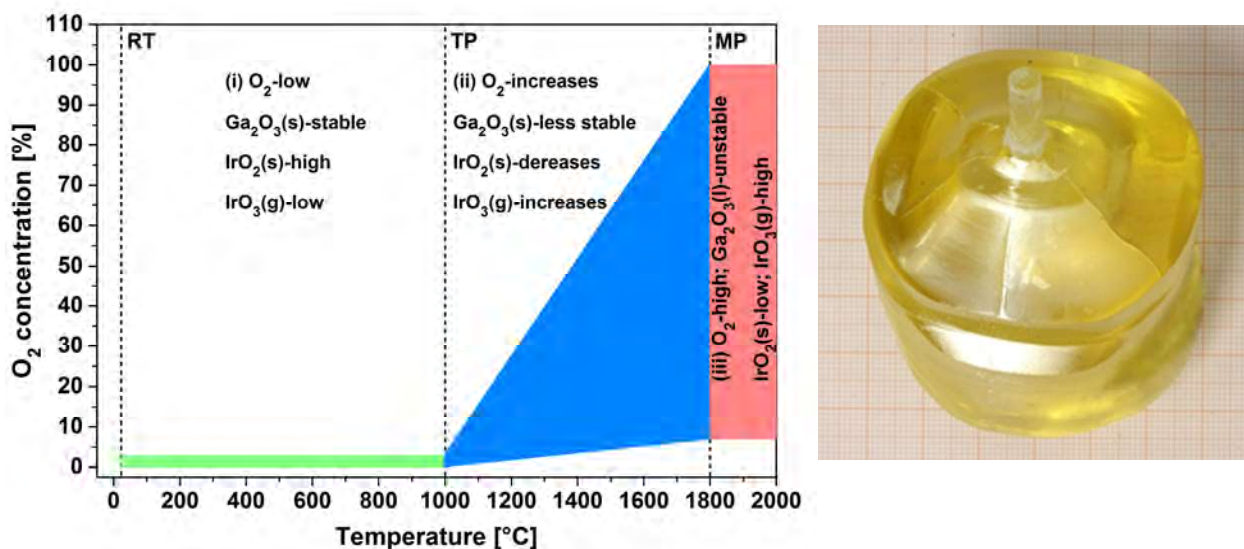


Fig. 2: Oxygen delivery vs. temperature for the growth of large diameter β -Ga₂O₃ single crystals from an Ir crucible (from [2]); 2-inch Al-doped β -Ga₂O₃ single crystal obtained by the Czochralski method (from [6])

- [1] Z. Galazka, K. Irmscher, R. Uecker et al., Journal of Crystal Growth **404** (2014) 184
- [2] Z. Galazka, R. Uecker, D. Klimm et al., ECS Journal of Solid State Science and Technology **6** (2017) Q3007
- [3] R. Uecker, H. Wilke, D.G. Schlom et al., Journal of Crystal Growth **295** (2006) 84
- [4] C. Gugushev, J. Hidde, T.M. Gesing et al., CrystEngComm **20** (2018) 2868-2876
- [5] K. Tetzner, E.B. Treidel, O. Hilt et al., IEEE Electron Device Letters **40** (2019) 1503
- [6] Z. Galazka, S. Ganschow, A. Fiedler et al., Journal of Crystal Growth **486** (2018) 82-90
- [7] Z. Galazka, K. Irmscher, R. Schewski et al., Journal of Crystal Growth **529** (2020) 125297
- [8] Z. Galazka, S. Ganschow, R. Schewski et al., Applied Physics Letters Materials **7** (2019) 022512
- [9] H.J. Haeni, P. Irving, W. Chang et al., Nature **430** (2004) 758
- [10] R. Uecker, R. Bertram, M. Brützam et al., Journal of Crystal Growth **457** (2017) 137–142
- [11] C. Gugushev, D. Klimm, M. Brützam et al., Journal of Crystal Growth **528** (2019) 125263
- [12] J. Pejchal, C. Gugushev, M. Schulze et al., Optical Materials **98** (2019) 109494
- [13] K.T. Stevens, W. Schlichting, G. Foundos et al., Laser Technik Journal (Wiley) 03/2016, p. 18

Growth of high-melting sesquioxides for laser applications

A. Uvarova, C. Gugushev, M. Bickermann and C. Kränkel

Leibniz-Institut für Kristallzüchtung, Max-Born-Straße 2, 12489 Berlin, Germany
E-mail: anastasia.uvarova@ikz-berlin.de

Lasers in the mid-infrared range are attractive in fields like laser surgery or atmospheric detection, due to the strong absorption of water in this spectral region. To achieve good beam quality and stable high-power laser operation, good mechanical, optical, and thermal properties are essential for potential laser materials. The rare-earth sesquioxide crystals Lu_2O_3 , Sc_2O_3 , and Y_2O_3 have been shown to be very suitable for high-power mid-infrared laser operation due to their high thermal conductivity and low phonon energies.

Despite these promising results, the growth of sesquioxide crystals with high optical quality is very challenging due to their high melting temperatures of more than 2400 °C. These materials were previously grown by the heat exchanger method from rhenium crucibles, as this is the only crucible material that is suitable for such crystals [1]. This method has shown good results, but the Re-crucibles are very sensitive to oxygen, which requires a very precise control of the growth atmosphere. Moreover, the fabrication of Re-crucibles is very expensive and thus this growth method is not suitable for commercial use.

Here, we report on the application of the optical floating zone technique (OFZ) for the growth of high-melting sesquioxide crystals to avoid the use of expensive and sensitive crucible materials. This method has several advantages compared to previous growth methods. It is crucible free and does not require zirconia insulation. Therefore, high oxygen partial pressures and free choice of the growth atmosphere are possible.

By using our high-pressure high-temperature OFZ furnace undoped Lu_2O_3 , as well as Er^{3+} and Yb^{3+} -doped Lu_2O_3 crystals were grown (Fig. 1). The growth experiments were carried out under Ar atmosphere at elevated pressure, the growth speed was varied between 2 mm/h and 7.5 mm/h at a lamp power of 5 kW. The pressed powder feeding rods were made from 5N purity powders. The doped rods were prepared by mixing Lu_2O_3 and Er_2O_3 or Lu_2O_3 and Yb_2O_3 powders, respectively, by using a 3-dimensional mixer. All rods were pressed in an isostatic press and then sintered in the oven.

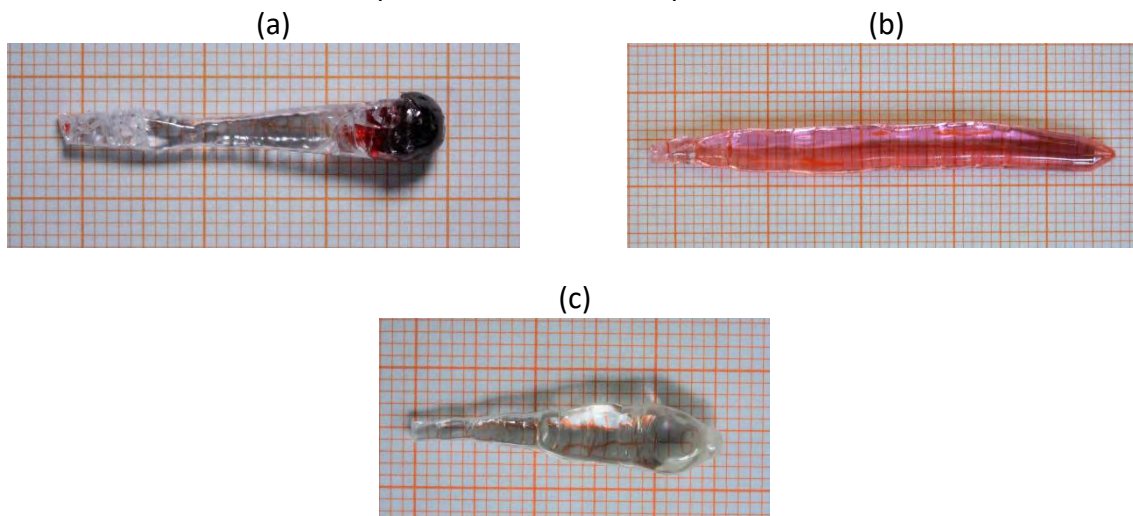


Fig. 1: Lu_2O_3 (a), Er^{3+} (b) and Yb^{3+} -doped Lu_2O_3 (c) crystals grown by the optical floating zone method.

In future, we aim to utilize these crystals for laser experiments to advance the progress in 3 μm laser operation with Er^{3+} -doped and 1 μm laser operation with Yb^{3+} -doped sesquioxides. We are convinced that the OFZ-technique is a well suited method for the growth of rare-earth doped sesquioxide crystals for laser applications.

[1] R. Peters, C. Kränkel, K. Petermann, and G. Huber, "Crystal growth by the heat exchanger method, spectroscopic characterization and laser operation of high-purity $\text{Yb}:\text{Lu}_2\text{O}_3$ ". J Cryst. Growth, 310(7-9), 1934-8, 2008

**COMMEMORATIVE EVENT
50 YEARS DGKK
Schüler Preis
DGKK Nachwuchspreis
DGKK Preis
Thursday 12.03.2020
14:50 – 17:50**

Solution Growth as a Powerful Tool for the Solid-State Physicist

A. Jesche^a

^a EP VI, Center for Electronic Correlations and Magnetism, Institute of Physics,
University of Augsburg, D-86159 Augsburg, Germany
E-mail: anton.jesche@physik.uni-augsburg.de

Summary

Whether for optimization of sample size and quality, detailed substitution series or exploratory work: solution growth is a versatile tool that offers many benefits. Once a suitable solvent (or flux) is found, the growth can be performed at reduced reaction temperature, reduced vapor pressure, and with small amounts of material (compared to using mirror furnaces, Czochralski or Bridgeman methods). Furthermore, an ‘in situ purification’ of the starting materials is often associated with crystallization from solutions.

I’m going to show how the successful single crystal growth from solution allowed for immediate progress in understanding various, primarily magnetic and superconducting materials. A couple of representative single crystals is shown in Fig. 1.

First example is the prominent family of FeAs high-temperature superconductors with critical temperatures of more than 50 K. Elevated synthesis temperatures beyond 1000°C in combination with the high vapor pressure of As pose a particular challenge. FeAs self-flux [1], KI salt flux [2], and Sn flux [3] were successfully applied to grow single crystals of several millimeter along a side. Those samples allowed to solve the magnetic structure and revealed important similarities and differences to the cuprate superconductors.

A significant number of binary systems with known crystal structure but unknown physical properties were grown as single crystals and investigated by temperature-dependent magnetization, specific heat and electric transport. Interesting and unexpected was, for example, the observation of strong quantum oscillations in the large-unit-cell compound Cu_{13}Ba [4] and nearly-itinerant ferromagnetism in CaNi_2 and CaNi_3 [5].

The latter were grown from Ca-rich flux that is highly reactive and required some effort in designing suitable crucibles that were made from Nb or Ta. Such crucibles were also used to grow single crystals from Li flux. Several Li-based materials and in particular various nitrides were successfully grown [6], for example pure and transition-metal doped Li_3N , Li_4SrN_2 , and $\text{LiSr}_2\text{CoN}_2$. A significant increase of the solubility of transition metals in Li is caused by the presence of N.

A completely unexpected side product was the growth of single crystalline α -Fe in Li-N flux [7]. We have found well faceted, rhombic dodecahedral α -Fe single crystals with diameters in the range of millimeters.

Furthermore, there is ongoing progress in the development of a ‘feedback’ furnace that allows for the in-situ detection of nucleation from a melt [8]. Liquidus temperature and other phase transitions are determined directly in the crystal growth apparatus leading to significantly improved process control and efficiency. Larger single crystals can be obtained by seed selection and slow cooling rates in the vicinity of the liquidus as shown for α -PdBi.

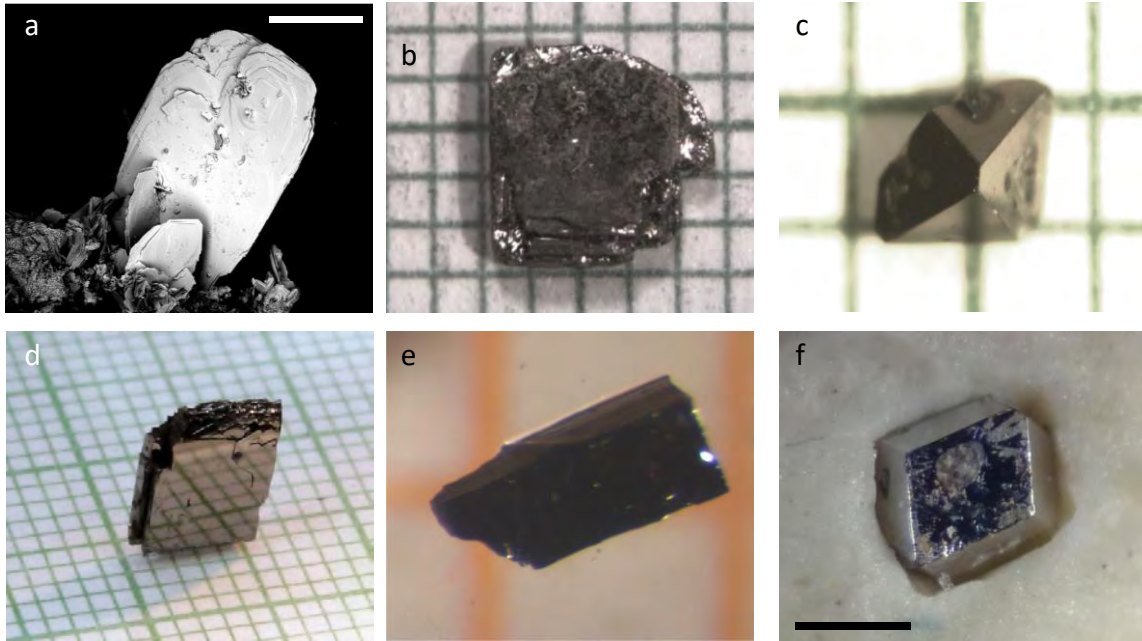


Fig. 1: Selection of single crystals obtained from high-temperature solution growth. a) CeFeAsO grown from KI flux. b) Cu_{13}Ba grown from $\text{Ba}_{38}\text{Cu}_{62}$. c) CaNi_2 grown from $\text{Ca}_{67}\text{Ni}_{33}$. d) Li_3N grown from $\text{Li}_{90}\text{N}_{10}$. e) Fe-substituted Li_4SrN_2 grown from Li-rich flux. f) $\alpha\text{-Fe}$ grown from $\text{Li}_{84}\text{N}_{12}\text{Fe}_3$. Scalebar in a) and f) is 0.5 mm, all other samples are shown on millimeter grid.

To summarize, “the ‘we find solutions’ approach is based on the development of broadly versatile melts that will allow for the explorations of a new sets of phase spaces; new pathways into a poorly explored part of the forest... hic sunt leones.” [9]

Acknowledgment

C. Krellner, C. Geibel, P.C. Canfield, A.A. Tsirlin, and P. Gegenwart are acknowledged for various fruitful conversations. The author thanks R. Weise, A. Herrnberger, and K. Wiedenmann for technical support. A cooperative project with the ScIDre GmbH (Dresden) was funded by the ZIM program of the German Ministry for Economic Affairs and Energy (BMWi). This work was supported by the Deutsche Forschungsgemeinschaft (DFG, German Research Foundation) - Grant No. JE748/1.

- [1] M. Kumar, M. Nicklas, A. Jesche, N. Caroca-Canales *et al.* Phys. Rev. B **78**, 184516 (2008)
- [2] F. Nitsche, A. Jesche, E. Hieckmann, T. Doert, and M. Ruck, Phys. Rev. B **82**, 134514 (2010)
- [3] A. Jesche, C. Krellner, M. de Souza, M. Lang, and C. Geibel, Phys. Rev. B **81**, 134525 (2010)
- [4] A. Jesche, S.L. Bud’ko, and P.C. Canfield, J. Alloys Compd. **587**, 705–709 (2014)
- [5] A. Jesche, K.W. Dennis, A. Kreyssig, and P.C. Canfield, Phys. Rev. B **85**, 224432 (2012)
- [6] A. Jesche and P.C. Canfield Philos. Mag. **94**, 2372–2402 (2014)
- [7] M. Fix, H. Schumann, S.G. Jantz, F.A. Breitner *et al.* J. Cryst. Growth **486**, 50 (2018),
- [8] A.G.F. Schneider, P. Sass, R. Schöndube, and A. Jesche Cryst. Res. Technol. **1900109** (2019)
- [9] P.C. Canfield, Prog. Phys. **83**, 016501 (2020)

MOVPE GROWTH OF GaAs WITH GROWTH RATES UP TO 280 $\mu\text{m}/\text{h}$

R. Lang^a, F. Habib^b, M. Dauelsberg^b, F. Dimroth^a, D. Lackner^a

^a Fraunhofer Institut für Solare Energiesysteme, Heidenhofstraße 2, 79110 Freiburg, Germany

^b AIXTRON SE, Dornkaulstraße 2, 52134 Herzogenrath, Germany

E-mail: robin.lang@ise.fraunhofer.de

Metal organic vapor phase epitaxy (MOVPE) of III-V compound semiconductors is a well-established technique used in industry for the production of multi-junction solar cells, LEDs, or lasers. MOVPE grown III-V multi-junction solar cells outperform all other solar cells in terms of efficiency. Still, the epitaxial production process is time consuming and expensive due to moderate growth rates and the inefficient use of the precursor materials. In this work, we address both issues simultaneously by increasing the growth rate and optimizing the process conditions of the reactor chamber. Additionally, we show the influence of high growth rates on material and solar cell properties. All samples were grown with an AIXTRON CRIUS Close-Coupled Showerhead reactor in a 7x4" configuration. In this reactor design, the gap distance between ceiling and susceptor can be adjusted. Standard precursors including TMGa, TMIn, TMAI, PH₃, and AsH₃ were used. A dual-layer anti-reflection coating (ARC) was applied to the solar cells and they were measured under the AM1.5g spectrum.

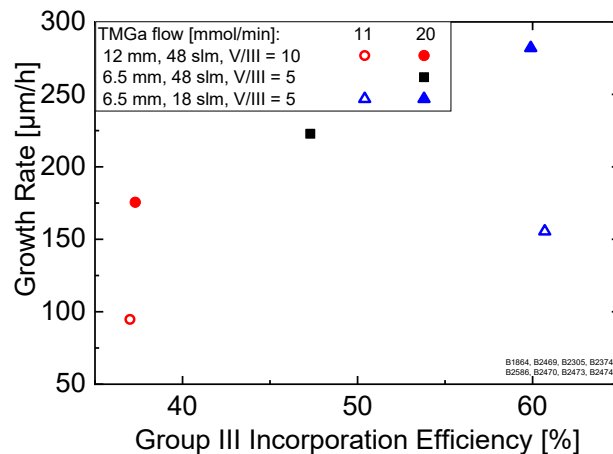


Fig. 1: GaAs growth rate plotted versus the incorporation efficiency of TMGa, calculated for one 12" wafer for different reactor conditions.

We demonstrate that growth rates up to 280 $\mu\text{m}/\text{h}$ for GaAs with group III incorporation efficiencies above 60 % are possible using MOVPE (see Fig. 1) [1]. These values were achieved by increasing the concentration gradient between the showerhead and the substrate and therefore the material transport to the wafer surface. In this reactor type, the concentration gradient can be increased by reducing the process gap height as well as the total H₂ carrier gas flow. The experimental results could be reproduced both by accurate numerical simulation [2] and with a simple calculation using a control volume ansatz. Furthermore, the influence of the growth rate on properties like surface morphology, surface roughness, growth rate homogeneity and background doping was studied. In terms of solar cell properties, the minority carrier diffusion length and the solar cell performance were investigated up to growth rates of 140 and 100 $\mu\text{m}/\text{h}$, respectively [3] (see Fig. 2 and Table 1).

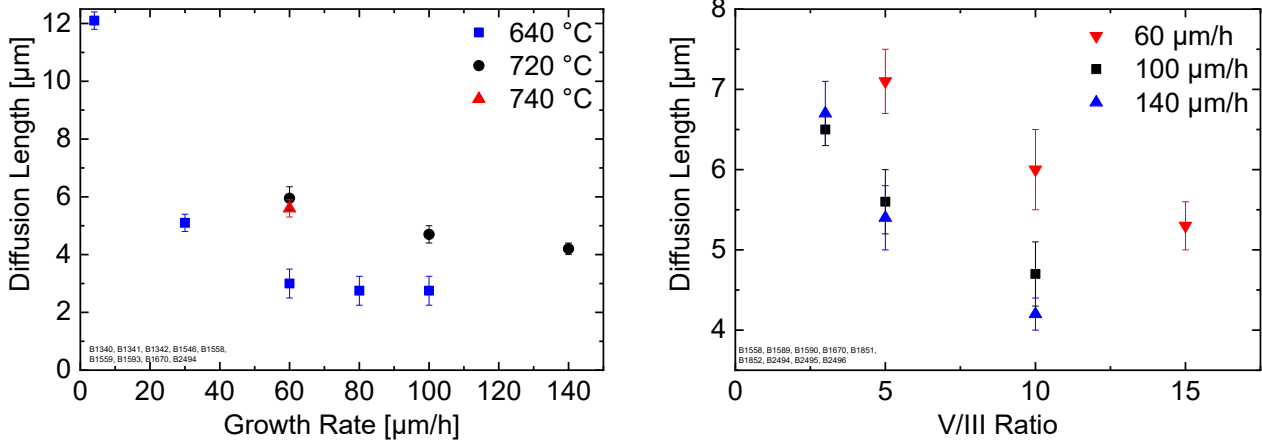


Fig. 2: Diffusion length in $2 \cdot 10^{17} \text{ cm}^{-3}$ doped p-GaAs plotted versus the growth rate for different growth temperatures at a V/III ratio of 10 (A) and versus the V/III ratio for different growth rates at a growth temperature of 720°C (B).

Table 1: Best 4 cm^2 cell results (measured under the AM1.5g spectrum).

Growth Rate [$\mu\text{m}/\text{h}$]	T_G [$^\circ\text{C}$]	V/III Ratio	V_{oc} [V]	J_{sc} [mA/cm^2]	FF [%]	η [%]
4	640	10	1.055	28.6	81.6	24.6
60	720	5	1.036	28.4	79.7	23.5
80	720	5	1.021	28.3	80.9	23.4
100	720	5	1.019	28.3	81.1	23.3
100	720	3	1.028	28.5	80.7	23.6

We found that an increase in the growth rate leads to a reduction of the diffusion length from 12 to $2.5 \mu\text{m}$ if all other parameters are kept constant. This is attributed to an increase in the amount of EL2 defects which is connected to As antisites (As_{Ga}) [4]. Higher growth temperatures and lower V/III ratios can suppress the formation of As_{Ga} and thus the diffusion length recovers. In the end, we achieved a diffusion length of more than $6 \mu\text{m}$ at a growth rate of $140 \mu\text{m}/\text{h}$. The combination of high growth rates and low V/III ratios opens up opportunities for significant cost reduction for the III-V epitaxy growth.

Solar cell measurements reflect the diffusion length results (Table 1). At a growth rate of $100 \mu\text{m}/\text{h}$, an open-circuit voltage of 1.028 V and an efficiency of 23.6 % under the AM1.5g spectrum were achieved at a V/III as low as three. This is only 1.0 %_{abs} below a reference solar cell grown at a growth rate of $4 \mu\text{m}/\text{h}$. The results show the potential of using MOVPE to reach lower cost GaAs epitaxy through the optimization of growth conditions.

Acknowledgment

The authors would like to acknowledge financial support by the German Federal Ministry of Education and Research under Grant “MehrSi” 03SF0525A and by the Marie Skłodowska-Curie “ENHANCE” Grant Agreement 722496.

- [1] R. Lang, F. Habib, M. Dauelsberg, F. Dimroth, D. Lackner, submitted to Journal of Crystal Growth
- [2] D. Brien, M. Dauelsberg, K. Christiansen, J. Hofeldt, M. Deufel, M. Heuken, Journal of Crystal Growth, **303**, 1, 330-333 (2007)
- [3] R. Lang, J. Schön, F. Dimroth, D. Lackner, IEEE Journal of Photovoltaics, **8**, 6, 1596-1600 (2018)
- [4] K. J. Schmieder, E. A. Armour, M. P. Lumb, M. K. Yakes, Z. Pulwin, J. Frantz, R. J. Walters, IEEE Journal of Photovoltaics, **7**, 1, 1596-1600 (2017)

The “amazing” group-III nitrides – epitaxy for optical and electronic applications

Stacia Keller^a

^a *Electrical & Computer Engineering Department, University of California Santa Barbara,
Santa Barbara, CA 93106, USA
E-mail: stacia@ece.ucsb.edu*

In the past decades group-III nitride technology has developed at an enormous pace. Optical devices such as LEDs and lasers have become part of everyday life in light bulbs, street lights, automotive lights, or digital cinema. Less visibly, electronic applications have emerged and (Al,Ga)N transistors are utilized in base stations, communications and RADAR. The application of (Al,Ga,In)N materials for electronic components is, however, still evolving. The large band gap, the high breakdown field, and the high electron mobility make group-III nitride based transistors attractive in particular for high power and high frequency applications.

One current direction of research is the exploration of nitride based transistors for 5G communication networks. In this area, new developments in epitaxial growth have led to a breakthrough in the device performance. In difference to traditional group-III nitride devices, which are typically based on epitaxial layers grown in the Ga-polar (0001) direction of the hexagonal lattice, these novel devices are fabricated via growth in the N-polar (000-1) direction, taking advantage of the opposite direction of the internal electric fields in N- compared to Ga-polar III-N heterostructures. While N-polar nitrides were explored early on, their utilization for device applications was hampered by their poor structural properties and high residual impurity concentrations. In particular films grown by metal-organic chemical vapor deposition, the most common epitaxial technique used for the deposition of III-N heterostructures, exhibited dense arrays of surface defects, which were believed to be immanent to the N-polar growth direction. A closer look at the impact of the epitaxial growth parameters, however, indicated that limitations in the surface mobility of adsorbed species may play a role in the defect formation. Adjustments in the growth procedure allowed the deposition of high purity N-polar III-N films on sapphire, SiC, and (111) silicon substrates and enabled the fabrication of N-polar transistors demonstrating a record output power density of 8.8 W/mm at 94 GHz with a power added efficiency of 27%. [1,2]

Another area of intense research is the fabrication of micro-LEDs for display applications, which led to an increased interest in nitride LEDs with InGaN active regions emitting at wavelength longer than green. The demonstration of high performance LEDs emitting in the yellow and red, however, poses several challenges, one being the large 10 % lattice mismatch between InN and GaN. In order to mitigate the lattice mismatch between base material and active region, substrates with a lattice constant larger than GaN are very attractive. One possible path is the fabrication of relaxed InGaN pseudo-substrates. Two approaches will be discussed. The first involves the coalescence of relaxed III-nitride nano-features, utilizing the natural relaxation observed in the nanoscale. [3] The second, more recently pursued technique takes advantage of the reduced mechanical stiffness of porous GaN, allowing the demonstration of relaxed and partially relaxed InGaN-on-porous-GaN 10 μm x 10 μm tile arrays. [4] Such pseudo-substrates have the potential to catalyze the development of full color micro-LED arrays.

[1] S. Keller et al., *Semicond. Sci. Technol.* **29**, 113001 (2014).

[2] B. Romanczyk et al., *IEEE Electron Device Letters*, Early Access Article DOI 10.1109/LED.2020.2967034 (2020).

- [3] S. Keller et al., *Semicond. Sci. Technol.* **30**, 105020 (2015).
- [4] S. Pasayat et al., *Materials* **13**, 213 (2020).

Session 7
Friday 13.03.2020
8:30 – 10:20

Model experiments for crystal growth

K. Dadzis ^a, O. Pätzold ^b, G. Gerbeth ^c

^a Leibniz-Institut für Kristallzüchtung (IKZ), Max-Born-Straße 2, 12489 Berlin, Germany

^b Institute of Nonferrous Metallurgy and Purest Materials, TU Bergakademie Freiberg,
Leipziger Str. 34, 09599 Freiberg, Germany

^c Institute of Fluid Dynamics, Helmholtz-Zentrum Dresden - Rossendorf, Bautzner Landstraße 400,
01328 Dresden, Germany

E-mail: kaspars.dadzis@ikz-berlin.de

Summary

Numerical simulations are widely used for process development and equipment design for crystal growth both on research and industrial scales. The underlying physical models require measurement data for validation. However, many crystal growth processes take place at high temperatures in a vacuum-sealed atmosphere, which significantly limits in-situ observation. Therefore, dedicated *model experiments* are applied, where the relevant physical phenomena are transferred (more exactly – scaled) to a model system working with a model material and having an appropriate in-situ access. We have recently reviewed the use of such model experiments to investigate melt and gas flows in crystal growth [1]. Two prominent examples are Czochralski (CZ) growth and directional solidification (DS) of silicon.

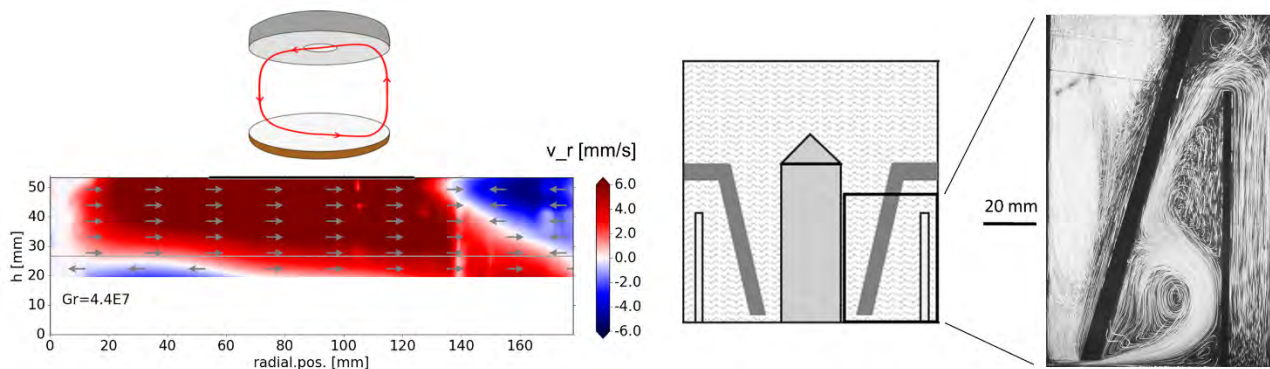


Fig. 1. Velocity measurements in model experiments for the CZ process: melt flow with an asymmetric structure (left); gas flow around the heat shield (right). See [1] for details.

Melt flow in the CZ Si growth has been modelled using liquid metal alloys such as GaInSn in heated containers with diameters up to 800 mm (see [1] and references therein). Early studies were focusing on the influence of various AC and DC magnetic fields and performed detailed measurements of the temperature field, which enabled the validation of turbulence models [2]. Application of ultrasonic velocity measurements recently revealed the presence of unexpected asymmetric flow patterns, which have not been fully explained by numerical simulation yet (see Fig. 1). What are appropriate boundary conditions for the temperature and velocity? Which turbulence models and discretization parameters are suitable? Such questions are still under active discussion today as demonstrated by recent simulations for the 300 mm CZ Si process [3]. Gas flows in CZ growth have been modelled using isothermal model liquids to describe the forced flow around the heat shield (see Fig. 1). While no comparisons with simulations have been published yet, the experiments have provided important hints about the long-range influence of inlet conditions and about the presence of 3D instabilities.

Model experiments with liquid metals for the melt flow in DS Si growth under AC magnetic fields have reached melt width up to 420 mm (see [1] and references therein). Advanced ultrasonic measurements of the 2D velocity fields in an experimental parameter study have enabled the classification of a large number of flow structures [4]. Although the corresponding numerical models still need further validation for the interaction with the solid-liquid boundary in particular, the confidence in the modeling results has been greatly improved.

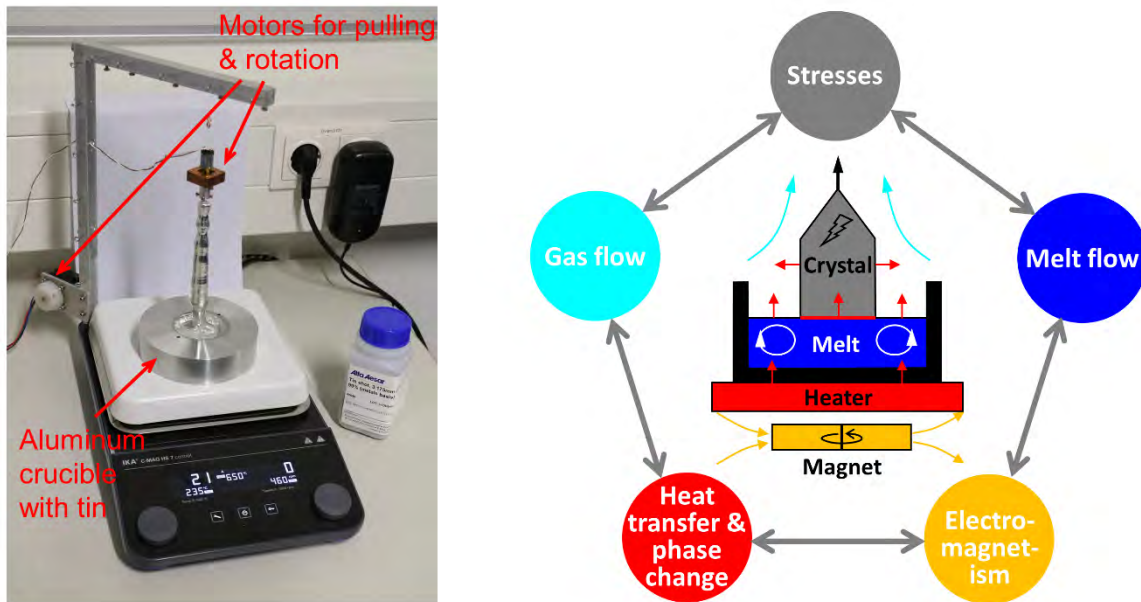


Fig. 2. Multi-physical model experiments for crystal growth: demo setup with CZ growth of Sn (left) and sketch of physical phenomena (right).

Melt and gas flows in crystal growth are a part of a larger landscape of interacting physical phenomena on several time and length scales. This physics landscape is common to many crystal growth processes – from the century-old experiments by Jan Czochralski with molten metals to industrial CZ pullers for 300 mm Si monocrystals. Fig. 2 shows a modern version of Czochralski's experiment and selects the key physical phenomena. It is important to realize that every crystal growth experiment needs to manage all these aspects. And every complete crystal growth simulation needs to include validated models (also, validated simplifications) of all these aspects. But how can we perform the necessary in-situ measurements for the validation of such coupled models? Note that the requirements for the modeling accuracy increase if we want to analyze complex phenomena such as transport of oxygen in solid, liquid and gas phases in CZ growth of Si.

These questions are being addressed within the Starting Grant NEMOCRYG funded by the European Research Council (ERC) for the time period Feb 2020 – Jan 2025 at the IKZ. We will develop accessible multi-physical model experiments for crystal growth and integrate modern measurement techniques (infrared imaging, ultrasonic velocimetry, etc.). The obtained in-situ measurement data will be used to reach a new level of physical understanding and establish a new generation of multi-physical models for crystal growth processes.

- [1] K. Dadzis, O. Pätzold, G. Gerbeth, *Cryst. Res. Technol.*, 1900096 (2019).
- [2] A. Krauze, N. Jekabsons, A. Muiznieks, A. Sabanskis, U. Lacis, *J. Cryst. Growth*, **312**, 3225–3234 (2010).
- [3] V. Kalaev, *J. Cryst. Growth*, **532**, 125413 (2020).
- [4] N. Thieme, M. Keil, D. Meier, P. Bönisch, K. Dadzis, O. Pätzold, M. Stelter, L. Büttner, J. Czarske, *J. Cryst. Growth*, **522**, 221–229 (2019).

NUMERICAL MODELING OF METALLIC IMPURITY INCORPORATION DURING DIRECTIONAL SOLIDIFICATION OF MULTI-CRYSTALLINE SILICON ASSISTED BY EXPERIMENTAL PROOF

S. Schwanke^{a*}, K. Schuck^a, T. Jung^a, M. Trempa^a, C. Kranert^b, C. Reimann^{a,b}, M. Kuczynski^c, G. Schroll^c,
J. Sans^c, J. Stenzenberger^d, K. Hesse^d, J. Heitmann^b, J. Friedrich^{a,b}

^aFraunhofer IISB, Schottkystr. 10, 91058 Erlangen, Germany

^bFraunhofer THM, Am St.-Niclas-Schacht 13, 09599 Freiberg, Germany

^cAlzChem Trostberg GmbH, Dr.-Albert-Frank-Str. 32, 83308 Trostberg, Germany

^dWacker Chemie AG, Johannes-Hess-Straße 24, 84489 Burghausen, Germany

E-mail: Stanislaus.schwanke@iisb.fraunhofer.de

Summary

During the crystallization process of multi-crystalline silicon (mc-Si) metal impurities (like Fe, Co etc.) are mainly incorporated into the silicon melt and hence into the ingot via diffusion from the quartz crucible through the silicon nitride (Si_3N_4) coating or from the coating itself. As a consequence, the highly contaminated peripheral areas of the grown ingots known as “redzones” cannot be used for further production of solar cells resulting in a high wafer yield loss, as well as the ingot center is limited in electrical performance due to fast diffusing metal impurities.

In order to get a better understanding of the metal impurity input during the crystallization process two numerical models were developed and evaluated by comparison to real annealing and crystallization experiments. The 1D model, which was written in the programming language Python [1], describes the solid-state diffusion of metals from Si_3N_4 coated crucible substrates into silicon blocks during annealing experiments and was used to identify suitable diffusion parameters. Afterwards these parameters were transferred to a 2D crystallization model, which is based on a self-written solver using the finite volume method and is implemented in the C++ program package OpenFOAM [2]. For validation of the numeric models several annealing experiments using mono-crystalline Cz blocks $70 \times 70 \times 55 \text{mm}^3$ in size were performed and mc-Si ingots with a weight of 15kg were grown in a Vertical Gradient Freeze (VGF) furnace, while different consumables (ceramic silica crucible, Si_3N_4 coating and silicon feedstock) with varying purity levels were used. The numerically calculated metal profiles along the block/ingot height were compared to measured Fe_i -profiles and metal concentrations determined by neutron activation analysis (NAA). Furthermore, numerically observed differences in the metal content between the grown ingots were qualitatively compared to the trends derived from carrier-lifetime measurements.

It will be shown that the trends from the real experiments can be directly predicted using the numerical models. Afterwards, the numerical crystallization model is scaled up to the industrial G6 scale and an overview about the correlation between the purity variations of the raw materials and the effect on the red zone expansion as well as the lifetime values of the center region will be shown. Purity variations of the Si_3N_4 coating and feedstock come only into effect in modern setups containing crucible diffusion barriers. In this case, the redzone expansion among others can be decreased down to 35%, if the Fe concentration of the coating would be reduced by one order of magnitude, while the full potential is limited by the contamination level of the silicon feedstock.

Acknowledgment

These research and development activities were carried out within the SYNERGIE project (0324150) funded by the German Federal Ministry for Economic Affairs and Energy.

- [1] Van Rossum, G., Python programming language, In USENIX Annual Technical Conference (2007)
- [2] OpenFOAM 4.x UserGuide, 2011-2019 OpenFOAM Foundation Ltd., Berkshire, UK

Forced convection by high-speed rotation in Czochralski growth from high-temperature solutions

O. Harder^a, P. Eschenbacher^a, E. Hanfstaengl^a, K. Dadzis^b, P. Gille^a

^a *Sektion Kristallographie, Ludwig-Maximilians-Universität München, Theresienstraße 41, 80333 München, Germany*

^b *Leibniz-Institut für Kristallzüchtung (IKZ), Max-Born-Straße 2, 12489 Berlin, Germany*
E-mail: oliver.harder@campus.lmu.de

Summary

In crystal growth of intermetallics, the Czochralski method has proved to be a powerful technique for bulk single crystals [1]. Many intermetallic compounds show peritectic melting behavior and can, therefore, only be crystallized from incongruent melts below their decomposition temperature. Combined with a restricted solubility, mass transport in the solution next to the growth interface is the limiting factor for growth rates and inclusion-free single crystal growth. Various techniques of forced convection, e.g. ACRT [2] or IRB [3], are known from literature to effectively suppress inclusion formation due to increased mass transport. Since the Czochralski method uses crystal and crucible counter-rotation anyway, we carried out a combined experimental and numerical modelling study to investigate the influence of high crystal rotation rates on mass transport in the Czochralski growth of intermetallic compounds from metallic solutions.

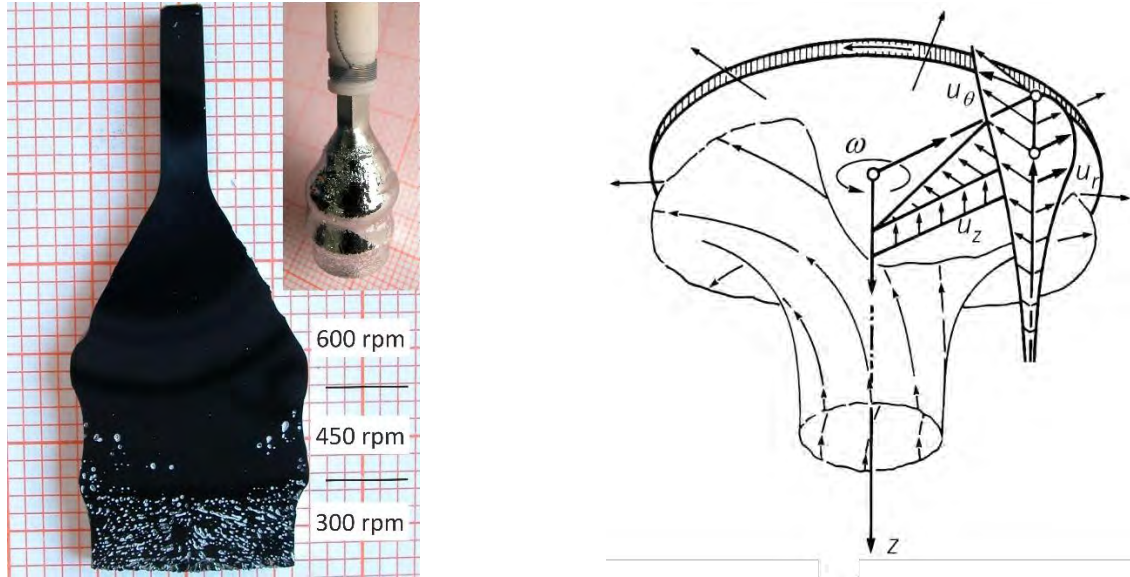


Fig. 1: Ga₃Ni₂ single crystal and inclusion distribution at varying crystal rotation rates (left). Schematic drawing of the rotating-disk model according to Hurle [5] (right).

As a first approximation, the rotating crystal can be described as a rotating disc attached to the melt surface. In this model, mass transport in the melt close to the crystal is dominated by diffusion in a boundary layer while convection dominates the remainder of the melt. This general case was analytically solved long time ago [4] and has been treated for Czochralski growth purposes by Hurle [5]. Its key idea is a reduced diffusion boundary layer (also named Ekman layer) thickness δ depending on the disc's rotation rate ω according to $\delta \sim (\nu/\omega)^{1/2}$ for a melt with kinematic viscosity ν .

Experimentally, several single crystal growth experiments were conducted in a modified self-built Czochralski apparatus using crystal rotation rates of up to 600 rpm. Ga_3Ni_2 and Ga_7Pd_3 served as model compounds due to their well-known tendency for severe inclusion formation at usual growth conditions. Despite such conditions, inclusion-free single crystal growth of Ga_3Ni_2 and Ga_7Pd_3 could be demonstrated with crystal rotation rates exceeding 400 rpm.

Further understanding about the impact of rotation rates and changes in rotation rates on the crystal growth dynamics was gained from experiments. As expected, there seems to be a critical rotation rate at which a system of formerly inclusion-free growth changes to the usual state of high inclusion density when the crystal rotation rate is lowered. Additionally, we could demonstrate that a state of abundant inclusions can return to one of inclusion-free growth. Lastly, we observed the impact of a sudden change in rotation rates on crystal growth dynamics.

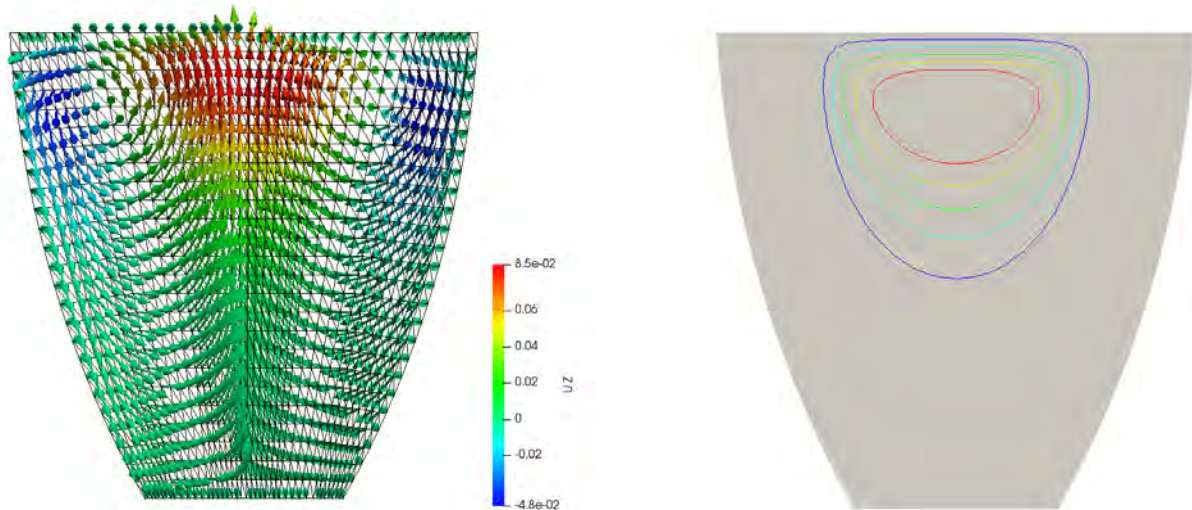


Fig. 2: Velocity vector field (in m/s) of fluid flow in a crucible (ratio of crystal to crucible radii 0.7) established by a crystal rotating with 600 rpm (left). Isolines of the vertical velocity component indicating the geometry of the boundary layer (right).

Numerical simulations with the computational fluid-dynamics package OpenFOAM were primarily used to investigate and support the experimental findings. Their most important result is the extension of the model of a uniform boundary layer thickness proposed by Hurlé [5] to one of a radially outwards increasing boundary layer thickness. Hence, the three-phase coexistence line has been found to be the experiment's most vulnerable region. Further results concern the impact of experimental parameters on mass transport. Experimental confirmation of these predictions was achieved by single crystal growth in a wider range of temperatures and rotation rates.

Acknowledgment

We are very grateful for the surface polishing of the samples by Stefanie Hoser. Experimental contributions by Christina Glassl are gratefully acknowledged.

- [1] P. Gille, in: *Crystal Growth of Intermetallics*, P. Gille, Yu. Grin (Eds.), de Gruyter, Berlin/Boston, 61-90 (2019).
- [2] H.J. Scheel, *J. Crystal Growth*, **13/14**, 560-565 (1972).
- [3] M. Pillaca et al., *J. Crystal Growth*, **475**, 346-353 (2017).
- [4] T. v. Kármán, *Z. Angew. Math. Mechan.*, **1**, 233-252 (1921).
- [5] D.T.J. Hurlé, in: *Advanced Crystal Growth*, P.M. Dryburgh et al. (Eds.), Prentice Hall, 97-123 (1987).

Theoretical analysis, critique and validity limits of Haasen-Alexander-Model for predicting the dislocation density

D.V. Berkov

General Numerics Research Lab, Moritz-von-Rohr-Str. 1^a, D-00745 Jena, Germany

E-mail: d.berkov@general-numerics-rl.de

In this talk we analyze in detail the widely used phenomenological Haasen-Alexander (HA) model [1,2] and its extension - Haasen-Alexander-Sumino (HAS) [3,4] model, which are used for predicting the dislocation density in crystals. We recall that both the original model and its extension are based on four equations of the meso- and macroscopic dislocation dynamics, namely:

- The Orowan law relating the **plastic** shear rate $\dot{\varepsilon}_p$, density of mobile dislocations n_m and the dislocation velocity v :

$$\frac{d\varepsilon_p}{dt} = \frac{1}{F} n_m \cdot v \cdot b \quad (A)$$

- The empirical law relating the growth rate of the dislocation density dn_m/dt to the effective stress τ_{eff} , the density n_m itself and the dislocation velocity v :

$$\frac{dn_m}{dt} = K \cdot \tau_{\text{eff}}^\lambda \cdot n_m \cdot v \quad (B)$$

- The Arrhenius-type relation between the dislocation velocity v and the effective stress τ_{eff} via the activation energy of the dislocation motion Q :

$$v = v_0 \exp\left[-Q/k_B T\right] \cdot \tau_{\text{eff}}^m \quad (C)$$

- The definition of the effective stress τ_{eff} via the applied stress τ_{ext} and the 'hardening' term τ_h :

$$\tau_{\text{eff}} = \max(S \cdot \tau_{\text{ext}} - \tau_h, 0), \quad \text{with } \tau_h = \alpha \cdot Gb \cdot \sqrt{n_m} \quad (D)$$

Whereas the Orowan law is a direct consequence of the definition of a plastic deformation due to the dislocation movement (factor F accounts for different contributions of different dislocation types), equations (B), (C) and (D) cannot be obtained from any basic physical principles and should be viewed as empirical relations based on more or less uncontrollable assumptions. In particular, non-linear dependencies on the effective stress on the r.h.s. in Eqs. (B) and (C) are purely phenomenological and have no proper physical basis.

The most important point, however, is the absence of any physical justification for the functional form of the dependence of the hardening term $\tau_h \sim \sqrt{n_m}$ on the dislocation density n_m used in the key equation (D) of the HAS model. First, we point out, that in the original work of Haasen [1] this dependence was introduced on a purely phenomenological basis to explain the non-monotonicity of the stress-strain dependence. Haasen made an attempt to explain this term stating that the 'effective' stress is the sum of the external stress and the **average dislocation-induced stress**.

However, we show that this explanation is incorrect, because components of the dislocation-induced stress are **odd** functions of Cartesian coordinates, so that for the random (and most other kinds of) dislocation arrangement the **average dislocation-induced stress is zero**.

Next, we analyze the possibility that the 'effective' stress is the sum of the external stress and the **standard deviation** of the dislocation-induced stress. The latter quantity would indeed be proportional

to $\sim\sqrt{n_m}$ (according to the central limit theorem), but this interpretation would be incorrect nevertheless, because the **random variable cannot be replaced** (even after averaging) **by its standard deviation** in any physical application.

The only possibility to assign a real physical meaning to the hardening term is to suggest, that **material ‘hardening’ is due to the presence of other (immobile!) dislocations** which generate a stress landscape for mobile dislocations. However, in this case the dislocation density in the hardening term would be different from the density of moving dislocations (these two dislocation populations are entirely different), which would also mean the failure of the HAS model.

Finally, we analyze the extended HAS model and summarize its advantages and further limitations. To the most serious limitations (in addition to the discussed above) belong:

- A very large number of freely adjustable parameters in the basic HA model; this number is even larger in the extended version, where many dislocation types and glide planes are taken into account.
- Complicated dislocation interactions (elastic forces, jogs, intersections etc.) are ‘squeezed’ into a single ‘hardening’ parameter α
- Any structures in the dislocation arrangement (cellular structures, dislocation walls etc.) are neglected
- All model parameters have to be determined experimentally anew not only for each new material, but also for each new type of the growth process
- These model parameters should be, strictly speaking, time-dependent due to the possible appearance of new dislocation structures during the growth and annealing processes
- The model is not applicable to crystals with the low dislocation density, because the dislocation configuration in such crystals should be described in terms of separated dislocations.

Following the line of arguments presented above, we strongly recommend the development and usage of really physical models, where the complicated matter of the dislocation interaction and multiplication is treated based on established physical relations.

ACKNOWLEDGMENT. The author acknowledges the financial support of BMWi (grant Nu. 03ET1331A)

- [1] P. Haasen, *Zeitschrift für Physik* **167** (1962) 461
[2] H. Alexander, P. Haasen, *Solid State Physics* **22** (1969) 27
[3] M. Suezawa, K. Sumino and I. Yonenaga, *phys. stat. sol. (a)* **51** (1979) 217
[4] K. Sumino, I. Yonenaga, *phys. stat. sol. (a)* **138** (1993) 573

Session 8
Friday 13.03.2020
11:00 – 12:50

Towards 80 mm dia. ultra-high purity germanium single crystals by Czochralski growth

Alexander Gybin, Kevin-Peter Gradwohl, Jozsef Janicskó-Csáthy, Natasha Dropka, Uta Juda,
Jörg Fischer and Radhakrishnan Sumathi*

Leibniz-Institut für Kristallzüchtung (IKZ), Max-Born-Str. 2, 12489 Berlin, Germany

**e-mail: radhakrishnan.sumathi@ikz-berlin.de*

Summary

High-purity germanium (HPGe) single crystals are very promising for their applications as radiation, spectroscopy detectors and are mostly used in experiments dealing with highest resolution, like dark matter research, neutrinoless events (e.g. LEGEND), and as best solution for precise gamma and x-ray spectroscopy. In comparison to silicon (Si), germanium (Ge) is much more efficient for radiation detection due to its high mass number, needing less energy for electron-hole pair creation and can have a larger depletion region (cm thickness) for total absorption. Growing “detector-grade” HPGe single crystals, with engineered structural defects and controlled properties, uniform throughout the crystal, represents one of the challenging tasks in these type of semiconductor materials’ crystal growth. For low background and high-resolution detection, the impurity concentration in the crystal should be ultra-low ($n < 10^{10} \text{ cm}^{-3}$). Numerous process steps are involved to obtain ultra-pure Ge source material and to cultivate single crystals. Additional challenges arise as Ge is one of the few substances that expands as it solidifies.

We have been establishing the following principal process steps at IKZ, all in-house under a single roof, to obtain HPGe crystals: (i) Reduction of GeO_2 to Ge for preparing poly-crystalline Ge bars, (ii) multi-zone-refining of the starting Ge metal bars up to ultra-high purity (12 N); (iii) Czochralski (Cz) growth of single crystals. The most challenging steps are, zone refining to reach the unprecedented purity and the Cz growth, both in H_2 atmosphere. In order to obtain the required purity level, the growth equipment has been specially constructed with an inductive heating set-up. However, it makes the control of the thermal field much more complicated as compared to resistive heating systems. The suitability of the constructed equipment has been tested for growing 2-inch crystals, before implementing a scaling-up process to grow larger diameter (≈ 3 -inch), massive crystals of few kgs in weight. For higher sensitivity and larger volume for detecting dark matter events, large diameter HPGe crystals are prerequisite.

The 3-inch diameter crystals are grown along the [100] direction (Fig.1a), which allow the dislocations to glide out and terminate at the crystal surface. The dislocation densities in these crystals are relatively higher ($\approx 10^4 \text{ cm}^{-2}$), but uniform all along the grown crystals. The 2-inch crystals grown under well-optimised conditions, usually have a dislocation density in the mid. 10^3 cm^{-2} , which is in the required range ($10^2 - 10^4 \text{ cm}^{-2}$) for the applications. [111] oriented crystals were also grown (Fig. 1b, nice facets seen from the top view). During the scaling-up process of massive crystals, further optimisation of the hot-zone and growth parameters are decisive. The most influencing factor in HPGe crystal growth is the process gas (H_2) environment, which makes the thermal field difficult to be controlled and thereby the temperature gradient in the growth regime. The H_2 atmosphere is used to reduce the oxides and minimize trapping centers. H_2 has a large thermal conductivity, low viscosity and also large convective heat transfer coefficient. Further, its purity, flow rate, convection, etc., will

additionally play a role on the final impurity concentration and defect density in the crystals. In our growth equipment, all the internal parts were home-designed and constructed specifically to take care of the concerns of high purity. A realistic three-dimensional computer-aided-design (3D-CAD) model was used to define the geometry, and for a good understanding of the thermal field and transport kinetics, computational fluid dynamics (CFD) simulations have been carried out (Fig.1c).

The grown crystals were investigated in the limelight of crystal perfection, defect density, defect nature and concentration of impurities. Different segregation coefficients of acceptors (B, having a very high segregation coefficient in Ge, $k_0 > 17$) and donors (P, very low $k_0 \approx 0.08$) give raise to a p-n transition around the middle part of the crystal. The shape of the solid-melt interface during the growth process is also important to predict the radial homogeneity of the wafers. The detailed properties obtained from various measurements will be presented, especially for large diameter crystals. The issues related to the diameter enlargement and retaining the control over purity and defect density will also be elucidated.

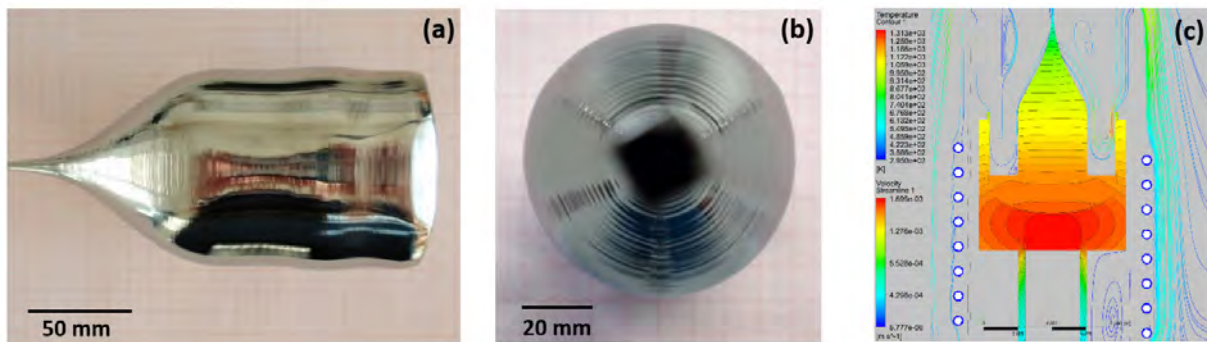


Fig. 1: a) Photo of a 3-inch dia. [100] HPGe crystal grown at IKZ; b) [111] oriented HPGe crystal; c) Numerical simulation of temperature field and gas convection in the crystal growth system.

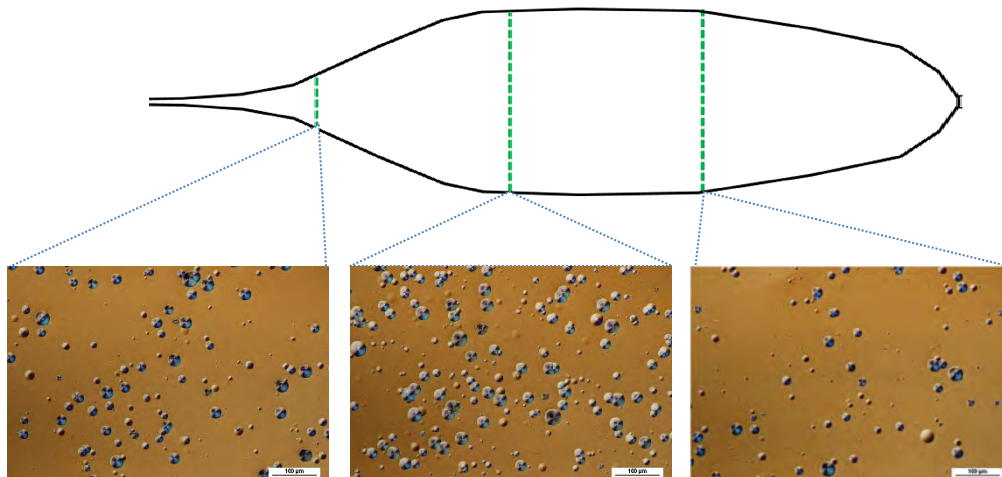


Fig. 2: Controlled EPD in the crystal grown in the newly scaled-up system. Top: Sketch showing the places where the samples were taken for EPD analyses; Bottom: Etched surfaces of the wafers cut from their respective top, middle, and bottom parts.

Acknowledgment

Authors gratefully acknowledge the German Federal Ministry for Education and Research (BMBF) for the financial support through a research grant (number 05A17BC1).

Formation of vacancy related defects in high-purity germanium

K.-P. Gradwohl^a, A. Gybin^a, J. Janicsko-Csathy^a, M. Roder^b, A. Danilewsky^b, R.R. Sumathi^a

^a Leibniz-Institut für Kristallzüchtung, Max-Born-Str. 2, 12489 Berlin, Germany

^b Kristallographie, ALU Freiberg, Hermann-Herder-Str. 5, 79104 Freiburg, Germany

E-mail: radhakrishnan.sumathi@ikz-berlin.de

Large mass radiation detectors with high resolution can be fabricated from high-purity germanium. The production of such detectors has recently gained large interest, since they might aid in the search of the neutrinoless double beta decay within the experimental program of the LEGEND collaboration [1]. For these applications, Ge single crystals with a very high crystalline perfection are required, to say more precisely, a high purity (net concentration of electrically active impurities $< 10^{10} \text{ cm}^{-3}$) and a homogeneous distribution of less structural defects such as dislocations and voids are required.

[100] single crystals of HPGe with a diameter of 2-inch were grown in pure H_2 atmosphere by the Czochralski method as described elsewhere [2]. The structural defects in these crystals were investigated by white beam X-ray imaging conducted at the topography station at the imaging cluster of the Karlsruhe Research Accelerator (KARA) synchrotron – a 2.5 GeV electron storage ring situated at Karlsruhe Institute of Technology (KIT), Germany [3]. The top part of the crystal was mostly dislocation-free and the dislocation density increases towards the tail of the crystal to a value of 2600 cm^{-2} , as can be seen in the X-ray topographs of Fig. 1. In a Ge crystal, the equilibrium vacancy (V) concentration at the melting point which ultimately originates from the growth process is 10^{15} cm^{-3} , while the concentration of self-interstitials is only around 10^9 cm^{-3} , which has been shown by first-principles calculations [4] as well as experimentally [5]. Hence, the mechanism $\text{Ge}_i + \text{V}_{\text{Ge}} \rightarrow \text{Ge}_{\text{Ge}}$ (Frank-Turnbull) does not noticeably reduce the concentration of Vs in the crystal. Vs can only be absorbed in parts of the crystal with dislocations of partly edge character, which consequently climb. Consequently, dislocation-free crystals exhibit huge excess Vs, which tend to form clusters (e.g. voids) or even electrically active V-related complexes when grown under H_2 atmosphere. We have observed that these Vs cluster into voids in the dislocation-free parts of the crystal, while no voids can be observed in parts with moderate dislocation density. The voids are identified by a black-white contrast in the topographs (Fig.1a), which is caused by a dynamical diffraction effect. It results from a modulation of the diffracted intensity, induced by a shift of the tie point position on the dispersion surface by the bending of lattice planes, due to the tensile strain around voids [6]. We estimate that the void density in the top part of the crystal is $< 10^5 \text{ cm}^{-3}$ and therefore very hard to detect them directly by microscopy.

The comparison of etching features originating from a modified CP-4 etch of samples from dislocation-free with non-dislocation-free samples of the crystal showed clear differences, indicating different defect structures. Charge carrier lifetime in dislocation-free wafers, laterally mapped by microwave detected photoconductivity (MDP), was determined to be less than $100 \mu\text{s}$, which is only a fraction of the typical lifetime ($>500 \mu\text{s}$) in comparable samples with a moderate dislocation density along with homogeneous distribution. At the middle of the wafers the charge carrier lifetime of dislocation-free crystals can even locally drop below $20 \mu\text{s}$. Since this behavior is not explicable by the simple presence of voids, further vacancy-related defects such as V-H complexes or vacancy condensation in the form of intrinsic stacking faults may exist in the crystals.

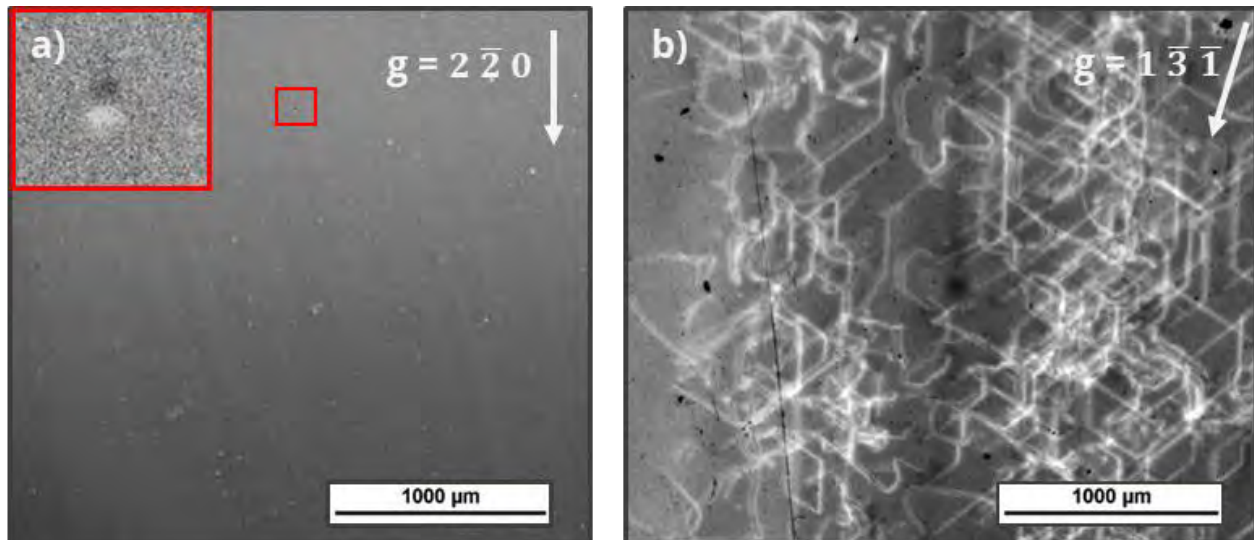


Fig. 1: White beam X-ray topographs of [100] Cz-Ge grown in H_2 atmosphere. (a) depicts an almost dislocation-free part of the crystal ($>1 \text{ cm}^2$) with a void depicted in the inset, while (b) shows a part of the same crystal with a moderate dislocation density of 2600 cm^{-2} and no indication of voids.

Acknowledgment

We thank the Karlsruhe Institute of Technology for the beam time at the Karlsruhe Research Accelerator synchrotron for investigation of our samples in the framework of the BIRD contract. We acknowledge the support by the German Federal Ministry for Education and Research (BMBF) within the collaborative project under the grant number 05A2017-GERDA.

- [1] N. Abgrall, et al., AIP Conference Proceedings, **1894**, No. 1 (2017)
- [2] N. Abrosimov, M. Czupalla, N. Dropka, J. Fischer, A. Gybin, K. Irmscher, J. Janicskó-Csáthy, U. Juda, S. Kayser, W. Miller, M. Pietsch, F. M. Kießling, Journal of Crystal Growth, **532**, 125396 (2020)
- [3] A. Rack, T. Weitkamp, S. Bauer Trabelsi, P. Modregger, A. Cecilia, T. dos Santos Rolo, T. Rack, D. Haas, R. Simon, R. Heldele, M. Schulz, B. Mayzel, A. N. Danilewsky, T. Waterstradt, W. Diete, H. Riesemeier, B. R. Müller, T. Baumbacha, Nuclear Instruments and Methods in Physics Research Section B: Beam Interactions with Materials and Atoms, **267.11**, 1978-1988 (2009)
- [4] P. Śpiewak, K. Sueoka, J. Vanhellemont, K. J. Kurzydłowski, K. Młynarczyk, P. Wabiński, I. Romandice, Physica B: Condensed Matter, **401**, 205-209 (2007)
- [5] J. Vanhellemont, P. Śpiewak, K. Sueoka, Journal of Applied Physics, **101**, 036103 (2007)
- [6] T. Tuomi, R. Rantamäki, P. J. McNally, D. Lowney, A. N. Danilewsky, P. Becker, Journal of Physics D: Applied Physics, **34**, 10A (2001)

CaWO₄ CRYSTAL GROWTH FOR THE CRESST DARK MATTER SEARCH

A. Kinast^a, A. Erb^{a,b}, F. Hamilton^a, M. Kaznacheeva^a, A. Langenkämper^a,
E. Mondragon^a, T. Ortmann^a, L. Pattavina^a, W. Potzel^a, S. Schönert^a,
R. Strauss^a and V. Wagner^a

^a Physik Department, Technische Universität München, James-Franck-Str. 1, 85748 Garching, Germany

^b Walther-Meißner-Institut, Bayerische Akademie der Wissenschaften, Walther-Meißner-Straße 8,
85748 Garching, Germany

E-mail: angelina.kinast@tum.de

Summary

The CRESST (Cryogenic Rare Event Search with Superconducting Thermometers) experiment is searching for elastic scattering of light dark matter particles using CaWO₄ single crystals. It is located deep underground at the Laboratori Nazionali del Gran Sasso (LNGS) in Italy and surrounded by several layers of active and passive shielding to reduce various backgrounds such as cosmic radiation or radiation from radioactive decays. CRESST is the world leading experiment in the mass range up to 0.5 GeV/c². A low detector threshold and a low background have a crucial impact on the sensitivity [1]. For both, the quality of the CaWO₄ crystals is essential. In order to fulfill the requirements of CRESST, a dedicated Czochralski crystal growth facility (see fig 1a) has been set up at the Technical University of Munich (TUM), starting from the production of the CaWO₄ powder from the raw materials CaCO₃ and WO₃ up to the final steps of cutting the detector crystals from the ingot [2]. An important milestone was the growth of the crystal TUM40 (see Fig. 1b,c) which showed an exceptional performance and a much higher radio-purity compared to commercially purchased crystals Daisy (dashed red line) and VK31 (dashed black line) [3],[4].

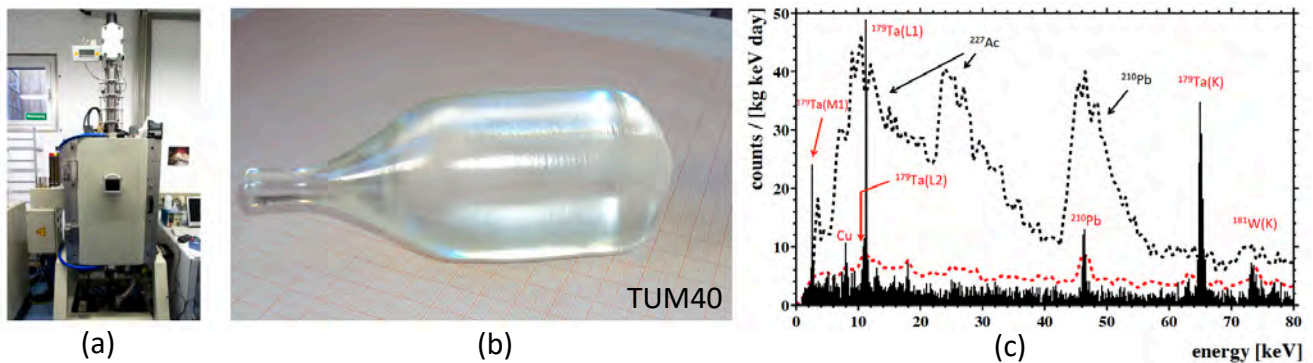


Fig. 1: (a) Picture of the Czochralski furnace in which the CaWO₄ single crystals are grown at TUM. The facility is exclusively used for CaWO₄ crystal growth to avoid cross contamination from impurities of other materials.
(b) The CaWO₄ crystal ingot TUM40.
(c) Histogram of the low-energy events of the detector TUM40 (black bars) recorded during CRESST-II Phase 2. The most prominent peaks are labelled. In comparison the two commercially bought crystals Daisy (dashed red line) and VK31 (dashed black line). Figure from [4].

In order to further improve the quality of the CaWO_4 crystals two approaches are followed. First and most important the improvement of the crystals' radiopurity by two orders of magnitude. For this a synthetization of the CaWO_4 powder via a precipitation reaction (see Fig. 2a) as well as an extensive powder purification for both the raw materials and the synthesized CaWO_4 powder has been developed and conducted at TUM. Screening of the powder using HPGe detectors shows a significant improvement of the radiopurity.

The second way to improve the crystal quality is the reduction of internal stress which is introduced to the crystal lattice from temperature gradients during the growth. To target this, a simulation of the temperature distribution in the furnace was developed with the help of the Leibniz-Institut für Kristallzüchtung (IKZ) using COMSOL Multiphysics (see Fig. 2b). The Czochralski setup was adapted accordingly and first measurements of the crystals in a stress birefringence setup show promising results.

In August 2019 the crystal TUM93 was grown from the first batch of the extensively chemically purified powder. Three CRESST detector crystals have been cut from the ingot and installed in the CRESST setup. This is an important milestone to reach the goals of the CRESST dark matter search.

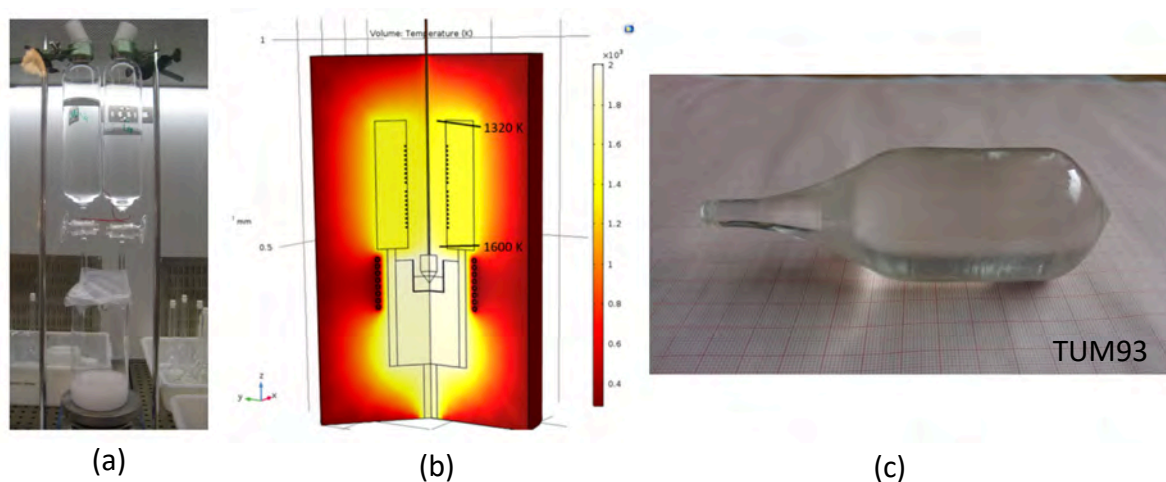


Fig. 2: (a) Picture of the precipitation reaction of the CaWO_4 powder from the raw materials CaCO_3 and WO_3 which are brought in an aqueous solution and are chemically purified prior to the reaction.
(b) Temperature distribution during the Czochralski growth. This simulation was performed with the program COMSOL Multiphysics in order to understand the temperature gradients during the growth better which are causing stress in the crystal lattice. The setup was then modified accordingly to lower these gradients.
(c) The CaWO_4 crystal TUM93 which was grown from the first batch of an extensively chemical purified powder. Three detector crystals have been cut from the ingot. They are currently operated in the ongoing CRESST run.

Acknowledgments

This research was supported by the DFG cluster of excellence Origins, by the BMBF Verbundprojekt 05A2017 CRESST-XENON and by the SFB1258.

- [1] A. H. Abdelhameed, et al, *arXiv:1904.00498* (2019).
- [2] A. Erb, J.-C. Lanfranchi, **CrystEngComm**, 15.12 (2013): 2301-2304.
- [3] R. Strauss, et al., **The European Physical Journal**, C 75.8 (2015): 352.
- [4] R. Strauss, et al., **Journal of Cosmology and Astroparticle Physics**, 2015.06 (2015): 030.

Investigation of particle incorporation in a transparent melt system under μg conditions

T. Jauß^a, T. Sorgenfrei^a

^a*Kristallographie, Albert-Ludwigs-Universität Freiburg, Hermann-Herder-Straße 5, 79104 Freiburg, Germany*

E-mail: thomas.jauss@fmf.uni-freiburg.de

The incorporation of foreign phase particles during crystal growth is a common occurrence, for example during the directional solidification of multi crystalline silicon for photovoltaic applications or string casting processes. These foreign phases generate several limitations, starting with acting as sources for dislocation clusters, disturbing the post growth material processing like wafering during wire sawing, and may be responsible for electrical problems, i.e. for solar cells by acting as shunts, short-circuiting the device. During earlier investigations of the incorporation behavior of silicon carbide (SiC) and silicon nitride (Si₃N₄) particles into growing silicon crystals [1, 2], we experienced the need to study the local reaction of the approaching phase boundary to the particle in front of it more in detail. With silicon as an opaque crystal and equally opaque melt, the only available way to investigate is post growth, and therefore, it is impossible to see the incorporation of a particle at the time of its engulfment. This requirement leads to the use of a transparent melt system with direct visual observability of the particles in the melt, in front of the phase boundary, and during the engulfment process.

The model system studied in this work is ice-water-glass-polystyrene. H₂O shows a clear and planar solid-liquid phase front while it can be crystallized in a suitable range of growth velocities. Different species of spherical particles were used to investigate the influence of different material parameters like density (density ratio to surrounding fluid), heat capacity, heat conductivity, etc. Hollow spheres of glass (9-13 μm diameter) and spheres of polystyrene (10, 30, and 100 μm diameter) were engulfed by a moving ice/water phase boundary. This setup was used under terrestrial conditions as well as on board of the TEXUS 56 sounding rocket payload, under microgravity conditions.

During the experiments, we could observe that in this system, similar to the Si-SiC-Si₃N₄ system, a critical growth velocity exists, below which a particle gets pushed along by the solid liquid interface, and above which a particle gets incorporated. Further, we could observe that the moving phase boundary also enriches the particles in front of itself, while it only incorporates particles with the “correct” radius (Fig 1).

As mentioned above, the focus of this work lies in the investigation of the direct, short-term, and local response of the moving phase boundary on the stationary/static particle in the fluid while getting closer. In μg as well as in reference experiments on ground it was observed that there is no determinable reaction of the phase boundary like forming hillocks or trenches, when a particle is engulfed and incorporated. The growth front stays flat, while the particle is overgrown laterally (Fig 2). This behavior is also in accordance to a silicon crystal engulfing a SiC particle (Fig 3). The acquired data points can now be used to further calibrate and validate quantitative FEM-models, so numerical predictions about particle incorporation can be made.

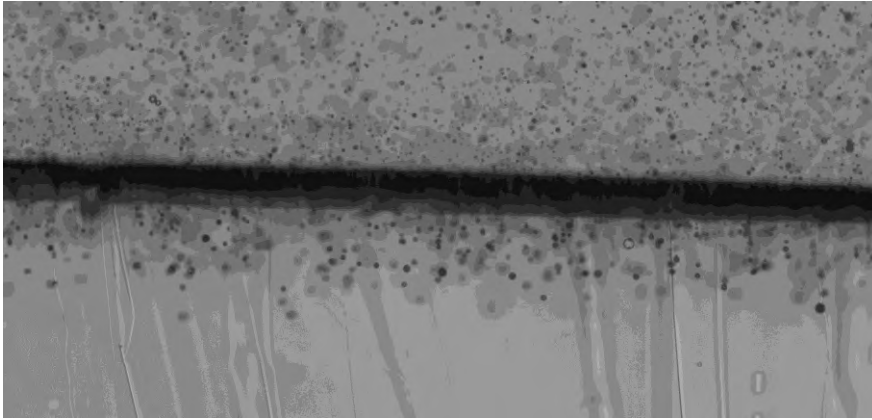


Fig. 1: Hollow glass sphere particles incorporated as a horizon by the moving ice-water phase boundary.

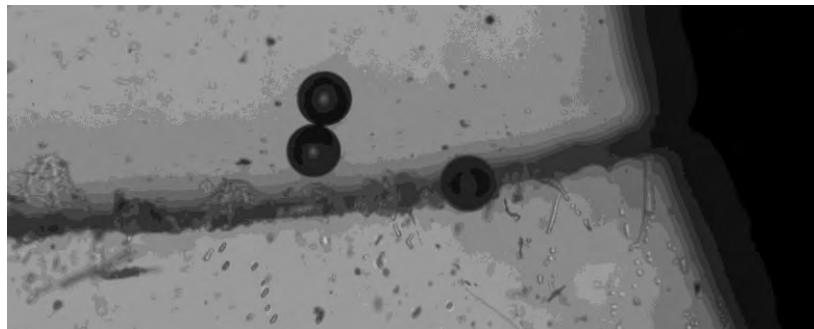


Fig. 2: Polystyrene particles with 30 µm diameter are engulfed by the moving ice-water phase boundary without determinable deformation of the phase boundary into hillocks or trenches.

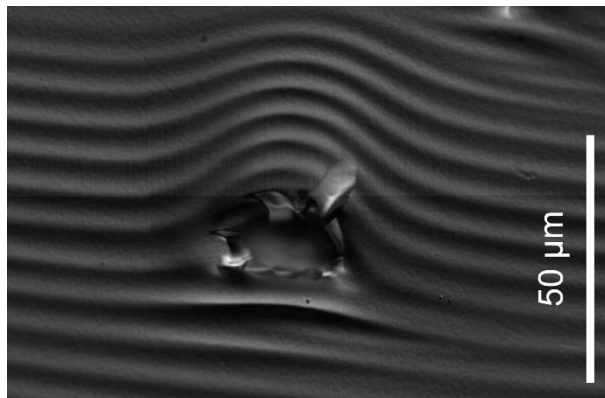


Fig. 3: SiC particle engulfed during growth. The striations indicate no reaction of the phase boundary to the particle prior to engulfment

Acknowledgment

We would like to thank Ms. Nadine Pfändler for her work during the preparations and execution of the TEXUS 56 sounding rocket mission. Our thanks also go to the teams of Airbus D&S, OHB, and SSC for their invaluable technical support. Financial support by DLR/BMWi under FKZ 50WM1756 is gratefully acknowledged.

[1] J. Friedrich, C. Reimann, T. Jauss, A. Cröll, T. Sorgenfrei, *J Cryst Growth*, **447**, 18-26 (2016)

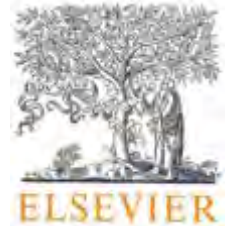
[2] J. Friedrich, C. Reimann, T. Jauss, A. Cröll, T. Sorgenfrei, Y. Tao, J.J. Derby, *J Cryst Growth*, **475**, 33 (2017)

Posterprize

A prize for the best poster presented during the poster session on Wednesday March 11, 2020 will be given by DGKK.

The winner will receive the volume “Fundamentals: Thermodynamics and kinetics” of the Handbook of Crystal Growth.

The volume is sponsored by Elsevier



Postersession
Wednesday 11.03.2020
15:00 – 16:30

Influence of the surface morphology on the defect distribution in the faceted region of 4H-SiC single crystals

Matthias Arzig^a, Michael Salamon^b, Ta Ching Hsiao^c, Norman Uhlmann^b and Peter J. Wellmann^a

^a Crystal Growth Lab, Materials Science Department 6, Friedrich-Alexander-Universität Erlangen-Nürnberg, Martensstraße 7, 91058 Erlangen, GERMANY

^b Fraunhofer Institute for Integrated Circuits, Development Center for X-Ray Technology (EZRT), Flugplatzstraße 75, 90768 Fürth, Germany

^c Industrial Technology Research Institute of Taiwan (ITRI), 195, Sec 4, Chung Hsing Rd., Chutung, Hsinchu 31040, Taiwan (TaChingHsiao@itri.org.tw)

For the growth of silicon carbide (SiC) crystals, the physical vapor transport (PVT) method has matured to become the industrial standard route [1-4]. The wafer quality has improved continuously making micropipe (MP) free material commercially available. By the optimization of the process conditions, the generation of new defects during growth is reduced as far as possible, leading to a steady reduction of defect densities in the wafers. Besides the suppression of defect formation also a distinct reduction of defects is possible in SiC crystals, for example by the conversion of defects as observed in the solution growth method [5]. It is believed that due to high surface steps threading defects are deflected into the basal plane. Using our in-situ computed tomography system we can observe the effect of changed process conditions directly during the growth. A different evolution of the growth interface shape was observed during crystal growth runs, caused by the application of insulation materials of differing thermal conductivity. A higher thermal conductivity leads to a larger radial thermal gradient in front of the growing crystal as confirmed by numerical simulation. Insulation material with lower thermal conductivity leads to a smaller radial temperature gradient at the crystal growth interface. Therefore, differently shaped growth interfaces evolve and different step morphologies are formed.

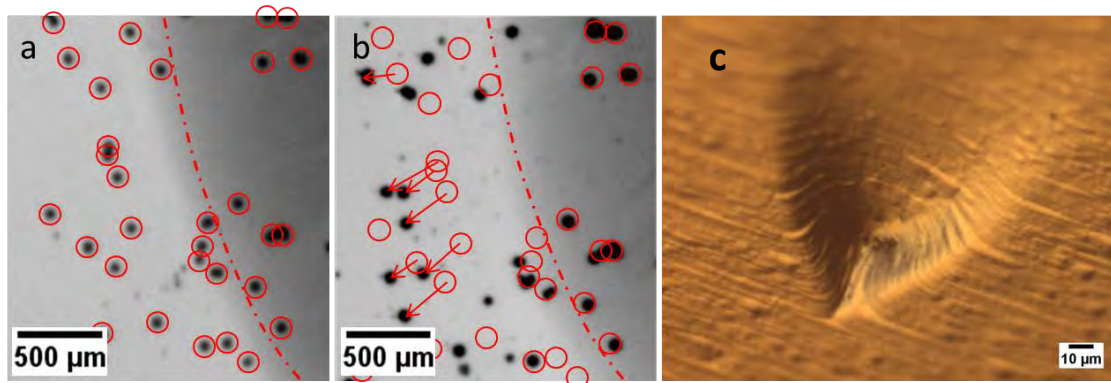


Fig. 1: micropipes in the stepflow area changing their position from bottom (a) to top (b) in the crystal.
(c) micropipe penetrating the crystal surface in the step-flow area

Due to the higher radial temperature gradient a smaller facet and steeper crystal flanks evolved compared to the growth run using an insulation material of lower thermal conductivity. The steep crystal flanks feature high surface steps as visible in Figure 1c, which strongly interact with the crystal defects. Two different mechanisms for the bending of micropipes (MPs) away from the $[1\bar{1}00]$ direction were found. Figure 1 a and b depicts the step flow area where the MPs are deflected collectively in the direction of the step flow by big surface steps. In the facet area the repulsive interaction of selected MPs led to a slight deflection restricted to the $\{1\bar{1}00\}$ prismatic plane in the $\langle 11\bar{2}0 \rangle$ direction as depicted in Figure 2, caused by repulsive interaction.

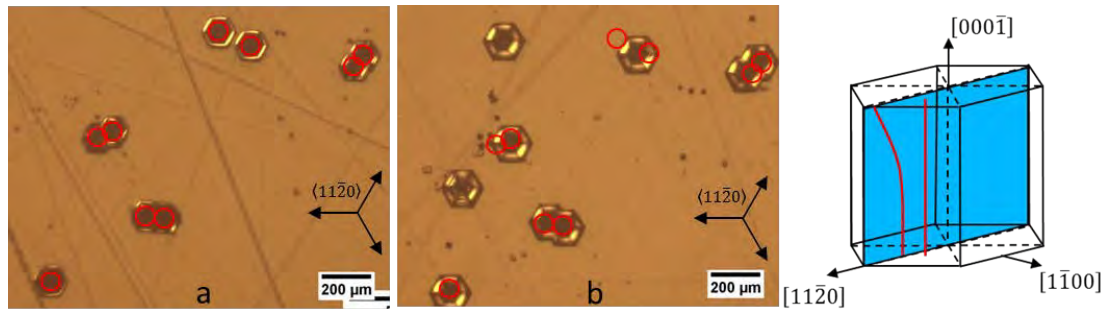


Fig. 2: micropipes in the facet area changing their position from bottom (a) to top (b) in the crystal.
(c) illustration of the repulsive interaction of two MPs with the same burgers vector

The defect densities listed in table 1 indicate that the large surface steps on the surface of crystal B convert a large amount of TEDs into BPDs leading to a reduction of this defect during the growth process.

Table 1: Densities of defects for crystal A grown under smaller radial thermal gradient and Crystal B grown under larger radial thermal gradient. Wafer #1 denotes the Wafer closer to the growth surface and Wafer #2 denotes the Wafer closer to the seed, respectively.

	TED [$1/\text{cm}^2$]	TSD [$1/\text{cm}^2$]	BPD [$1/\text{cm}^2$]
Crystal A Wafer #1	$(2.33 \pm 0.03)\text{E}4$	$(0.94 \pm 0.02)\text{E}3$	$(4.58 \pm 0.05)\text{E}3$
Crystal A Wafer #2	$(2.18 \pm 0.02)\text{E}4$	$(1.00 \pm 0.03)\text{E}3$	$(5.27 \pm 0.05)\text{E}3$
Crystal B Wafer #1	$(0.44 \pm 0.08)\text{E}4$	$(0.88 \pm 0.29)\text{E}3$	$(3.14 \pm 0.61)\text{E}3$
Crystal B Wafer #2	$(1.12 \pm 0.30)\text{E}4$	$(1.00 \pm 0.33)\text{E}3$	$(3.07 \pm 0.58)\text{E}3$

For the growth of large SiC boules the application of large radial gradients for defect reduction seems not appropriate as large radial strain will lead to the generation of new defects. Therefore, the application of an off-axis angle to produce a surface morphology featuring large steps would be a better method. Measurements of the angle between the facet plane and the crystal flanks, reveal an inclination angle of 10° directly around the rim of the facet and going up to 20° further away at the steepest regions. The growth on seeds cut with a large off-axis angle between $10\text{-}20^\circ$ can be a promising approach to achieve defect reduction in PVT grown SiC by large surface steps, while avoiding large radial thermal gradients.

Acknowledgment

The authors acknowledge funding by the DFG under the grant numbers WE2107/12-1 and UH246/4-1

- [1] I. Manning, G. Y. Chung, E. Sanchez, Y. Yang, J. Q. Guo, O. Goue, B. Raghothamachar, M. Dudley, Materials Science Forum, **924**, 11-14 (2018)
- [2] A. R. Powell, J. J. Sumakeris, Y. Khlebnikov, M. J. Paisley, R. T. Leonard, E. Deyneka, S. Gangwal, J. Ambati, V. Tsevtkov, J. Seaman, A. McClure, C. Horton, O. Kramarenko, V. Sakhalkar, M. O'Loughlin, A. A. Burk, J. Q. Guo, M. Dudley, E. Balkas, Materials Science Forum, **858**, 5-10 (2016)
- [3] T. L. Straubinger, E. Schmitt, S. Storm, M. Vogel, A. D. Weber, A. Wohlfart, Materials Science Forum, **645-648**, 3-8 (2010)
- [4] A. K. Gupta, P. Wu, V. Rengarajan, X. P. Xu, M. Yoganathan, C. Martin, E. Emorhokpor, A. Souzis, I. Zwieback, T. Anderson, Materials Science Forum, **717-720**, 3-8 (2012)
- [5] S. Harada, Y. Yamamoto, S. Xiao, D. Koike, T. Mutoh, K. Murayama, K. Aoyagi, T. Sakai, M. Tagawa, T. Ujihara, Materials Science Forum, **821-823**, 3-8 (2015)

Limitations during Vapor Phase Growth of Bulk (100) 3C-SiC Using 3C-SiC-on-SiC Seeding Stacks

M. Schöler^a, P. Schuh^a, J. Steiner^a, F. La Via^b, Marco Mauceri^c, Marcin Zielinski^d,
Peter J. Wellmann^a

^a Crystal Growth Lab, Materials Department 6 (i-meet), FAU Erlangen-Nuremberg, Martensstr. 7,
D-91058 Erlangen, Germany

^b CNR-IMM, sezione di Catania, Stradale Primosole 50, I-95121 Catania, Italy

^c LPE S.P.A., Sedicesima Strada, I-95121 Catania, Italy

^d NOVASiC, Savoie Technolac, BP267, F-73375 Le Bourget-du-Lac Cedex, France
E-mail: michael.schoeler@fau.de

Summary

Certain condition including a high supersaturation, a silicon-rich gas phase and a high vertical temperature gradient during the growth of 3C-SiC are key challenges to obtain high quality material. We have developed a transfer method creating high-quality 3C-SiC-on-SiC (100) seeding stacks, suitable for use in the so-called sublimation “sandwich” epitaxy (SE) [1]. A series of growth runs with different source to seed distances were performed and characterized by XRD and Raman spectroscopy. The measurements revealed a decrease in material quality with increasing source to seed distances.

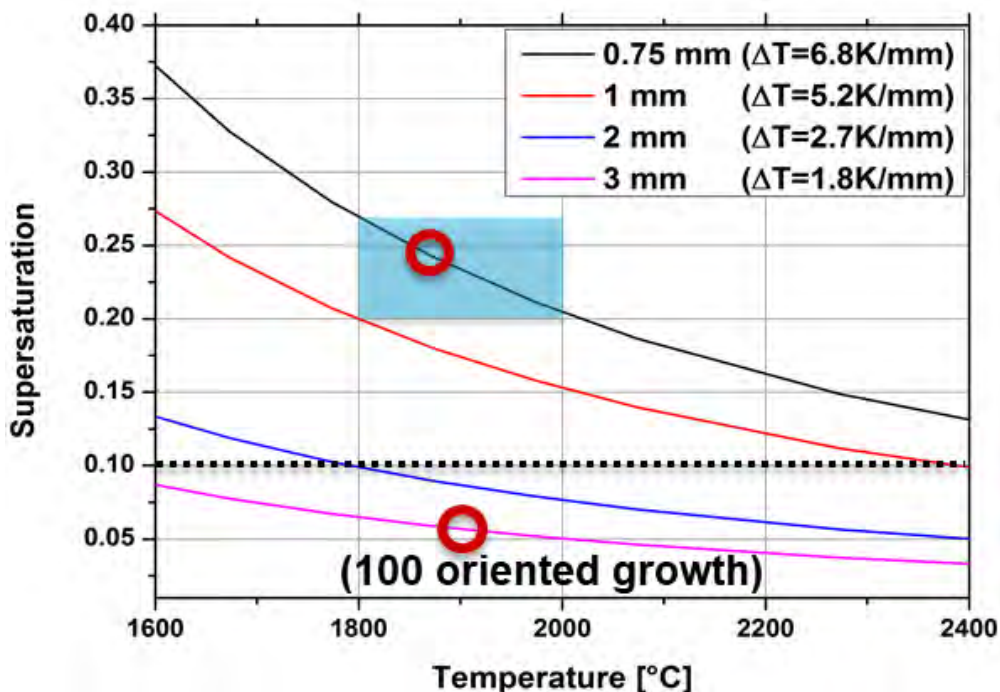


Fig. 1: From simulation data calculated supersaturation of the growth-limiting gas species SiC₂ as a function of temperature for varying source-to-substrate distances. Highlighted areas are extracted from the literature and experiments were performed on (100)-oriented material. The dashed line marks the minimal necessary supersaturation for stable growth of 3C-SiC.

For a better understanding, simulations of the used SE setup were carried out using COMSOL Multiphysics. Thereby a quantitative estimation for the temperature gradient and consequently the supersaturation of the growth limiting gas species SiC_2 was created. Different source-to-seed distances were taken into account as well as various temperatures. The simulated data showed a decrease in supersaturation of the growth-limiting SiC_2 gas species with increasing source-to-seed distances (Fig. 1). The observed decline in crystal quality during the growth runs with increasing spacing could therefore be explained by the reduction in supersaturation.

The main defect limiting the growth of cubic silicon carbide appears to be the protrusion defect which is already present in the seeding layers [2]. Morphology analysis of as-grown material indicates an increasing protrusion dimension with increasing crystal thickness. This effect limits the achievable maximal thickness. During growth of an approximately 2.7 mm thick crystal additional polytype inclusions could be observed. They began to occur at low supersaturation ($S \leq 0.06$) and prolonged during growth (increase of carbon gas-species). Nevertheless, switch-backs to the cubic polytype could be observed at later growth stages. Together with the simulated data, we were therefore able to suggest a necessary minimal supersaturation of 0.1 for the stable growth of 3C-SiC.

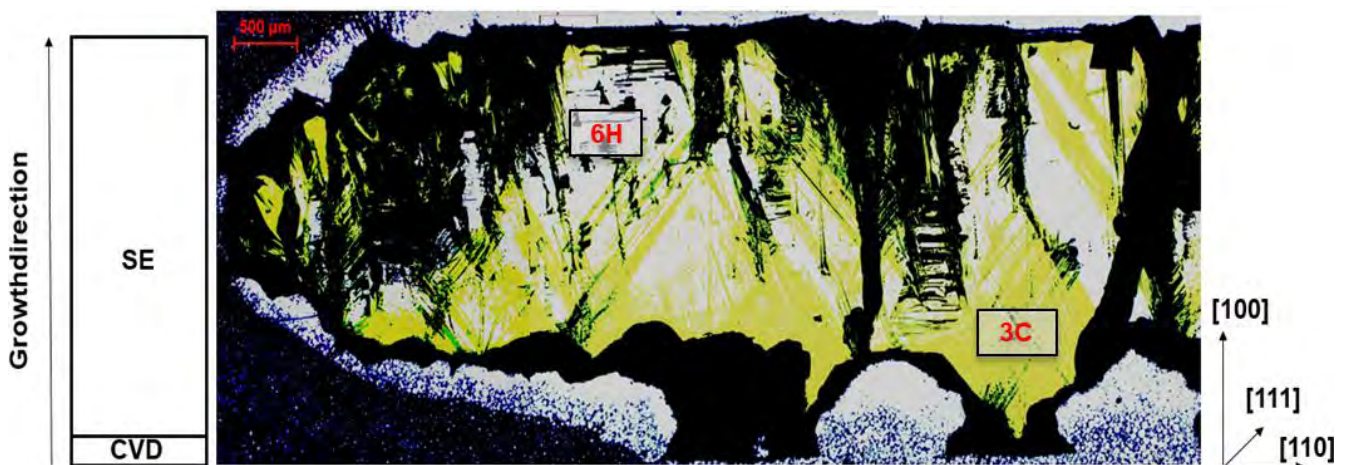


Fig. 2: Crosscut from an approx. 2.7 mm thick one-inch sample in through-light set up viewed with an optical microscope. The growth conditions were near the limit of stable 3C-SiC growth (yellow areas) as can be seen by the white inclusions representing polytype switches to 6H. Backside sublimation also occurred during the growth (removed areas located at the bottom).

Acknowledgment

This work is funded by the European H2020 framework program for research and innovation under grant agreement number 720827 (CHALLENGE).

[1] P. Schuh, M. Schöler, M. Wilhelm, M. Syväjärvi, G. Litrico, F. La Via, M. Mauceri, P.J. Wellmann, Sublimation growth of bulk 3C-SiC using 3C-SiC-on-Si (100) seeding layers, *J. Cryst. Growth*, **478**, 159-162 (2017).

[2] F. La Via, A. Severino, R. Anzalone, C. Bongiorno, G. Litrico, M. Mauceri, M. Schoeler, P. Schuh, P.J. Wellmann, From thin film to bulk 3C-SiC growth: Understanding the mechanism of defects reduction, *Mater. Sci. Semicond. Process*, **78**, 57–68 (2018).

X-Ray Analysis of Defects in 4H-SiC

M. Roder^a, J. Steiner^b, B. Nguyen^c, S. Haaga^{a,d}, M. Kabukcuoglu^{a,d}, S. Bode^d, D. Hänschke^d,
T. Baumbach^{d,e}, P. Wellmann^b, S. Sandfeld^c, A. Danilewsky^a

^a Crystallography, Albert Ludwigs University Freiburg, 79104 Germany

^b Crystal Growth Lab, Material Department 6 (i-meet), University of Erlangen-Nürnberg, 91058 Erlangen

^c Micromechanical Materials Modelling (MMM), Institute of Mechanics and Fluid Dynamics, Technical University Bergakademie Freiberg (TUBAF), Lampadiusstr. 4, D-09599 Freiberg

^d Laboratory for Applications of Synchrotron Radiation (LAS), Karlsruhe Institute of Technology (KIT), D-76131 Karlsruhe, Germany

^e Institute for Photon Science and Synchrotron Radiation (IPS), Karlsruhe Institute of Technology (KIT), D-76344 Eggenstein, Germany

E-mail: melissa.roder@krist.uni-freiburg.de

Silicon carbide (SiC) used as semiconductor material for high power devices often degrades the device's performance by a high variety and density of defects [1]. The wafers of several 4H-SiC crystals, grown by Physical Vapor Transport [2, 3] at various growth conditions were characterized. For each crystal, one wafer close to the crystal seed and one wafer close to the crystal cap was investigated. Synchrotron White Beam X-ray Topography (SWXRT) measurements in back-reflection geometry were carried out at the topography station at imaging cluster of KIT light source [4] to investigate and distinguish the different defect types. Further, High Resolution X-ray Diffractometry (HRXRD) measurements were performed at selected wafer areas, capturing the interplay between different dislocations or one specific dislocation type. The same defect types occur in all investigated wafers, namely Threading Screw Dislocations (TSD), Micropipes (MP), Small-angle grain boundaries (SAGB) in form of Threading Edge Dislocation (TED) arrays and Basal Plane Dislocations (BPD). Full wafer mappings, recorded in 0004 reflection show an inhomogeneous distribution of the mentioned defects (see Fig.1 (a) and (d)). In all wafer mappings, the defect density is lowest in the wafer center and increases towards the wafer border. The region between wafer middle and border is made up by a BPD network (see Fig.1 (b)), which corresponds to the crystal area with the highest calculated resolved shear stress distribution inherent during the growth temperature of 2250 °C [5]. In this area the shear stress exceeds a critical value for the formation of BPDs [6]. The network shows a connection to TSDs, whereas MPs are mostly isolated. Near the border there's a spontaneous change of the BPD network to an area of dominating SAGBs with a connection to MPs (see Fig. 1(c)). This change can be caused by a transition of BPDs into TEDs due to changing temperature and stress gradients during the cool down phase. By comparing the wafer close to the seed with the one close to the crystal cap, it becomes apparent that density, types and distribution of the occurring defects do not change along the crystal. Further, by using one wafer as seed for the next growth, defect types, density and distribution remains similar. Therefore, all types of threading dislocations and SAGBs continue during growth. HRXRD measurements were performed at different wafer areas to investigate the crystal quality more quantitatively. Rocking curves in 0004 reflection show a difference in their curve shape and full-width at half maximum (FWHM) depending on the crystal quality, which is in good agreement with the SWXRT results. More meaningful are the recorded Reciprocal Space Maps (RSM), to separate the effect of different defects on crystal lattice strain and tilt. Depending on the dominant defect type in the measured area the shape of the RSM and the relation of crystal lattice strain to crystal lattice tilt changes. A pure BPD network results in pure crystal lattice tilt, whereas mixed types of dislocation result in different amounts of strain and tilt. Even for the largest MPs, in combination with any type of edge dislocation, the contribution of pure lattice strain decreases. So in conclusion, there is no far-

reaching influence of one type of dislocations on the crystal lattice. Further, since most of the defects propagate through the whole length of the crystal, the crystal lattice strain and tilt conditions remain similar on the same wafer areas, irrelevant on the wafer position inside the crystal.

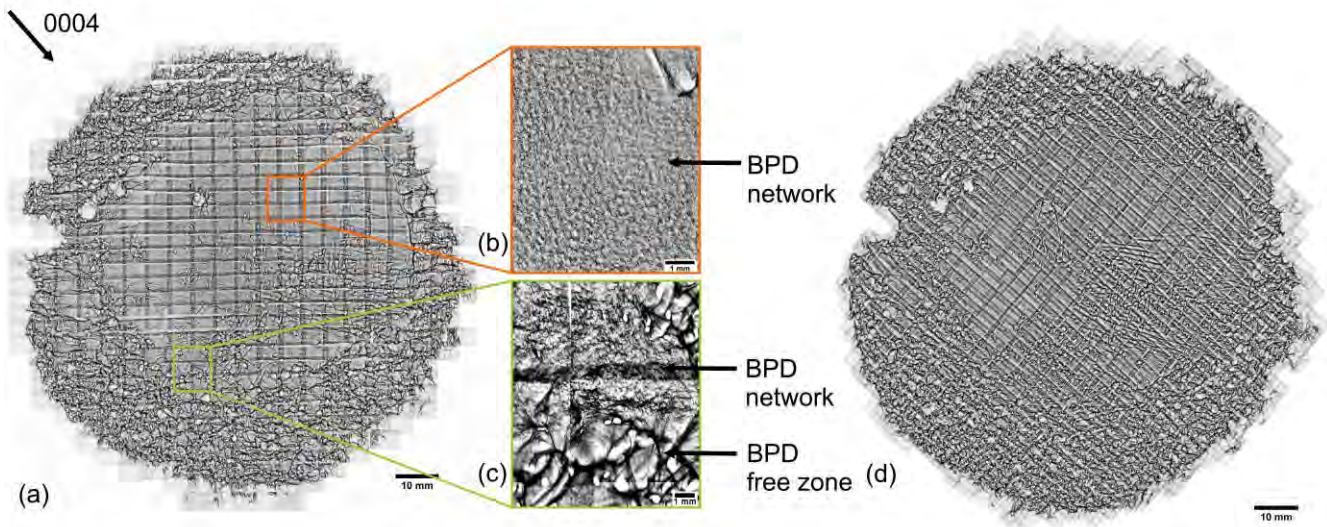


Fig. 1: (a) SWXRT wafer mappings recorded in 0004 of wafer A1, close to the crystal seed. (b) Circular arranged BPD network around the wafer center. (c) Abrupt transition from BPD network area to area with increased SAGBs. (d) SWXRT wafer mapping recorded in 0004 of wafer A2, close to the crystal cap. The mapping shows a similar defect arrangement as for wafer A1.

Acknowledgment

I want to thank our team at crystallography Freiburg. Mr. Harald Schade, Marcus Zuber and Elias Haman from KIT for technical support and all the help during beamtime and the "Deutsche Forschungsgemeinschaft" (DFG) for financial support, Project-Nr: 2083562101.

- [1] Neudeck, Ph G et al. "Breakdown degradation associated with elementary screw dislocations in 4H-SiC p+ n junction rectifiers." MRS Online Proceedings Library Archive 483 (1997).
- [2] Wellmann, P. J. et al. "Review of SiC crystal growth technology." Semiconductor Science and Technology 33.10 (2018): 103001.
- [3] Wellmann, P.J., et al. "Growth of SiC bulk crystals for application in power electronic devices—process design, 2D and 3D X-ray in situ visualization and advanced doping." Crystal Research and Technology 50.1 (2015): 2-9
- [4] Rack, A., et al. "The micro-imaging station of the TopoTomo beamline at the ANKA synchrotron light source." Nuclear Instruments and Methods in Physics Research Section B: Beam Interactions with Materials and Atoms 267.11 (2009): 1978-1988.
- [5] Steiner, Johannes, et al. "Analysis of the Basal Plane Dislocation Density and Thermomechanical Stress during 100 mm PVT Growth of 4H-SiC." Materials 12.13 (2019): 2207.
- [6] Selder, M., et al. "Numerical simulation of thermal stress formation during PVT-growth of SiC bulk crystals." Materials Science Forum. Vol. 353. Trans Tech Publications Ltd., Zurich-Uetikon, Switzerland, 2001.

Impact of Varying Parameters on the Temperature Gradients in 100 mm Silicon Carbide Bulk Growth in a Computer Simulation Validated by Experimental Results

J. Steiner^a, Matthias Arzig^a, Michael Salamon^b, Alexey Denisov^c, Norman Uhlmann^b,
Peter J. Wellmann^a

^a Crystal Growth Lab, Materials Science Department 6, Friedrich-Alexander-Universität Erlangen-Nürnberg, Martensstraße 7, 91058 Erlangen, Germany

^b Fraunhofer Institute for Integrated Circuits, Development Center for X-Ray Technology (EZRT), Flugplatzstraße 75, 90768 Fürth, Germany

^c PVA Crystal Growing Systems GmbH Im Westpark 10–12, 35435 Wettenberg, Germany
E-mail: johannes.steiner@fau.de

Summary

The extraordinary electrical properties of silicon carbide (SiC) established it as one of the currently relevant wide-band gap semiconductor materials for high power, high temperature, and high frequency electronic applications. Due to the increasing industrial standard size for SiC wafers from 100 mm up to 200 mm in the future, a fundamental understanding of the growth process and the corresponding conditions are crucial to achieve a crystal quality high enough for further processing. Commonly, SiC is grown by the physical vapor transport (PVT) method [1]. Changes of the growth conditions like axial and radial temperature gradients due to the growth of the SiC boule and shrinkage of the SiC source material lead to thermoelastic stresses and, as a result, defects are formed [2, 3]. The adaption of thermal gradients inside the hot zone is one way to reduce such defect generation. However, the high process temperatures prevent a straightforward in situ data acquisition from specific points inside of the crucible via thermocouples. Instead, numerical modeling can be used for hot zone engineering and to facilitate a better understanding of the complex dynamics during the PVT growth of SiC [4-6]. A major obstacle in the accurate modeling of the PVT growth process is the lack of precise material data at temperatures well above 2000°C of the applied carbon-based thermal isolations and crucible parts, as well as the highly dynamic SiC powder source. Moreover, material inhomogeneities can lead to further deviations of expected results. In this work, a quantification of the effects of these uncertainties on numerical modeling was done by utilizing the temperature data of growth runs inside a 75 mm PVT and two different 100 mm PVT setups and creating a simulation tool accurate enough to depict the process temperature fields with high accuracy covering a wide range of hot zone geometry and process parameters. Complementing X-ray imaging was done to characterize the evolution of crystal and source during the growth processes and further verify the numerical calculations [7, 8]. In addition, experimental validation was carried out by the comparison of simulated isothermals with experimental doping striations of the axial and radial temperature gradient and the evolution of the shape of the crystal growth interface (see fig. 1). This validated model enabled us to study the influence of changing materials properties of the graphite crucible, the SiC powder source or the graphite isolation on the accuracy of the simulation.

The impact of the cooling solution of a PVT setup either based on water or air on the temperature gradients inside the hot zone was investigated by growing two 100 mm crystals in two different PVT setups. It could be proved numerically and experimentally that the cooling solution has no influence on thermal gradients and the resulting crystals. Two additional 100 mm crystals were grown with varying source powder packaging densities. Using X-ray imaging, a correlation between the sources' packaging density and the curvature of the resulting crystal growth front could be demonstrated. Radial and axial temperature gradients will be influenced by the porosity of the source charge, as

validated by our model. Furthermore, the evolution of the source charge and its properties was investigated using an in situ CT-system. The insignificance of the source powder's electrical properties due to limited induction heating could be shown. While changing the thermal properties of the graphite hot zone will impact the radial gradient only to a minor degree, the axial gradients will be altered by a moderate amount. In case of unreliable thermal isolation material data the uncertainty can be lessened by adjusting the applied power in the simulation according to measured temperatures without losing too much accuracy. This however requires reliable temperature data on top and below the hot zone. Finally, the influence of the process pressure on the isolation has been investigated. The simulation is expanded by implementing a dependency between the pressure acting on the isolation and the resulting changes in thermal conductivity. With this implementation, the model can predict changes in temperature based on different growth pressures with high accuracy.

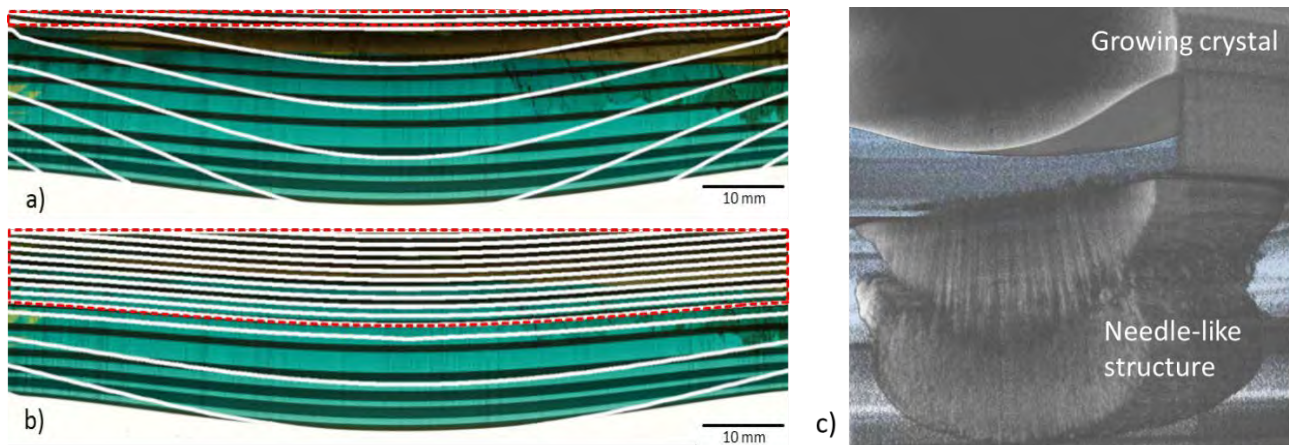


Fig. 1: Cross-section of a crystal grown with increasing power between 12.6 kW and 14.4 kW overlaid with isotherms derived from the simulation at a) the beginning of the growth and b) after 20 h growth. The seed and grown crystal is outlined in by the dashed line. c) In-situ 3D-CT-image of changing mass distribution inside the growth chamber.

Acknowledgment

The authors acknowledge funding by the DFG under the grant numbers WE2107/12-1 and UH246/4-1.

- [1] Y. M. Tairov, V. F. Tsvetkov, *Journal of Crystal Growth*, **43**, 209-212 (1978)
- [2] E. Schmitt, T. Straubinger, M. Rasp, A. D. Weber, *Superlattices and Microstructures*, **40**, 320-327 (2006)
- [3] D. Hofmann, E. Schmitt, M. Bickermann, M. Kölbl, P. J. Wellmann, A. Winnacker, *Materials Science and Engineering*, **61-62**, 48-53 (1999)
- [4] E. L. Kitanin, M. S. Ramm, V. V. Ris, A. A. Schmidt, *Materials Science and Engineering B*, **55**, 174-183 (1998)
- [5] M. Selder, L. Kadinski, Y. Makarov, F. Durst, P. Wellmann, T. Straubinger, D. Hofmann, S. Karpov, M. Ramm, *Journal of Crystal Growth*, **211**, 333-338 (2000)
- [6] D. D. Avrov, A. S. Bakin, S. I. Dorozhkin, V. P. Rastegaev, Y. M. Tairov, *Journal of Crystal Growth*, **198-199**, 1011-1014 (1999)
- [7] P. J. Wellmann, M. Bickermann, D. Hofmann, L. Kadinski, M. Selder, T. L. Straubinger, A. Winnacker, *Journal of Crystal Growth*, **216**, 263-272 (2000)
- [8] P. Wellmann, G. Neubauer, L. Fahlbusch, M. Salamon, N. Uhlmann, *Crystal Research and Technology*, **50**, 2-9 (2015)

NUMERICAL MODELLING OF THE CZOCHRALSKI GROWTH OF NEODYMIUM-SCANDATE SINGLE CRYSTALS

Klaus Böttcher, Wolfram Miller and Steffen Ganschow

Leibniz-Institut für Kristallzüchtung (IKZ) im FVB e.V., 12489 Berlin, Max-Born-Straße 2, Germany
E-mail: klaus.boettcher@ikz-berlin.de

NdScO₃ belongs to the group of the rare-earth scandates which has the perovskite structure. Concerning the lattice cell parameters, those rare-earth scandate perovskites meet other important perovskites, and so they are suitable substrates for the epitaxial growth of perovskite thin films because they are structurally, chemically and thermally compatible with them [1].

As most other perovskite-type rare-earth scandates, NdScO₃ melts congruently, NdScO₃ single crystals can be grown by the conventional Czochralski method with rf-heating and automatic diameter control. The most challenging property of NdScO₃ crystals is probably the semitransparency concerning internal radiative heat transfer.

In the present investigation, for solving of the heat transfer problem we have used the software CGSimTM [2] which is a tool for modelling crystal growth from the melt. For the solution of the radiative transport equation, CGSimTM uses a variant of the Discrete Transfer Method, that was adjusted to treat axisymmetric problems in complex domains, i.e. CGSimTM is able to solve the radiative transport equation for the full range of optical thickness.

Currently, NdScO₃ Czochralski crystals can be successfully grown up to a geometry of 45 mm length and 18 mm radius. However, from time to time they crack during wafer preparation, for that reason we are interested in the investigation of thermal stresses.

For treating the radiative heat transfer, as a first approach, we have defined different value ranges of a grey absorption coefficient μ in order to meet the various branches of the dimensionless optical thickness τ : for $\mu = 0.01 \dots 3 \text{ m}^{-1}$ we get $\tau < 0.1$, i.e. the medium is optical thin, for $\mu = 400 \dots 800 \text{ m}^{-1}$ we get $\tau > 10$, i.e. the medium is optical thick, and for $\mu = 10 \dots 200 \text{ m}^{-1}$, the medium is modelled as moderately optical thick.

The computations are performed in two steps: A: axisymmetric calculation of the temperature field in the entire furnace and of the field distribution of velocity for melt and gas using CGSim, whose algorithms performs power control in order that the temperature at the contact line between crystal, melt and gas keeps the melting point temperature and carries out the relocation of the finite-element mesh in order to track the shape of the crystal/melt interface. Then step B: from the crystal we take geometry and temperature field and expand them to 3D by rotating their data along 360 degree. This new data structure is put into software COMSOL[3]: now the anisotropic coefficients of thermal expansion and elasticity can take effect in order to make 3D displacements and thermal stresses in terms of the von Mises stress.

In Fig. 1 is shown the von Mises stress at the crystal surface for the 12 cases of absorption coefficients (ranging from optically thin via intermediate to thick). Additionally we see at the x-y line plots the deflections of the crystal/melt interface and the maximum values of the von Mises stress: we see that the cases with the largest stress values have intermediate absorption. Exactly these data sets have a similar deflection of the crystal/melt interface as in experiments: between 3 and 4 mm. This could explain the large residual stresses which lead to mechanical cracking at wafer preparation. For those cases (enboxed in Fig. 1) in Fig. 2 is shown the stress distribution within the crystals along a cross cut plane, for both cases: with and without the initial seed cone. The absence of the initial seed cone does not essentially change the thermal stress distribution near the crystal/melt interface.

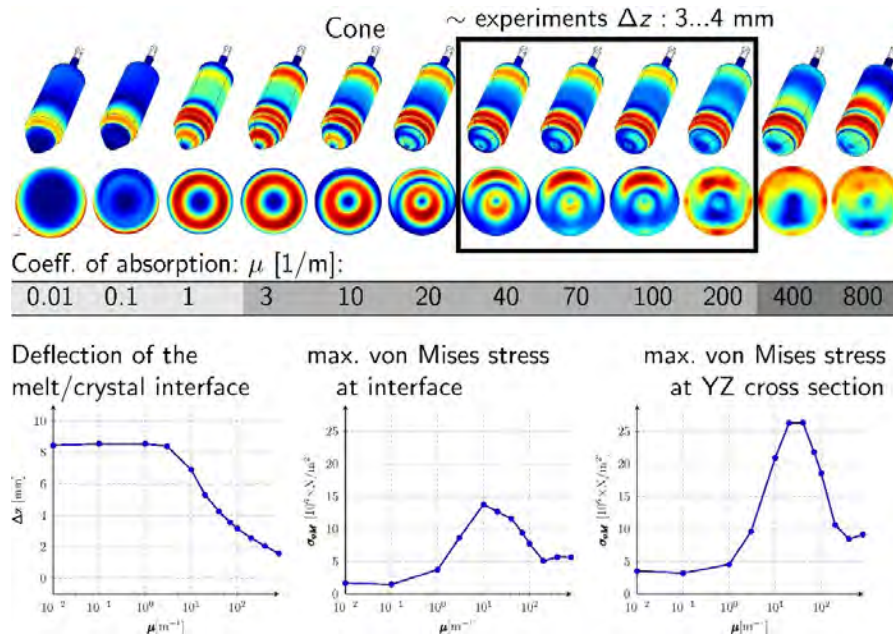


Fig. 1: Top: Von Mises stress at the crystal surface and at the crystal/melt interface (the circle below) as a result of the action of the absorption coefficient (see gray-scaled row from 0.01 ... 800 1/m), Bottom: Some results items in dependence of the absorption coefficient along the full range.

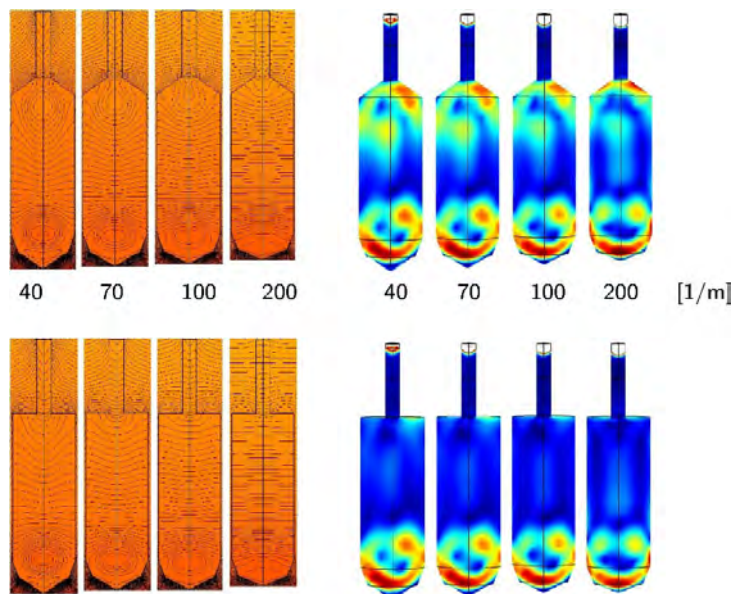


Fig. 2: Top: Temperature field and Von Mises stress at a crystal cross cut for the cases where the crystal/melt interface is in the range of the experimentally observed values:
 Top: Case with crystal conus after seed, bottom: Case without crystal conus after seed.

References:

[1] R. Uecker et al., Properties of rare-earth scandate single crystals (Re=Nd-Dy), Journal of Crystal Growth **310**, 2649-2658 (2008)
 [2] STR Group Inc.: CGSim Crystal Growth Simulator: Software for modelling of crystal growth from the melt, Theory manual (Ch. 7.1), Version 18.1, 2018, Saint Petersburg, Russian Federation.
 [3] Fa. COMSOL Inc.: COMSOL Multiphysics™, User Guide, Version 5.4, 2018, Burlington, USA.

Synthesis and characterization of the triangular antiferromagnets NaYbO₂, KYbO₂ and NaYbS₂

F. Grußler^a, P. Gegenwart^a, A. A. Tsirlin^a

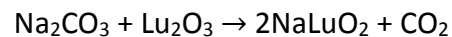
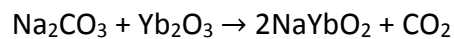
^a Experimental physics VI, Center for Electronic Correlations and Magnetism, University of Augsburg,
Augsburg, Germany.

E-mail: franziska.grussler@physik.uni-augsburg.de

Summary

NaYbO₂, KYbO₂ and NaYbS₂ feature the same space group $R\bar{3}m$ as the spin liquid candidate YbMgGaO₄ but evade structural disorder pertinent to that compound. Here, we present a way to synthesize polycrystalline NaYbO₂ and KYbO₂ as well as KYbS₂ single crystals.

The NaYbO₂ samples as well as the non-magnetic reference compound NaLuO₂ were synthesized via solid state reactions:



The precursors were weighed in the ratio of Na/Yb = 11. The excess of Na₂CO₃ is necessary, since at temperatures above 900°C some Na₂CO₃ is lost due to evaporation. They were pressed into pellets and subsequently heated according to the heating program shown in Fig. 1. Polycrystalline NaYbO₂ was synthesized by this method, no impurity phases were detected in synchrotron XRD measurements. Heat capacity measurements down to 100 mK in various magnetic fields revealed a field-induced order. Furthermore, spin-liquid behavior was demonstrated in NaYbO₂ [1].

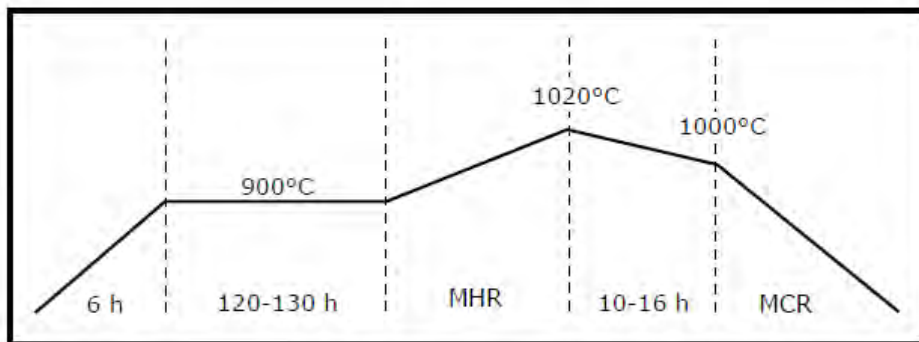


Fig. 1: Temperature profile used for the synthesis of NaYbO₂. The abbreviations MHR and MCR stand for the maximum heating rate and maximum cooling rate, respectively.

The approach of preparing KYbO₂ is based on the synthesis reported in [2]. The starting materials (Yb₂O₃ and KO₂) were weighed in a glove box filled with argon gas to prevent a reaction of KO₂ with the air moisture. As suggested in [2], an excess of KO₂ was used, the percentage of additional KO₂ was varied. In this case 75% additional KO₂ yields the best synthesis result. The precursors were filled into a platinum crucible and heated to 650°C in a horizontal furnace under argon flow. After the heat treatment the samples were stored in a glovebox under argon atmosphere since they are sensitive to the air moisture. XRD measurements revealed minor impurity phases of Yb₂O₃ and KOH·H₂O in the KYbO₂ samples.

KYbS₂ single crystals were synthesized using the KCl flux, with the ratio of Yb:S:KCl=2:3:80 [3]. S and KCl were weighed accordingly and thoroughly mixed in a mortar. Small pieces of Yb were placed in a quartz tube and covered with the S-KCl mixture. Subsequently, the precursors were sealed in the quartz tube under argon atmosphere. The sealed ampoule was placed in a furnace and heated in accordance to the heating program shown in Fig. 2 (left). Small KYbS₂ single crystals (<0.5mm) were formed shown in Fig. 2 (right). The success of the synthesis was verified via powder XRD measurements.

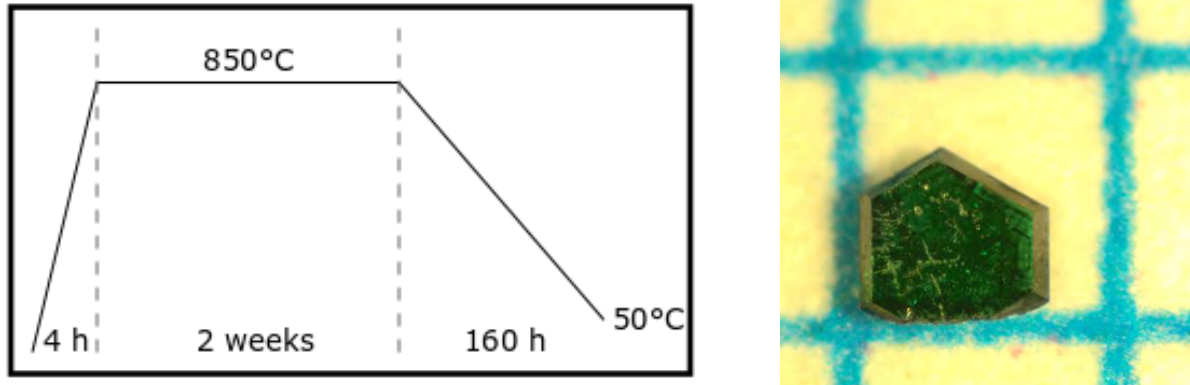


Fig. 2: Left: Temperature profile used for the synthesis of KYbS₂. Right: KYbS₂ single crystal.

Subject: Abstract Poster

- [1] L. Ding, P. Manuel, S. Bachus, F. Gräßler, P. Gegenwart, J. Singleton, R. D. Johnson, H. C. Walker, D. T. Adroja, A. D. Hillier, and Al. A. Tsirlin, *Physical Review B*, **100**, 144432 (2019)
- [2] B. Dong, Y. Doi, and Y. Hinatsu, *Journal of Alloys and Compounds*, **453(1)**, 282 – 287 (2008)
- [3] Ryosuke Iizaka et al. (Saitama University Japan)

The Influence of Sodium Dodecyl Sulfate on the Growth and Properties of Triglycine Sulfate Crystals

Ella Supik¹, Saskia Mihalic¹, Jannick Fammels¹, Rayhane Ghane-Motlagh²,
Peter Woias², and Andreas Danilewsky¹

¹ *Kristallographie, Institut für Geo- und Umweltnaturwissenschaften, Albert-Ludwigs-Universität Freiburg, Hermann Herder Str. 5, 79104 Freiburg, Germany*

² *Professur für Konstruktion von Mikrosystemen, Institut für Mikrosystemtechnik, Albert-Ludwigs-Universität Freiburg IMTEK, Georges-Köhler-Allee 102, 79110 Freiburg
E-mail: ellasusannsupik@googlemail.com*

Summary

This project investigates the influence of sodium dodecyl sulfate (SDS) on the morphology and structural properties of triglycine sulfate (TGS). TGS crystallises monoclinic in the space group $P2_1$ and shows a high pyroelectric effect parallel to the [010]-direction. The highest growth velocity of pure TGS is in the [010]-direction, as a result the (010)-faces disappear and will only appear as corners or edges. For a facilitated production of TGS infrared detectors the enlargement of the (010)-face is of great interest, if the pyroelectric figures of merit (FOM) are not heavily impacted.

J. Fammels [1] and S. Mihalic [2] started with several detergents to slow down the growth velocity in the [010]-direction. Sodium dodecyl sulfate (SDS) showed most promising results as described by R. Ghane [3,4]. The addition of SDS did not affect the pyroelectric coefficient (p_c) of 168 C/(m²K) at room temperature. However, the relative permittivity of 105 of TGS is decreased to 75 if SDS is added during growth. As a result, the figures of merit for voltage generation and for energy harvesting increased by 29 % to 201 kV/(mK) and 42,52 J/(m³K²) [4]. The pyroelectric coefficient was determined using a dynamic measuring method [3].

In this work a more suitable concentration of SDS was determined to further enlarge the (010)-face of the triglycine sulfate (TGS) crystals. Accordingly, the crystals were grown from aqueous solution with various concentrations of 0,00302 - 0,00306 Mol% of SDS, by the means of the temperature lowering method. The concentration of 552,04 g/l TGS resulted in a saturation temperature of 48,00 °C of the initial solution. The temperature was decreased at a rate of 0.08 °C/day, while continuously stirring with 60 rpm to ensure a homogenous concentration and temperature distribution during growth, without disturbing crystal growth. In all experiments, parasitic growth occurred on the bottom of the growth vessel, this however did not disturb the crystal growth. At higher concentrations of SDS (0.338 Mol% SDS), the parasitic crystals showed a needle-like structure [1,2], whereas parasites that formed during crystal growth of TGS with lower concentrations of SDS (<0.00306 Mol% SDS) showed a tabular habitus. The parasitic crystals were investigated and compared by the means of X-ray-powder-diffraction (XRD). The powder diffractometry of pure TGS, the tabular and needle shaped parasites show entirely different results. This leads to the assumption that the parasites are composed of different substances than TGS, the substance has not been identified yet.

One of five crystals, grown from solutions with low concentrations of SDS (<0.00306 Mol% SDS) developed monocrystalline (Fig. 2) with clear and well-developed faces, whereas four crystals started twinning (Fig. 1) in the course of the growth process. The twinning was initiated by sudden temperature changes and oversaturation of the solution and caused an acceleration of growth in [010]-direction. Thus, the (010)-face did not develop in the twinned crystals as shown in Fig. 1. Assuring a stable temperature reduction of 0.08 °C/day prevents the crystals from twinning.

Accordingly, monocrystalline TGS crystals with an enlarged (010)-face can be produced. The addition of 0,00306 Mol% SDS caused the largest reduction of growth velocity in [010]-direction. A monocrystalline crystal with a large (010)-face resulted, as shown in Fig. 2. The grown crystals were characterized by Laue measurements and X-ray-powder diffraction (XRD). The XRD analysis did not show any changes compared to pure TGS. Furthermore, IR-spectra of TGS crystals grown with 0,39 Mol% SDS, show the same peaks as pure TGS, thus no incorporation of SDS in the TGS crystals occurs [4].

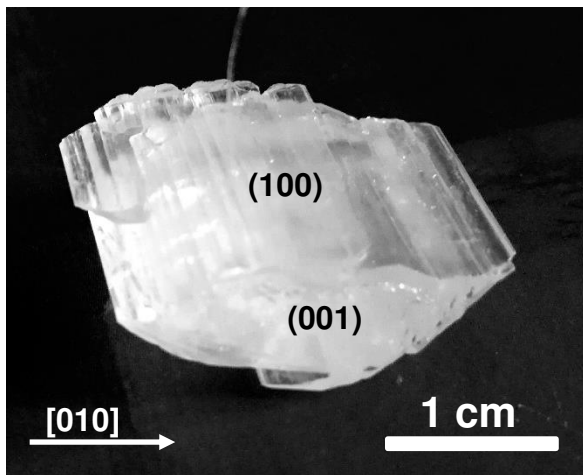


Fig. 2: Twinned TGS crystal grown with 0,00304 Mol% SDS. The twinning plane is parallel to the (100)-face.

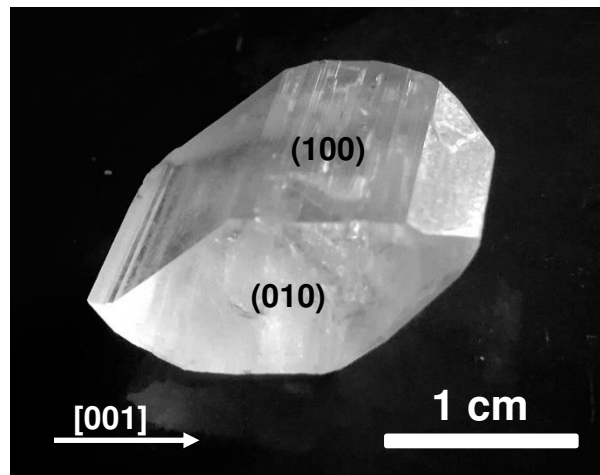


Fig. 2: Monocrystalline TGS crystal grown with 0,00306 Mol% SDS. The crystal inhibits a large (010)-face.

Acknowledgment

The authors thank Otto Schäfer, Müllheim for helpful discussions.

- [1] J. Fammels, BSc-thesis Albert-Ludwigs-Universität Freiburg, (2017), unpublished.
- [2] S. Mihalic, BSc-thesis Albert-Ludwigs-Universität Freiburg, (2019), unpublished.
- [3] R. Ghane-Motlagh, M. Kroener, F. Goldschmidtboeing, A.N. Danilewsky, P. Woias, Smart Mater. Struct. 27 (2018), 084004.
- [4] R. Ghane-Motlagh, J. Fammels, A. N. Danilewsky, U. Pelz, and P. Woias, J. Crystal Growth & Design, (2020), submitted.

Single-crystal growth and magnetic phase diagram of TbFeO₃

Alexander Engelhardt^a, Georg Benka^a, Andreas Bauer^a, Andreas Erb^b, Christian Pfeleiderer^a

^a Fakultät für Physik, Technische Universität München, James-Franck-Straße 1,
85748 Garching, Germany

^b Walther-Meißner-Institut, Bayerische Akademie der Wissenschaften, Walther-Meißner-Straße 8,
85748 Garching, Germany
E-mail: alexander.engelhardt@tum.de

Summary

The results are presented of the experimental investigation of the magnetic properties of the orthorhombic perovskite TbFeO₃. This compound has two magnetic sublattices resulting in complex magnetic phases. Furthermore, using neutron diffraction it was shown that it hosts a magnetic soliton lattice, a complex and anharmonic magnetic structure [1]. In the presented work, single crystal TbFeO₃ was synthesized by means of a combination of a solid-state reaction and the optical floating zone technique. X-ray powder diffraction patterns recorded at different temperatures revealed an anomaly in the thermal expansion at the antiferromagnetic ordering temperature of the iron spins at $T_N = 688$ K. Measurements of the zero-field magnetic susceptibility and of the heat capacity between 2 K and 300 K revealed the presence of two magnetic phase transitions, namely a ordering of the terbium spins around 8 K and a spin-reorientation of the two magnetic sublattices around 3 K. Based on measurements of the longitudinal ac susceptibility, various magnetic spin configurations were identified in detailed phase diagrams at low temperatures for magnetic fields applied along the three major crystallographic axes of the orthorhombic system. The main result, in particular, concerned the observation of the soliton lattice state by means of measurements of the transverse susceptibility when the external magnetic field is applied along the c-axis.

Acknowledgment

We wish to thank Andreas Erb and Astrid Habel for the supervision during the preparation of polycrystalline oxide rods for the optical floating zone technique. We acknowledge Susanne Mayr for the preparation of oriented single crystals. Financial support was provided through DFG TRR80.

[1] S. Artyukhin, M. Mostovoy, Nature Materials, **11**, 694-699 (2012)

Crystalgrowth of Fe-doped Li_3N

F. Breitner^a, M. Fix^a and A. Jesche^a

^aEP VI, Electronic Correlations and Magnetism, University of Augsburg, Germany
E-mail: franziska.breitner@physik.uni-augsburg.de

Summary

$\text{Li}_2(\text{Li}_{1-x}\text{Fe}_x)\text{N}$ shows fascinating magnetic properties with high magnetic anisotropy and huge hysteresis. The spin reversal is dominated by quantum tunneling of the magnetization and the system can be considered a single atom magnet [1]. Here, we present a method for growing $\text{Li}_2(\text{Li}_{1-x}\text{T}_x)\text{N}$ single crystals doped with iron and other transition metals $T = \{\text{Mn}, \text{Co}, \text{Ni}, \text{Cu}\}$ from a lithium-rich melt. Liquid lithium has a low melting point as well as a high solubility for nitrogen already at comparatively low temperatures of 800°C and below [2]. The low solubility of transition metals in pure lithium can be considerably improved by adding a third element, in this case nitrogen. Both these properties make lithium a promising flux for the growth of nitride-based single crystals.

Crystal growth of $\text{Li}_2(\text{Li}_{1-x}\text{T}_x)\text{N}$ is performed using a three-cap-crucible which is made from a niobium tube, two caps and a strainer also made from niobium. Due to the high reactivity of lithium and the air and moisture sensitivity of the reactants and the final product, all manipulations were carried out in an argon-filled glovebox (with O_2 and H_2O below 0.5 ppm). After loading the starting materials (Li, Li_3N and T), the crucible is sealed by welding the cap to the tube using an arc-melter. This crucible is again sealed in a quartz ampoule under argon atmosphere to prevent the niobium from oxidation and placed in a furnace. The mixture is then heated to a maximum temperature of 850°C, cooled down to 750°C within an hour and slowly cooled down to 500°C over typically 150 hours. After the growth process is finished, the crystals are separated from the flux via high temperature centrifugation which is performed within seconds after the sample has been removed from the furnace at 500°C [3].

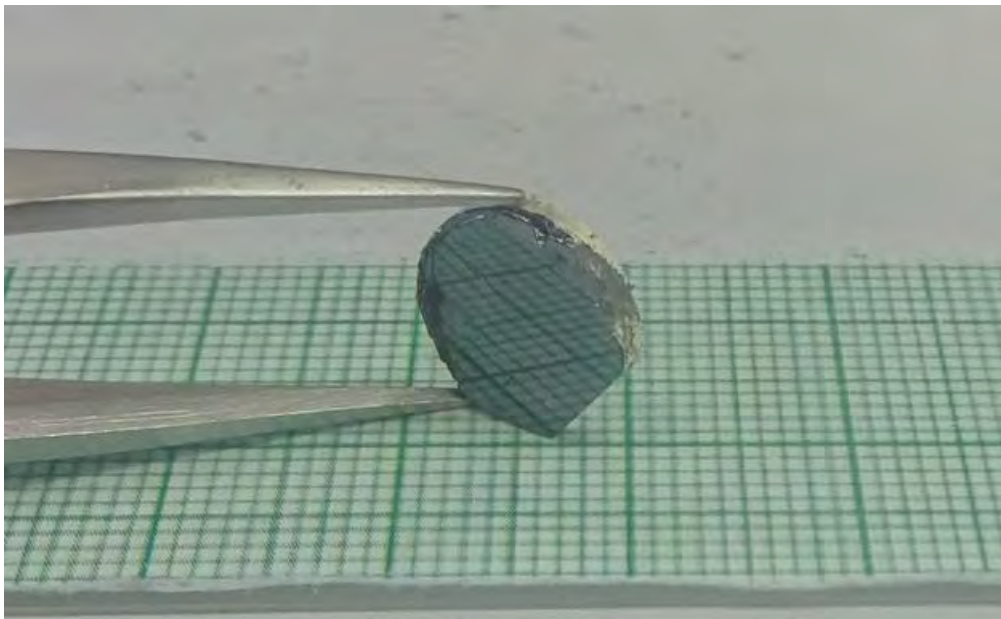


Fig. 1: As-grown Li_3N single crystal obtained from lithium-rich flux on a millimeter grid.

The obtained single crystals show a hexagonal symmetry and a side length of several millimeters. In some cases, the size of the crystals is limited by the diameter of the used niobium crucible of 12mm. A significant amount of lithium in the crystals grown using this method can be substituted with transition metals, e.g. $x = 30 \%$ for $T = \text{Fe}$. The habit and size of the resulting crystals are significantly influenced by the introduction of the different transition metals. Structural characterization was performed using X-Ray diffraction and chemical analysis by means of inductively coupled plasma optical emission spectrometry measurements.

The size and quality of the single crystals allow for a plethora of experiments to be performed such as measurements of the anisotropic magnetic, thermodynamic and optical properties.

Acknowledgment

This work was supported by the Deutsche Forschungsgemeinschaft (DFG, German Research Foundation) - Grant No. JE748/1.

- [1] M. Fix, J.H. Atkinson, P.C. Canfield, E. del Barcon, and A. Jesche, Phys. Rev. Lett. **120**, 147202 (2018)
- [2] T. Massalski, Binary Alloy Phase Diagrams, Volume **3**, 2448 (1990)
- [3] A. Jesche and P. Canfield, Phil. Mag. **94**, 2372-2402 (2014)

Microstructural evolution of intermetallics under the influence of magnetic field annealing – exemplified by Mn_3Ga

G. Kirste^a, C.G.F. Blum^a, J. Freudenberger^a, S. Wurmehl^a, B. Büchner^a

^a Leibniz-Institut für Festkörper- und Werkstoffforschung, Helmholtzstraße 20, 01069 Dresden, Germany

E-mail: g.kirste@ifw-dresden.de

Summary

Magnetic field annealing is a valuable tool for influencing microstructure and texture. The origin of this approach lies within the interaction of an external magnetic field with the sample's magnetic anisotropy. Although anisotropic magnetic susceptibility may even be found in diamagnetic materials, magnetic field annealing is especially interesting for materials with exceptional ferromagnetic properties. Among these materials with high response to external magnetic fields are Heusler related intermetallics - like Mn_3Ga , showing a $D0_{22}$ structure.

The Mn-Ga phase diagram being rather complex, this phase cannot be obtained by a simple melting process. In such cases magnetic field annealing provides another advantage. With the aid of the magnetic contribution to Gibbs free energy the applied external magnetic field may act as key to promoting phase formation or even enable new phase formation routes. For Mn_3Ga , *Ener et al.* depicted the magnetic field-assisted formation of the $D0_{22}$ phase [1].

Referring to those previous findings, Mn_3Ga samples were annealed for up to two weeks within this study. The results of conventional annealing were contrasted with those of magnetic field annealing in a superconducting magnet using a magnetic flux density of 7 T (*Figure 1*). Beforehand the arc melted samples received rotary swaging to increase the defect concentration, which further forwards the phase transformation. In the course of characterization, we focused on the progression of microstructure using microscopical methods, supplemented by some analysis via X-ray diffraction and SQUID magnetometry.

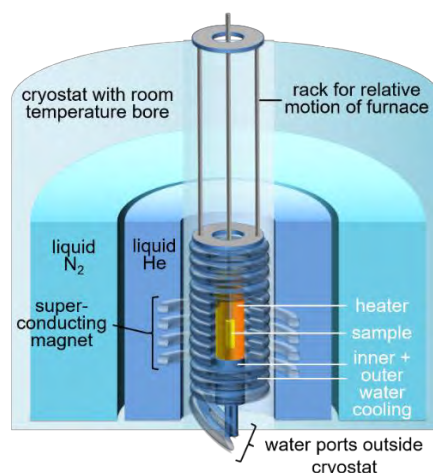


Fig. 1: Experimental setup for magnetic field annealing in a superconducting magnet.

The achieved differences in microstructural evolution with and without application of an external magnetic field will be discussed. Furthermore, the example of Mn_3Ga will be used to sketch the capabilities of magnetic field processing for tailoring the microstructure of intermetallics in general.

References

- [1] S. Ener, K.P. Skokov, D.Y. Karpenkov, M.D. Kuz'min, O. Gutfleisch, *Journal of Magnetism and Magnetic Materials*, **382**, 265-270 (2015)

ZF NMR AS A TOOL TO CLARIFY CRYSTALLOGRAPHIC, MAGNETIC AND ELECTRONIC STRUCTURE OF MAGNETICALLY ORDERED MATERIALS

P.Fritsch^a, F. Hammerath^a, J. Lucassen^b, C. F Schippers^b, M. A. Verheijen^{b,c}, E. J. Geluk^d, B. Barcones^d, R. A. Duine^{b,e}, H. J. M. Swagten^b, B. Kopmans^b, R. Lavrijsen^b, S.Wurmehl^{a,f}

^a IFW Dresden, Institute for Solid State Research, Helmholtzstraße 20, 01069 Dresden, Germany

^b Department of Applied Physics, Eindhoven University of Technology, P.O. Box 513, 5600 MB Eindhoven, the Netherlands

^c Eurofins Materials Science BV, High Tech Campus 11, 5656 AE Eindhoven, The Netherlands

^d NanoLab@TU/e, Eindhoven University of Technology, P.O. Box 513, 5600 MB Eindhoven, the Netherlands

^e Institute for Theoretical Physics, Utrecht University, Princetonplein 5, 3584 CC Utrecht, the Netherlands

^f Institute of Solid State and Materials Physics, TU Dresden, 01062 Dresden, Germany

E-mail: p.fritsch@ifw-dresden.de

Macroscopic properties of (magnetically ordered) materials are inseparably linked to their (local) structure. Hence, any specific functionality can only be understood and tailored if the structure-property relationships are taken into account.

Nuclear magnetic resonance spectroscopy (NMR) is a known standard technique for structure analysis on a wide range of materials. The basis of NMR is the interaction of the nucleus' spin with an external magnetic field, neighboring nuclei and the surrounding electrons. The externally applied field is the determining factor in paramagnetic and diamagnetic matter. However, for magnetically ordered materials the strongest contribution stems from the hyperfine field originating in the hyperfine interaction of the nuclear magnetic moment with the magnetic field deriving from the spin and orbital currents of the surrounding electrons. Therefore magnetically ordered materials can be probed with ease under zero external field. Zero-field nuclear magnetic resonance spectroscopy (ZF NMR) is a tool to probe the local environment of the NMR active nuclei on an integral scale. This tool enables a variety of local properties, such as local crystallographic defects, lattice strain, magnetic stiffness, local magnetic moments and even the local electronic structure [1-3].

We use ZF NMR to investigate Co thin films with the different thicknesses $t = 10$ nm and $t = 25$ nm. The objective in this work is to explain the increase in magnetic anisotropy with increasing film thickness [4]. The investigation with ZF NMR as a local probe gives us information about the ratio and magnetic stiffness of different crystallographic phases and stacking faults present in the films. Figure 1 shows the ⁵⁹Co ZF NMR spectrum for the sample $t = 25$ nm. The spectrum is fitted with an appropriate Gaussian model to extract the exact resonance frequencies of each specific crystallographic environment and their corresponding ratio in the overall film. The resonance frequencies are compared with the literature and assigned accordingly [5]. Two allotropes can be found within the thin film: fcc (blue line) and hcp (magenta line). While hcp Co is the stable allotrope under ambient condition, Co grows in the fcc structure on top of Pt due to lattice mismatch. Between the fcc and hcp environment two distinguishable stacking fault (sfs) environments can be found. Concerning the magnetic anisotropy and how this is linked to the structural finding, there are two possible sources for the increase in this property. Either the observed magnetic anisotropy stems from a magnetocrystalline (intrinsic) effect due to the larger contribution of hcp Co in the thicker film which is inherently more anisotropic than fcc Co or the anisotropy originates in the magnetoelastic (extrinsic) effect, due to defect pinning on the sites of the stacking faults between the fcc and hcp Co. We will

give an answer to this question as well as more examples from our recent research underlining the potential of ZF NMR to understand structure-property relationships in modern materials.

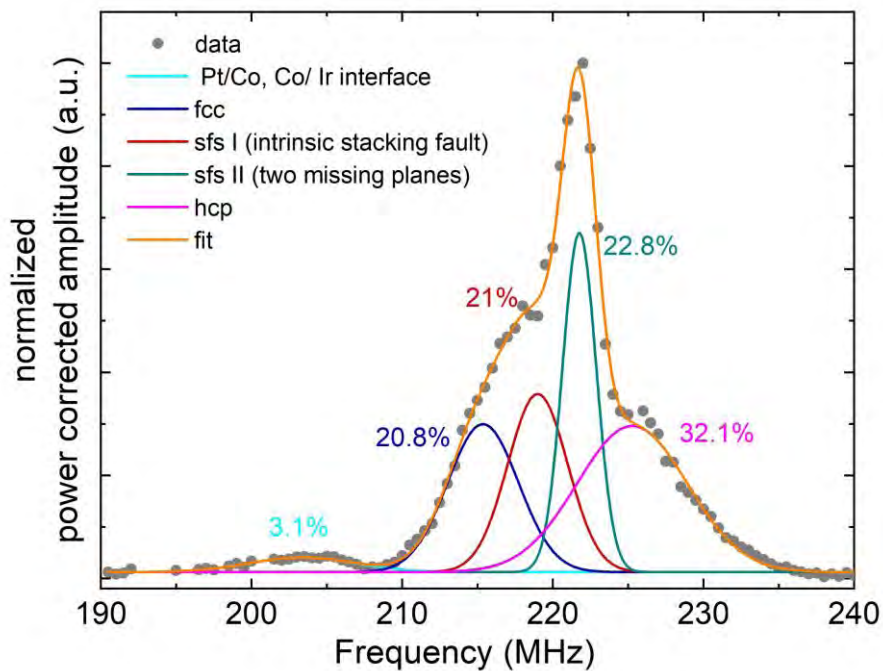


Fig. 1: ^{59}Co ZF NMR frequency spectrum of a Co thin film (thickness $t = 25$ nm).

Acknowledgment

Financial support is acknowledged from the Deutsch Forschungsgemeinschaft (DFG) through Grants No. WU595/3-3 and WU595/14-1

- [1] A. C. Gossard and A. M. Portis, Phys. Rev. Lett., **3**, 164 (1959)
- [2] P. Panissod and C. Mény, Appl. Magn. Reson., **19**, 447-460 (2000)
- [3] S. Wurmehl and J. T. Kohlhepp, J. Phys. D: Appl. Phys., **41**, 173002 (2008)
- [4] J. Lucassen, C. F. Schippers, M. A. Verheijen, P. Fritsch, E. J. Geluk, B. Barcones, R. A. Duine, S. Wurmehl, H. J. M. Swagten, B. Koopmans, R. Lavrijsen, arXiv:1909.02467, (2019)
- [5] G. J. Strijkers, J. T. Kohlhepp, H. J. M. Swagten, W. J. M. de Jonge, Appl. Magn. Reson., **19**, 461-469 (2000)

LnMn₂Ge₂ (Ln = Nd, Sm, Dy): SINGLE CRYSTAL GROWTH AND CHARACTERIZATION

K. Kliemt, M. Ocker, R. Möller and C. Krellner

Kristall- und Materiallabor, Goethe-Universität Frankfurt, Max-von-Laue-Str.1, 60438 Frankfurt, Germany
kliemt@physik.uni-frankfurt.de

Among the 122 compounds which crystallize in the ThCr₂Si₂-type structure, the compounds LnMn₂Ge₂, where Ln is a rare earth element, stand out since they exhibit a complex magnetic behaviour. At high temperatures, the magnetism is dominated by the ordering of the 3d electrons of Mn, while at low temperatures it is determined by the ordering of the rare earths local moments [1, 2].

There are many studies of polycrystalline samples or small single crystals, but large and pure single crystals suitable for spectroscopic studies are missing. In previous work, the possibility of the growth of single crystals from indium flux was reported [3]. Our attempts to grow the LnMn₂Ge₂ (Ln=Nd, Sm, Dy) from indium or tin flux failed. Instead, we succeeded to grow these compounds from a stoichiometric mixture of the elements.

In this contribution, we present the details of the growth by Czochralski method. Preliminary differential thermal analysis (DTA) showed that the compounds do not grow congruently. Furthermore it turned out that the evaporation of Mn from the stoichiometric melt is considerably large. Therefore, we applied the Czochralski method using a levitating melt under enhanced Ar pressure for the growth (Fig. 1, left). Recently, this procedure was developed and successfully applied to the single crystal growth of the ferromagnetic quantum-critical compound YbNi₄P₂ [4]. From the grown samples, mm-sized single crystals of LnMn₂Ge₂ were extracted (Figs. 2 and 3). In this contribution, we will present the chemical and structural characterization of the Czochralski grown LnMn₂Ge₂ crystals and some physical measurements around the magnetic transitions.



Fig. 1: *Left*: Crystal growth by Czochralski method from a levitating melt. *Right*: ThCr₂Si₂-type structure of the LnMn₂Ge₂ compounds.

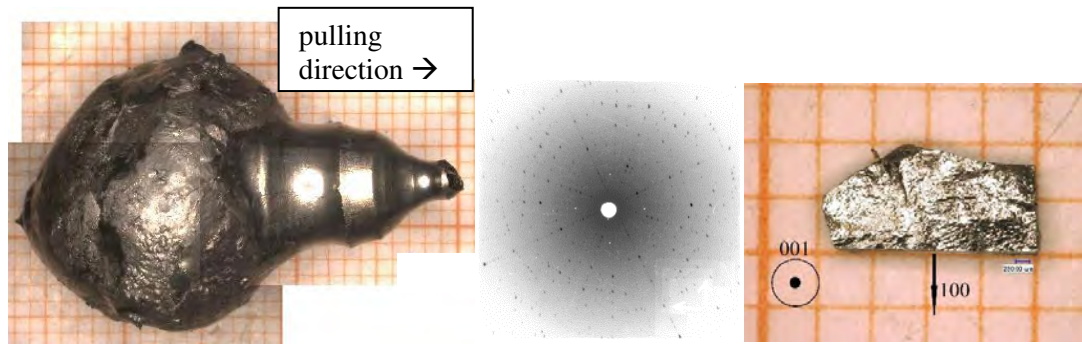


Fig. 2: *Left*: SmMn₂Ge₂ Czochralski grown sample. *Middle*: Laue pattern view along the tetragonal axis. *Right*: Extracted single crystal grain of SmMn₂Ge₂.

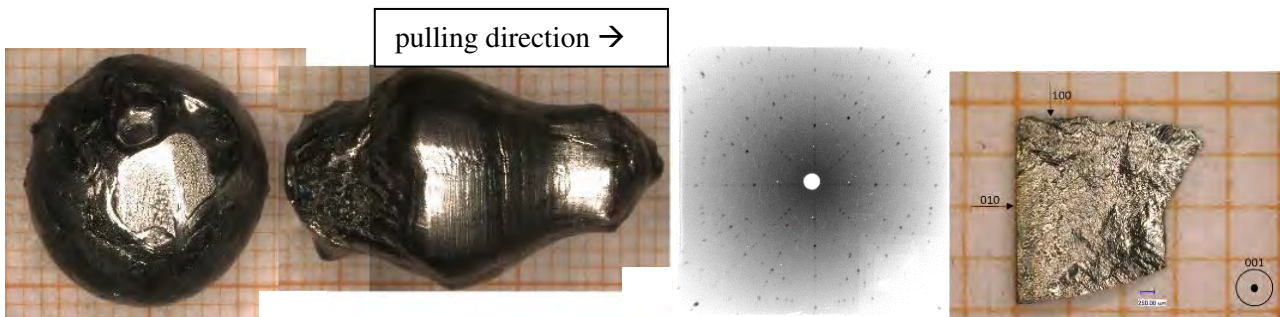


Fig. 3: *Left*: NdMn₂Ge₂ Czochralski grown sample separated from the residual flux. *Middle*: Laue pattern, view along the tetragonal axis. *Right*: Extracted single crystal grain of NdMn₂Ge₂.

- [1] G. Guanhua et al., Journal of Experimental and Theoretical Physics 93, 796 (2001).
- [2] N. P. Kolmakova et al., Low Temperature Physics 28, 653 (2002).
- [3] E. M. Gyorgy et al., Journal of Applied Physics 61, 4237 (1987).
- [4] K. Kliemt, C. Krellner, J. Cryst. Growth 449, 129 (2016).

Directly analyzing the depth dependent properties of $\text{Cu}(\text{In,Ga})(\text{S,Se})_2$ wedges manufactured by exfoliation and a nontoxic, adjustable etching process

M. Schuster ^a, U. Künecke ^a, P.I. Reyes Figueroa ^b, R. Klenk ^b, P.J. Wellmann ^a

^a Institut Materialien der Elektronik und der Energietechnologie (i-MEET), Friedrich-Alexander Universität, Martensstr. 7, 91058 Erlangen, Germany

^b PVcomB, Helmholtz Zentrum Berlin (HZB), Hahn-Meitner-Platz 1, 14109 Berlin, Germany
E-mail: msc.matthias.schuster@fau.de

Summary

The material system of $\text{Cu}(\text{In,Ga})(\text{S,Se})_2$ (CIGS) is well-established among high efficiency thin film solar cells. The physical properties of CIGS throughout the absorber layer depend on the depth distribution of composition profiles, especially elemental profiles of Ga and S. Thus a reliable quantification technique is required, especially to tune the optoelectronic properties like the band gap energy. In this work a nontoxic and adjustable etching process was used to prepare wedge-shaped samples for further direct analysis – both from CIGS absorbers on glass substrates (provided by Helmholtz Zentrum Berlin) as well as from exfoliated CIGS films. Large area energy dispersive X-ray spectroscopy (EDX) with different acceleration voltages from the front (CIGS on substrate) and from the back side (exfoliated CIGS film) was used to acquire a first determination of the element composition. The CIGS wedges were characterized by field emission scanning electron microscopy (FESEM) to evaluate the morphology, EDX at 10 kV to determine the local element composition and distribution, and photoluminescence (PL) to investigate the optoelectronic properties. A schematic of the sample preparation and characterization processes can be seen in Fig.1.

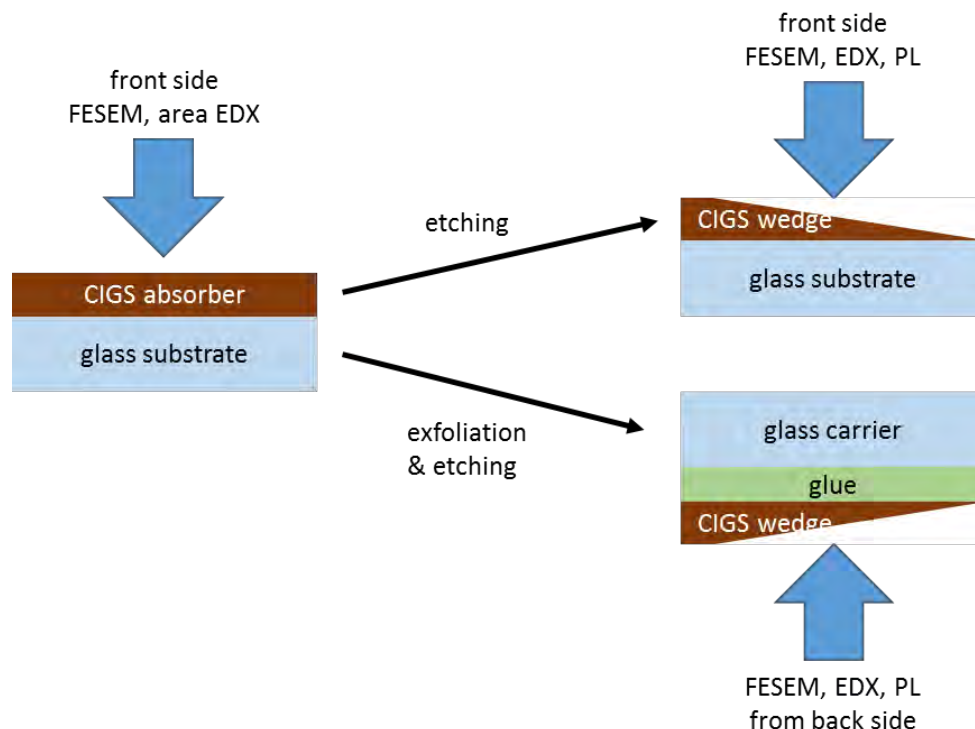


Fig. 1: Schematic of the CIGS wedge sample preparation and the performed characterization measurements.

In Fig.2 the different sample types are compared concerning their Cu(In+Ga) and Ga(In+Ga) ratios as well as their Sulfur and Selenium content throughout the CIGS film. The respective amounts were measured by area EDX with different acceleration voltages from the front side and the back side. After etching the CIGS on substrate and exfoliated CIGS films, low voltage EDX measurements are used to further analyze and confirm the expected elemental profiles.

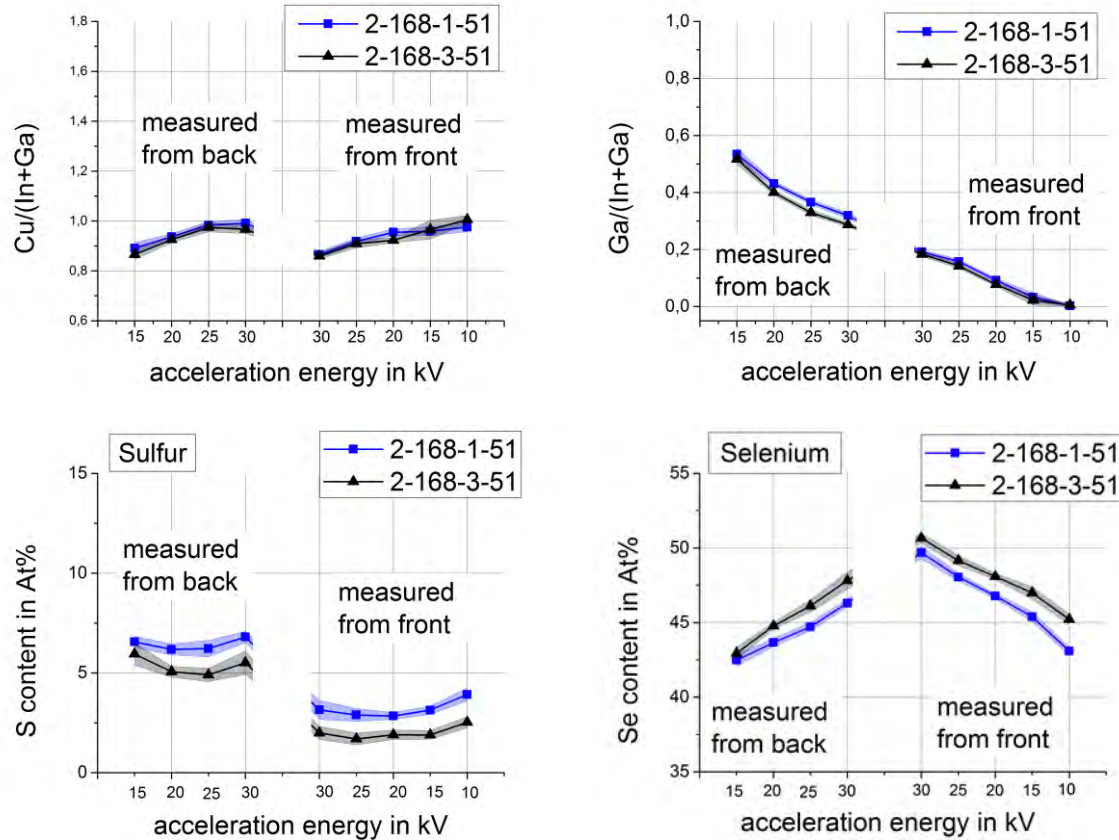


Fig. 2: Values of Cu(In+Ga), Ga(In+Ga) and S content throughout the layer as measured with area EDX with different acceleration voltages from the front (CIGS on substrate) and from the back (exfoliated CIGS films).

The directly measured (PL) minimum band gap energy is slightly lower than the estimated value from the composition gradients that were measured by glow discharge optical emission spectroscopy (GDOES). Moreover throughout the CIGS film a rise in band gap energy can be measured, as the amount of Ga increases towards the back contact.

Acknowledgment

The authors thank Erik Waack and Ralf Haberecht from HZB for providing the CIGS films. This project is funded under support code 0324154 by the German Ministry of Economic Affairs and Energy (BMWi) on the basis of a decision by the German Bundestag.

Crystal growth of (Cd,Zn)Te under microgravity Vampir-F: Characterization of ground experiments

J. Zou¹, A. Fauler¹, A.S. Senchenkov², N.N. Kolesnikov³, M. Fiederle¹

¹ Materials Research Center FMF, Freiburg, Germany

² Research and Development Institute for Launch Complexes NIISK, Moscow, Russia

³ Institute of Solid State Physics of Russian Academy of Sciences, Chernogolovka, Russia

E-mail: jiaona.zou@fmf.uni-freiburg.de

Cadmium zinc telluride ((Cd,Zn)Te) has been considered a promising material for the fabrication of room temperature X- and Gamma-Ray detectors, owing to its excellent electrical properties and its high density. Travelling Heater Method (THM), which is a solution growth technique, allows the preparation of monocrystalline material with the required electrical properties regarding high resistivity and high carrier mobility-lifetime-products. The THM method provides a uniform crystal composition of ternary materials such as (Cd,Zn)Te.

Nevertheless, the application is limited by the presence of material defects, such as Te inclusions, twins and even cracks. The growth of defect-free quality (Cd,Zn)Te crystals still remains a challenge. Microgravity conditions provide unique possibilities to improve the quality of the crystals owing to suppression of buoyancy convection. To study the influence of microgravity on the crystal quality, two space experiments 'VAMPIRE-F' are scheduled for 2021. The preparation of these experiments includes the growth of several crystals using THM and the characterization of these crystals as well as the growth of seed material in our 3 inch THM facility.

Some of the important parameters of the ground experiments are shown in Tab. 1. After performing the first two ground experiments, two problems have been found. Firstly, there was a large zinc concentration variation at the boundary between the seed and the grown crystal. And secondly, both of the seeds were almost not dissolved. Therefore, some parameters have been adjusted for the third experiment aiming to solve these problems. First, the CdTe concentration in the Te Zone was increased from 5 % to 10 %. In addition, the heater temperature at the beginning of the translation was increased and then went back slowly. At last, the starting position of the heater was moved 5 mm towards the seed direction.

Tab. 1: experimental parameters of the three ground experiments

sample No.	doping	CdTe % in Te Zone	heater temperature	RMF	heater position
F1-01-GM	In (5 ppm)	5%	1080-1100 °	no	Zone centre
F1-02-GM	In (5 ppm)	5%	1100-1110 °	2 mT, 100 Hz	Zone centre -2 mm
F1-03-GM	In (5 ppm)	10%	1110-1100-1110 °	2 mT, 100 Hz	Zone centre -5 mm

In this study, Infrared Transmission Microscope was used to analyze the defects distribution, like Te inclusions. Birefringence measurement and optical microscopy were performed to analyze the stress distribution in the crystals. Further, X-ray Diffraction (XRD) and Energy Dispersive X-ray Spectroscopy (EDX) were done to obtain further information of the Zn concentration and defects in the crystals. In addition, Contactless Resistivity Mapping (COREMA) was used to measure the resistivity of the crystals.

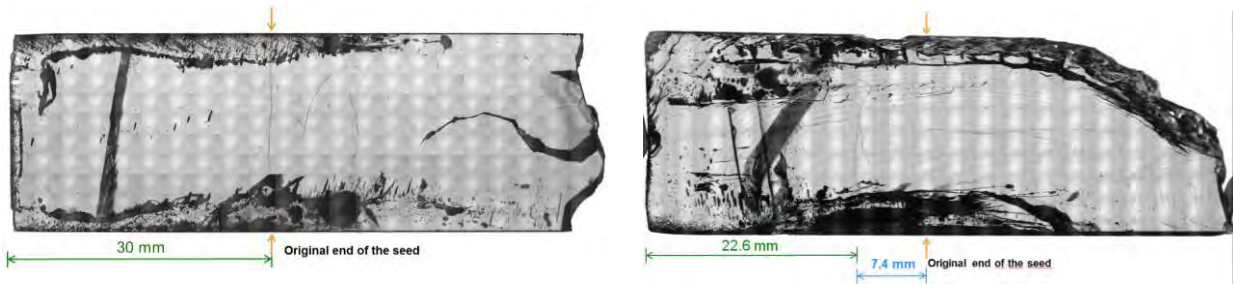


Fig. 1: IR images of F1-02-GM (left) and F1-03-GM (right). The seed of the second sample F1-02-GM was not dissolved, while the seed of F3-03-GM was dissolved for 7.4 mm after adjustment of the experimental parameters.

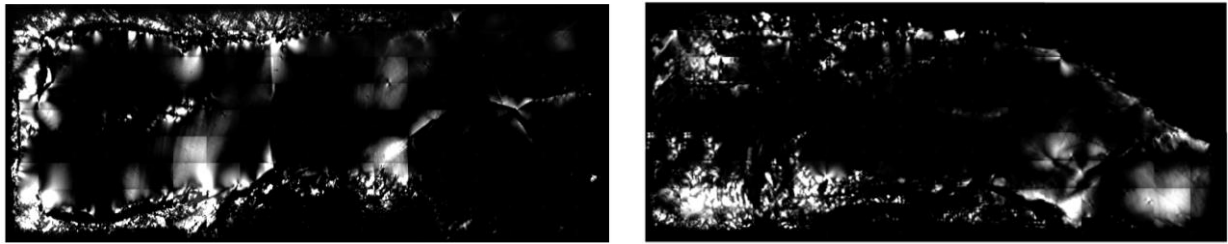


Fig. 2: Birefringence mappings of F1-02-GM (left) and F1-03-GM (right). Some stress was found at the boundary of F1-02-GM, while the boundary of F1-03-GM is free from dramatic stress.

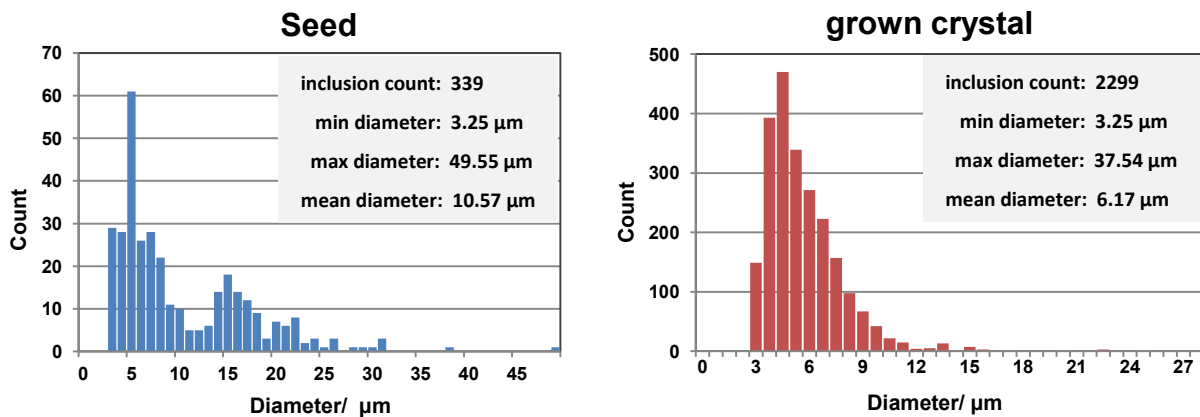


Fig. 3: histogram of the two areas with the same size in sample F1-03-GM. The grown crystal has much more inclusions but with smaller mean diameter (10.57 μm) when compared to the seed (6.17 μm).

In-situ detection of crystallization processes and seed selection in high temperature solutions

Andreas Schneider¹ and Anton Jesche¹

¹*University of Augsburg, Universitätsstraße 2, 86135 Augsburg, Germany*

andreas-gabriel.schneider@physik.uni-augsburg.de

anton.jesche@physik.uni-augsburg.de

Summary

Solution growth is a powerful tool for single crystal growth of various materials [1] and particularly useful for basic research in solid state physics and chemistry. Compared to procedures like Czochralsky or Bridgeman growth it doesn't depend on congruent melting of the respective compound. In contrary, a decrease of the formation temperatures of the desired compounds by several hundred degrees as well as reduced vapor pressures and higher diffusion rates can be achieved. Accessing the exact onset and temperature of nucleation on the other hand remains almost impossible. A prediction of this instant gets also hampered by the uncertainties of the published liquidus temperatures (if available at all). This gets aggravated by supercooling, which stays undetected during the growth procedure. The difference between the displayed furnace temperature and the actual sample temperature makes this even more difficult.

Here we present a way to accurately measure the complete time-temperature profile including small temperature changes caused by dissolution or nucleation. This is achieved by contacting the growth crucible (ceramic) with a measurement wire of high thermal and mechanical stability such as pure or alloyed tungsten. By sawing grooves into the crucible's bottom side and placing the wire into them in a meandering way, the wire gets as close as possible to the melt without direct contact covering a major part of the crucible bottom. An alumina based high temperature ceramic glue with high thermal conductivity covers and stabilizes the wire inside the grooves. By connecting the thin wire with massive metallic rods (3 mm in diameter) of tungsten or molybdenum that lead from the heating zone to the outside of the furnace the voltage at the measurement wire can be detected directly by using a Lock-in amplifier. Due to the linear temperature dependence of the wire resistance, the measured Lock-In voltage directly follows the crucible temperature. Additional contributions by released or absorbed heat inside the solution cause anomalies within this curve. Information about the absolute temperature is provided by a thermocouple the crucible is placed onto during growth.

Without the necessity of a reference crucible, the signal-to-noise ratio approaches the level of conventional DTA-signals. The detection of nucleation enables seed selection using oscillations within a well-defined temperature range. The system can be applied to various solvents including aqueous solutions and has been proven up to 1300°C. Furthermore, promising tests on metallic crucibles such as tantalum have been successfully conducted. The entire measurement setup is placed in a tube furnace, providing high heating and cooling rates, a temperature accuracy of 0.5 Kelvin and stable atmosphere conditions. The reaction chamber can be flooded with inert gas allowing the growth of air sensitive samples as well as protecting metallic crucibles and the measurement wire. The processes are

controlled by a graphical user interface offering the possibility of real time observation of the sample state together with in-situ analysis tools.

Eight well explored binary systems showing phase transitions between 147°C and 1121°C have been investigated and compared with DTA measurements of the same composition. Obtained results are in good agreement with the literature as well with DTA. Single crystals of binary PdBi were investigated in detail and the growth optimized. The obtained crystals were successfully enhanced in size in comparison to conventionally grown ones.

Furthermore they are not only significantly larger but also of excellent quality as shown by the emergence of dHvA-oscillations at comparatively high temperatures and low fields of 3 Tesla at 2 Kelvin. Besides the liquid-solid phase transitions also a solid-solid phase transition of β -PdBi₂ to α -PdBi₂ [2] and vice versa has been detected successfully, showing the sensitivity and versatility of the system.

The established setup offers a considerable increase in efficiency and accuracy for various solution growth processes, suitable for a wide variety of systems. The application to other such growth systems as well as further improvements of sensitivity and precision are anticipated.

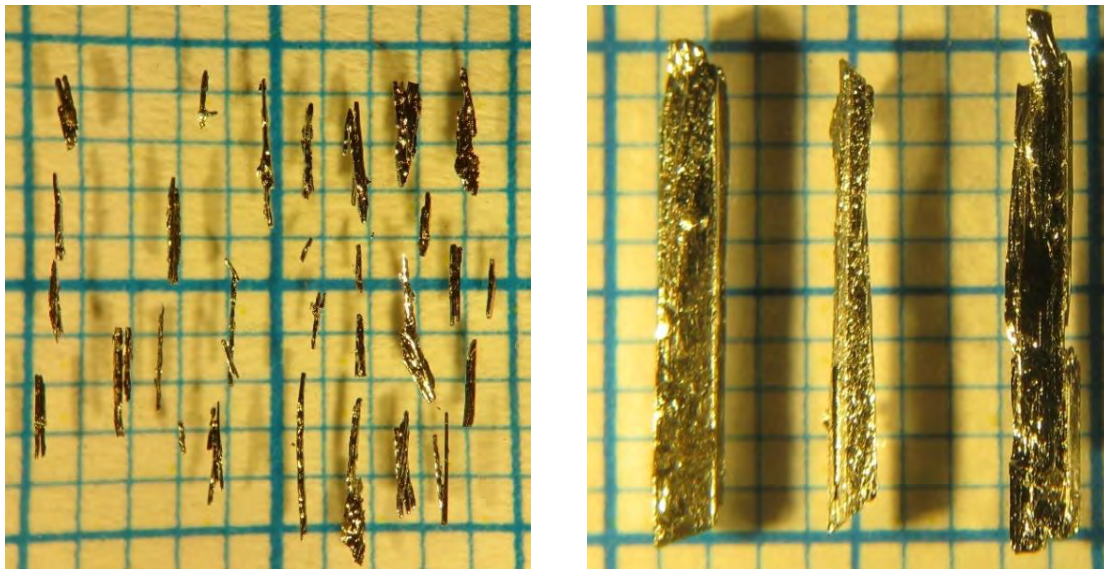


Fig: Conventional grown PdBi-crystals from a box furnace (left) in direct comparison with seed selected PdBi-crystals (right)

Acknowledgment

This work was supported by the Deutsche Forschungsgemeinschaft (DFG, German Research Foundation) - Grant No. JE748/1. The crystal growth apparatus is developed in a cooperative project with the SciDre GmbH, Dresden, with financial support from the ZIM program of the German Ministry for Economic Affairs and Energy (BMWi).

[1] M. M. Kanatzidis, R. Pöttgen, W. Jeitschko, *Angew. Chem. Int. Ed.* **2005**, *44*, 6996.

[2] T. B. Massalski (ed.), *Binary Alloy Phase Diagrams* (Vol. 1), ASM International, Materials Park, OH **1986** → Bi-Pd (Bismuth-Palladium)

[3] A. G. Schneider, P. Sass, R. Schöndube, A. Jesche, *Cryst. Res. Technol.* **2019**, 1900109

A KMC model for homoepitaxial growth of Ga₂O₃

W. Miller^a, Dennis Meiling^b, Robert Schewski^a, Andreas Popp^a, Saud Bin Anooz^a,
and Martin Albrecht^a

^a Leibniz-Institut für Kristallzüchtung (IKZ), Max-Born-Str. 2, 12489 Berlin, Germany

^b Electrical Energy Storage Technology (EET) TU Berlin, Einsteinufer 11, EMH 2, 10587 Berlin, Germany
E-mail: wolfram.miller@ikz-berlin.de

Introduction

β -Ga₂O₃ has recently become of great interest because it is an excellent candidate for power electronics and optoelectronic applications [1,2]. Large progress has been made in the homoepitaxy by MBE, MOVPE, and HVPE. Nevertheless, many details of the process are not yet known. Kinetic Monte Carlo methods are one possibility to gain a deeper insight into the surface kinetics. A set of experiments followed by surface analysis using STEM and AFM give us the possibility to compare both experimental and numerical results. We consider only MOVPE on (100) planes because this was the only surface where step growth was achieved [3–5].

Kinetic Monte Carlo Method

We set up a KMC model, which reflects the structure of Ga₂O₃ with its 8 Ga atoms and 20 O atoms in the unit cell. Ga and O₂ can adsorb. The sticking coefficient is set according to the particular atomic configuration of the surface atoms (details see [6]). Ga and O atoms can diffuse, also GaO_x species can diffuse in *c*-direction. There is evidence from experiments that Ga₂O can desorb [7] and thus, we consider this in KMC. We make a list of all possible events with their probabilities and chose in every iteration one event randomly with respect to its relative probability to the sum of probabilities of all events. The diffusion energies were set in the range of 1.5 eV because a 1D mean field approach for island growth gave a value of this order by comparison with experimental results [4].

Results

We performed runs on flat (on-oriented) and vicinal (6° miscut) surfaces. STEM HAADF images of the surfaces reveal that the terraces are always B1 or B2-plane (see Fig. 1) [8].

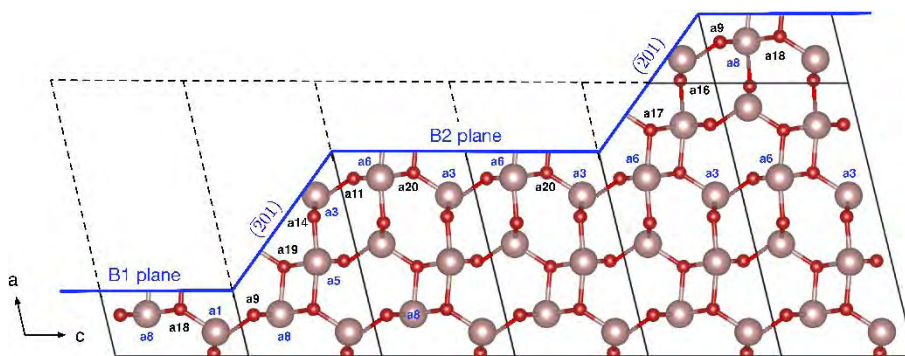


Fig. 1: Surface planes as observed in the STEM analysis. Atoms are labeled according to their number in the KMC code.

On flat surfaces we modify the ratio O/Ga. For small O/Ga ratio no critical nucleus could be formed. The larger the ratio the faster the growth. Nevertheless, no 3D growth is observed but first the next B-plane is filled up. This corresponds with the experimental observations. Choosing a fixed O/Ga ratio we performed

runs for 750°C, 800°C, and 850°C. For the latter we observe large 2D islands as in the experiments [6]. At lower temperature the growth is faster but structure sizes are smaller.

On the vicinal surface we change the desorption rates. For an intermediate desorption rate (as used for the flat surface) we obtain step growth (case B in Fig. 2). For high desorption rate (case C) we observe step bunching because every fluctuation in edge growth leads to a growth instability. In the opposite case (case A) we observe random growth on the terraces but eventually ending up in a double step. The final morphology looks similar to that of Case C. Please note that we have only two steps in our KMC run and cannot make any realistic statement beyond the 20 s shown in Fig. 2.

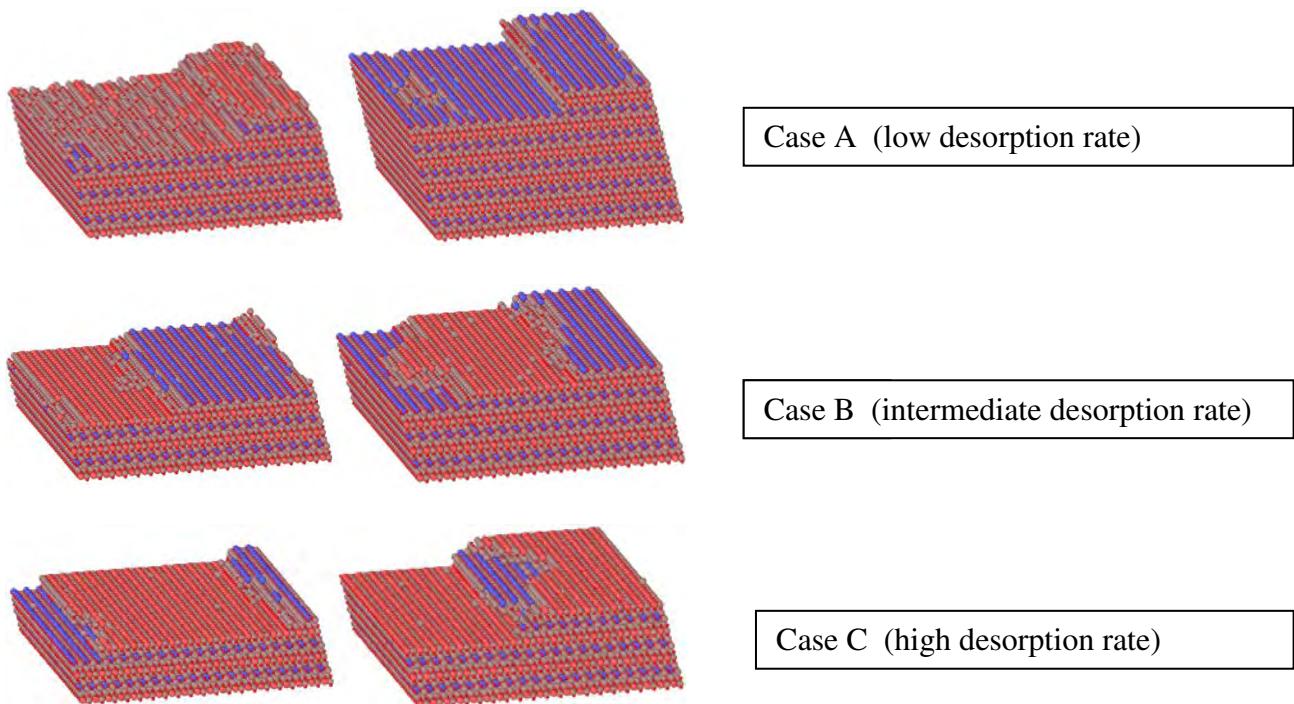


Fig. 2: Surface morphologies for runs with different desorption rates. Left: 10s, Right: 20s.

Acknowledgment

This work was partially conducted in the frame of Science Campus for Growth and Fundamentals of Oxides (GraFox) supported by the Leibniz Association.

- [1] M. Higashiwaki, H. Murakami, Y. Kumagai, A. Kuramata, *Jap. J. Appl. Phys.*, **55**, 1202A1 (2016).
- [2] M. Zhong, Z. Wei, X. Meng, F. Wu, J. Li, *J. Alloys Comp.*, **619**, 572 (2015).
- [3] T. Oshima, N. Arai, N. Suzuki, S. Ohira, S. Fujita, *Thin Solid Films*, **516**, 5768 (2008).
- [4] R. Schewski, M. Baldini, K. Irmischer, A. Fiedler, T. Markurt, B. Neuschulz, T. Remmele, T. Schulz, G. Wagner, Z. Galazka, et al., *J. Appl. Phys.*, **210**, 225308 (2016).
- [5] M.-Y. Tsai, O. Bierwagen, M. E. White, J. S. Speck, *J. Vac. Sci. Technol. A* **28**, 354 (2010).
- [6] W. Miller, D. Meiling, R. Schewski, A. Popp, S. Bin Anooz, M. Albrecht; submitted to *Phys. Rev. Research*
- [7] P. Voigt, O. Bierwagen; *Appl. Phys. Lett.* **109**, 062103 (2016)
- [8] R. Schewski, K. Lion, A. Fiedler, C. Wouters, A. Popp, S. V. Levchenko, T. Schulz, M. Schmidbauer, S. Bin Anooz, R. Grüneberg, et al., *APL Mater.*, **7**, 022515 (2019).

Investigation of soluto-capillary convection in $\text{Ge}_x\text{Si}_{1-x}$ melts

J. P. Wöhrle, T. Jauß, T. Sorgenfrei

Crystallography, Albert-Ludwigs-University Freiburg, Hermann-Herder-Straße 5, 79104 Freiburg,
Germany

E-mail: jan.philipp.woehrle@krist.uni-freiburg.de

The requirements for industrial semiconductor materials used for device applications are constantly rising – one example is the upcoming development of the 5G mobile network technology and the following advancement of autonomous driving. Therefore, high quality bulk crystals are needed – to solve the technical obstacles, a profound comprehension of the respective material systems is required. Especially in mixed systems, additional challenges concerning the homogeneity of the grown material are rising due to varying properties of the different chemical composition of the components, such as germanium and silicon.

$\text{Ge}_x\text{Si}_{1-x}$ is an elemental semiconductor material which is extremely attractive for various applications like thermoelectrics, microelectronics, photovoltaic, or various functional applications due to its lattice constant and band gap tuning based on the composition. A major challenge in growing high quality $\text{Ge}_x\text{Si}_{1-x}$ bulk crystals from melt, is the fact that the surface tension of silicon is 30% higher than germanium, while on the other hand the density is only half as large (see table 1).

Table 1: Surface tension and density of Ge and Si.

	germanium	silicon
surface tension	$\gamma(T) = 591 - 0.08 \cdot (T - T_m)$ mN/m [1]	$\gamma(T) = 765 - 0.016 \cdot (T - T_m)$ mN/m [2]
density	5.323 g/cm ³ at 20 °C [3]	2.336 g/cm ³ at 20 °C [3]

Due to the large segregation coefficient of Si in Ge of $k_0 \leq 5$, germanium is enriched in front of the solid/liquid interface, which leads to a strong soluto-capillary convection and solutal buoyancy convection. It is shown that this specific type of convection is significantly influencing the shape of the solid-liquid interface and consequently the complete growth process, if a growth technique with free melt surfaces is used (e.g. Float-Zone, detached Bridgman, etc.). Therefore, a deeper understanding of the influence of convection flux and capillary phenomena on the resulting crystal quality is needed. Under normal gravity conditions on earth (1g), it is not possible to investigate the effect of the buoyancy force and different surface-tension-driven convections separately on the crystal growth process – in microgravity (μg) the influence of density-driven convection is suppressed including the strong buoyancy convection. These experiments under μg conditions provide the possibility to investigate the flow behavior in-situ on and in the liquid phase without the disturbing impact of the buoyancy convection.

Therefore, we perform experiments in parabolic flights (see fig. 1) which provide several μg phases up to 22 seconds, where we can quantitatively and qualitatively determine the effect of soluto-capillary convection in the Ge-Si system. In the used setup, the solid/liquid interface is running perpendicular to the melt surface so that impacts of surface tension driven flows and their effects on the growth front can directly be observed. By analyzing the movement of small boron nitrite tracer particles on the melt surface during solidification we can track the movement processes and estimate the velocities of these particles. Different $\text{Ge}_x\text{Si}_{1-x}$ mixtures (3-35 at% Si) are used to investigate the effect of the composition on the soluto-capillary Marangoni convection.

To handle the short parabolic phases, we have to ensure that we can heat up and cool down the samples rapidly – therefore we use a double ellipsoid mirror furnace with an argon atmosphere as inert gas (scheme of used furnace in fig. 2). To record the tracer paths (e.g. fig. 3), we use a top mounted high-speed CCD camera. A current view on the results of the parabolic flight campaigns of the last years will be presented.

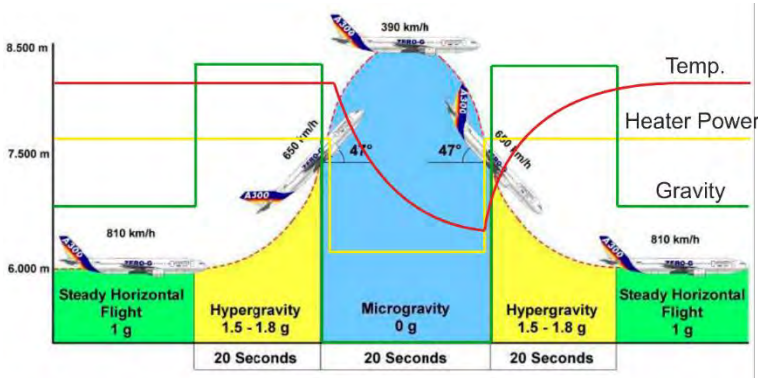


Figure 1: Parabolic flight setup during one parabola (image by Novespace, France). One flight day offers 30 parabolas with 20 seconds of microgravity each. Guaranteed maximum deviations of $\pm 0.005g$.

Figure 2: Left: Double ellipsoid mirror furnace allows rapid heating and cooling of the samples. Right: A high-speed camera above the top window records tracer movements on the solidifying melt surface. The crucible consists of SiC coated graphite.

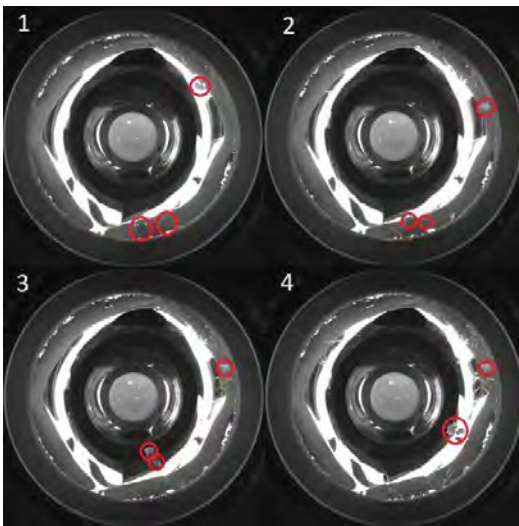
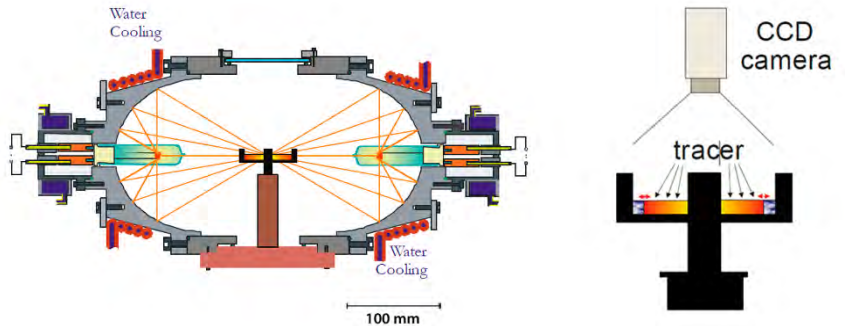


Figure 3: Four stages during a μg experiment: (1) In the initial state, the sample is completely molten. The pBN tracers remain on the starting position. (2) Solidification starts on the top. The tracer is moved by soluto capillary convection and thermocapillary convection. (3) Solidification starts also on the lower crucible wall. Second tracer movement is initiated. (4) In the final state, the complete sample is solid and will be heated again for the next parabola.

[1] Kaiser, N., Cröll, A., Szofran, F.R., Cobb, S.D., Benz, K.W. Journal of Crystal Growth 231 (2001), 4, 448-457

[2] Rhim, W.-K., Ohsaka, K.: Journal of Crystal Growth 208 (2000) 313-321

[3] Greenwood, N.N., Earnshaw, A.: *Chemie der Elemente*. 1. Auflage. VCH, Weinheim 1988, S. 482

Parameter study on n-type multicrystalline ingots with tailored resistivity profiles

I. Buchovska, N. Dropka, M. Pietsch, F.M. Kiessling

Leibniz-Institut für Kristallzüchtung, Max-Born-Str. 2, D-12489 Berlin, Germany

Nowadays multicrystalline silicon (mc-Si) produced by directional solidification (DS) is the most popular substrate material for manufacturing of solar cells. It covers more than 60% of PV market and is expected to keep a significant share in the next decade. The trend towards high efficiency and low cost solar devices results in multiple changes and improvements both in solar cell technology and crystallization methods. One of the most promising concepts is solar cells and modules based on n-type crystalline silicon material, which already demonstrates world record efficiencies and is the most suitable candidate to be the next industry standard. In general, crystallization of standard n-type material does not imply any dramatic changes in comparison to p-type growth. However, some specific differences related to the peculiarities of dopant element still exist. For instance, strong segregation of phosphorus in silicon leads to broader resistivity variation of n-type phosphorus-doped ingots in comparison to p-type ones, which in turn results in lower yield and higher cost of crystalline material.

Recently the method for reduction of resistivity variation in phosphorus-doped directionally solidified mc-Si was proposed. It is based on the ability of phosphorus to evaporate from silicon melt surface not only in case of high vacuum but also at pressures typical for DS crystallisation [1]. The method implies controlling and altering phosphorus transport both in liquid and gaseous phases by the complex arrangements of ambient pressure, gas flow and melt mixing performed by travelling magnetic fields (TMF). It was shown that this approach can be effectively used to control and tailor resistivity distribution along the ingots height. However, it has not yet been investigated how the manipulations with gas pressure and melt mixing affect other parameters of multicrystalline ingots, which are important for solar cell operation.

In this work we present the results for n-type DS-Si ingots, which were grown using complex arrangements on influencing phosphorus transport during growth process. These involve variation of melt stirring, ambient gas flow and gas pressure. In the row of experiments on homogenization of resistivity profiles different process conditions and their combinations were tested on G1-size (22 x 22 x 12 cm³) n-type DS ingots, including both conventional and high performance mc-Si material. The quality of ingots was characterized in terms of minority carrier lifetime, as well as the presence of impurities and inclusions (Cs, Oi, SiC, Si₃N₄, metals etc.)

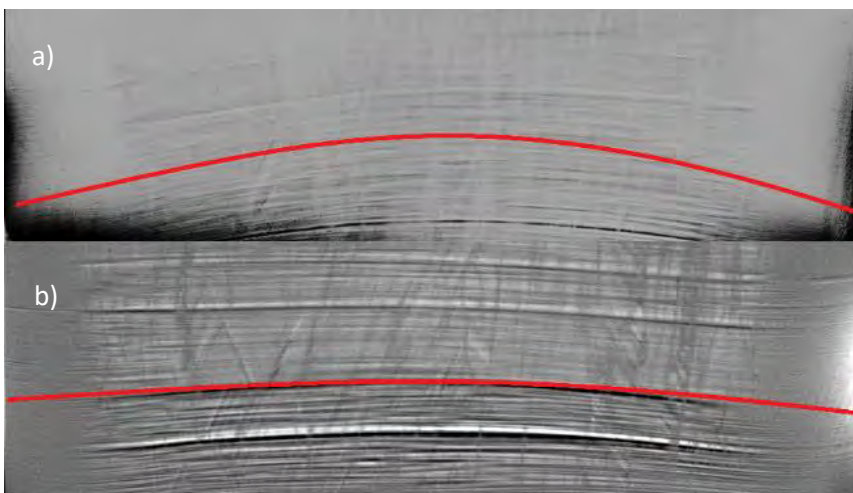


Fig. 1: The shape of solid-liquid interface of mc-Si ingots:
a) without TMF stirring,
b) with TMF stirring

The influence of each process parameter on material quality will be discussed. It will be shown that enhanced melt stirring with double-frequency TMF not only promote uniform resistivity profile in the first half of mc-Si, but also ensures flatter crystallization front (Fig. 1.), which is beneficial for stable crystal growth [2].

A particular attention will be given to the influence of gas pressure on ingot quality and process safety. It is well known that low ambient pressure during crystallization provokes erosion of crucible coating as well as migration of oxygen from a crucible into silicon melt and its evaporation from melt surface [3]. It will be shown that even at the process pressure of 50 mbar no sticking between a quartz crucible and the ingot was observed and no harmful Si_3N_4 inclusions were found in crystallized ingots. The used crucibles were coated with Si_3N_4 according to a developed in-house procedure. Furthermore, although such low pressures result in somewhat increased concentration of O_i in the second half of mc-Si ingots, it was on an acceptable level and significantly lower than regular elevated values at the bottom of DS ingots (Fig. 2).

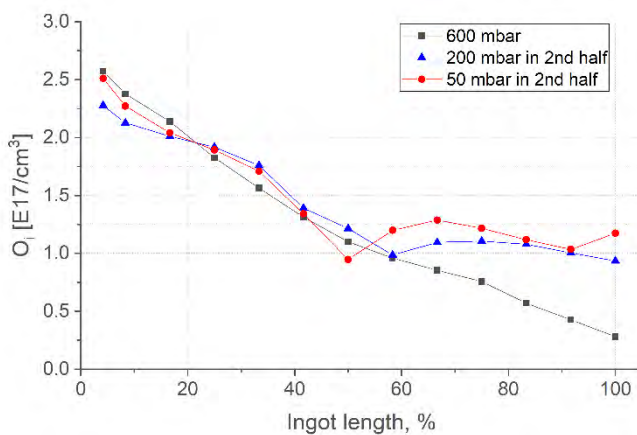


Fig. 2: Distribution of interstitial oxygen for mc-Si ingots grown with different ambient pressure

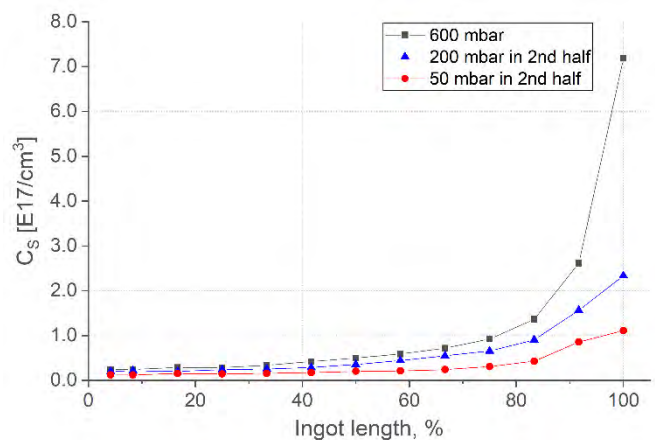


Fig. 3: Distribution of substitutional carbon for mc-Si ingots grown with different ambient pressure

It will be shown that a complex approach to melt stirring and gas transport ensure not only improved resistivity distribution along the height of n-type phosphorus-doped DS-Si ingots, but also provide multicrystalline material of high quality suitable for production of high efficiency solar cells and modules.

Acknowledgment

The authors are thankful to M. Imming-Friedland and T. Wurche for sample preparation.

- [1] I. Buchovska, N. Dropka, S. Kayser, F.M. Kiessling, J. Cryst. Growth, **507**, 299 (2019)
- [2] F.M. Kiessling, F. Büllesfeld, N. Dropka, Ch. Frank-Rotsch, M. Müller, P. Rudolf, J. Cryst. Growth, **360**, 81 (2012)
- [3] X.M. Huang, K. Saitou, S. Sakai, K. Terishima, K.Hoshikawa, Jpn. J. Appl. Phys. **37**, 3188 (1998)

Investigation of directionally solidified quasi-mono silicon for future gravitational-wave detector test-mass mirrors

Frank M. Kiessling^{1,*}, Iryna Buchovska¹, Graeme McGhee², Maya Kinley-Hanlon², Iain Martin², Peter Murray², Roman Schnabel³, Jessica Steinlechner^{4,5}, Simon Tait²

¹Leibniz-Institut für Kristallzüchtung, Max-Born-Str. 2, D-12489 Berlin, Germany

²SUPA, School of Physics and Astronomy, University of Glasgow, Glasgow, G12 8QQ, Scotland

³Institut für Laserphysik und Zentrum für Optische Quantentechnologien, Universität Hamburg, Luruper Chaussee 149, D-22761 Hamburg, Germany

⁴Maastricht University, P.O. Box 616, 6200 MD Maastricht, The Netherlands

⁵Nikhef, Science Park 105, 1098 XG Amsterdam, The Netherlands

*email: frank.kiessling@ikz-berlin.de

In 1916, Albert Einstein predicted the existence of gravitational waves (GW). A century later on 09-14-2015, the Laser Interferometer Gravitational-wave Observatory (LIGO) observed GW from the merging of two black holes for the first time [1]. In order to detect more gravitational waves from a wider range of sources, the detection sensitivity has to be continuously improved. The European Einstein Telescope (ET) is a vision for the next (3rd) generation of GW detectors [2]. One component of the conceptual ET design study are 200 kg test-mass mirrors from single crystalline silicon.

Although there exist various techniques to produce silicon single crystals, the diameter of the crystals is the first criterion to consider. Since the size of a mirror has to be about 50 cm in diameter, single crystalline silicon of highest perfection cannot be provided by the crucible-free float zone technique. Even dislocation free silicon single crystals, which have been grown by the Czochralski (Cz) method, might not fulfill the proposed size and purity required for the Einstein Telescope [2, 3]. An interesting approach to overcome the size problem is the use of silicon grown by directional solidification (DS). DS-Si can be grown as quasi-mono ingots with far bigger sizes needed here and might be available on the market by request. Unfortunately, this quasi-mono silicon has the lowest material quality compared to the dislocation-free silicon crystals mentioned above. But, since the oxygen level in directional solidified silicon material is lower than the one in Cz-Si and even magnetic Cz-Si crystals, the use of DS-Si might be a promising approach. Thus, the defect limits have to be investigated in order to evaluate its suitability for the use as a future gravitational-wave detector test-mass mirrors material.

Samples of different sizes have been prepared using a quasi-mono silicon ingot grown by directional solidification. The material has been characterized regarding carrier lifetime, concentration of substitutional carbon C_s, interstitial oxygen O_i and electrical resistivity. Microwave detected photoconductivity method, FTIR and conductivity measurements are performed, respectively. Additionally, photoluminescence measurements reveal possible recombination active dislocation clusters. These data will be discussed in relation to preliminary results of mechanical loss (which determines the level of thermal noise) and optical absorption (a crucial parameter for maintaining cryogenic operating temperature) values.

References

- [1] B. P. Abbott et al., *Phys. Rev. Lett.* 116, 061102 (2016).
- [2] <http://www.et-gw.eu/index.php/etdsdocument>
- [3] J. Steinlechner, *Phil. Trans. R. Soc. A* 376, 20170282 (2018).

Single crystal growth of Sn- and Ge-substituted GaPd₂ for basic research in catalysis

S. Püschel, K. Bader, and P. Gille

Ludwig-Maximilians-Universität München, Department of Earth and Environmental Sciences,
Crystallography section, 80333 München, Germany
E-mail: stefan.pueschel@campus.lmu.de

Summary

According to recent studies, intermetallic compounds may have better catalytic properties than presently used industrial catalysts that are based on noble metal elements or substitutional alloys from them [1]. The latter ones suffer diffusion and segregation under operation conditions, while intermetallics have well-defined structures with the catalytically active atoms at specific atomic sites. Therefore, they may have better long-term stability and considerably higher catalytic selectivity, according to the *active-site isolation concept* [2].

Several binary compounds in the Ga-Pd system have already been grown with the Czochralski technique from Ga-rich solutions as cm³-sized single crystals [3], which are required for fundamental studies in surface physics and crystallography. The intermetallic compound GaPd₂ has been shown to be the best candidate for heterogeneous catalysis in hydrogenation processes, with catalytically active Pd sites, being well isolated. More recently, it has been found that partially replacing Ga by Sn in GaPd₂ may further increase the activity of this catalyst [4].

Substituting a part of the Ga atoms by an element from the fourth group in the periodic table, thus growing solid solutions, e.g. (Ga,Ge)Pd₂ or (Ga,Sn)Pd₂, allows to study the electronic influence of an additional valence electron on the material's catalytic properties while the crystal structure remains almost unchanged. Unfortunately, little is known about the ternary Ga-Ge-Pd and Ga-Sn-Pd phase diagrams. In the pseudobinary GaPd₂-GePd₂ system, the substitution of Ga by Ge is restricted since GaPd₂ crystallizes in the Co₂Si structure type (*Pnma*) and GePd₂ in the Fe₂P structure type with hexagonal symmetry (*P $\bar{6}$ 2m*). An isothermal section through the ternary phase diagram at 700°C has been published as early as 1975 [6] indicating a maximum Ge substitution according to approx. Ga_{0.57}Ge_{0.43}Pd₂. GaPd₂ and SnPd₂ are isostructural in the Co₂Si structure type (*Pnma*) and therefore form a complete solid solution series. However, pure SnPd₂ cannot be grown from a liquid phase, but decomposes in a peritectoid reaction at 820°C [5]. Thus, ternary Ga_{1-x}Sn_xPd₂ solidification from a native melt or solution is expected to result in an upper limit of Sn substitution for Ga.



Fig. 1: Ga_{0.7}Sn_{0.3}Pd₂ single crystal, grown with the Czochralski technique in [010] direction.



Fig. 2: Ga_{0.8}Ge_{0.2}Pd₂ single crystal, grown with the Czochralski technique in [001] direction.

This contribution presents the results of a high number of slow-cooling experiments in order to investigate parts of the unknown liquidus surface, i.e. to study the primary crystallization fields of the 1:2 phase solid solutions and the relevant tie-lines for the crystal growth in the two ternary systems Ga-Ge-Pd and Ga-Sn-Pd. These small-scale experiments were done with typically less than 1 g of material in graphitized fused silica ampoules. The obtained spherical samples were investigated using X-ray powder diffraction, optical microscopy and electron-probe microanalysis. The maximum Ga substitution by Sn has been determined as $\text{Ga}_{0.46}\text{Sn}_{0.54}\text{Pd}_2$ that primarily crystallized from a solution of composition $(\text{Ga}_{0.4}\text{Sn}_{0.6})_{0.38}\text{Pd}_{0.62}$. Based on these findings, Czochralski growth experiments from incongruent melts, being either (Ga,Sn)- or (Ga,Ge)-rich, were successfully done using binary GaPd_2 seeds of different crystallographic orientations. As already known from growth experiments with binary GaPd_2 , extremely low pulling rates down to $25 \mu\text{m/h}$ were necessary to avoid fluid inclusion formation. Weak segregation effects along the pulling direction (Fig. 3) indicate pseudobinary segregation coefficients that are only slightly lower than unity.

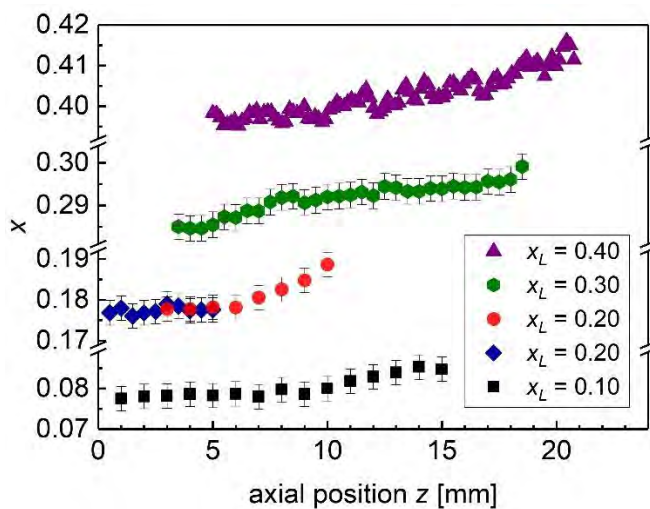


Fig. 3: Axial composition profiles of single crystals of the $\text{Ga}_{1-x}\text{Sn}_x\text{Pd}_2$ solid solution grown from different starting melts. The Sn content of the starting charge is given in terms of the pseudobinary mole fraction x_L according to $(\text{Ga}_{1-x_L}\text{Sn}_{x_L})_{1-y_L}\text{Pd}_{y_L}$ [7].

Acknowledgments: The authors are grateful to Juri Grin (MPI for Chemical Physics of Solids, Dresden) and Marc Armbrüster (TU Chemnitz) for fruitful discussions as well as to the Deutsche Forschungsgemeinschaft for financial support under grant no. GI 211/15-1.

References

- [1] M. Armbrüster, R. Schlögl, Yu. Grin, *Sci. Technol. Adv. Mater.*, **15**, 1-17 (2014).
- [2] W.M.H. Sachtler, *Catal. Rev. Sci. Engin.*, **14**, 193-210 (1976).
- [3] J. Schwerin, D. Müller, S. Kiese, P. Gille, *J. Crystal Growth*, **401**, 613-616 (2014).
- [4] O. Matselko, R.R. Zimmermann, A. Ormeci, U. Burkhardt, R. Gladyshevskii, Yu. Grin, M. Armbrüster, *J. Phys. Chem. C* **122**, 21891–21896 (2018).
- [5] T.B. Massalski et al., *Binary Alloy Phase Diagrams*, ASM International, Ohio (1990).
- [6] S. Heinrich, K. Schubert, *Z. Metallkd.* **66**, 353-355 (1975).
- [7] K. Bader, A. Dorner, P. Gille, *J. Crystal Growth*, **532**, 125401 (2020).

Thermally stimulated dislocation generation in silicon crystals grown by the Floating Zone method

Hans - Joachim Rost, Iryna Buchovska, Kaspars Dadzis, Uta Juda, Robert Menzel, Matthias Renner*

*Leibniz-Institut für Kristallzüchtung, Max-Born-Str. 2, 12489 Berlin, Germany
email: hans-joachim.rost@ikz-berlin.de

Previously, the dislocation behavior from the view point of photovoltaics was studied during melting and crystallization of large-area single crystal seeds at near-equilibrium conditions using the so-called NeoGrowth technique [1], [2]. Alternatively, the authors investigated the crucible-free growth of low-defect single crystals on large-diameter silicon seeds by a new, modified FZ- technique [3] without using the common Dash technique. All grown crystals, independent of the seed structure or preparation procedure, reproducibly developed a dislocation network in the temperature range between 900 °C and 1200 °C already during heating to the melting temperature and before the growth started.

In the present study, a long dislocation-free crystal with a diameter of 20 mm and smaller than the inner hole diameter of the RF-coil was grown using the standard Floating Zone method. Then the grown crystal, without any mechanical or chemical treatment, was stepwise heated up in the temperature range from 700 °C till 1180 °C controlled by a pyrometric system. After reaching a quasi-stationary state for a chosen temperature, the crystal was shifted by a certain distance relative to the fixed coil. The crystal was then cut into segments of about 100 mm in length. Plates with a thickness of 2 mm were cut parallel to the growth direction and double-side polished. Additionally, wafers were cut perpendicular to the growth direction between the segments. The samples were analyzed by Lateral Photovoltage Scanning (LPS), photoluminescence (PL) and etch pit density (EPD) as well as the lifetime were measured.

Comparing the results of the different methods a strong correlation between the dislocation density and the lifetime was found in dependence of the temperature increase in the investigated range. The region of the dislocations generation and its spreading behavior could be revealed. Possible origins and correlations will be discussed.

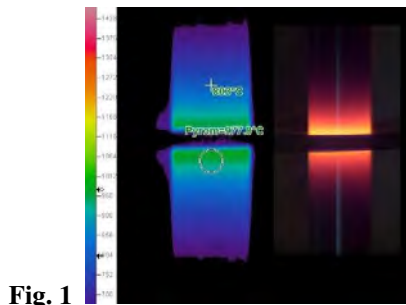


Fig. 1

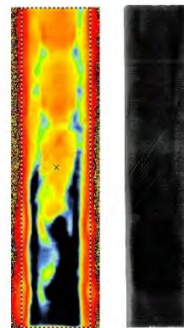


Fig. 2

Figure 1 – Temperature (pyrometer)(left) and crystal picture (right) during the heating.

Figure 2 – Lifetime (left) and EPD (right) measured on a longitudinal cut

References:

- [1] N. Stoddard, B. Gründig-Wendrock, A. Krause, D. Oriwol, M. Bertoni, T. Uberg Naerland, I. Witting, L. Sylla, J. Crystal Growth 452 (2016) 272–275.
- [2] N. Stoddard, J. Russell, E.C. Hixson, H. She, A. Krause, F. Wolny, M. Bertoni, T. Uberg Naerland, L. Sylla, W. von Ammon, Prog. Photovolt. Res. Appl. (2018) 1–8.
- [3] H.-J. Rost, R. Menzel, D. Siche, U. Juda, S. Kayser, F.M. Kießling, L. Sylla, T. Richter Journal of Crystal Growth 500 (2018) 5–10

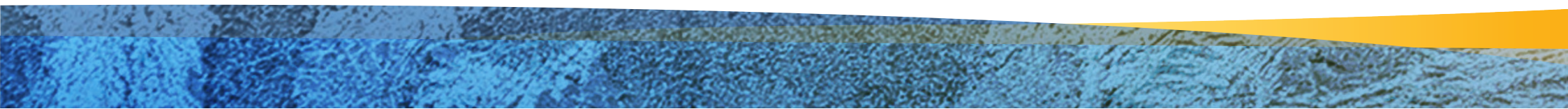


Crystals (ISSN 2073-4352) is an open access journal that covers all aspects of crystalline material research. *Crystals* provides a forum for the advancement of our understanding of the nucleation, growth, processing, and characterization of crystalline and liquid crystalline materials. Their mechanical, chemical, electronic, magnetic, and optical properties, and their diverse applications, are all considered to be of importance. Additionally, we encourage contributors to send articles focused on crystals research (of small and high molecular weight). Their characterization by using modern techniques for crystal growth and high resolution characterization such as synchrotron radiation and modern methods for the growth of crystals for X-ray free electron lasers (XFELS) would also be welcome.

IMPACT
FACTOR
2.06

<https://www.mdpi.com/journal/crystals>

Crystals sponsored the Special Prize of the Scholar's Competition „Wer züchtet den schönsten Kristall“.



X-ray diffraction systems

... highly precise
... versatile
... customized

XRD diffractometers for
stress analysis
texture analysis
phase analysis
high resolution applications

- XRD Space universal
large sample space
large angular and translation ranges
- XRD Charon SXL
largest sample space
largest sample weight

versatile, camera-controlled sample
mounting
automatic positioning and sampling
of large sample batches



XRD crystal orientation systems

- XRD Galaxy SCL
precision laue systems for fast ori-
entation of crystals, ingots, wafers,
turbine blades
- XRD Galaxy SCD
high precision scanning systems for
orientation of ingots and wafers

versatile, camera-controlled sample
mounting
automatic positioning and sampling of
large sample batches



Ihre Spezialisten für Diamantdrahttechnologie

www.didras.com

Über DIDRAS:

DIDRAS GmbH wurde 2019 aus einem Steinbeis Forschungsinstitut heraus gegründet. Die Technologie des Diamantdrahtsägens verfolgen wir schon seit 2009 durch mehrere Forschungs- und Entwicklungsprojekte.

Technologie:

Das Diamantdrahtsägen überzeugt mit einem präzisen Schnitt und nahezu geschliffenen Oberflächen. Beinahe alle Werkstoffe können durch das Diamantdrahtsägen getrennt werden. Besonders geeignet ist der Diamantdraht zum Trennen von sehr harten und spröden Werkstoffen.

Mit den sehr dünnen Drahtschlaufen von DIDRAS, können kleine Bauteile wie zum Beispiel Elektronik-Widerstände getrennt werden.

Produkt:

- DWLS-650 die CNC-gesteuerte Diamantdrahtsäge
- Für 2D-Schnitte
- Schnittgeschwindigkeit bis zu 80m/s
- Verfahrweg in X/Y = 200 mm
- Drahtschlaufen in allen Längen von 120µm bis 240µm Draht-Ø



PRÄZISIONSTECHNIK

HK-Präzisionstechnik GmbH

Kooperationspartner zu DIDRAS GmbH für die Entwicklung und Herstellung von Diamantdrahtsägen für den industriellen Einsatz.

Mehr als 70 Jahre Erfahrung und eine ganz besondere Auffassung von Qualität, Zuverlässigkeit und Präzision begründen heute den herausragenden Ruf der HK-PRT. Besonders auf dem Spezialgebiet der Diamantdrahtsäge-Technik und deren Anwendung in der Siliziumbearbeitung setzt die HK-PRT Technologie neue Maßstäbe.



aprotec – advanced process technologies

Unser Name steht für innovative und fortschrittliche Lösungen in der Prozessanlagen- und Automatisierungstechnik

Prozessanlagentechnik

Entwicklung und Herstellung von schlüsselfertigen Anlagen für kundenspezifischen Prozesse mit speziellen Prozessumgebungen wie Vakuum, Überdruck, hohen Temperaturen oder reinsten Gasatmosphären für die industrielle Produktion oder im Labormaßstab für folgende Anwendungen:

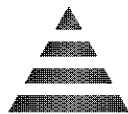
- Kristallzüchtung
- Schmelzen & Gießen
- Tempern, Reduktion und Synthese
- spezielle Hochtemperaturprozesse
- Spezielle Vakuum-/Hochdruckprozesse



Dafür steht unser Team aus Ingenieuren und Technikern mit fundiertem Wissen und langjähriger Branchenerfahrung.

Material-Technologie & Kristalle für Forschung, Entwicklung und Produktion

- ▲ Kristallzüchtungen von Metallen, Legierungen und Oxiden
- ▲ Kristallpräparation (Formgebung, Polieren und Orientieren)
- ▲ Reinstmaterialien (99,9 – 99,99999 %)
- ▲ Substrate (SrTiO₃, MgO, YSZ, ZnO, Al₂O₃, etc.)
- ▲ Wafer (Si, Ge, ZnTe, GaAs und andere HL)
- ▲ Sputtertargets
- ▲ Optische Materialien (Fenster, Linsen, etc.)
- ▲ Auftragsforschung für Werkstoffe und Kristalle



MaTeck

Im Langenbroich 20
52428 Jülich
Tel.: 02461/9352-0
Fax: 02461/9352-11
eMail: info@mateck.de

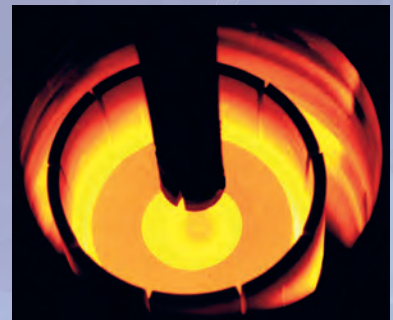
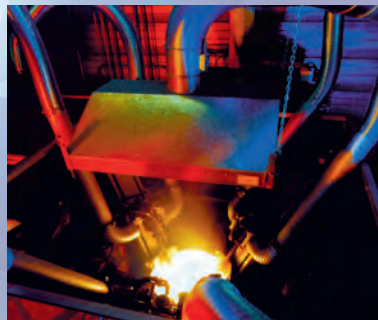
Besuchen Sie uns im Internet (inkl. Online-Katalog):
www.mateck.de

SurfaceNet

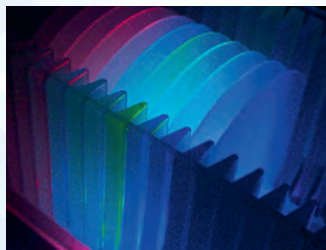
Crystals



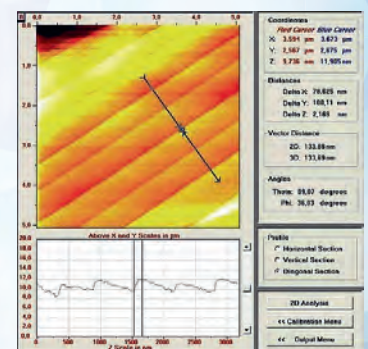
Crystal Puller



Wafers



Analytical Services



Substrates

Custom Parts

Sputter Targets

PLD Targets

Custom Crystal Growth

SurfaceNet GmbH

Oskar-Schindler-Ring 7 · 48432 Rheine – Germany

Fon +49 (0)5971 4010179 · Fax +49 (0)5971 8995632

sales@surfacenet.de · www.surfacenet.de

- Reine und hochreine Metalle & Anorganika
- Aufdampfmaterialien
- Sputtertargets
- Seltene Erden
- Edelmetall-Halbzeuge



chemPUR
Ihr Partner für Chemie & Physik

ChemPur Feinchemikalien und Forschungsbedarf GmbH

Rüppurrer Straße 92
D-76137 Karlsruhe

Tel.: + 49 (0) 7 21 - 9 33 81 40
info@chempur.de **www.chempur.de**



SCIDRE

SCIENTIFIC INSTRUMENTS DRESDEN GMBH

Exploitation of ideas towards novel research equipment



**You have research equipment ideas which are waiting for realization?
You use self-developed technology for your research?**

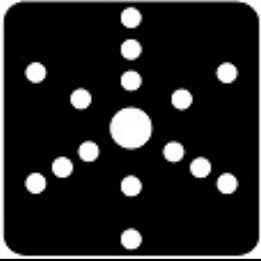


**Contact us to benefit from commercialization of your ideas and for
joint R&D projects towards novel equipment in your lab!**

- Research technologies also have market potential — together we can make successful products out of your equipment ideas!
- Working in science and bringing ideas to the market is compatible — with the right partner there is no impairment of your scientific work
- You earn license fees on every sold product and benefits from successful technology transfer
- You do not bear entrepreneurial risk and become visible as inventor
- We will advise you concerning third-party funds during joint R&D projects

Scientific Instruments Dresden GmbH
Gutzkowstraße 30
01069 Dresden
Germany

Web page www.scidre.de
E-mail info@scidre.de
Phone +49 (0) 351 - 84 22 14 70
Fax +49 (0) 351 - 84 22 89 38



MULTIWIRE LABORATORIES, Ltd.
 95 Brown Rd. MS 1018
 266A Langmuir Building
 Ithaca, NY 14850
Phone: (607) 257-3378
Email: salesinfo@multiwire.com

LAUE-CAMERA GmbH
 Sonnenweg 4b
 85386 Eching
Tel. 0170- 8238306
salesinfo@lauecamera.com
www.lauecamera.com

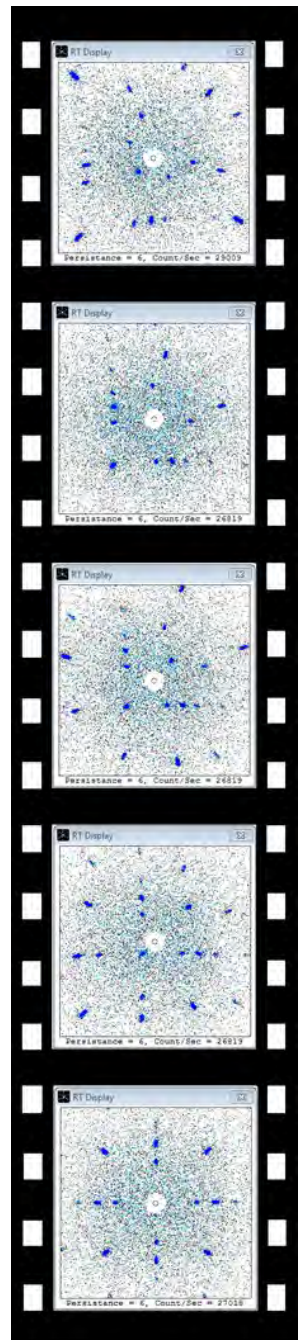
MWL120 Real-Time Back-Reflection X-Ray Camera System



MWL120 REAL-TIME LAUE DETECTOR

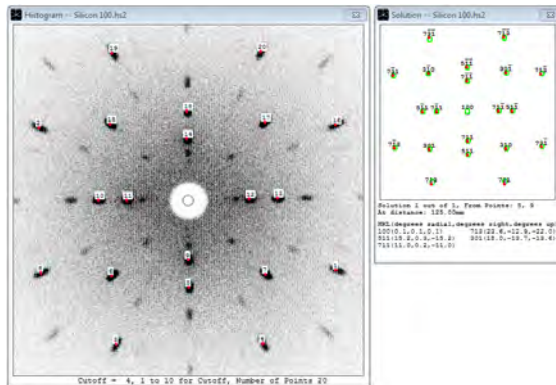
- Ideal replacement for the Polaroid XR-7 back-reflection cassette (film no longer available)
- NorthStar 7 indexes cubic, hexagonal, triclinic crystal systems and creates stereographic projections
- Provides an accuracy of 0.25° in standard Laue mode and 0.05° in high-resolution mode
- Operates best with the MWL motorized orientation stages
- Ideal for research applications, industrial process control, or academic laboratories
- Earlier model MWL110 systems can be upgraded to MWL120 capability

REAL-TIME IMAGE SEQUENCE



NORTHSTAR SOFTWARE

Crystal orientation is fast and easy with the latest NorthStar 7 software. Display real-time images while you rotate your sample, then use the collection mode to capture histograms for analysis. Northstar can automatically detect diffraction spots, determine the Miller index for each reflection, and calculate the angles to any crystal axis, all with a simple point-and-click interface.



MOTORIZED CRYSTAL ORIENTATION

Motorized sample stages allow manipulation of your sample position and orientation during measurements, improving productivity and safety.

- The **MWL706 Three-Axis Motorized Goniometer** makes positioning crystal samples fast and easy with real-time adjustment of pitch, yaw, and roll for samples up to 1 kg in size.
- The **MWL701A Jack & Translation Stage** allows easy vertical and horizontal motion to place the sample correctly in the beam or to image different parts of larger samples.
- The **MWL703 Motorized Bond Barrel** is ideal for orienting crystals



MWL706 3-Axis Goniometer



for **MWL701 Jack & Translation**



MWL703 Motorized Bond Barrel

Abstract Book
DKT2020

ISBN 978-3-00-064845-8

Copyright and responsible :

Deutsche Gesellschaft für
Kristallwachstum und Kristallzüchtung e.V.
DGKK e.V. (WW6, z.Hd. P. Wellmann)
Martensstr. 7
91058 Erlangen
Germany

Editor:
Prof. Dr. Andreas Erb
Walther Meissner Institut
für Tieftemperaturforschung
Bayerische Akademie der Wissenschaften
Walther-Meissnerstr. 8
85748 Garching
Germany



Fraunhofer

IISB

FRAUNHOFER-INSTITUT FÜR INTEGRIERTE SYSTEME UND BAUELEMENTE TECHNOLOGIE IISB

DU BIST STUDENT/-IN
DER ELEKTROTECHNIK,
MECHATRONIK,
WERKSTOFF-
WISSENSCHAFTEN, PHYSIK,
ENERGIETECHNIK ODER
EINES VERGLEICHBAREN
STUDIENGANGS?
STARTE JETZT DEINE
KARRIERE AM
FRAUNHOFER IISB
IN DEN BEREICHEN
LEISTUNGSELEKTRONIK &
HALBLEITERTECHNOLOGIE.



www.recruiting.fraunhofer.de

BEWERBERPORTAL:

www.IISB.fraunhofer.de/jobs